BST

BioScience Trends

IRCA
BSSA

IACMHR

www.biosciencetrends.com

BioScience Trends is one of a series of peer-reviewed journals of the International Research and Cooperation Association for Bio & Socio-Sciences Advancement (IRCA-BSSA) Group and is published bimonthly by the International Advancement Center for Medicine & Health Research Co., Ltd. (IACMHR Co., Ltd.) and supported by the IRCA-BSSA and Shandong University China-Japan Cooperation Center for Drug Discovery & Screening (SDU-DDSC).

BioScience Trends devotes to publishing the latest and most exciting advances in scientific research. Articles cover fields of life science such as biochemistry, molecular biology, clinical research, public health, medical care system, and social science in order to encourage cooperation and exchange among scientists and clinical researchers.

BioScience Trends publishes Original Articles, Brief Reports, Reviews, Policy Forum articles, Case Reports, News, and Letters on all aspects of the field of life science. All contributions should seek to promote international collaboration.

Editorial Board

BioScience Trends

CONTENTS

Volume 10, Number 4, 2016

Original Articles

CONTENTS   (*Continued*)

Brief Reports

Commentary

Guide for Authors

Copyright

Original Article

Hepatitis B virus dampens autophagy maturation *via* negative regulation of Rab7 expression

Tianhui Zhou[1,*], Min Jin[3,*], Yongsen Ding[1], Yi Zhang[4,5], Ye Sun[1], Shiqian Huang[2], Qing Xie[1,**], Congfeng Xu[2,3,**], Wei Cai[1,**]

[1] *Department of Infectious Diseases, Ruijin Hospital, Shanghai Jiao Tong University School of Medicine, Shanghai, China;*
[2] *Shanghai Institute of Immunology, Institutes of Medical Sciences, Shanghai Jiao Tong University School of Medicine, Shanghai, China;*
[3] *Key Laboratory of Stem Cell Biology, Institute of Health Sciences, Shanghai Institutes for Biological Sciences, Chinese Academy of Sciences and Shanghai Jiao Tong University School of Medicine, Shanghai, China;*
[4] *Biomedical Research Center, Zhongshan Hospital, Fudan University, Shanghai, China;*
[5] *Shanghai Key Laboratory of Organ Transplantation, Shanghai, China.*

Summary   **Hepatitis B virus (HBV) infection brings a huge challenge for medical health practitioners. It has been reported that invaded HBV escapes autophagic degradation through inhibiting lysosome maturation following enhanced autophagy formation, which putatively contributes to HBV replication and infection. However, the underlying mechanism by which HBV escapes from autophagic degradation remains elusive. In this study, we monitored the autophagic process using HepG2 cells and mice without or with transient HBV DNA plasmid transfection (pHepG2) or stable HBV infection (HepG2.2.15 cells) *in vitro* and *in vivo*. The results of Western blot, transmission electron microscopy and confocal microscopy, confirmed that HBV induced autophagy, while the fusion of autophagosomes with lysosomes was arrested. Furthermore, Rab7, a small GTPase that functions as a molecular switch responsible for the autophagosome-lysosome fusion, was inhibited, suggesting a potential mechanism for HBV-induced inhibition of autophagic degradation. In conclusion, our study proposes a potential mechanism for how HBV escapes autophagic degradation, which might be a novel therapeutic target for controlling HBV infection.**

Keywords: HBV, Rab7, Autophagy, Autophagosome-lysosome fusion

1. Introduction

Hepatitis B virus (HBV) infection threats about 248

million individuals' health globally. It remains a dreadful public health problem worldwide although the pervasive application of effective vaccination limits the number of newly HBV-infected patients dramatically (*1*). The availability of potent antiviral drugs decreases the morbidity and mortality inflicted by HBV infection. Nevertheless, almost all the current therapeutic measures are unable to completely eradicate the HBV DNA even after long-term antiviral therapy (*2*), and HBV could be reactivated when host immunity is compromised. The persistence of HBV DNA in the nucleus of infected hepatocytes is one of the intractable enigmas in approaches for the cure of chronic hepatitis B (CHB) (*3*). A better understanding of this refractory challenge may help to develop reliable priorities against HBV infection.

Macroautophagy (hereafter autophagy), a highly conserved cellular self-digestive process, plays a pivotal role in the degradation of dysfunctional proteins and

damaged organelles to maintains cellular homeostasis or responses to harmful stimuli in higher eukaryotes (*4*). Autophagy initiates with the formation of an autophagosome, following docking and fusion with a lysosome. Only after the fusion can the contents of the autophagosome be degraded (*5*). Moreover, accumulating evidence shows that autophagy is also involved in many pathophysiologic processes of human diseases including microbial infection (*6*). For HBV, Sir D *et al.* first reported that HBV could activate the early autophagic pathway (*7*). But it seems like autophagy causes no harm to HBV (*8*). The precise underlying mechanisms why the enhanced autophagosomes promote HBV DNA replication instead of engulfing it need to be elucidated.

Rab7, a small GTPase of Rab superfamily, functions as a key organizer of multiple membrane trafficking processes. It has been well established that Rab7 serves as a master regulatory component for the biogenesis of autophagosomes, lysosomes and other lysosome-related organelles (*9*). More recently, Rab7 has been implicated in the maturation of autophagosomes and their fusion with lysosomes. Hampered fusion of autophagosomes and lysosomes caused by deficiency of Rab7 has been covered in mycobacterium tuberculosis and human parainfluenza virus infection (*10,11*). Nevertheless, it is still uncertain whether Rab7 also plays an indispensable role in HBV-induced incomplete autophagy.

In the study, HBV infection induced autophagy was investigated, and the potential molecular mechanism that hindered autophagosome-lysosome fusion in HBV induced incomplete autophagic degradation was further explored.

2. Materials and Methods

2.1. Cell culture

HepG2 cells were obtained from the American Type Culture Collection (ATCC) and maintained according to ATCC instructions. HepG2.2.15 cells, which contained a stably integrated 1.3-copy HBV genome and could support persistent replication of HBV and produce intact HBV particles (*12*), was provided by the Department of Infectious Diseases of Changzheng Hospital. It was maintained in Dulbecco's Modified Eagle Medium (Invitrogen) supplemented with 10% (vol/vol) heat-inactivated fetal bovine serum (Invitrogen), 380 μg/mL G418 (Sigma), 125 μg/mL penicillin and 50 μg/mL streptomycin at 37°C in a humidified incubator containing 50 mL/L CO_2 (*13*).

2.2. Plasmids and cell transfection

HBV DNA plasmid (pHBV), which contains the 1.3-mer overlength HBV genome, and backbone plasmid pUC19 were a kind gift of professor James Ou from University of Southern California, Los Angeles, CA (*14*).

Transient transfection into HepG2 of pHBV (pHepG2) or the backbone plasmid pUC19 (as the mock-transfected HepG2) were performed using Fugene 6 reagent (Roche) according to the manufacturer's instructions, respectively. HepG2 cells were lysed for both protein and RNA analysis after 48 h transfection. Meanwhile, level of HBsAg in the cell supernatant was determined using the ARCHITECT i2000SR HBsAg QT assay (Abbott). The cut-off value for determining if HBsAg is positive is S/N ratio ≥ 0.05, and the reporting units are S/N ratio. Level of HBV DNA in the cell supernatant was detected using the Roche COBAS HBV Amplicor MonitorTM assay. Tandem mRFP-GFP-LC3 expressing plasmid ptfLC3 (Addgene) was obtained from Addgene (*15*), and transfection was performed using Lipofectamine 2000 (Invitrogen).

2.3. Animal analysis

C57BL/6 mice (8 weeks old, male) were injected *via* the tail vein with phosphate buffer saline (PBS) in a volume that was equivalent to 8% of the body weight. The PBS with or without 10 μg of pHBV was delivered within 5 to 8 sec. Four days later, mice were sacrificed and liver tissues or serums were collected. Total liver protein was analyzed. Serum levels of HBsAg and HBV DNA of the mice were determined. The animal experiments were approved by the Ethics Committee of Ruijin Hospital.

2.4. Immunoblotting

Cells were directly lysed with RIPA containing protease and phosphatase inhibitors (Roche) and proteins were separated by SDS-PAGE after denaturation (*16*). Immunoblot analysis was performed by initial transfer of proteins onto polyvinylidenefluoride filters using a Mini Trans-Blot (Bio-Rad) followed by a blocking step with 5% nonfat dried milk plus 0.1% Tween 20 for 2 hours at room temperature and exposed to primary antibodies diluted 2,000-fold that recognized microtubule-associated protein light chain 3 (LC3, Cell Signal), autophagy-related protein 5 (Atg5, Cell Signal), Rab7 (Cell Signal), or 5000-fold for GAPDH (Santa Cruz) overnight at 4°C and subsequently washed. The blots were then incubated with a secondary antibody conjugated with Horse Radish Peroxidase diluted 5000-fold for 1 hour at room temperature. Signals were detected by a FluorChem E system (Alpha Innotech Corp). For some immunoblots, band densitormetry was quantified using ImageJ software (National Institutes of Health).

2.5. RT-PCR

RT-PCR for Rab7 was performed as previously described (*17*), the primer pairs used in the study were as follows: Forward: 5'-ATGACCTCTAGGAAGAAAGTGTTGC TG-3'; Reverse: 5'-TCAGCAACTGCAGCTTTCTGCC

GAG-3'. Total RNA was extracted using TRIzol reagent (Invitrogen), and RNA was reverse transcribed using Superscript II (Invitrogen) and a random hexamer primer. The cDNA was used as template for PCR with Rab7-specific primer pairs, and PCR products were analyzed by agarose gel electrophoresis and visualized under UV light with ethidium bromide.

2.6. *Transmission electron microscopy*

For ultrastructure analysis, cells were trypsinized, centrifuged, and fixed with 2.0% glutaraldehyde in 0.2M PBS (pH 7.2) for 12 h at 4°C, and washed with PBS, then post-fixed with 1% OsO_4 in 0.2M PBS (pH 7.2) for 2 h at 4°C. After a further wash with PBS, cells were dehydrated *via* a graded ethanol series and then embedded before trimming and sectioning. Embedded cells were sectioned at a thickness of 75 nm using a Reichert Ultramicrotome and mounted onto 200-mesh copper grids. After counterstaining with uranyl acetate and lead citrate for 5 min, the grids were visualized using a CM-120 transmission electron microscope (Philip) with an operating voltage of 80kV (*18*).

2.7. *Fluorescence confocal microscopy*

Fluorescence confocal microscopy was performed as previously described (*16*). Cells grown on coverslips were fixed in BD Cytofix/Cytoperm solution (BD Biosciences) at room temperature for 15 min. These coverslips were visualized with single-line excitation at 488 or 594 nm for Alexa Fluor on an Olympus Fluoview confocal microscope with appropriate emission filters (Olympus).

2.8. *Autophagy analyses*

For starvation, the cells were incubated in serum-free Earle's balanced salt solution (Invitrogen) for 6 hours. Autophagy was analyzed by immunoblotting or fluorescence microscopy, as described previously (*19*). In the immunoblotting analysis, cells were treated as indicated, and cell lysates were immunoblotted with anti-LC3 antibody to monitor the LC3-II generated during the formation of autophagosomes. In the fluorescence confocal microscopy analysis, cells were transfected with a mRFP-GFP-LC3 expressing plasmid ptfLC3 construct and treated as indicated. These cells were imaged by fluorescence confocal microscopy and autophagy cell numbers were recorded. Total LC3-positive dots (GFP^+RFP^+ and GFP^-RFP^+ dots), early autophagosomes (GFP^+RFP^+ dots) and autolysosomes ($GFP^- RFP^+$ dots) were analyzed.

2.9. *Statistical analysis*

The 2-tailed Student t test or one-way analysis of variance followed by the Turkey post-hoc test was used for all statistical analyses in the study using SPSS 18.0. A value of $p < 0.05$ was considered as statistically significant.

3. Results

3.1. *HBV DNA stimulates the formation of autophagosomes*

In order to study whether HBV DNA induces autophagy, first we established an HBV infection cellular system. In our system, the levels of HBsAg and HBV DNA in cell supernatant were monitored. Compared to the HepG2 control and the mock-transfected HepG2, HepG2.2.15 and pHepG2 showed significantly higher levels of both HBsAg and HBV DNA (Figure 1A, B). Atg5 and LC3, two pivotal ubiquitin-like proteins that are involved in the initiation of autophagy, serve as hallmarks of the formation of autophagosomes (*5*). In the current study, markedly elevated LC3-II and Atg5 were detected in pHepG2, and HepG2.2.15 cells, similar to that in starved HepG2 cells (Figure 1C, D). Additionally, autophagy-featured intracellular double membrane structures were readily observed in pHepG2 under transmission electron microscopy, whereas there were barely double membrane vacuoles in HepG2 (Figure 1E). Collectively, it suggests that HBV infection induces autophagosome formation.

3.2. *HBV infection induces autophagosome accumulation in vivo*

To decipher whether HBV infection could induce autophagosome formation *in vivo*, pHBV was injected into C57BL/6 mice to simulate infection of HBV. Compared with those in the control, serum HBsAg and HBV DNA levels significantly increased in the pHBV injection group (Figure 2A and B). Histology showed disorganized hepatic lobules and lymphocytic infiltration in portal tracts, which indicated obvious inflammation in liver tissue (Figure 2C). Higher expression of LC3-II and Atg5 protein levels were observed in liver tissue of pHBV transfected mice than that of control mice (Figure 2D). Thus, our data indicates that HBV infection induces the formation of autophagosomes *in vivo*.

3.3. *Autophagy maturation is hampered in pHepG2 cells*

Autophagy maturation (docking and fusion of lysosome) is a key step for microbial degradation and is susceptible to pathogen hijacking. To uncover the underlying mechanism by which HBV induced autophagy promoted HBV replication instead of engulfing it, HepG2 cells were transfected with pHBV, followed by transfection with mRFP-GFP-LC3 plasmid. GFP is susceptible to
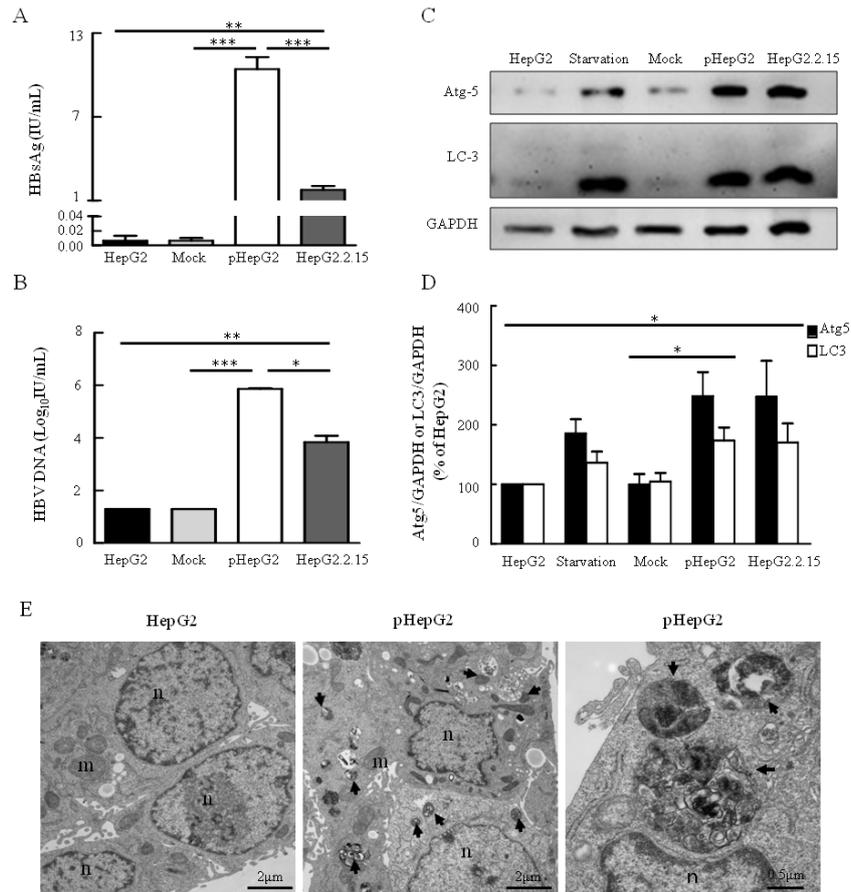
Figure 1. HBV DNA induces autophagosome accumulation. HepG2 cells were starved, transfected with pHBV or pUC19 for 48h, respectively. **(A, B)** Levels of HBsAg and HBV DNA in supernatant of HepG2, mock-transfected HepG2, pHepG2 and HepG2.2.15 were measured. *, $p < 0.05$; **, $p < 0.01$; ***, $p < 0.001$. **(C)** The Atg5 and LC3 levels in HepG2, starvation treated HepG2, mock-transfected HepG2, pHepG2 and HepG2.2.15 were assessed by Western blot. **(D)** The bands density ratios of Atg5/GAPDH or LC3-II/GAPDH were determined by Western blot, and the results of control HepG2 was taken to be 100%. It was calculated as the average value of the data obtained from 3 independent experiments. *, $p < 0.05$. **(E)** Autophagic vacuoles in HepG2 and pHepG2 were observed by electron microscopy. The arrow indicates autophagosome, "m" represents mitochondria, and "n" represents nuclear.
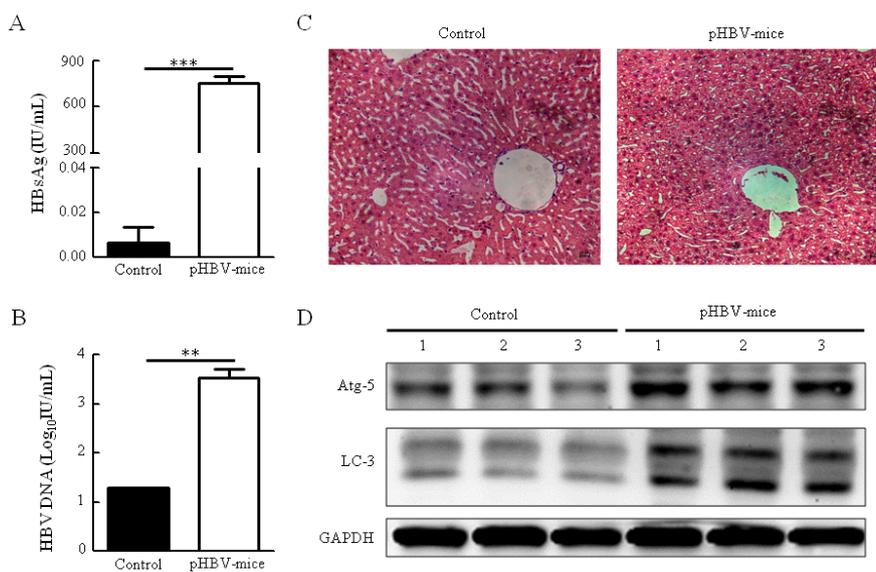
Figure 2. pHBV increases autophagosome formation in mice. Male C57BL/6 mice (8 weeks old) were randomly injected with (pHBV, $n = 3$) or without (control, $n = 3$) 10 μg of pHBV. Ninety-six hours later, mice were sacrificed and liver tissues or sera were collected. **(A and B)** Mice serum HBsAg and HBV DNA levels were measured. **, $p < 0.01$; ***, $p < 0.001$. **(C)** Liver tissues of mice in control and pHBV-treated mice were stained with hematoxylin-eosin staining. **(D)** Atg5 and LC3 levels in mice liver tissue were assessed by Western blot.

acidified conditions, while mRFP signals are relatively stable, so the autophagosome is displayed as yellow punctate dots (both red and green) before fusion with lysosome, and red for mature autolysosomes. As shown in Figure3A, yellow punctate dots were more obvious in pHepG2 cells than HepG2, while only sporadic red punctate dots were observed, confirming dominant presence of autophagosomes (yellow punctate dots), with rather few autolysosomes (red punctate dots). Cell numbers of HepG2 with autophagy were significantly

increased after transfection with pHBV (Figure 3B). Above all, our data indicates inhibitory effects on autopahgy maturation.

3.4. *HBV infection induces reduction of Rab7*

Small GTPase Rab7 has been considered as a master molecular switch during the formation of autolysosomes (*20*). Consequently, the expression of Rab7 was investigated to determine the role of Rab7 in HBV induced autophagy. Our results showed significant drops in Rab7 protein expression in pHepG2 cells and HepG2.2.15 cells (Figure 4A, B), as well as in Rab7 mRNA level (Figure 4C, D). Thus, it shows that HBV infection inhibits Rab7 expression and dampens autophagy maturation.

4. Discussion

Autophagy, a conserved cellular protective mechanism, has been regarded as a key component of the innate immune system (*21*). Induction of autophagy results in the elimination of invading pathogens, whereas some microbes have evolved strategies to manipulate autophagy for their own benefit. Several reports have proclaimed that HBV infection is able to induce autophagy (*7,22,23*), and transfection of pHBV in hepatic and hepatoma cell lines both promote formation of autophagosomes (*23*). Consistently, our results also discovered increased autophagy in pHepG2 cells and HBV-expressing HepG2.2.15 cells. Furthermore, the *in vivo* results support our conclusion when transfecting C57BL/6 mice with pHBV.

HBV-induced autophagy have been extensively investigated, and the views of its effect on HBV and chronic infection were still elucidated. Several studies suggested that HBV could manipulate autophagy to affect virus production and chronic infection

Figure 3. Autophagosome-lysosome fusion-block by pHBV transfection. (A) HepG2 cells transfected without or with HBV DNA plasmid (pHepG2) were grown on coverslips, then transiently transfected with mRFP-GFP-LC3 expressing plasmid ptfLC3. Digital images were captured with confocal microscopy. **(B)** Under confocal microscopy, cells with yellow punctate dots was identified as cells with autophagy. The number of autophagic cells was recorded in every 100 cells counted. The results were calculated as the average value of the data obtained from 3 independent experiments. ***, *p* < 0.001.

Figure 4. HBV DNA downregulates Rab7 expression. HepG2 cells were starved, transfected with pHBV or pUC19 for 48h, respectively. **(A)** The cellular lysis was subjected to Western blot for Rab7 protein expression analysis. **(C)** The cellular Rab7 mRNA levels in HepG2, starvation treated HepG2, mock-transfected HepG2, pHepG2 and HepG2.2.15 were detected by RT-PCR. **(B, D)** The bands density ratios of Rab7/GAPDH were determined by Western blot and RT-PCR, and the results of control HepG2 was taken to be 100%. It was calculated as the average value of the data obtained from 3 independent experiments. *, *p* < 0.05.

establishment (*24,25*). On the contrary, Tian *et al.* indicated that incomplete autophagy could regulate HBV DNA replication instead of HBV virions *in vivo* (*26*). However, how autophagy might implement regulation and help pathogen escape from the following autophagic degradation still remained elusive. A recent study demonstrated that hepatitis B virus x protein impaired lysosomal degradative capacity by disturbing its acidification without influencing the fusion of autophagosomes and lysosomes (*27*). Intriguingly, one of the most important findings from our current study turned out that the fusion of autophagosomes and lysosomes was hampered in pHepG2 cells. This discrepancy might be due to transfection of a different pHBV in our experiment system. Besides, the effects of different cell lines also should be considered. Some intracellular pathogens, mycobacterium tuberculosis and human parainfluenza virus (*10,11*), hijack autophagy and inhibit its maturation for their replication, prompting us to speculate that HBV might induce autophagosome formation as its replication site to facilitate the viral life cycle but block the following autophagosomes-lysosomes fusion to evade autophagic degradation.

Fusion proteins, such as VAMP1, 2, 7 and 8, Vti1b, syntaxin1, and 8, VPS28, LAMP2 and Rab7, play a key role in the fusion of autophagosomes and lysosomes. Our data suggested that a difference merely existed in Rab7 mRNA levels between HepG2 and pHepG2. Rab7, a late endosome-/lysosome-related small GTPase, may be the only lysosomal Rab protein identified so far (*9*), which functions as a crucial molecular switch in autophagy. Rab7 can act as a master factor to regulate the biogenesis and maintenance of lysosomes (*28*). Furthermore, blocking Rab7-mediated trafficking machineries downregulate autophagy-mediated clearance (*29*). Extensive research delineated that Rab7 could promote maturation of autophagosomes and regulate their fusion with lysosomes (*30*). However, abnormal expression of Rab7 has been implicated in invasion of many other pathogens. For example, Hu D *et al.* reported that Rab7 could be blocked to prevent autophagosome-lysosome fusion in mycobacterium tuberculosis infection (*10*). Hampered fusion of autophagsomes and lysosomes caused by deficiency of Rab7 has also been covered in human parainfluenza virus infection (*11*). Moreover, Inoue J *et al.* has reported that HBV could hijack Rab7 for its replication, as siRNA-mediated depletion of Rab7 dramatically augmented the secretion of virions (*31*). Accordingly, our data showed that HBV infection inhibited Rab7 expression in pHepG2 cells and HepG2.2.15 cells. Whereas, starvation treatment, which induced autophagy in the whole process, increased expression of Rab7 in HepG2 cells. Combined with these findings, our study made it clear that Rab7 might be responsible for the HBV-induced incomplete autophagic progress, which could convincingly show how HBV could enhance the formation of autophagosomes and

escape subsequent autophagic degradation.

In conclusion, this study confirms that HBV induces autophagosome formation but blocks autophagy maturation. Moreover, it supports the idea that HBV dampens Rab7 expression, which is responsible for the autophagosome-lysosome fusion. Our findings help to clarify the role of Rab7 in HBV-induced incomplete autophagic degradation and provide a potential target for further manipulation of autophagy in the treatment of HBV infection.

Acknowledgements

References

1. Schweitzer A, Horn J, Mikolajczyk RT, Krause G, Ott JJ. Estimations of worldwide prevalence of chronic hepatitis B virus infection: a systematic review of data published between 1965 and 2013. The Lancet. 2015; 386:1546-1555.
2. Liang TJ, Block TM, McMahon BJ, Ghany MG, Urban S, Guo JT, Locarnini S, Zoulim F, Chang KM, Lok AS. Present and future therapies of hepatitis B: From discovery to cure. Hepatology. 2015; 62:1893-908.
3. Thomas D, Zoulim F. New challenges in viral hepatitis. Gut. 2012; 61 Suppl 1:i1-5.
4. Shintani T, Klionsky DJ. Autophagy in health and disease: a double-edged sword. Science. 2004; 306:990-995.
5. Yang Z, Klionsky DJ. Eaten alive: a history of macroautophagy. Nat Cell Biol. 2010; 12:814-822.
6. Kudchodkar SB, Levine B. Viruses and autophagy. Rev Med Virol. 2009; 19:359-378.
7. Sir D, Tian Y, Chen Wl, Ann DK, Yen TSB, Ou JhJ. The early autophagic pathway is activated by hepatitis B virus and required for viral DNA replication. Proceedings of the National Academy of Sciences. 2010; 107:4383-4388.
8. Zhong L, Hu J, Shu W, Gao B, Xiong S. Epigallocatechin-3-gallate opposes HBV-induced incomplete autophagy by enhancing lysosomal acidification, which is unfavorable for HBV replication. Cell Death Dis. 2015; 6:e1770.
9. Zhang M, Chen L, Wang S, Wang T. Rab7: roles in membrane trafficking and disease. Biosci Rep. 2009; 29:193-209.
10. Hu D, Wu J, Wang W, Mu M, Zhao R, Xu X, Chen Z, Xiao J, Hu F, Yang Y, Zhang R. Autophagy regulation revealed by SapM-induced block of autophagosome-lysosome fusion *via* binding RAB7. Biochem Biophys Res Commun. 2015; 461:401-407.
11. Ding B, Zhang G, Yang X, Zhang S, Chen L, Yan Q, Xu M, Banerjee AK, Chen M. Phosphoprotein of human parainfluenza virus type 3 blocks autophagosome-

lysosome fusion to increase virus production. Cell Host Microbe. 2014; 15:564-577.

12. Sells MA, Chen ML, Acs G. Production of hepatitis B virus particles in Hep G2 cells transfected with cloned hepatitis B virus DNA. Proc Natl Acad Sci U S A. 1987; 84:1005-1009.

13. Xu WS, Zhao KK, Miao XH, Ni W, Cai X, Zhang RQ, Wang JX. Effect of oxymatrine on the replication cycle of hepatitis B virus *in vitro*. World J Gastroenterol. 2010; 16:2028-2037.

14. Zheng Y, Li J, Johnson DL, Ou JH. Regulation of hepatitis B virus replication by the ras-mitogen-activated protein kinase signaling pathway. J Virol. 2003; 77:7707-7712.

15. Kimura S, Fujita N, Noda T, Yoshimori T. Monitoring autophagy in mammalian cultured cells through the dynamics of LC3. Methods Enzymol. 2009; 452:1-12.

16. Xu C, Feng K, Zhao X, Huang S, Cheng Y, Qian L, Wang Y, Sun H, Jin M, Chuang TH, Zhang Y. Regulation of autophagy by E3 ubiquitin ligase RNF216 through BECN1 ubiquitination. Autophagy. 2014; 10:2239-2250.

17. Cai W, Du A, Feng K, Zhao X, Qian L, Ostrom RS, Xu C. Adenylyl cyclase 6 activation negatively regulates TLR4 signaling through lipid raft-mediated endocytosis. J Immunol. 2013; 191:6093-6100.

18. Jiang Y, Tong Y, Lu S. Visualizing the three-dimensional mesoscopic structure of dermal tissues. J Tissue Eng Regen Med. 2014; 8:794-800.

19. Xu C, Liu J, Hsu LC, Luo Y, Xiang R, Chuang TH. Functional interaction of heat shock protein 90 and Beclin 1 modulates Toll-like receptor-mediated autophagy. FASEB J. 2011; 25:2700-2710.

20. Ng EL, Gan BQ, Ng F, Tang BL. Rab GTPases regulating receptor trafficking at the late endosome-lysosome membranes. Cell Biochem Funct. 2012; 30:515-523.

21. Devenish RJ, Lai SC. Autophagy and burkholderia. Immunol Cell Biol. 2015; 93:18-24.

22. Sir D, Ann DK, Ou JH. Autophagy by hepatitis B virus and for hepatitis B virus. Autophagy. 2010; 6:548-549.

23. Tang H, Da L, Mao Y, Li Y, Li D, Xu Z, Li F, Wang Y, Tiollais P, Li T, Zhao M. Hepatitis B virus X protein sensitizes cells to starvation-induced autophagy *via* up-regulation of beclin 1 expression. Hepatology. 2009; 49:60-71.

24. Li J, Liu Y, Wang Z, Liu K, Wang Y, Liu J, Ding H, Yuan Z. Subversion of cellular autophagy machinery by hepatitis B virus for viral envelopment. J Virol. 2011; 85:6319-6333.

25. Yang H, Fu Q, Liu C, Li T, Wang Y, Zhang H, Lu X, Sang X, Zhong S, Huang J, Mao Y. Hepatitis B virus promotes autophagic degradation but not replication in autophagosome. Biosci Trends. 2015; 9:111-116.

26. Tian Y, Sir D, Kuo CF, Ann DK, Ou JH. Autophagy required for hepatitis B virus replication in transgenic mice. J Virol. 2011; 85:13453-13456.

27. Liu B, Fang M, Hu Y, Huang B, Li N, Chang C, Huang R, Xu X, Yang Z, Chen Z, Liu W. Hepatitis B virus X protein inhibits autophagic degradation by impairing lysosomal maturation. Autophagy. 2014; 10:416-430.

28. Bucci C, Thomsen P, Nicoziani P, McCarthy J, van Deurs B. Rab7: a key to lysosome biogenesis. Mol Biol Cell. 2000; 11:467-480.

29. Rawet-Slobodkin M, Elazar Z. PLEKHM1: a multiprotein adaptor for the endolysosomal system. Mol Cell. 2015; 57:1-3.

30. Ganley IG, Wong PM, Jiang X. Thapsigargin distinguishes membrane fusion in the late stages of endocytosis and autophagy. Autophagy. 2011; 7:1397-1399.

31. Inoue J, Krueger EW, Chen J, Cao H, Ninomiya M, McNiven MA. HBV secretion is regulated through the activation of endocytic and autophagic compartments mediated by Rab7 stimulation. J Cell Sci. 2015; 128:1696-1706.

Original Article

miR-613 suppresses ischemia-reperfusion-induced cardiomyocyte apoptosis by targeting the programmed cell death 10 gene

Zhenhua Wu[1], Yujuan Qi[1], Zhigang Guo[2,*], Peijun Li[1], Ding Zhou[3]

[1] *ICU, Departmentof Cardiac Surgery, Tianjin Chest Hospital, Tianjin, China;*
[2] *Department of Cardiac Surgery, Tianjin Chest Hospital, Tianjin, China;*
[3] *TEDA International Cardiovascular Hospital, Tianjin, China.*

Summary   **MicroRNAs (miRNAs) are important gene regulators in both biological and pathological processes, including myocardial ischemia/reperfusion (I/R) injury. This study investigated the effect of miR-613 on I/R-induced cardiomyocyte apoptosis and its molecular mechanism of action. Hypoxia/reoxygenation (H/R) significantly increased the release of lactate dehydrogenase (LDH), levels of malondialdehyde (MDA), and cardiomyocyte apoptosis, but these effects were attenuated by an miR-613 mimic. Programmed cell death 10 (PDCD10) was identified as a target gene of miR-613. miR-613 significantly increased the phosphorylation of Akt (p-Akt). An miR-613 mimic lowered the level of expression of pro-apoptotic proteins, C/EBP homologous protein (CHOP), and phosphorylated c-Jun N-terminal kinase (p-JNK), and it up-regulated the expression of the anti-apoptotic protein B-cell lymphoma-2 (Bcl-2). All of these effects were reversed by restoration of PDCD10. Taken together, the current findings indicate that miR-613 inhibits I/R-induced cardiomyocyte apoptosis by targeting PDCD10 by regulating the PI3K/AKT signaling pathway.**

Keywords: *miRNAs, hypoxia/reoxygenation, C/EBP homologous protein, B-cell lymphoma-2, PI3K/AKT*

1. Introduction

Myocardial ischemia/reperfusion (I/R)-induced cardiac injury after myocardial ischemia, cardiac surgery, or cardiac arrest leads to a high mortality rate in humans with coronary heart disease. I/R injury causes local myocardial inflammation and apoptosis, resulting in irreversible damage to the myocardium (*1*). Several mechanisms underlying myocardial I/R injury have been elucidated, including formation of oxygen free radicals, intracellular Ca$^+$ overload, neutrophil activation, and vascular endothelium damage (*2*). However, the complete profile of molecular pathways associated with myocardial I/R injury is not yet fully understood.

MicroRNAs (miRNAs) are highly conserved, small, noncoding RNAs that can regulate cell proliferation, migration, differentiation, apoptosis, and immune response at the post-transcriptional level. Recent studies have reported that miRNAs play an important role in myocardial I/R injury and may become potential targets for diagnosis and therapy. As an example, miR-93 inhibits I/R-induced cardiomyocyte apoptosis by targeting PTEN (*3*). miR-17 attenuates apoptosome formation and cardiomyocyte apoptosis by regulating apoptotic protease activation factor 1 (*4*).

Mounting evidence has indicated that miR-613 is involved in multiple processes, including tumorigenesis, metastasis, lipogenesis, and lipoprotein metabolism (*5-8*). However, the role of miR-613 in myocardial I/R injury has not been examined. The current study found that miR-613 suppresses cardiomyocyte apoptosis induced by hypoxia/reoxygenation (H/R) in H9c2 cells. PDCD10 was identified as a direct target of miR-613. This study also examined the level of expression of p-Akt and downstream signaling proteins such as CHOP, p-JNK, and Bcl-2. miR-613 was found to affect I/R-induced cardiomyocyte apoptosis by regulating the

PI3K/Akt signaling pathway. Together, these findings reveal part of the miR-613/PDCD10 /PI3K/Akt pathway that mediates I/R-induced cardiomyocyte apoptosis.

2. Materials and Methods

2.1. *Cell culture and miRNA transfection*

H9c2 cells were cultured in DMEM containing 10% fetal bovine serum (FBS) at 37°C with 5% CO_2. An miR-613 mimic, an miR-613 inhibitor, and a corresponding control (miR-NC) were synthesized by GenePharma (Shanghai, China). H9c2 cells were cultured in six-well plates and transfected with an miR-613 mimic, an miR-613 inhibitor, or miR-NC using Lipofectamine 2000 reagent according to the manufacturer's instructions (Invitrogen, USA).

2.2. *Construction of vectors*

The EGFP coding region from the pEGFP-N2 vector was subcloned into pcDNA3. The 3'-UTR of wild-type or mutant-type PDCD10 was then cloned into a pcDNA3-EGFP vector. A PDCD10 expression plasmid, pcDNA3-PDCD10, was constructed by cloning the coding sequence of PDCD10 into a pcDNA3 vector.

2.3. *Detection of LDH and MDA*

Lactate dehydrogenase (LDH) and malondialdehyde (MDA) commercial kits were purchased from Sangon Biotech (Shanghai, China). LDH and MDA were measured according to the manufacturer's instructions.

2.4. *In vitro hypoxia/reoxygenation (H/R) model*

Cardiomyocytes were perfused in normal Hank's solution with a gas mixture of 95% O_2-5% CO_2 at 37°C, pH 7.4. To simulate an ischemic environment, cardiomyocytes were perfused in Hank's solution at a pH of 7.4 at 37°C without glucose or calcium. Cells were then exposed to a gas mixture of 95% N_2-5% CO_2. To simulate a reperfusion environment, cells were again perfused in normal Hank's solution with a gas mixture of 95% O_2-5% CO_2 at 37°C, pH 7.4 (*9*). Cells in a normoxic environment served as the corresponding control.

2.5. *Analysis of apoptosis*

Cell apoptosis were detected using the Annexing V-FITC/propidium iodide (PI) apoptosis detection kit (BD Biosciences, Shanghai, China). Cells were harvested and collected after centrifugation for 5 to 10 minutes at 2,000 rpm. Cells were then washed with phosphate-buffered saline (PBS) and suspended in 300 µL of Binding Buffer. An Annexin V-FITC solution (5 µL) was added to the cell suspension, which was incubated for 15 min in the dark. Five µL of PI was then added to the suspension.

Cell apoptosis was analyzed with a flow cytometry system (BD Bioscience, Shanghai, China). Healthy living cells are denoted as FITC-/PI- cells, early apoptotic cells are denoted as FITC+/PI- cells, and necrotic and late apoptotic cells are denoted as FITC+/PI+ cells.

2.6. *Reverse transcription-quantitative polymerase chain reaction (RT-qPCR)*

Total RNA and microRNA were extracted using Trizol reagent (Invitrogen) and the mirVana miRNA isolation kit (Ambion, Austin, TX, USA). RNA integrity was verified with agarose gel electrophoresis. cDNA was obtained using the Taqman® RNA reverse transcription kit. cDNA was then subjected to RT-qPCR using SYBR Premix Ex Taq (TaKaRa, Dalian, China) to measure the relative level of miR-613 and PDCD10 mRNA expression. β-actin and U6 served as corresponding controls. The relative level of gene expression was analyzed using the $2^{-\Delta\Delta Ct}$ method.

2.7. *Western blot analysis*

Cell protein was extracted with the RIPA lysis buffer (BLKW Biotechnology, Beijing, China). Equal amounts of protein were separated by sodium dodecyl sulfate-polyacrylamide gel electrophoresis (SDS-PAGE) and then transferred to nitrocellulose membranes. The membranes were blocked with 5% skim milk for 2 h and then incubated with primary antibodies that were purchased from Cell Signaling Technology. The primary antibodies used were as follows: PDCD10 (1:500), p-AKT (1:1,000), glucose-regulated protein (GRP) 78 (1:500), caspase-12 (1:500), CHOP (1:1,000), p-JNK (1:1,000), and Bcl-2 (1:500). Goat anti-rabbit secondary antibody was added and cells were incubated at room temperature for 2 h. Bands were visualized with an enhanced chemiluminescence (ECL) regent (Santa Cruz Biotechnology, CA, USA). Glyceraldehyde phosphate dehydrogenase (GAPDH) served as the internal control.

2.8. *EGFP reporter assay*

Cells were transfected with an miR-613 mimic, an miR-613 inhibitor, or a reporter plasmid carrying a wild-type or mutant PDCD10-3'UTR. Fluorescence intensity was detected with an F-4500 fluorescence spectrophotometer (Hitachi, Tokyo, Japan). An RFP expression vector served as a reporter control. The relative fluorescence intensity of EGFP was determined with respect to the RFP intensity.

2.9. *Statistical analysis*

The statistical software Graphpad 5.0 was used to

analyze data. Data are expressed as the mean ± standard deviation (mean ± S.D.). One-way ANOVA was used to compare differences among groups. A two-tailed Student's *t*-test was used to compare differences between two groups. A p-value of less than 0.05 was considered statistically significant.

3. Results

3.1. *miR-613 was down-regulated in H9c2 cells after H/R*

To explore the potential role of miR-613 in myocardial I/R injury, the expression of miR-613 was detected in H9c2 cells after 10 h in a hypoxic environment and 2 h of deoxygenation. Data indicated that miR-613 expression was reduced by almost 43% in H9c2 cells after H/R treatment compared to cells under normoxia. This result suggested that miR-613 may play a role in the H/R injury of H9c2 cells (Figure 1).

3.2. *MiR-613 alleviated H/R-induced cardiomyocyte injury*

Since the release of LDH is an important sign of cell injury, the release of LDH by H9c2 cells was examined. Results indicated that H/R treatment significantly increased the release of LDH. The miR-613 mimic decreased the release of LDH by approximately 49% while the miR-613 inhibitor increased the release of LDH by almost 1.3-fold in response to H/R in H9c2 cells (Figure 2A).

MDA is a key index of membrane lipid peroxidation. Levels of MDA were also measured. As shown in Figure 2B, levels of MDA in cells increased significantly after H/R treatment in comparison to levels in control cells. Similarly, miR-613 decreased an H/R-induced increase in MDA levels by 52% while inhibition of miR-613 increased MDA levels by almost 1.4-fold (Figure 2B).

3.3. *miR-613 suppressed H/R-induced cardiomyocyte apoptosis in vitro*

The above results suggested that miR-613 expression decreased in H9c2 cells after H/R, so the question was then whether or not miR-613 protected cardiomyocytes from H/R-induced injury by affecting cell apoptosis. The effect of miR-613 on cardiomyocyte apoptosis was detected using flow cytometry. Data indicated that overexpression of miR-613 significantly reduced the rate of apoptosis during H/R. However, inhibition of miR-613 markedly increased the rate of apoptosis compared to that in cells treated with H/R alone (Figure 3A).

To further explore the potential molecular mechanism of action of miR-613, expression of apoptosis-related proteins such as GRP78, caspase-12, cytochrome c, Bax, and caspase-3 was examined. Results suggested that H/R markedly increased the level of expression of these proteins, but that increase was reversed by miR-613 overexpression. In contrast, inhibition of miR-
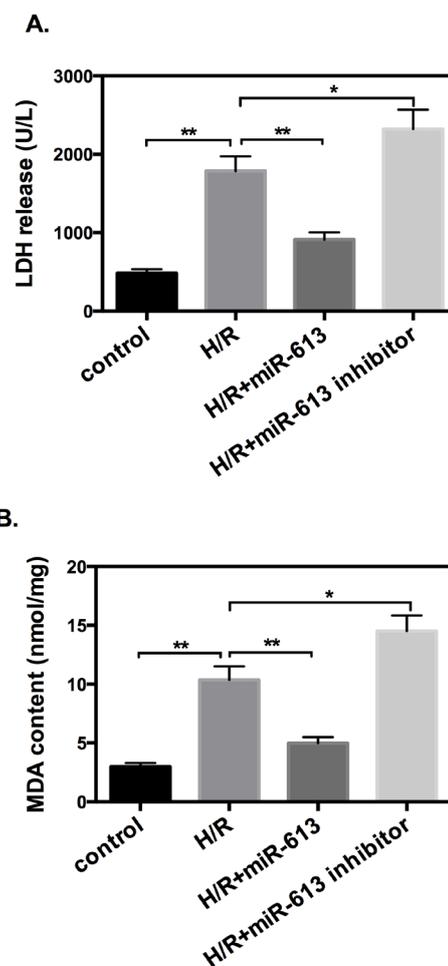
Figure 2. miR-613 alleviated H/R-induced cardiomyocyte injury. (A), Release of LDH. **(B)**, Levels of MDA. *$p < 0.05$, **$p < 0.01$. (*Note*: H/R+miR-613: H9c2 cells were transfected with an miR-613 mimic after H/R treatment; H/R+miR-613 inhibitor: H9c2 cells were transfected with an miR-613 inhibitor after H/R treatment. Data are expressed as the mean ± S.D.)

Figure 1. miR-613 was down-regulated in H9c2 cells after H/R. RT-qPCR was used to detect the expression of miR-613 in H9c2 cells after H/R or under normoxia. Cells under normoxia served as the control group. The level of miR-613 expression in the control group was normalized to 1. U6 served as a loading control. *$p < 0.05$.
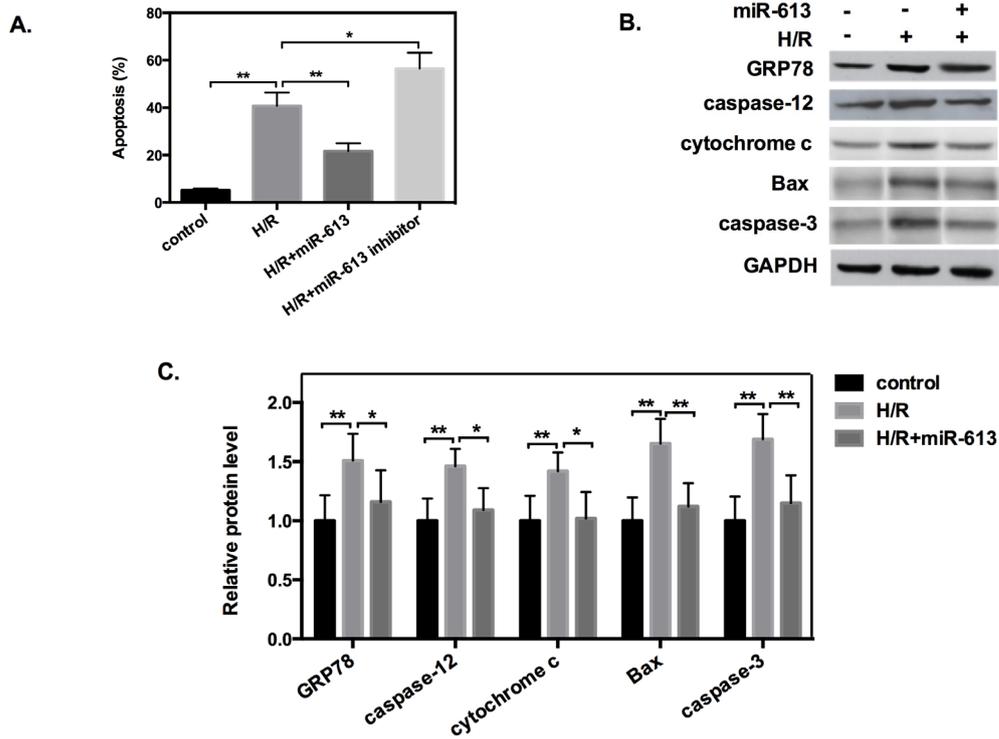
Figure 3. miR-613 suppressed H/R-induced cardiomyocyte apoptosis *in vitro*. (A) The rate of cell apoptosis was detected with an Annexin V/Propidium iodide apoptosis assay after transfection with an miR-613 mimic or inhibitor. **(B)**, Western blot analysis of the level of GRP78, caspase-12, cytochrome c, Bax, and caspase-3 proteins with or without transfection of miR-613 after H/R treatment. Levels of protein expression in the control group were normalized to 1. GAPDH served as the internal control. **(C)**, Statistical analysis of levels of protein expression. The histogram shows the mean ± S.D. for normalized GAPDH. *$p < 0.05$, **$p < 0.01$.
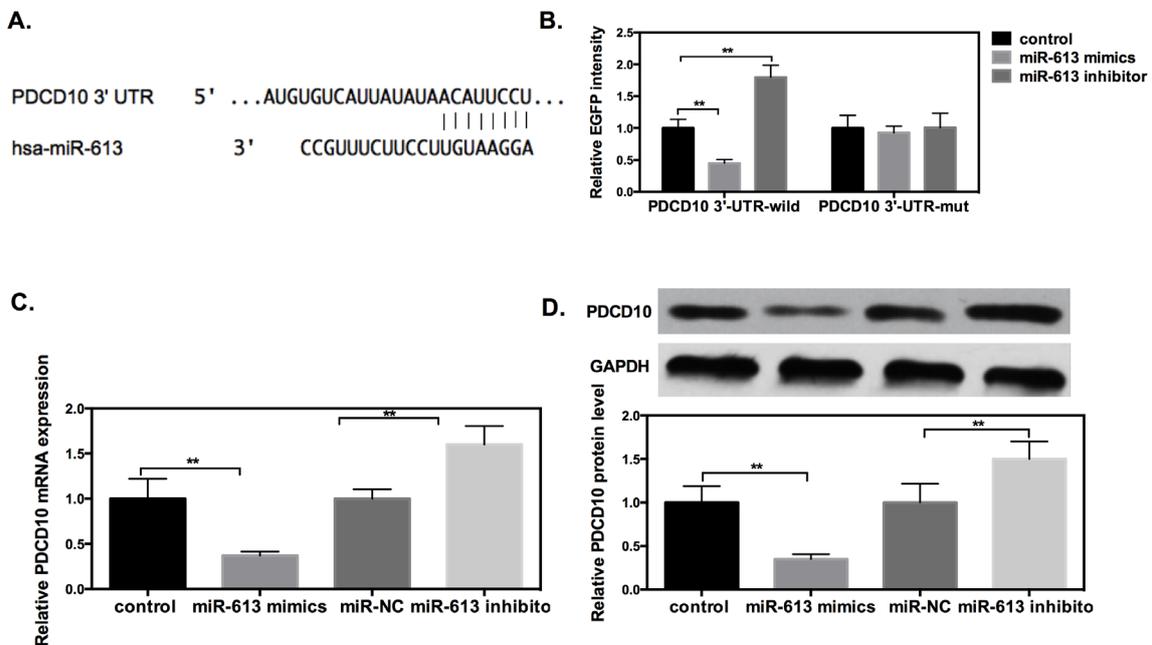
Figure 4. miR-613 directly targeted PDCD10 by binding to its 3'-UTR. (A) The potential binding site for miR-613 in the 3'-UTR of PDCD10 mRNA. **(B)** EGFP reporter analysis was performed to detect relative EGFP activity after a wild-type or mutant-type reporter plasmid was co-transfected with an miR-613 mimic, an miR-613 inhibitor, or miR-NC control in H9c2 cells. Relative EGFP intensity was determined as the ratio to the RFP intensity. **(C)** RT-qPCR was used to detect the level of PDCD10 mRNA in transfected cells. β-actin was used as the corresponding control. **(D)** The level of PDCD10 protein was detected with Western blot analysis in transfected H9c2 cells. Normalization was performed using GAPDH. **$p < 0.01$.

613 significantly increased the level of expression of apoptosis-related proteins (Figure 3B and 3C).

3.4. *miR-613 directly targeted PDCD10 by binding to its 3'-UTR*

miRNAs act by regulating target genes. To investigate the exact mechanism by which miR-613 affects cell apoptosis induced by H/R, TargetScan, miRanda, and PicTar were used to predict the potential target genes of miR-613. PDCD10 was chosen for further study along with genes that may be responsible for cell apoptosis. Bioinformatic analysis revealed that the 3'-UTR of PDCD10 contains a putative binding region of miR-613 (Figure 4A). To determine whether or not miR-613 directly targets PDCD10, an EGFP reporter analysis was performed. EGFP reporter vectors carrying the 3'-UTR of wild-type or mutant-type PDCD10 were transfected into H9c2 cells when miR-613 was over-expressed or inhibited. When miR-613 was overexpressed, the level of expression of the 3'-UTR of the wild-type decreased by almost 55%, while inhibition of miR-613 increased the the level of expression of the 3'-UTR of the wild-type by approximately 1.8-fold (Figure 4B). However, the level of expression of the 3'-UTR of the mutant-type was not affected by a change in miR-613 expression.

RT-qPCR and Western blot analysis suggested that the miR-613 mimic decreased the level of expression of PDCD10 mRNA and PDCD10 protein; when miR-

613 was inhibited, however, PDCD10 expression was up-regulated (Figure 4C and 4D). All of these findings indicated that miR-613 down-regulates PDCD10 expression by directly binding to its 3'-UTR.

3.5. *miR-613 affected I/R-induced cardiomyocyte apoptosis by regulating the PI3K/Akt signaling pathway*

PI3K/Akt is an intracellular signaling pathway that is associated with cardioprotection (*10*). To further explore whether or not miR-613 also protected cardiomyocytes from I/R-induced injury by regulating the PI3K/Akt pathway, the level of expression of marker proteins such as p-Akt, the level of expression of the pro-apoptotic proteins CHOP and p-JNK, and the level of expression of the anti-apoptotic protein Bcl-2 were detected. Results suggested that miR-613 reduced the level of CHOP expression by 42% and that of p-JNK by 52% while it

Figure 6. Restoration of PDCD10 counteracted the effect of miR-613 on the release of LDH, levels of MDA, and H/R-induced cardiomyocyte apoptosis. (A) Western blot analysis was performed to detect PDCD10 protein expression in h9c2 cells with or without restored PDCD10. **(B)** Ectopic expression of PDCD10 neutralized inhibition of the release of LDH by miR-613. **(C)** Ectopic expression of PDCD10 neutralized inhibition of MDA levels by miR-613. **(D)** Ectopic expression of PDCD10 counteracted inhibition of cardiomyocyte apoptosis by miR-613. **(E)** Restoration of PDCD10 counteracted the effect of miR-613 on the PI3K/Akt pathway. *$p < 0.05$, **$p < 0.01$.

Figure 5. miR-613 suppressed I/R-induced cardiomyocyte apoptosis by regulating the PI3K/Akt signaling pathway. (A) Western blot analysis of the level of p-Akt, CHOP, p-JNK, and Bcl-2 proteins when an miR-613 mimic was transfected into H9c2 cells. **(B)** Statistical analysis of levels of protein expression. The histogram shows the mean ± S.D. of normalized GAPDH. *$p < 0.05$, **$p < 0.01$.

increased the expression of p-Akt by 1.8-fold and the expression of Bcl-2 by 1.5-fold (Figure 5).

3.6. *miR-613 affected I/R-induced cardiomyocyte apoptosis by directly targeting PDCD10*

The data above indicate that miR-613 down-regulates the expression of PDCD10 at both the mRNA and protein levels. To further determine whether or not PDCD10 was the functional target gene, a rescue experiment was performed. miR-613 and a PDCD10 expression plasmid without the 3'-UTR were transfected into H9c2 cells, and results indicated that overexpression of PDCD10 neutralized the decrease in PDCD10 expression induced by miR-613 (Figure 6A). Restoration of PDCD10 counteracted the effect of miR-613 on the release of LDH, levels of MDA, H/R-induced cardiomyocyte apoptosis, and PI3K/Akt signaling pathways (Figure 6B-6D). These findings suggest that miR-613 acts on I/R-induced cell apoptosis by directly regulating PDCD10.

4. Discussion

Recent animal experiments and clinical studies have indicated that cell apoptosis is closely related to myocardial I/R-induced injury. Thus far, numerous miRNAs have been reported to be associated with myocardial I/R injury by regulating target genes, including miR-451, miR-133a, and Lin28a (*11-13*). The current study investigated the potential role of miR-613 in myocardial I/R injury and results indicated that the level of miR-613 expression decreased by 43% in H9c2 cells after H/R treatment in comparison to the level of expression in the controls. This finding suggests that miR-613 may play a role in I/R injury to cardiomyocytes.

The specific effects of miR-613 were determined. Results indicated that an miR-613 mimic decreased an H/R-induced increase in the release of LDH, levels of MDA, and cardiomyocyte apoptosis. Furthermore, several apoptosis-related proteins were significantly up-regulated as a result of H/R injury, but this increase was reversed by overexpression of miR-613. These findings indicate that miR-613 suppressed cardiomyocyte apoptosis and it protected cardiomyocytes from H/R-induced injury.

To further illustrate the molecular mechanism by which miR-613 functions, its target genes were predicted and eventually verified. PDCD10 is also known as cerebral cavernous malformation 3 (CCM3), and it plays an important role in regulating apoptosis, neoangiogenesis, and certain tumor signaling pathways (*14-16*). Mounting evidence indicates that PDCD10 plays a pivotal role in regulating cell survival and death. In different type of cells, PDCD10 is reported to be both pro-apoptotic (*17*) and anti-apoptotic (*18*), suggesting that apoptosis by PDCD10 is context-dependent.

Bioinformatic analyses suggested that PDCD10 is a potential target of miR-613. This prediction was confirmed by an EGFP reporter assay. Moreover, miR-613 down-regulated the expression of PDCD10 at both the mRNA and protein levels. A rescue experiment was performed to further explore whether or not PDCD10 is a target gene of miR-613. A PDCD10 expression plasmid without the 3'-UTR and an miR-613 mimic were co-transfected into H9c2 cells. Results showed that restoration of PDCD10 counteracted the effect of miR-613 on the release of LDH, levels of MDA, H/R-induced cardiomyocyte apoptosis. That is, miR-613 acts in I/R-induced cardiomyocyte apoptosis by directly targeting PDCD10.

The PI3K/Akt signaling pathway is a major signaling that promotes cell survival and proliferation (*19*). When PI3K is activated, it acquires the ability to phosphorylate PIP2 into PIP3 and leads to activation of Akt. Activated Akt then translocates from the cell membrane to the cytoplasm and nucleus and can activate or suppress many downstream proteins to regulate cellular functions (*20*). Phosphorylated PI3K/Akt inhibits pro-apoptotic substrates, such as CHOP and p-JNK, while it promotes the anti-apoptotic substrate Bcl-2 (*21*). Recent evidence suggests that PDCD10 is associated with the activation of Akt signaling protein (*22*). The current study found that miR-613 significantly increased the level of p-Akt and Bcl-2 expression; when miR-613 was overexpressed, however, the level of expression of the pro-apoptotic proteins CHOP and p-JNK decreased significantly. Furthermore, ectopic expression of PDCD10 restored the effect of miR-613 on the PI3K/Akt signaling pathway. These findings indicate that miR-613 can inhibit I/R-induced cardiomyocyte apoptosis by targeting PDCD10 by regulating PI3K/Akt signaling pathways.

Taken together, the current findings are the first to show that miR-613 can suppress I/R-induced cardiomyocyte apoptosis by down-regulating PDCD10 and activating PI3K/Akt pathways. PDCD10 is a direct target gene of miR-613. The current results reveal the molecular mechanism by which miR-613 affects I/R-mediated apoptosis, and this finding may help facilitate the treatment of myocardial I/R injury.

Acknowledgements

References

1. Hu X, Zhou X, He B, Xu C, Wu L, Cui B, Wen H, Lu Z, Jiang H. Minocycline protects against myocardial ischemia and reperfusion injury by inhibiting high mobility group box 1 protein in rats. Eur J Pharmacol. 2010; 638:84-89.
2. Thind GS, Agrawal PR, Hirsh B, Saravolatz L, Chen-Scarabelli C, Narula J, Scarabelli TM. Mechanisms

of myocardial ischemia-reperfusion injury and the cytoprotective role of minocycline: Scope and limitations. Future Cardiol. 2015; 11:61-76.

3. Ke ZK, Xu P, Shi Y, Gao AM. MicroRNA-93 inhibits ischemia-reperfusion induced cardiomyocyte apoptosis by targeting PTEN. Oncotarget. 2016; 7:28796-28805.

4. Song S, Seo HH, Lee SY, Lee CY, Lee J, Yoo KJ, Yoon C, Choi E, Hwang KC, Lee S. MicroRNA-17-mediated down-regulation of apoptotic protease activating factor 1 attenuates apoptosome formation and subsequent apoptosis of cardiomyobytes. Biochem Biophys Res Commun. 2015; 465:299-304.

5. Wang W, Zhang H, Wang L, Zhang S, Tang M. miR-613 inhibits the growth and invasiveness of human hepatocellular carcinoma *via* targeting DCLK1. Biochem Biophys Res Commun. 2016; 473:987-992.

6. Fu X, Cui Y, Yang S, Xu Y, Zhang Z. MicroRNA-613 inhibited ovarian cancer cell proliferation and invasion by regulating KRAS. Tumour Biol. 2016; 37:6477-6483.

7. Zhong D, Zhang Y, Zeng YJ, Gao M, Wu GZ, Hu CJ, Huang G, He FT. MicroRNA-613 represses lipogenesis in HepG2 cells by downregulating LXRα. Lipids Health Dis. 2013; 12:32.

8. Sacco J, Adeil K. MicroRNAs: Emerging roles in lipid and lipoprotein metabolism. Curr Opin Lipidol. 2012; 23:220-225.

9. Zhai C, Tang G, Peng L, Hu H, Qian G, Wang S, Yao J, Zhang X, Fang Y, Yang S, Zhang X. Inhibition of microRNA-1 attenuates hypoxia/re-oxygenation-induced apoptosis of cardiomyocytes by directly targeting Bcl-2 but not GADD45Beta. Am J Transl Res. 2015; 7:1952-1962.

10. Yao H, Han X, Han X. The cardioprotection of the insulin-mediated PI3K/Akt/mTOR signaling pathway. Am J Cardiovasc Drugs. 2014; 14:433-442.

11. Xie J, Hu X, Yi C, Hu G, Zhou X, Jiang H. MicroRNA-451 protects against cardiomyocyte anoxia/reoxygenation injury by inhibiting high mobility group box 1 expression. Mol Med Rep. 2016; 13:5335-5341.

12. Li S, Xiao FY, Shan PR, Su L, Chen DL, Ding JY, Wang ZQ. Overexpression of microRNA-133a inhibits ischemia-reperfusion-induced cardiomyocyte apoptosis by targeting DAPK2. J Hum Genet. 2015; 60:709-716.

13. Zhang M, Sun D, Li S, Pan X, Zhang X, Zhu D, Li C, Zhang R, Gao E, Wang H. Lin28a protects against cardiac ischemia/reperfusion injury in diabetic mice through the insulin-PI3K-mTOR pathway. J Cell Mol Med. 2015; 19:1174-1182.

14. He Y, Zhang H, Yu L, Gunel M, Boggon TJ, Chen H, Min W. Stabilization of VEGFR2 signaling by cerebral cavernous malformation 3 is critical for vascular development. Sci Signal. 2010; 3:ra26.

15. Fidalgo M, Guerrero A, Fraile M, Iglesias C, Pombo CM, Zalvide J. Adaptor protein cerebral cavernous malformation 3 (CCM3) mediates phosphorylation of the cytoskeletal proteins ezrin/radixin/moesin by mammalian Ste20-4 to protect cells from oxidative stress. J Biol Chem. 2012; 287:11556-11565.

16. Aguirre AJ, Brennan C, Bailey G, Sinha R, Feng B, Leo C. Zhang Y, Zhang J, Gans JD, Bardeesy N, Cauwels C, Cordon-Cardo C, Redston MS, DePinho RA, Chin L. High-resolution characterization of the pancreatic adenocarcinoma genome. Proc Natl Acad Sci U S A. 2004; 101:9067-9072.

17. Schleider E, Stahl S, Wustehube J, Walter U, Fischer A, Felbor U. Evidence for anti-angiogenic and pro-survival functions of the cerebral cavernous malformation protein 3. Neurogenetics. 2011; 12:83-86.

18. Zhu Y, Wu Q, Xu JF, Miller D, Sandalcioglu IE, Zhang JM, Sure U. Differential angiogenesis function of CCM2 and CCM3 in cerebral cavernous malformations. Neurosurg Focus. 2010; 29:E1.

19. Shaw RJ, Cantley LC. Ras, PI(3)K and mTOR signalling controls tumor cell growth. Nature. 2006; 441:424-430.

20. Zhang J, Yu XH, Yan YG, Wang C, Wang WJ. PI3K/Akt signaling in osteosarcoma. Clin Chim Acta. 2015; 444:182-192.

21. Atif F, Yousuf S, Stein DG. Anti-tumor effects of progesterone in human glioblastoma multiform: Role of PI3K/Akt/mTOR signaling. J Steroid Biochem Molr Biol. 2015; 146:62-73.

22. Lambertz N, EI Hindy N, Kreitschmann-Andermahrl, Stein KP, Dammann P, Oezkan N, Mueller O, Sure U, Zhu Y. Downregulation of programmed cell death 10 is associated with tumor cell proliferation, hyperangiogenesis and peritumoral edema in human glioblastoma. BMC cancer. 2015, 15:759.

Silence of MACC1 decreases cell migration and invasion in human malignant melanoma through inhibiting the EMT

Yingguo Ding[*], **Xiaomin Li, Dongsheng Hong, Li Jiang, Yong He, Hong Fang**

Department of Dermatology, The First Affiliated Hospital of Zhejiang University, Zhejiang, China.

Summary	**Metastasis-associated colon cancer 1 (MACC1) has been demonstrated to promote metastasis of several cancers via regulating epithelial-mesenchymal transition (EMT). However, its biological behavior in human malignant melanoma remains unclear. In this study, MACC1 downregulation was established in two melanoma cell lines (A375 and G361 cells) using RNA interference, as confirmed by quantitative real time PCR (qRT-PCR) and Western blot analysis. Subsequently, we investigated the effects of MACC1 silencing on cell mobility, migration and invasion using scratch wound and Transwell assays. Our results indicated that knockdown of MACC1 significantly suppressed cell migration and invasion ability of both melanoma cell lines. Moreover, downregulation of MACC1 upregulated E-cadherin, N-cadherin and Vimentin, as confirmed by qRT-PCR, Western blot and immunofluorescent Staining analysis. These findings suggest MACC1 might serve as a new molecular target for the treatment of melanoma by a novel mechanism underlying the metastasis of melanoma cells.**

Keywords: Melanoma, Metastasis-associated colon cancer 1 (MACC1), migration, invasion, epithelial-mesenchymal transition (EMT)

1. Introduction

Human malignant melanoma is characterized as highly aggressive with metastatic potential, which has been considered as one of the deadliest forms of skin cancer (*1*). It is estimated that more than seventy thousand melanoma cases were diagnosed in 2014 in the United States (*2*) and is still rapidly increasing compared to any other solid tumors (*3*). Over the past years, some progress has been made in surgery removal, chemotherapy and radiotherapy (*4,5*). However, the incidence and mortality rate have been increasing for higher recurrence and metastasis. Considering the lack of effective therapies, better understanding of molecular mechanisms underlying malignant melanoma metastasis and development is urgently required to improve the

treatment strategies for this devastating disease.

Metastasis-associated colon cancer 1 (MACC1), was first identified in colon cancer by genome-wide data analysis (*6*), and subsequently has been found to be overexpressed in various other types of cancer, including lung cancer (*7*), gastric cancer (*8*) and hepatocellular carcinoma (*9*). Moreover, MACC1 could promote tumor proliferation and invasion *in vitro* in these cancer types. In addition, MACC1 has been demonstrated to be an independent prognostic indicator of recurrence and disease-free survival, as well as be involved in cancer initiation and development (*10*). Recently, various studies have revealed that MACC1-induced tumorigenesis is closely correlated with hepatocyte growth factor (HGF)/c-MET signaling pathway activation (*6,10*) leading to enhanced cell motility, invasion and metastasis (*11*). Furthermore, MACC1 could increase vimentin and suppress E-cadherin in colon cancer cells, but its silencing reversed these changes (*12*). To our knowledge, there is no report on its role regulating cell metastasis, as well as the underlying mechanism in carcinogenesis of malignant melanoma in the literature.

In the present study, RNA interference was first used to knockdown MACC1 expression in melanoma cell

lines. Then the biological behavior of MACC1 silencing was analyzed on melanoma cells, including cell mobility, migration and invasion, as well as possible mechanisms underlying these functional assays.

2. Materials and Methods

2.1. *Cell lines and culture*

Two human malignant melanoma cell lines, A375 and G361 were obtained from American Type Culture Collection (ATCC; Manassas, VA, USA) and maintained in Dulbecco's modified Eagle's medium (Welgene, Daegu, Korea) supplemented with 10% fetal bovine serum and 100 U/mL each of penicillin and streptomycin (Gibco, Grand Island, NY, USA). All cells were cultured in a fully humidified atmosphere containing 5% CO_2 at 37°C.

2.2. *Small interfering RNA (siRNA) sequences and transfection*

The targeted MACC1 and one scrambled siRNA sequences (5'-AAAGACAGAAGGAGAAAGGAA-3' and 5'-AAAGACAGAAGGAGAAAGGAA-3') were chemically synthesized and purified. For MACC1 silencing, A375 or G361 cells were placed in 6-well plates, seeded at a quantity of 1×10^5 cells, and transfected with siRNA against MACC1 (siMACC1) or negative scrambled siRNA (siCtrl) using Lipofectamine™ RNAiMAX (Invitrogen, Merelbeke, Belgium) according to the manufacturer's instructions. Forty-eight hours after transfection, cells were harvested for mRNA expression detection and Western blot analysis. Stably transfected cells were selected for migration and invasion assays.

2.3. *Quantitative real time PCR (qRT-PCR)*

Total RNA was extracted from cells using Trizol reagent (Ambion/Thermo-Fisher Scientific, Grand Island, NY, USA) according to the manufacturer's instructions. For cDNA synthesis, 1 μg RNA was transcribed using the SuperScript First-Strand Synthesis Kit (Invitrogen, Carlsbad, CA, USA). Quantitative real-time PCR was performed using Power SYBR green PCR Master Mix (Applied Biosystems, Foster City, CA, USA) according to the manufacturer's protocol on a LightCycler® 480 II (Roche, West Sussex, UK). Primers used included the following: MACC1 (forward): 5'-TTCTTTTGATTCCTCCGGTGA-3'; MACC1 (reverse): 5'-ACTCTGATGGGCATGTGCTG-3'; E-cadherin (forward): 5'-TCTGGAAGGAATGGA GGAGTC-3'; E-cadherin (reverse): 5'-AATTGGGCAAATGTGTTCAGC-3'; N-cadherin (forward): 5'-GCTCCCTTAATTCCTCAAGT AGTG-3'; N-cadherin (reverse): 5'-TTCAGTCATCACCT

CCACCATAC-3'; Vimentin (forward): 5'-ATTCCACTTTGCGTTCAAGG-3'; Vimentin (reverse): 5'-CTTCAGAGAGAGGAAGCCGA-3'; GAPDH (forward): 5'- TGACTTCAACA GCGACACCCA-3'; GAPDH (reverse): 5'- CACCCTG TTGCTGTAGCCAAA-3'. GAPDH was used as a control to normalize amounts of cDNA among samples. Differences were calculated using the threshold cycle (Ct) and comparative Ct methods for relative quantification. Results were expressed as the relative expression of mRNA levels compared to controls. The experiment was performed in triplicate.

2.4. *Western blot analysis*

Total cellular protein were extracted from A375 and G361 cells using 2 × SDS sample buffer (100 mM Tris-HCl, 10 mM EDTA, 4% SDS, 10% Glycine) supplemented with protease inhibitors (PMSF, Sigma-Aldrich). Approximately 30 μg of protein were separated by 10% sodium dodecyl sulfate polyacrylamide gel electrophoresis (SDS-PAGE) and then transferred onto Polyvinylidene fluoride (PVDF) membranes (Millipore, Bedford, MA). Membranes were than blocked with 5% skim milk for 2 h at room temperature, and then incubated with primary antibodies against MACC1 (Sigma, Louis, MO), E-cadherin (Cell Signaling Technology, Danvers, MA), N-cadherin (Cell Signaling Technology, Danvers, MA), Vimentin (Cell Signaling Technology, Danvers, MA) and GAPDH (Santa Cruz Biotechnology, Santa Cruz, CA) overnight at 4°C. GAPDH was used as the loading control. The signals were detected by enhanced chemiluminescence (Millipore, Billerica, MA).

2.5. *Scratch wound assay*

Forty-eight hours after transfection with siRNAs, cells were incubated overnight until grown to about 90% confluency. Then a standard 200 μL plastic filter tip was drawn across the well to produce a wound. The floating cells were eliminated and wells were washed with PBS. The lodged cells were incubated in fresh complete medium for another 24 h. The wound areas were observed at 0 and 24 h time points and photographed under a fluorescence microscope. Wound healing effects were determined by measuring the percentage of the wound area compared with the area of total cells. Each sample was analyzed in triplicate. The experiment was performed in triplicate.

2.6. *Cell migration assay*

For cell migration assay, A375 (2.0×10^4 cells/well) and G361 cells (3.0×10^4 cells/well) were seeded in serum-free media in upper Transwell culture chambers (8 μm pore size, Millipore, MA, USA) coated with collagen

for 24 h. Then 1 mL medium was added to the bottom chamber. After 24 h incubation, migrated cells in the membrane were fixed with 4% paraformaldehyde and stained with 0.02% crystal violet. Finally, the number of migrating cells on the lower membrane surface was counted in five random 200× fields under a microscope. The mean number of cells per field was calculated as cell counts. Each sample was analyzed in triplicate. The experiment was performed in triplicate.

2.7. Cell invasion assay

For cell invasion assay, A375 (2.0×10^4 cells/well) and G361 cells (3.0×10^4 cells/well) were seeded in serum-free media in upper Transwell culture chambers (8 μm pore size, Millipore, MA, USA) coated with matrigel (BD Biosciences) for 24 h. Complete media containing 10% FBS was added to the lower chamber as chemoattractant. Finally, the number of invasive cells on the lower membrane surface was counted in five random 200× fields under a microscope. Similarly, the mean number of cells per field was calculated as cell counts. Each sample was analyzed in triplicate. The experiment was performed in triplicate.

2.8. Immunofluorescent staining

The A375 cells were cultured in a 24-well plate after 24 h transfection. The cells were then washed three times with PBS for 5 min and fixed with 4% paraformaldehyde in PBS, followed by permeabilization with 0.1% Triton X-100 in PBS for 5 min, and then blocked for 1h with PBS containing 5% bovine serum albumin. The cells were incubated with E-cadherin, N-cadherin or Vimentin antibody overnight and washed with PBS three times for 5 min. They were then incubated with the corresponding secondary antibodies for 1 h and washed three times with PBS for 5 min. A drop of 4', 6-diamidino-2-phenylindole (DAPI, Invitrogen) was added into the 24-well plate. The cells were visualized using a fluorescence microscope (VANOX-S, Olympus, Melville, NY, USA).

2.9. Statistical analysis

Numerical data were analyzed using SPSS13.0 software and expressed as means ± standard deviation (SD) of at least three independent determinations. Statistically significant differences between groups were assessed using analysis of the Student's t test. $p < 0.05$ was considered to be statistically significant.

3. Results

3.1. Establishment of MACC1 silencing A375 and G361 cells

It has been reported that MACC1 is closely associated with metastatic carcinomas in various tumors. To investigate the potential role of MACC1 in human malignant melnoma, the expression of MACC1 was specifically downregulated in melanoma cell lines A375 and G361 using siRNA transfection, as confirmed by qRT-PCR and Western blot analysis. As shown in Figure 1A, the mRNA ($p < 0.001$) and protein levels of MACC1 were significantly decreased in A375 cells following siMACC1 transfection, indicating a considerable knockdown efficiency. Similar results were also observed in G361 cells (Figure 1B, $p < 0.001$). Taken together, we successfully constructed a MACC1 silencing melanoma cell model.

3.2. MACC1 silencing inhibits the motility of A375 and G361 cells

To investigate whether MACC1 silencing inhibits A375 and G361 cell mobility, a wound healing assay was performed. As shown in Figure 2A and C, a continuous rapid movement was observed in the control group compared with cells following siMACC1 transfection. Quantitative analysis further indicated that the wound areas in the siCtrl group was significantly decreased compared to the siMACC1 group in both A375 (Figure 2B, $p < 0.001$) and G361 cells (Figure 2D, $p < 0.001$) after incubation for 24 h.
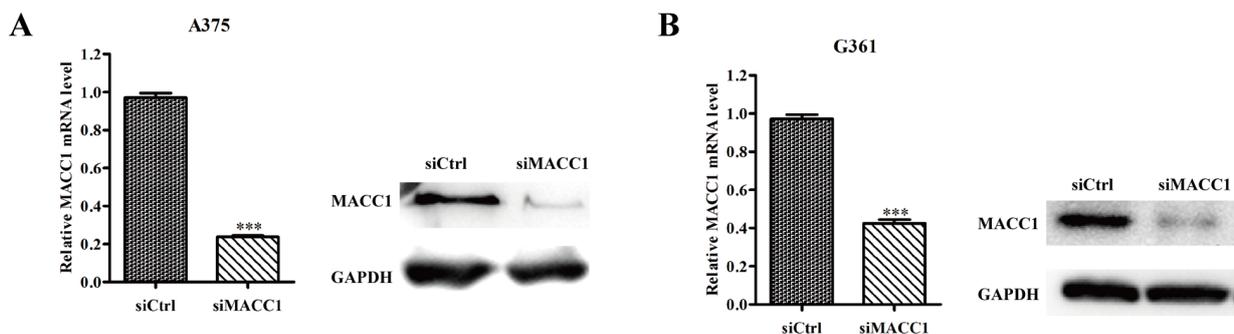
Figure 1. Stable knockdown of MACC1 was successfully constructed in melanoma cells. The mRNA and protein levels of MACC1 were analyzed in A375 **(A)** and G361 **(B)** by qRT-PCR and Western blot analysis. GAPDH was used as a loading control. ***$p < 0.001$, shown siMACC1 *vs*. siCtrl group.
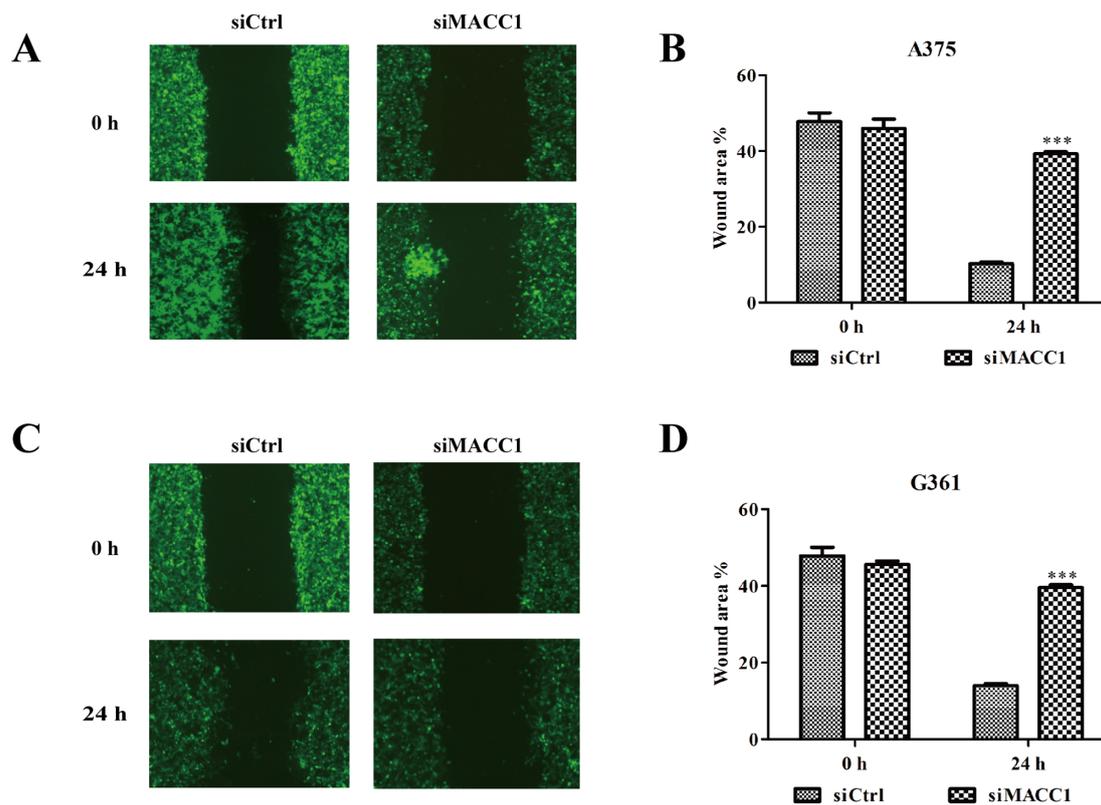
Figure 2. MACC1 silencing inhibits the mobility of melanoma cells. Cell in monolayers were wounded by 200 μl plastic filter tip and the remaining cell monolayers were incubated in the medium for 24 h. At the 0 h and 24 h, the wound areas were photographed in A375 **(A)** and G361 **(C)** under a fluorescence microscope and the percentage of wound area was calculated A375 **(B)** and G361 **(D)** as described in the methods section. ***$p < 0.001$, shown siMACC1 *vs.* siCtrl group.

3.3. *MACC1 silencing suppressed migration and invasion of melanoma cells*

It has been demonstrated that cancer metastasis is inseparable with cell migration and invasion. Therefore, the effects of MACC1 on A375 and G361 cell migration were determined by Transwell cell migration assay. As shown in Figure 3A and B, treatment of A375 and G361 cells with siMACC1 led to a significant decrease in cell vertical migration through the Transwell chamber ($p < 0.001$). Subsequently, cell invasion was measured by Transwell matrigel invasion assay and the results are shown in Figure 3C and D. This indicated that the invasive ability of A375 and G361 cells was remarkably reduced by siMACC1 treatment. These consistent results suggested that MACC1 silencing could effectively reduce the metastatic potentials of the melanoma cells.

3.4. *MACC1 silencing altered EMT expression in melanoma cells*

To further investigate the possible mechanisms underlying MACC1 silencing suppressed cell migration and invasion, the expression of the epithelial markers E-cadherin and N-cadherin, as well as the mesenchymal marker Vimentin were determined in A375 cells after transfection with siMACC1 or siCtrl using qRT-PCR and Western blot analysis. As shown in Figure 4A, the mRNA and protein levels of E-cadherin were obviously upregulated in A375 cells after MACC1 knockdown, whereas those of N-cadherin (Figure 4B) and Vimentin (Figure 4C) were both significantly downregulated in A375 cells induced by MACC1 silencing. Immunofluorescent staining of E-cadherin, N-cadherin and Vimentin showed the same results as those from qRT-PCR and Western blot analysis (Figure 5). Collectively, these results support the idea that knockdown of MACC1 decreased migratory and invasive ability through alteration of EMT expression in melanoma *in vitro*.

4. Discussion

Malignant melanoma is the most deadly type of skin cancer with a high metastatic potential. Due to the complicated mechanism underlying its metastasis, there is currently no effective treatment for malignant melanoma. In this study, we investigated for the first time the biological behavior of MACC1 in melanoma pathogenesis. We found decreased MACC1 resulted in significant inhibition of cell migration and invasion in melanoma through modulating EMT expression. Our
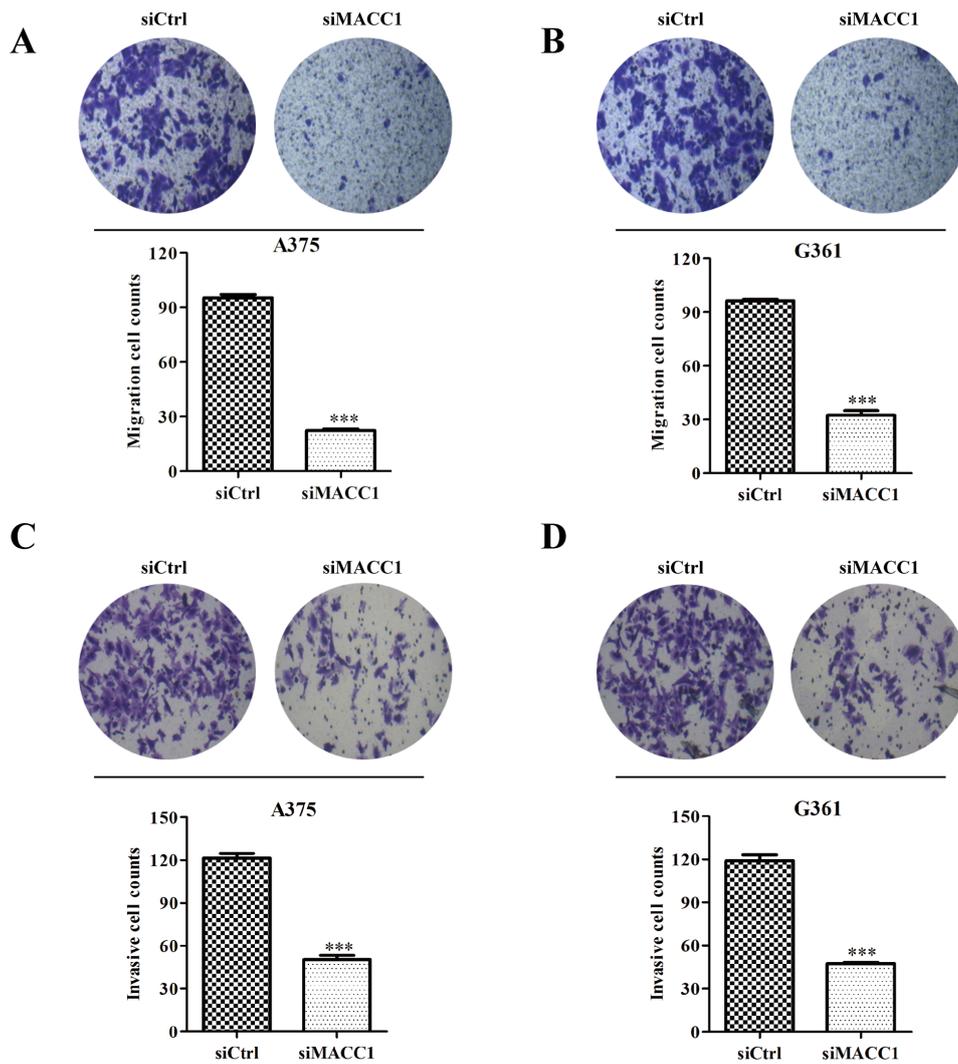
Figure 3. MACC1 silencing inhibited cell migration and invasion ability of melanoma cells. A375 and G361 cells were placed in upper Transwell culture chambers, which were coated with collagen or matrigel. Cell penetration through to the lower surface were stained with crystal violet and photographed under a light microscope, then counted in A375 **(A)** and G361 **(B)** cells. Cells that penetrated through with matrigel to the lower surface were stained with crystal violet and photographed under a light microscope, then counted in A375 **(C)** and G361 **(D)** cells. Quantitative results were obtained from three independent experiments. ***$p < 0.001$, shown siMACC1 *vs.* siCtrl group.
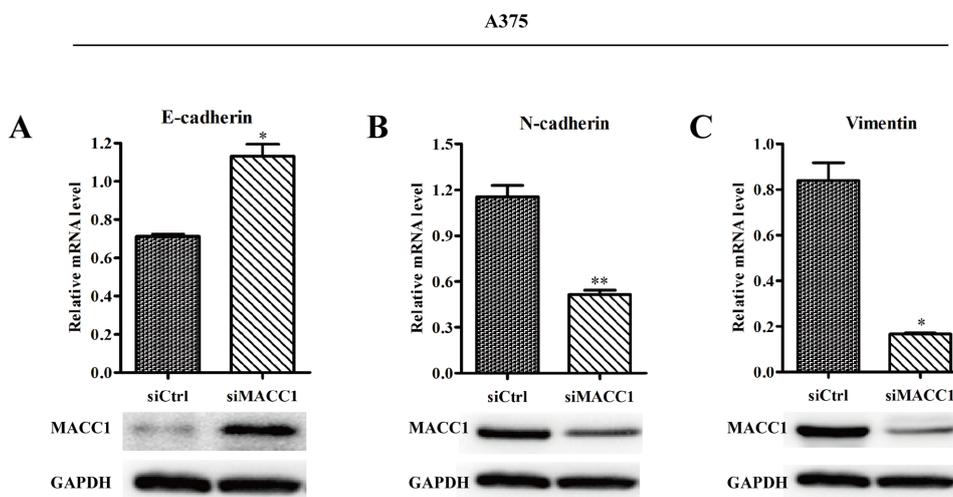
Figure 4. MACC1 silencing altered EMT expression in A375 cells. Knockdown of MACC1 increased E-cadherin expression, but decreased N-cadherin and Vimentin expression as shown by qRT-PCR and Western blot analysis. GAPDH was used as a loading control. **$p < 0.05$, *$p < 0.01$, shown siMACC1 *vs.* siCtrl group.
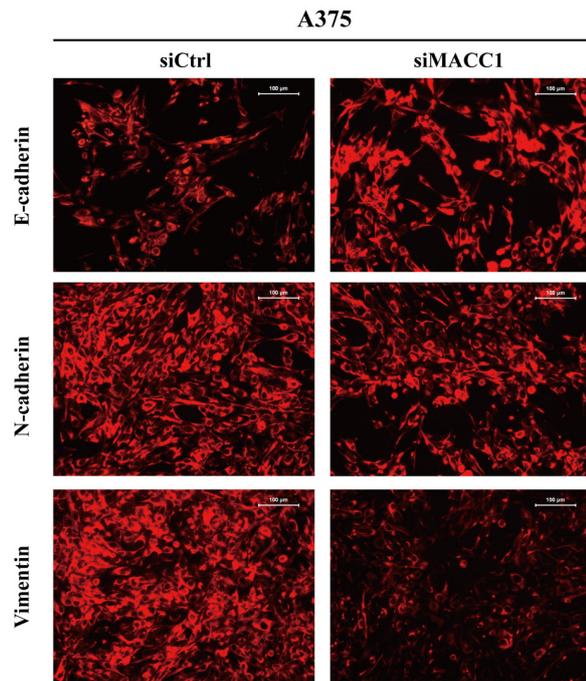
Figure 5. The expression of E-cadherin, N-cadherin and Vimentin in A375 cells was analyzed by immunofluorescent staining. The results showed that MACC1 silencing could increase the expression of E-cadherin, and decrease the expression of N-cadherin and Vimentin.

results may provide a new target for intervention in melanoma treatment.

Accumulating evidence have indicated there is a close relationship between MACC1 and proliferation and metastasis in a variety of tumors. Consistent with our results, downregulation of MACC1 remarkably inhibited cell migration and invasion in gastric cancer (*13*), glioma (*14*) and ovarian cancer (*15*). Previous studies have demonstrated that deregulation of HGF/c-MET signaling, governed by MACC1 induces various malignant behaviors in cancer (*16*). EMT plays an important role in HGF/c-MET signaling regulation, which are mainly involved in the initiating step for the cascade of tumor invasion driven by various genes (*11,17,18*). Therefore, we speculate MACC1 might be associated with the EMT phenotype. To confirm this speculation, we focused on hallmarks of EMT. Our results showed that MACC1 silencing could upregulate expression of E-cadherin, while downregulating expression of N-cadherin and vimentin.

E-cadherin, as the hallmark of EMT (*19*) is an essential adhesive tumor suppressor (*20*) in the establishment of epithelial adhesion junctions and a tight polarized cell layer, whose downregulation is a leading event in the progression of various tumors into the metastatic cascade (*21,22*). Thus, the upregulation of E-cadherin induced by MACC1 silencing in cells implicated that MACC1 plays a crucial role in impairing epithelial characteristics. N-cadherin is a mesenchymal marker and is also correlated with the

migratory and invasive phenotype (*23*). Vimentin, an intermediate filament during EMT, is shown to be required for remodeling of cytoskeleton elongation and facilitating mesenchymal cell migration (*24*). After downregulation of MACC1, we found that these two representative mesenchymal markers were consistently decreased. Collectively, MACC1 plays an important role in melanoma metastasis.

In summary, it is not hard to suggest how the oncogene MACC1 affects the malignancy of melanoma, as originally shown in our current cellular experiments. Our findings demonstrate MACC1 might be a potential therapeutic target for inhibiting EMT in melanoma invasiveness. Furthermore, more experiments are still needed to determine whether MACC1 silencing will reduce melanoma tumorigenicity in mouse xenograft models, as well as the specific mechanisms.

References

1. Zhu Y, Ye T, Yu X, *et al*. Nifuroxazide exerts potent anti-tumor and anti-metastasis activity in melanoma. Sci Rep. 2016; 6:20253.
2. DeSantis C, Ma J, Bryan L, Jemal A. Breast cancer statistics, 2013. CA Cancer J Clin; 2014; 64:52-62.
3. Azoury SC, Lange JR. Epidemiology, risk factors, prevention, and early detection of melanoma. Surg Clin North Am. 2014; 94:945-962.
4. Mort RL, Jackson IJ, Patton EE. The melanocyte lineage in development and disease. Development. 2015; 142:1387.
5. Cummins, DL, Cummins JM, Pantle H, Silverman MA, Leonard AL, Chanmugam A. Cutaneous malignant melanoma. Mayo Clin Proc. 2006; 81:500-507.
6. Stein U, Walther W, Arlt F, Schwabe H, Smith J, Fichtner I, Birchmeier W, Schlag PM. MACC1, a newly identified key regulator of HGF-MET signaling, predicts colon cancer metastasis. Nat Med. 2009; 15:59-67.
7. Shimokawa H, Uramoto H, Onitsuka T, Gu C, Hanagiri T, Oyama T, Yasumoto K. Overexpression of MACC1 mRNA in lung adenocarcinoma is associated with postoperative recurrence. J Thorac Cardiovasc Surg. 2011; 141:895-898.
8. Wang L, Wu L, Lin L, Liu P, Huang H, Liao W, Zheng D, Zuo Q, Sun L, Huang N, Shi M, Liao Y, Liao W. Metastasis-associated in colon cancer-1 upregulation predicts a poor prognosis of gastric cancer, and promotes tumor cell proliferation and invasion. Int J Cancer. 2013; 133:1419-1430.
9. Shirahata A, Fan W, Sakuraba K, Yokomizo K, Goto T, Mizukami H, Saito M, Ishibashi K, Kigawa G, Nemoto H. MACC 1 as a marker for vascular invasive hepatocellular carcinoma. Anticancer Res. 2011; 31:777-780.
10. Stein U, Dahlmann M, Walther W. MACC1 - more than metastasis? Facts and predictions about a novel gene. J Mol Med (Berl). 2010; 88:11-18.
11. Birchmeier C, Birchmeier W, Gherardi E, Vande Woude GF. Met, metastasis, motility and more. Nat Rev Mol Cell Biol. 2003; 4:915-925.
12. Zhen T, Dai S, Li H, Yang Y, Kang L, Shi H, Zhang F, Yang D, Cai S, He Y, Liang Y, Han A. MACC1 promotes carcinogenesis of colorectal cancer *via* beta-catenin

signaling pathway. Oncotarget. 2014; 5:3756-3769.

13. Guo T, Yang J, Yao J, Zhang Y, Da M, Duan Y. Expression of MACC1 and c-Met in human gastric cancer and its clinical significance. Cancer Cell Int. 2013; 13:121.

14. Sun L, Li G, Dai B, Tan W, Zhao H, Li X, Wang A. Silence of MACC1 expression by RNA interference inhibits proliferation, invasion and metastasis, and promotes apoptosis in U251 human malignant glioma cells. Mol Med Rep. 2015; 12:3423-3431.

15. Li H, Zhang H, Zhao S, Shi Y, Yao J, Zhang Y, Guo H, Liu X. Overexpression of MACC1 and the association with hepatocyte growth factor/c-Met in epithelial ovarian cancer. Oncol Lett. 2015; 9:1989-1996.

16. Stein U, Smith J, Walther W, Arlt F. MACC1 controls Met: What a difference an Sp1 site makes. Cell Cycle. 2009; 8:2467-2469.

17. Gherardi E, Birchmeier W, Birchmeier C, Vande Woude G. Targeting MET in cancer: Rationale and progress. Nat Rev Cancer. 2012; 12:89-103.

18. Ponzo MG, Lesurf R, Petkiewicz S, O'Malley FP, Pinnaduwage D, Andrulis IL, Bull SB, Chughtai N, Zuo D, Souleimanova M, Germain D, Omeroglu A, Cardiff RD, Hallett M, Park M. Met induces mammary tumors with diverse histologies and is associated with poor outcome and human basal breast cancer. Proc Natl Acad Sci U S A.
2009; 106:12903-12908.

19. Hajra KM, Chen DY, Fearon ER. The SLUG zinc-finger protein represses E-cadherin in breast cancer. Cancer Res. 2002; 62:1613-1618.

20. Pećina-Šlaus N. Tumor suppressor gene E-cadherin and its role in normal and malignant cells. Cancer Cell Int. 2003; 3:17.

21. Christofori G, Semb H. The role of the cell-adhesion molecule E-cadherin as a tumour-suppressor gene. Trends Biochem Sci. 1999; 24:73-76.

22. Cheng CW, Wu PE, Yu JC, Huang CS, Yue CT, Wu CW, Shen CY. Mechanisms of inactivation of E-cadherin in breast carcinoma: Modification of the two-hit hypothesis of tumor suppressor gene. Oncogene. 2001; 20:3814-3823.

23. Lamouille S, Xu J, Derynck R. Molecular mechanisms of epithelial-mesenchymal transition. Nat Rev Mol Cell Biol. 2014; 15:178-196.

24. Schoumacher M, Goldman RD, Louvard D, Vignjevic DM. Actin, microtubules, and vimentin intermediate filaments cooperate for elongation of invadopodia. J Cell Biol. 2010; 189:541-556.

The protective effects of human umbilical cord mesenchymal stem cells on damaged ovarian function: A comparative study

Jinjin Zhang[1], Jiaqiang Xiong[1], Li Fang[1], Zhiyong Lu[1], Meng Wu[1], Liangyan Shi[2], Xian Qin[1], Aiyue Luo[1], Shixuan Wang[1,*]

[1] *Department of Obstetrics and Gynecology, Tongji Hospital, Huazhong University of Science and Technology, Wuhan, Hubei, China;*
[2] *Department of Obstetrics and Gynecology, Hubei Province, Maternity and Child Health Care Hospital, Wuhan, Hubei, China.*

Summary	Numerous studies have reported that human umbilical cord mesenchymal stem cell (hUCMSC) therapy can rescue the structure and function of injured tissues. The aims of this study were to explore the protective role of hUCMSC transplantation in a model of accelerated ovarian aging and to compare 2 methods of transplanting hUCMSCs, *i.e. i*) via intravenous injection (IV) and *ii*) in situ ovarian micro injection (MI). Female mice were subjected to superovulation and ozone inhalation to create a model of accelerated ovarian aging with a decline in both the quantity and quality of oocytes. Cells were transplanted *via* IV or MI, and ovaries were removed after 2 weeks or 1 month of treatment. Ovarian reserve and function were evaluated based on the follicle counts, hormone levels, the estrous cycle, and reproductive performance. Cell tracking, terminal deoxynucleotidyl transferase-mediated dUTP nick end labeling (TUNEL), real-time polymerase chain reaction (PCR), and Western blot analysis were used to assess the inner mechanisms of injury and repair. Results indicated that ovarian function increased significantly after treatment with hUCMSCs. Immunofluorescence revealed reduced TUNEL staining and a decreased percentage of apoptotic cells. A higher level of expression of anti-apoptotic and antioxidant enzymes was noted in the ovaries of groups treated with hUCMSCs. These parameters were enhanced more when mice were treated with hUCMSCs for 1 month than when they treated with hUCMSCs for 2 weeks. IV was better able to restore ovarian function than MI. These results suggest that both methods of transplantation may improve ovarian function and that IV transplantation of hUCMSCs can significantly improve ovarian function and structural parameters more than MI transplantation of hUCMSCs can.

Keywords: Ovarian aging, hUCMSCs, model of accelerated ovarian aging, intravenous injection, in situ ovarian micro injection

1. Introduction

Aging of the ovaries is characterized by a gradual decline in both the quantity and quality of oocytes. At the 16th-20th week of fetal development, the ovaries contain 6-7 million primordial follicles (*1,2*), which serve as a source of developing follicles (*1,3,4*). Unfortunately, the number of oocytes inevitably declines with age. At birth, approximately 1-2 million primordial follicles remain in the ovaries (*5*). By the onset of puberty, the number of primordial follicles declines to only 300,000 to 400,000 (*6,7*). At child-bearing age, the number of primordial follicles decreases steadily at a rate of about 1,000 follicles per month and drops below 1,000 at the average age of 51 years (menopause) (*8-10*).

As the follicle count decreases with age, oocyte quality also diminishes. The products produced by oxidative stress during daily metabolism may cause aging (*11*). Long-term greater oxidative stress damage may be involved in the process of ovarian aging (*12,13*). Previous

studies have indicated that oxidative stress harms oocyte development. A study that examined the relationship between oxidative stress and poor oocyte quality suggested that women who undergo IVF have a higher proportion of degenerative oocytes and a significantly higher level of 8-hydroxy-2'-deoxyguanosine (8-OHdG, a marker of the degree of DNA oxidation) in the ovarian follicular fluid (*14*). When women who failed to become pregnant after IVF were given antioxidants, they had a markedly lower level of 8-OHdG in the follicular fluid and a higher pregnancy rate. Recent studies have also suggested that mitochondrial dysfunction is involved in age-related damage to oocytes. The undesirable changes caused by excessive free radicals can result in cellular injury that increases with age (*15,16*). Along with an age-related decrease in estrogen levels, the absence of the beneficial effects of estrogen on oxidative stress finally causes damage to the ovaries. This may explain the significantly increase in the rate of congenital birth defects in women over age 38 (*17*). The accumulation of oxidative damage and an accompanying diminishing of antioxidant defenses will ultimately lead to ovarian aging.

Based on these findings, a new a model of accelerated ovarian aging was created to induce a decline in both the quantity and quality of oocytes by superovulation and ozone inhalation. Repeated ovulation was induced in mice by sequentially administering pregnant mare serum gonadotropin (PMSG), human chorionic gonadotropin (hCG), and prostaglandin F2α (PGF2α) to reduce the primordial follicle pool. Ozone inhalation was used to increase oxidative damage throughout the body, including the ovaries.

Previous studies have suggested that stem cells have the ability to differentiate into a variety of cell phenotypes, so they can be used to treat various diseases. Given this contention, suitable stem cells could most likely be used to delay ovarian aging. Stem cell therapy has been found to restore the fertility of patients, although its mechanism is unclear (*18*). Mesenchymal stem cells (MSC) derived from Wharton's jelly of the human umbilical cord (human umbilical cord MSCs, or hUCMSCs) have displayed characteristics similar to those of bone marrow mesenchymal stromal cells (BMSCs). Compared to BMSCs, hUCMSCs have many merits as a cell treatment because of their relatively large capacity for *ex vivo* expansion, low risk of viral infection, lack of donor morbidity, and less pronounced immunogenicity (*19-21*). Evidence has shown that hUCMSCs have unique advantages compared to BMSCs (*22*), which make them a promising source of cells for treatment. According to previous studies, stem cells to treat ovarian injury are primarily administered *via* intravenous injection (IV) or in situ ovarian micro injection (MI) (*23-26*). However, very few studies have examined suitable forms of hUCMSC therapy to delay ovarian aging. The current study sought to evaluate 2 different forms of hUCMSC therapy for protection against ovarian aging in an animal model in order to offer a better form of cell therapy.

2. Materials and Methods

This study was conducted in the Stem Cell Research Laboratory in Gynecology & Obstetrics. This study followed procedures consistent with the guidelines for the care and use of laboratory animals issued by the Academy of Tongji Medical College at Huazhong University of Science and Technology.

2.1. *Preparation, culture, and identification of hUCMSCs*

hUCMSCs were prepared, identified, and cultured according to a recently published protocol (*23*). At passage 6, the expression of cell surface markers was analyzed with flow cytometry using fluorescein isothiocyanate (FITC)-conjugated human monoclonal antibodies such as CD14 (BioLegend, 325623), CD31 (BioLegend, 303103), CD34 (BioLegend, 343603), CD105 (BioLegend, 323203), CD45 (BioLegend, 304005), CD44 (BioLegend, 338803), CD73 (BioLegend, 344015), human leukocyte antigens-D region (HLA-DR, BioLegend, 307603), phycoerythrin (PE)-conjugated human antibodies against CD90 (BioLegend, 328109), and PE-CD29 (BioLegend, 303003). Adherent cells were detached by treatment with 0.25% trypsin ethylene diamine tetraacetic acid (EDTA) and incubated with monoclonal antibodies, re-suspended in 0.4mL phosphate buffer solution (PBS), and immediately analyzed using a flow cytometer. To further detect the differentiation potential of hUCMSCs, osteogenic and adipogenic experiments were conducted, and alkaline phosphatase (ALP) and oil red O staining were used to indicate differentiation.

2.2. *Creation of an animal model*

Female C57BL/6 mice (6 weeks old, weighing 16.7 ± 0.8 g) were obtained from Beijing HFK Bio-Technology (Beijing, China). All mice were housed in a specific pathogen-free (SPF)-grade facility with a controlled temperature (25°C) and light cycle (12 h light, 12 h dark). To create a model of accelerated ovarian aging, mice were super-ovulated *via* an intraperitoneal injection of 5 IU of pregnant mare serum gonadotropin (PMSG) (Hangzhou Animal Medicine Factory, Hangzhou, China). Forty-eight hours after PMSG administration, the mice were intraperitoneally administered 5 IU human chorionic gonadotropin (hCG) (Livzon Pharmaceutical Group Inc., Guangzhou, China); 19 hours later, 25 IU of PGF2α (Hangzhou Animal Medicine Factory, Hangzhou, China) was administered intraperitoneally. Five hours after PGF2α administration, the sequential administration of the

three agents was repeated 10 times in 30 days (*27*). To induce ozone inhalation, mice were placed in a half-open system in which an ozonator (manufactured by Beijing Kang Er Xing Technology Development Co. Ltd., Beijing, China) had been placed on a rack. An ozone meter (manufactured by Beijing Kang Er Xing Technology Development Co. Ltd., Beijing, China) was used to measure the ozone concentration inside the cage during the experiment. Once the ozonator was turned on, the fresh airflow that entered the ozonator was regulated to maintain the ozone concentration in the center of the cage at 1.2 mg/m^3 (*28,29*). The mice were exposed to ozone for 8 h (20:00-04:00) each day until the end of the last cycle of superovulation. A photograph of intraperitoneal injection and a diagram of the ozone chamber are shown in Figure 1.

2.3. Animal groups

One hundred and twenty-six mice were randomly divided into 2 groups. The normal control group (NC, *n* = 12) consisted of untreated normal mice and the model group (Mod, *n* = 114) consisted of mice with accelerated ovarian aging. Once the model was created, 6 mice from each group were sacrificed to assess ovarian function. The remaining mice were divided into 8 groups: IV-u2w, IV-p2w, MI-u2w, MI-p2w, IV-u1m, IV-p1m, MI-u1m, and MI-p1m. Each group consisted of 12 mice.

2.4. PKH26 labelling

hUCMSC membranes were labeled with a lipophilic dye, PKH26, usong the PKH26 Red Fluorescence Kit (Sigma-Aldrich) according to the manufacturer's instructions (*30*). The labeled cell suspension was diluted to almost 1×10^6 cells/mL. The collected cells were then stained with trypan blue to ensure cell viability was over 95%. Cells were then used for cell therapy.

2.5. hUCMSC transplantation

Mice in the IV-u2w and IV-u1m groups were administered hUCMSCs *via* the tail vein for 2 weeks and 1 month, respectively, and the IV-p2w and IV-p1m groups were treated with PBS. As shown in Figure 2, mice in the intravenous group (IV-u2w, IV-u1m) were injected intravenously with 1×10^6 hUCMSCs in 100 μL of PBS as described in previous studies (*31-33*). Mice in the IV-p2w and IV-p1m groups were injected with 100 μL of PBS alone. The same amount was injected the following day. In the IV-u1m group and IV-p1m group, PBS was injected again 15 and 16 days after the first injection.

In the in situ micro injection groups (MI-u2w and MI-u1m), a total of 2×10^6 hUCMSCs in 10 μL of PBS was injected directly into the bilateral ovaries with
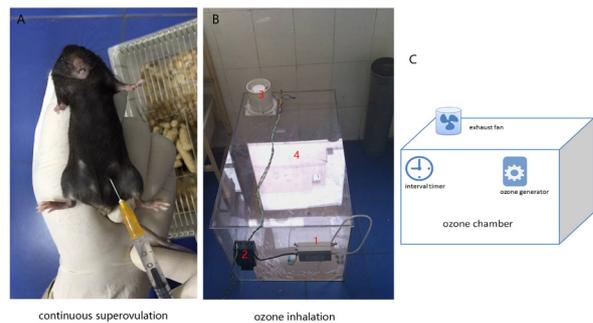
Figure 1. Model setup. (A) Intraperitoneal injection. **(B)** Ozone inhalation. **(C)** Diagram of the ozone chamber. *Note*: 1. Ozone generator; 2.Timer; 3. Exhaust fan; 4. Ozone chamber.
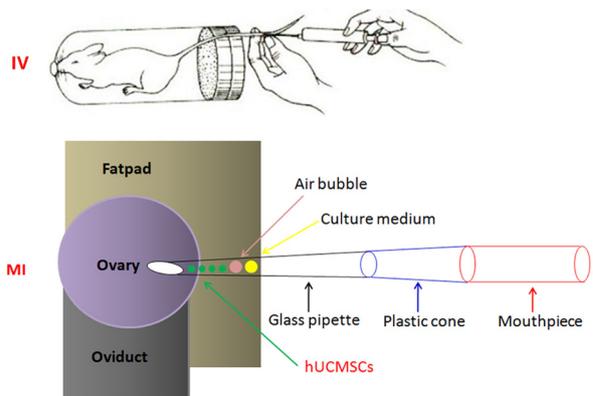
Figure 2. hUCMSC transplantation. IV: Intravenous injection; MI: In situ ovarian micro injection.

a micro injector while mice in the MI-p2w and MI-p1m groups were injected with 10 μL of PBS alone to serve as a control. No leakage was apparent after transplantation.

2.6. Ovarian follicle counts and morphological analysis

Two weeks or 1 month after cell transplantation, 6 mice from each group were sacrificed and their ovaries were removed and fixed for sectioning. Mouse ovaries fixed in 4% paraformaldehyde for 24 h were transferred to 70% ethanol, embedded in paraffin, and successively cut lengthwise into sections of 5 μm. Every fourth section was mounted on a glass slide. Ever other slide was stained with hematoxylin and eosin and analyzed under a microscope by 2 researchers who were blinded to the origin of the sections. Only follicles containing oocytes with a nucleus were scored in histomorphometric evaluation, as originally described (*34*). In all sections, the numbers of primordial, growing, and antral follicles were tallied to obtain the count of each type of follicle in a given ovary.

2.7. Hormone examination

Sterile non-heparinized tubes were used to collect blood samples from non-pregnant mice during the diestrus

of the estrous cycle in sterile non-heparinized tubes. The blood samples were centrifuged at 3,000 rpm for 5 minutes, and serum was collected and stored at -80°C until analysis. Levels of serum E2 and P were measured using an enzyme-linked immune sorbent assay (ELISA) according to the manufacturer's instructions (Cayman Chemical Company, Ann Arbor, MI, USA).

2.8. Estrous phase and fertility tests

Five mice in each group were used in estrous cycle and fertility tests. The estrous cycles of the female mice were regularly assessed every morning between 08:00 and 9:00 AM using vaginal cytology (*35,36*). Mating trials were initiated 20 days after hUCMSC treatment and lasted for 4 months. The number and survival rate of fetuses and the time of birth were recorded to evaluate reproductive performance.

2.9. Detection of apoptosis

Apoptotic cells in ovarian tissue sections were identified with an in situ Cell Death Detection Kit, POD (Roche, Germany) according to the manufacturer's instructions. Paraffin sections of the ovaries were dewaxed, rehydrated, digested with proteinase K (10 μM) for 5 min, incubated in TUNEL enzyme (10% v/v; Roche) and TUNEL label (90% v/v; Roche) for 60 min at 37°C, and mounted in ProLong Gold medium containing 4',6-diamidino-2-phenylindole (DAPI). Negative control sections were incubated with a TUNEL reaction mixture without enzyme (terminal deoxynucleotidyl transferase, TdT). Finally, the sections were observed and digital images were recorded using a Leica inverted SP5 confocal laser-scanning microscope (Leica Microsystems, Wetzlar, Germany).

2.10. Real-time fluorescence quantitative polymerase chain reaction (qPCR)

Total RNA in the ovaries was extracted. Real-time PCR was performed using the AB StepOne Plus PCR machine (Applied Biosystems, Foster City, CA, USA) as described in a previous study (*37*). The PCR amplification of all transcripts was performed with the gene-specific primers listed in Table 1. Primers were found in the literature or designed with software Primer 3.0. The quality and identity of each PCR product was determined using melting curve analysis. The expression of mRNA was calculated using the delta-delta Ct method, with relative gene expression $= 2^{-(\Delta Ct\ sample - \Delta Ct\ control)}$ (*38*). All data were normalized to expression of glyceraldehyde-3-phosphate dehydrogenase (GAPDH).

2.11. Western blot analysis

Western blot analysis was performed as previously

described (*39*). Cell membranes were incubated overnight at 4°C with a primary antibody against superoxide dismutase 2 (SOD2, Abcam, UK, ab13533, 1:5,000 dilution), catalase (CAT, Abcam, UK, ab16731,1: 2,000 dilution), Bcl-2 associated X protein (Bax, Abcam, UK, ab32503, 1: 5,000 dilution), Bcl2 (Abcam, UK, ab32124, 1:1,000 dilution), or β-actin (Sigma,1: 1,000 dilution). Afterwards, membranes were incubated with a horseradish peroxidase-conjugated anti-rabbit or antimouse antibody (1:3,000 dilution) for 30 minutes at room temperature and washed 3 times with tris-buffered saline tween20 (TBST). After incubation with a chemiluminescent substrate for 5 minutes, protein signals were detected with BIO-RAD ChemiDoc™ XRS (USA) and analyzed with Image LabTM Software.

2.12. Statistical analysis

Statistical analysis was performed using the software SPSS®17.0 with data expressed as the mean ± SEM. Student's t-test was used to compare the NC and Mod groups to assess the model. One-way analysis of variance (ANOVA) was used to compare hormones, follicle counts, apoptosis rates, and gene expression among the groups. Differences in estrous cycles were evaluated using ANOVA with a post-hoc Tukey's test. Values with $p < 0.05$ were considered to indicate a significant difference.

3. Results

3.1. Characterization of hUCMSCs

At least 10 days was needed for the first colonies of hUCMSCs to appear, and an extra week was required for them to reach 50-60% confluency. Isolated hUCMSCs in culture were characterized using microscopy and flow cytometry. The morphology of cultured hUCMSCs resembled fibroblasts with few other cells (Figure 3A). To determine the extent to which induction resulted in hUCMSC differentiation into adipocytes versus osteoblasts, the cells were examined with oil red O and ALP staining. As shown in Figure 3B and 3C (red cells), isolated hUCMSCs were able to differentiate into both adipocytes and osteoblasts. In addition, flow cytometry was used to recognize the expression of surface markers at passage 6. Results indicated that the cultured hUCMSCs were negative for HLA-DR, CD14, CD31, CD34, and CD45. However, more than 95% of the cell population was positive for the markers CD29, CD44, CD73, CD90, and CD105 (Figure 3D).

3.2. Assessment of the animal model

In order to assess whether the mouse model of accelerated ovarian aging was effectively created, ovarian morphology, ovarian follicle counts, plasma estrogen

Table 1. List of specific primers and amplification conditions for real-time PCR

NCBI accession	Aliases	Sequence (5'-3')		Tm, Cycles	Size (bp)
		Forward	Reverse		
NP_032110	GAPDH	AAGGGTGGAGCCAAAAGGG	GGGGGCTAAGCAGTTGGTG	60, 30	141
NP_031553	Bax	CCCGAGAGGTCTTCTTCCG	AGCCGCTCACGGAGGAAGT	60,30	181
NP_803129	Bcl2	GATGCTGGAGATGCGGACG	ACGACGGTAGCGACGAGAG	60,30	240
NP_033934	CAT	GGAGGCGGGAACCCAATAG	GTGTGCCATCTCGTCAGTGAA	60,30	102
NP_038699	SOD2	CAGACCTGCCTTACGACTATGG	CTCGGTGGCGTTGAGATTGTT	60,30	113
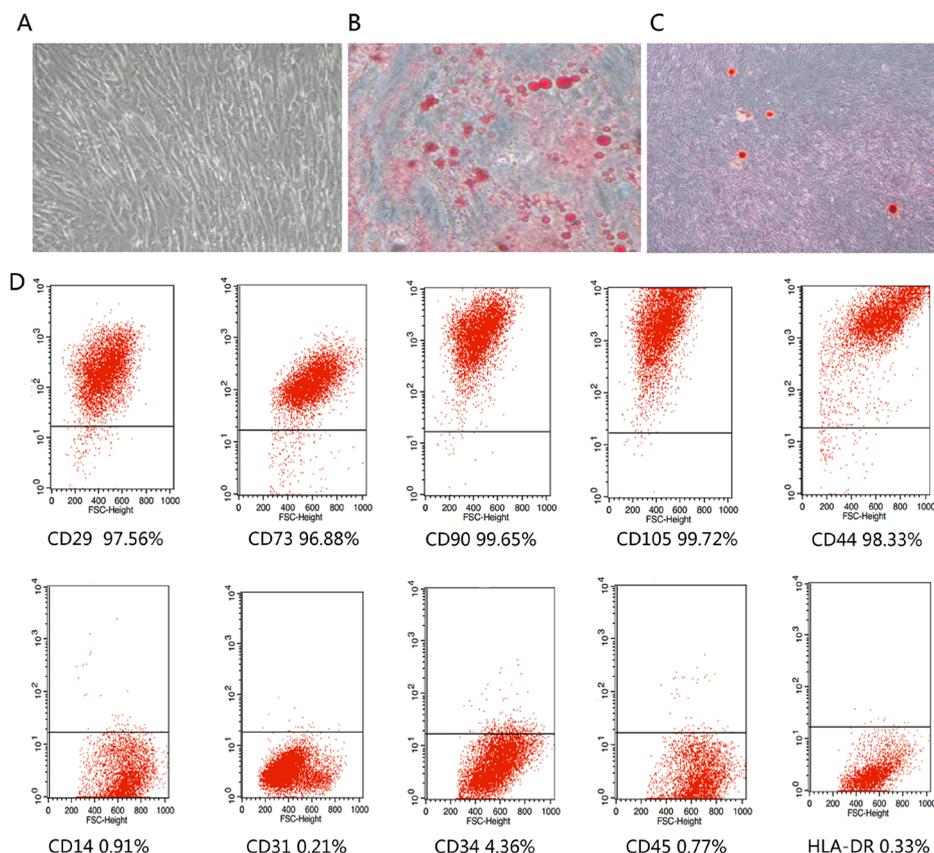
Figure 3. Isolation and identification of hUCMSCs. (A) hUCMSCs have a typical fibroblastic morphology. **(B)** hUCMSCs differentiate into adipocytes. **(C)** hUCMSCs differentiate into osteoblasts. **(D)** Flow cytometry analysis of hUCMSCs. Cells were positive for CD29, CD90, CD105, CD73, and CD44 and negative for CD14, CD31, HLA-DR, CD34, and CD45.

and progesterone levels, and reproductive performance were studied. Once the model was created, examination of the ovaries indicated that the ovaries of the NC mice contained numerous follicles in each stage. However, the ovaries of the mice in the Mod group mostly consisted of secondary follicles and atretic follicles, with fewer primordial follicles and primary follicles. Moreover, the plasma levels of estrogen and progesterone decreased, along with fertility, in the Mod group compared to levels in the NC group. These results indicated that the Mod group of mice had diminished ovarian reserve. The specific results are shown below.

3.3. *hUCMSCs restored ovarian function in terms of both ovarian follicle counts and morphology*

Two weeks after PKH26-labeled hUCMSCs were intravenously injected, those cells were tracked in mouse ovaries. However, the labeled cells did not develop into follicles or oocytes. Follicles stained with hematoxylin and eosin in each stage in all groups are shown in Figure 4A-J. Female mice who were super-ovulated and subjected to ozone inhalation exhibited physiological ovarian aging. The NC group of mice had 61.5 ± 10.3 primordial follicles, and the Mod group of mice had 38.0 ± 7.1 primordial follicles (Mod *vs.* NC, $p < 0.01$). There were fewer primordial and primary follicles in the ovaries of the mice in the Mod group than in the NC group. Moreover, the number of secondary follicles and atretic follicles in the Mod group was higher than that in the NC group ($p < 0.01$ for secondary follicles and $p < 0.05$ for atretic follicles).

The hUCMSCs were administered intravenously or *via* in situ micro injection. Ovaries were removed
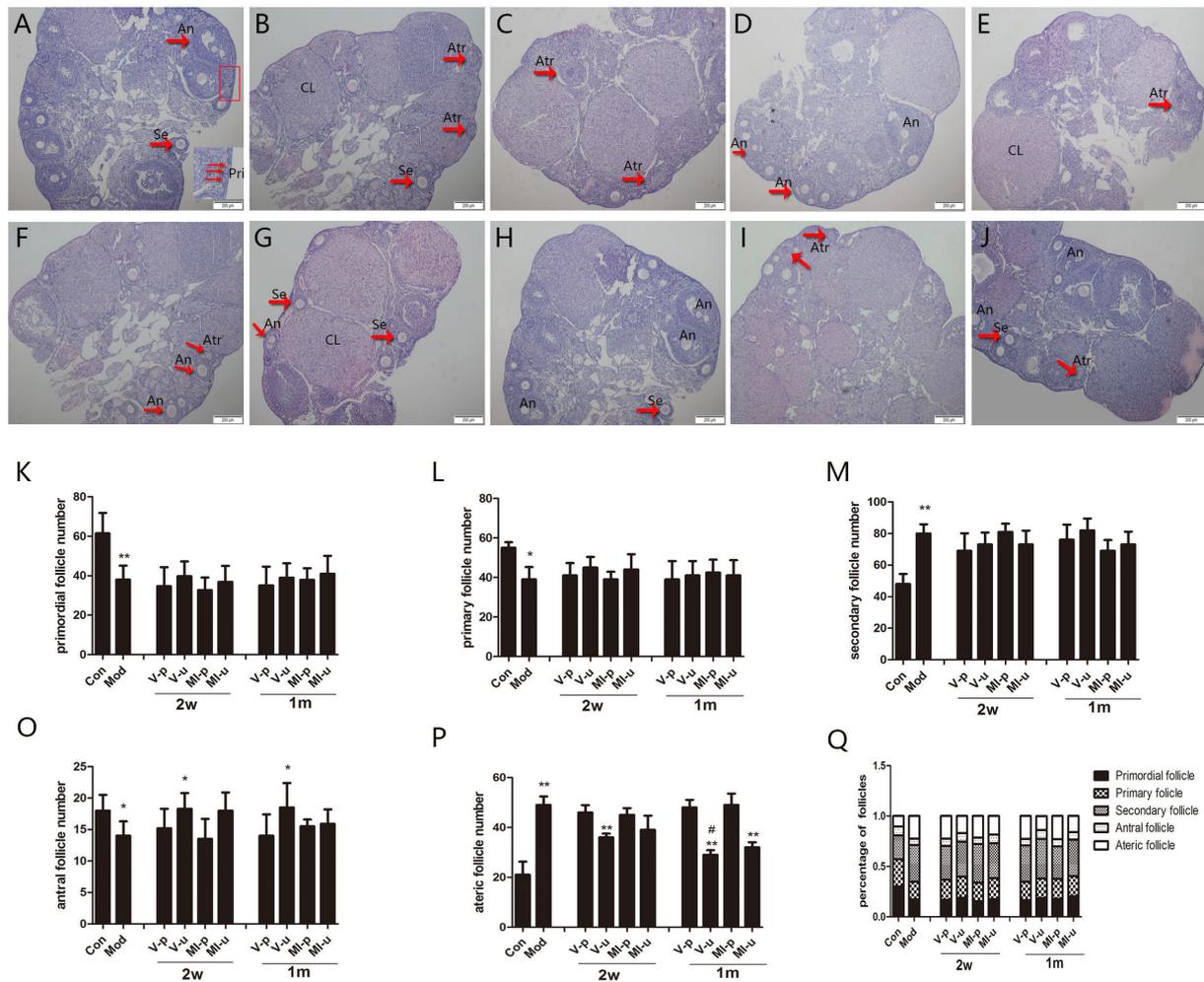
Figure 4. The effect of transplantation on follicle morphology and number in each group during various stages of development. (A-J) Representative histological images of the ovaries in each group of mice. Once the model was created, the ovaries of the Mod group had fewer primordial and primary follicles compared to the NC group. However, the number of secondary follicles and atretic follicles in the Mod group increased significantly. Atretic follicles decreased and healthy antral follicles increased after treatment with hUCMSCs for 2 weeks or 1 month. Bar = 200 μm; Pri: primordial follicles; Se: secondary follicles; An: antral follicles; Atr: atretic follicles; CL: corpus luteum. **(K-Q)** Numbers of each grade of follicles in all groups. **(K)** Primordial follicles. **(L)** Primary follicles **(M)** Secondary follicles **(O)** Antral follicles **(P)** Atretic follicles. **(Q)** The percentage of follicles in each group during various stages. The * symbol represents the Mod group versus the NC group or groups treated with hUCMSCs versus corresponding groups treated with PBS, *$p < 0.05$, **$p < 0.01$; The # symbol represents IV-u1m group versus IV-u2w group, #$p < 0.05$.

2 weeks or 1 month after treatment, and the number of each type of follicle was determined. Ovaries from mice that were treated with hUCMSCs (IV-u2w, IV-u1m, MI-u2w, and MI-u1m) had similar numbers of primordial follicles, primary follicles, and secondary follicles in comparison to the Mod group of mice and the corresponding groups treated with PBS (Figue 4K-M) ($p > 0.05$). Groups treated with hUCMSCs had a greater number of healthy antral follicles than did groups treated with PBS except for the MI-u2w and MI-u1m groups. After treatment, however, atretic follicles decreased in the IV-u2w, IV-u1m, and MI-u1m groups compared to the corresponding groups treated with PBS. The follicle count did not differ significantly in the IV-u1m group or the IV-u2w group except in terms of the number of atretic follicles. Nevertheless, the atretic follicle count decreased substantially with the duration of hUCMSC treatment in the IV-u1m group than in the IV-u2w group. As shown

in this study, 1 month may be the optimal duration of stem cell therapy. The number and percentage of follicles in each group during various stages of development are shown in Figure 4K-Q.

3.4. *hUCMSCs restored ovarian function in terms of sex hormone levels*

Follicular development was evaluated in all groups by monitoring estrous cycles with vaginal smears, and estrogen and progesterone levels in serum were measured. Two weeks or 1 month after hUCMSC treatment, the serum levels of estrogen and progesterone in the treated groups increased significantly compared to those in the corresponding groups treated with PBS ($p < 0.05$). Levels of estrogen and progesterone did not differ significantly in the MI-p2w group or the MI-u2w group. Estrogen levels in mice increased with the
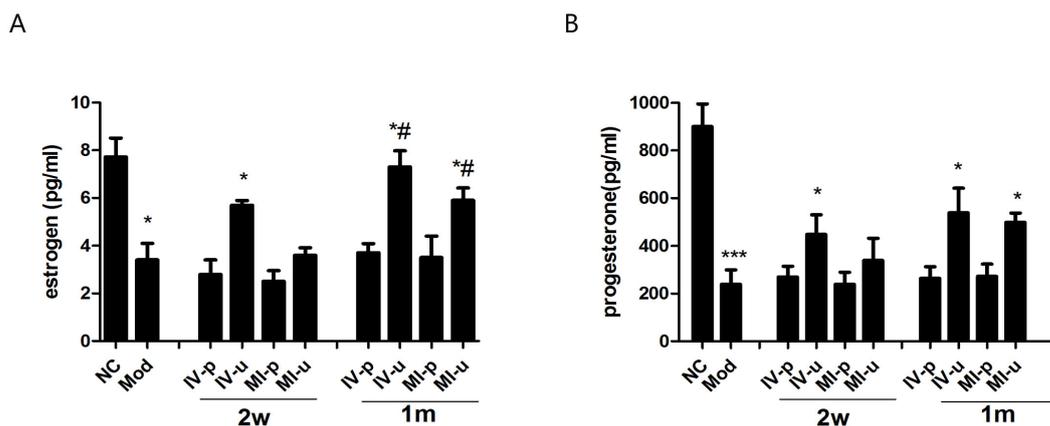
Figure 5. Estrogen and progesterone levels in different groups. After hUCMSC treatment, serum levels of estrogen **(A)** and progesterone **(B)** increased significantly compared to levels in the corresponding groups treated with PBS, and those levels did not differed significantly in the MI-u2w group and the MI-u2w group. The * symbol represents the Mod group versus the NC group or groups treated with hUCMSCs versus corresponding groups treated with PBS, $*p < 0.05$, $***p < 0.001$; The # symbol represents the IV-u1m group versus the IV-u2w group or the MI-u1m group versus the MI-u2w group, $#p < 0.05$.

**Table 2. Effect of hUCMSCs on the estrous cycle ($n = 5$) and reproductive performance ($n = 5$)**

Reproductive performance	NC	Mod	IV-p2w	IV-u2w	MI-p2w	MI-u2w	IV-p1m	IV-u1m	MI-p1m	MI-u1m
Regular cycles (%)	100	0	0	25	0	12.5	0	37.5	0	25
Irregular cycles (%)	0	37.5	25	37.5	12.5	25	37.5	50	50	37.5
Cessation of cycle (%)	0	62.5	75	37.5	87.5	62.5	62.5	12.5	50	37.5
Total number of newborns (n)	51	37	39	47	41	45	38	49	41	51
Mean litter size (n)	10.2 ± 1.5	$7.4 \pm 1.3^*$	7.8 ± 2.1	9.4 ± 1.0	8.2 ± 0.6	9 ± 1.1	7.6 ± 0.9	$9.8 \pm 1.7^*$	8.2 ± 2.1	$10.2 \pm 1.6^*$
Gross survival rate (%)	100	95.1	89.7	91.7	92.6	93.3	94.7	98.0	95.1	96.1

duration of treatment and differed significantly in groups treated with hUCMSCs for 1 month or 2 weeks (the MI-u1m group *vs.* the MI-u2w group, $p < 0.05$; the IV-u1m group *vs.* the IV-u2w group, $p < 0.05$) (Figure 5A-B). The levels of progesterone in the IV-u2w, IV-u1m, and MI-u1m groups increased significantly compared to the corresponding groups treated with PBS. Similar to estrogen, progesterone levels did not differ in the MI-u2w group or MI-p2w group.

3.5. hUCMSCs restored the estrous cycle and reproductive performance

All mice in the NC group exhibited a regular 4-5-d estrous cycle and each phase of the estrous cycle had a normal length. Once the model was created, the mice displayed a prolonged estrous cycle with a significant increase in the duration of the metaestrus phase; 37.5% of mice had irregular cycles and 62.5% had cycles that ceased. Two weeks or 1 month after hUCMSC treatment, a significantly higher percentage of mice in the IV-u2w (25%), MI-u2w (12.5%), IV-u1m (37.5%), and MI-u1m (25%) groups had regular cycles compared to the corresponding groups treated with PBS, *i.e.* the IV-p2w (0%), MI-p2w (0%), IV-p1m (0%), and MI-p1m (0%) groups. Mice treated with hUCMSCs for 1 month were compared to those treated with hUCMSCs for 2 weeks. Results revealed that the percentage of mice with a

regular cycle increased with the duration of hUCMSC treatment, regardless of the method of transplantation (Table 2). The decline in fertility and fecundity is the most obvious outcome of ovarian aging, so the mean litter size and mean number of litters were analyzed in both groups after 4 months of breeding. Both the number of newborns per litter and the total number of litters decreased markedly in the Mod group (7.4 ± 1.3; 37) compared to those in the NC group (10.2 ± 1.5; 51). The pregnancy rate did not decrease significantly in any group (Table 2). Moreover, no external morphological abnormalities were noted in the offspring of the groups. Mice treated with hUCMSCs for 2 months had similar numbers of litters and numbers of newborns per litter compared to their counterparts, which suggests that short-term transplantation of hUCMSCs does affect the reproductive performance of mice. When female mice were treated with hUCMSCs for 1 month and mated with normal males of proven fertility, those females were significantly more fertile than the female controls. The number of newborns per litter and the total number of litters increase in the IV-u1m (9.8 ± 1.7, 49) and MI-u1m (10.2 ± 1.6, 51) groups in comparison to those in the IV-p1m (7.6 ± 0.9, 38) and MI-p1m (8.2 ± 2.1, 41) groups, which suggests that 1 month of treatment may be more suitable to restore fertility ($p < 0.05$) (Table 2). In addition, the pregnancy rate and survival rate were similar among the groups.
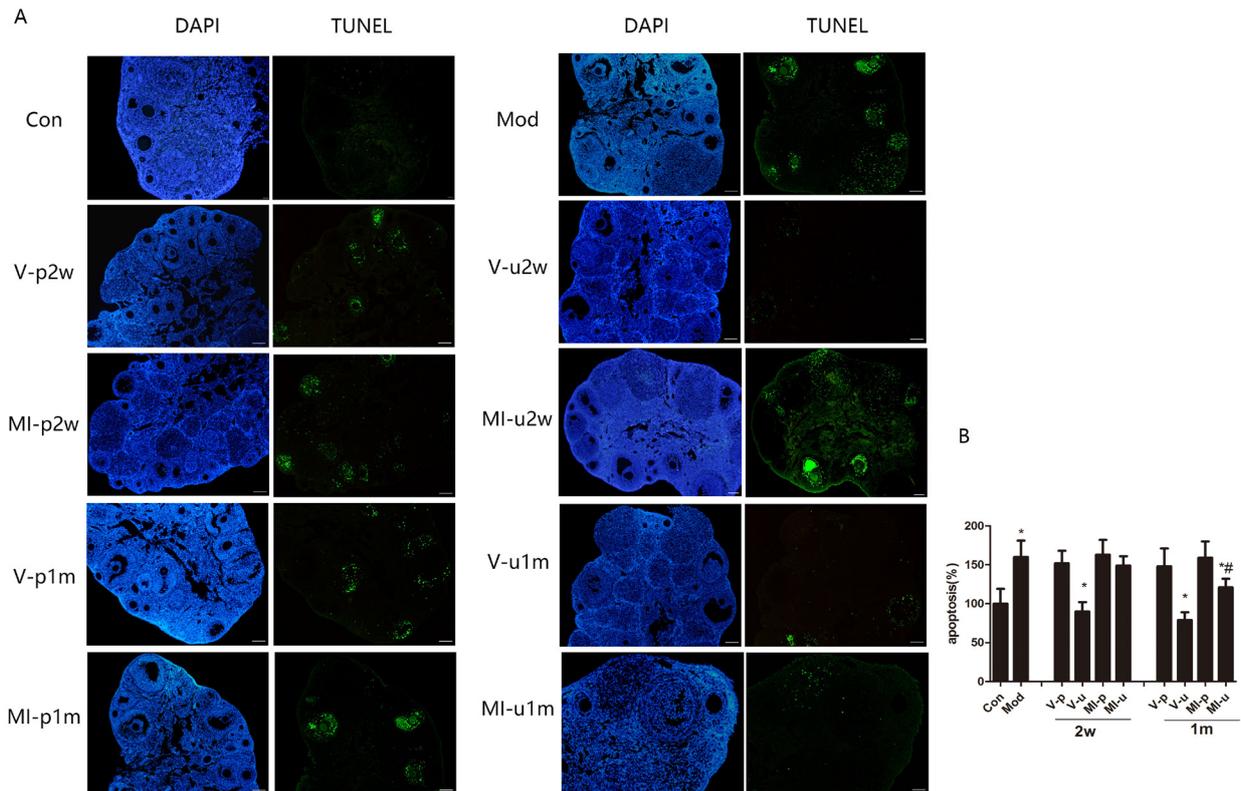
Figure 6. Apoptosis in the ovaries decreased after hUCMSC treatment. (A) Representative images of ovarian tissue obtained from all groups of mice. Data from 2 weeks and 1 month after hUCMSC treatment indicate that apoptosis was attenuated by the transplantation of hUCMSCs. Bar = 50 μm. **(B)** The rate of GC apoptosis in each group. Values are expressed as the mean ± SD. The * symbol represents the Mod group versus the NC group or groups treated with hUCMSCs versus corresponding groups treated with PBS, *p < 0.05; The # symbol represents the MI-u1m group versus the MI-u2w group, #p < 0.05.

3.6. hUCMSCs reduced the apoptosis of granulosa cells

Once the model was created, granulosa cells and other cells in the ovaries experienced dramatic apoptosis. Blue staining in the ovaries indicates the nucleus and green staining indicates TUNEL-positive GCs. The apoptosis of GCs in the Mod group was almost 1.5-fold of that in the NC group. Two weeks and 1 month after hUCMSC transplantation, the percentage of TUNEL-positive GCs in these 2 treated groups was significantly lower than that in groups treated with PBS, as shown in Figure 6A-B. The number of apoptotic GCs decreased after hUCMSC treatment (the IV-u2w group *vs.* the IV-p2w group, $p <$ 0.05; the IV-u1m group *vs.* the IV-p1m group, $p < 0.05$; the MI-u1m group *vs.* the MI-p1m group, $p < 0.05$). The percentage of apoptotic cells decreased in the MI-u1m group compared to that in the MI-u2w group ($p < 0.05$) but did not differ significantly in the MI-u2w group or the MI-p2w group. Values are expressed as the mean ± SEM.

3.7. hUCMSCs restored ovarian function via antioxidant and anti-apoptotic enzymes

Gene expression in the groups treated with hUCMSCs was compared to that in the groups treated PBS, revealing that some genes that regulate antioxidant and

anti-apoptotic action were altered. The groups treated with hUCMSCs expressed more SOD2, CAT, and Bcl2 mRNA and less Bax mRNA than did the groups treated with PBS (Figure 7). Levels of mRNA expression of some genes (SOD2 and Bcl2) were significantly higher in the IV-u1m group than in the MI-u1m group but those levels did not differ significantly in the IV-p1m group or the MI-p1m group (Figure 7A, D). The level of expression Bcl2 mRNA was much higher in the IV-u2w group than in the MI-u2w group ($p < 0.05$), as shown in Figure 7 D.

The level of protein expression was examined, revealing a trend like that observed with mRNA levels, as shown in Figure 8. Antioxidant and anti-apoptotic proteins increased and pro-apoptotic proteins decreased in the groups treated with hUCMSCs. hUCMSCs were found to restore ovarian function, and this observed effect was presumably due to high levels of antioxidant and anti-apoptotic enzymes since the ovaries did not form any oocytes or GCs. Hence, this action means that hUCMSCs are suitable for regenerative cell therapy.

4. Discussion

A woman's fertility is known to decline with age. The gradual loss of fertility becomes more prominent after the age of 35 and stops during menopause at a mean age of 50-51 years (*40*). The ovaries have accelerated aging
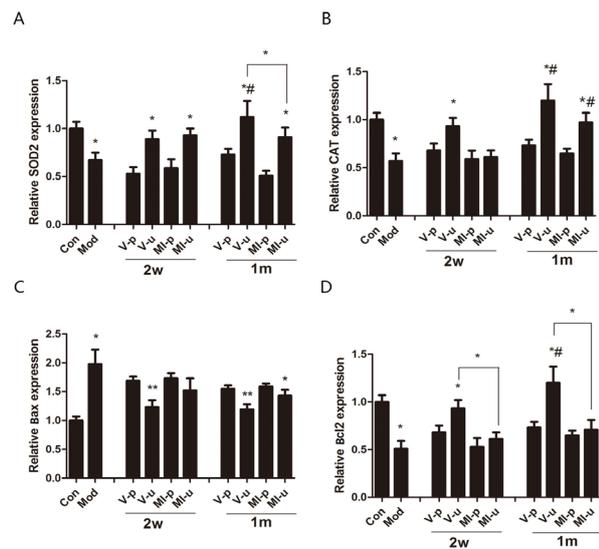
Figure 7. Effects of hUCMSCs on expression of mRNA of genes coding for antioxidant and anti-apoptotic enzymes in ovaries. Relative levels of expression of the genes SOD2 **(A)**, CAT **(B)**, Bax **(C)**, and Bcl2 **(D)** were determined using real-time PCR. The level of SOD2, CAT, and Bcl2 expression decreased significantly in the Mod group. After hUCMSC treatment, the expression of mRNA of antioxidant and anti-apoptotic genes increased significantly. Levels of expression increased more in the groups treated with hUCMSCs for 1 month than in those treated with hUCMSCs for 2 weeks. The levels of Bax increased in the Mod group and decreased in the IV-u 2m, IV-u 1m, and MI-u1m groups compared to the corresponding groups treated with PBS. The * symbol indicates the Mod group versus the NC group, groups treated with hUCMSCs versus corresponding groups treated with PBS, the MI-u1m group versus the IV-u1m group, or the MI-u2w group versus the IV-u2w group, *$p < 0.05$, **$p < 0.01$; The # symbol indicates the IV-u1m group versus the IV-u2w group or the MI-u1m group verus the MI-u2w group, #$p < 0.05$.

Figure 8. Effect of hUCMSCs on the expression of antioxidant and anti-apoptotic proteins in mice ovaries. (A) Representative Western blots of SOD2, CAT, Bax, and Bcl2 in the ovaries of mice. **(B-E)** The relative levels of expression of SOD2, CAT, Bax, and Bcl2 protein in each group. The level of expression of SOD2, CAT, and Bcl2 increased and the level of expression of Bax decreased in the IV-u1m, IV-u2w, and MI-u1m groups. The level of protein expression did not differ significantly in the MI-u2w or MI-p2w groups. The * symbol indicates the Mod group versus the NC group, groups treated with hUCMSCs versus corresponding 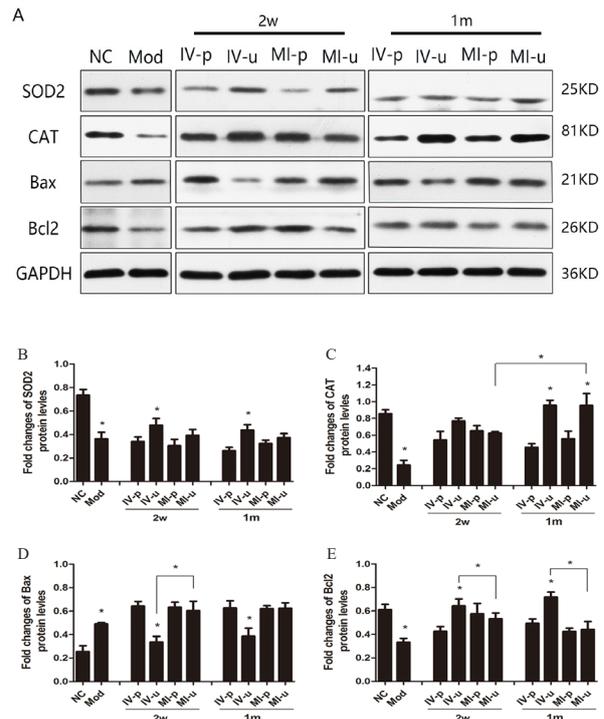groups treated with PBS, the MI-u1m group versus the IV-u1m group, or the MI-u2w group versus the IV-u2w group, *$p < 0.05$.

relative to the aging of other body systems, and ovarian aging is described as a gradual decline in the quantity and quality of ovarian follicles (41). The current study attempted to utilize continuous superovulation via repeated injections of PMSG, hCG, and PGF2α to accelerate the consumption of follicles as well as ozone inhalation to increase oxidative damage to the ovaries in order to create a model of accelerated ovarian in mice.

Once the model of accelerated ovarian aging was created, ovarian reserve diminished and the number of atretic follicles increased. Current evidence suggests that the estradiol level decreases relatively late in the process of ovarian aging and that the plasma level of progesterone does not change significantly (42-44). The current results indicated that the plasma levels of estradiol and progesterone decreased in the Mod group of mice. The estrous cycles of older mice were longer and then the capacity for maintaining cycles finally disappeared. Most of the vaginal lavages from acyclic mice were leukocytic (i.e. diestrus or metaestrus) (45). In the current study, the percentage of mice in the Mod group with irregular cycles and cycles that ceased increased markedly with a decrease in plasma levels

of estradiol and progesterone. Menstrual changes are therefore considered to be an early manifestation of ovarian dysfunction. A decrease in the follicle count with age indicates the onset of cycle irregularity and the final cessation of menses (46,47), which is the final step in the process of ovarian aging. Moreover, the corresponding age-related decline in oocyte quality is widely known to be a major impetus for low pregnancy rates in aging females. In the current study, fertility and fecundity declined markedly in the Mod group of mice.

The current results indicated that the plasma levels of estradiol and progesterone increased in the group treated with hUCMSCs for 1 month and the IV-u2w group. This finding may be due to the increase in normal healthy antral follicles and the decrease in atretic follicles. The percentage of regular cycles also increased after hUCMSC transplantation. A higher percentage of mice treated with hUCMSCs for 1 month exhibited regular cycles and higher numbers of newborns per litter. The current results indicated that transplantation via injection in the tail vein and treatment for 1 month are more suitable for restoration of ovarian function. In this study, both methods of transplantation yielded satisfactory results in terms

of restoring ovarian function, although these two approaches did differ significantly in some respects. Intravenous injection has several advantages over in situ ovarian micro injection. Intravenous injection is generally less invasive, it has more marked effects, and it can more effectively restore ovarian function.

After hUCMSC treatment, ovarian function in mice recovered as expected, although transplanted cells did not develop into follicle components. Apoptosis is likely to be a relevant mechanism in the process of ovarian aging (*48-50*). Previous studies have shown that stem cells can inhibit apoptosis through secretion of stanniocalcin-1 and paracrine factors and they can enhance the oxidative stress response pathway. Apoptosis generally increases to a very high level when mice are subjected to oxidative stress. After hUCMSC treatment, the number of TUNEL-positive cells decreased significantly, indicating that hUCMSCs can reduce apoptosis caused by superovulation and oxidative stress.

Reactive oxygen species (ROS) are considered to be an underlying factor for aging and may initiate aging by causing oxidative damage (*51*). Increased levels of endogenous ROS and diminished antioxidant defenses lead to a wide range of cellular oxidative damage, which includes a subsequent decrease in ovarian quality. The current results also indicated that ovarian expression of SOD2 and CAT decreased considerably compared to that in the NC group. After hUCMSC transplantation, expression of SOD2 and CAT increased in all groups except the MI-u 2w group. In the IV-u1m group of mice, the expression of SOD2 and CAT was markedly higher than that in the IV-u2w and MI-u1m groups. Thus, the observed effect was most probably due to enhanced expression of genes coding for antioxidant and anti-apoptotic enzymes.

Over the past few years, human MSCs have been extensively studied in clinical trials to treat various conditions such as neurological diseases, cardiovascular diseases, immune diseases, gastrointestinal diseases, and blood diseases. However, only a few studies have determined an optimal method for stem cell transplantation, at least in the field of reproductive medicine. The current study compared 2 general forms of stem cell therapy and findings revealed that IV, which is widely used in clinical settings, is more suitable to restoring ovarian function. Recent clinical studies have suggested that traditional Chinese medicines such as Kuntai capsules can effectively alleviate clinical symptoms, increase levels of estrogen, and decrease levels of follicle-stimulating hormone (FSH) and luteinizing hormone (LH) in the women with diminished ovarian reserve or premature ovarian failure (*52,53*). Traditional Chinese medicines are usually taken orally. Nonetheless, IV may be the best route for administration of traditional Chinese medicines. Regardless, a better understanding and proper use of hUCMSCs may offer hope to women with aging ovaries who wish to conceive.

References

1. Broekmans FJ, Knauff EA, te Velde ER, Macklon NS, Fauser BC. Female reproductive ageing: Current knowledge and future trends. Trends Endocrinol Metab. 2007; 18:58-65.
2. Djahanbakhch O, Ezzati M, Zosmer A. Reproductive ageing in women. J Pathol. 2007; 211:219-231.
3. Hansen KR, Knowlton NS, Thyer AC, Charleston JS, Soules MR, Klein NA. A new model of reproductive aging: The decline in ovarian non-growing follicle number from birth to menopause. Hum Reprod. 2008; 23:699-708.
4. McGee EA, Hsueh AJ. Initial and cyclic recruitment of ovarian follicles. Endocr Rev. 2000; 21:200-214.
5. Markström E, Svensson ECh, Shao R, Svanberg B, Billig H. Survival factors regulating ovarian apoptosis – dependence on follicle differentiation. Reproduction. 2002; 123:23-30.
6. te Velde ER, Pearson PL. The variability of female reproductive ageing. Hum Reprod Update. 2002; 8:141-154.
7. Block E. A quantitative morphological investigation of the follicular system in newborn female infants. Acta Anat (Basel). 1953; 17:201-206.
8. Alviggi C, Humaidan P, Howles CM, Tredway D, Hillier SG. Biological versus chronological ovarian age: Implications for assisted reproductive technology. Reprod Biol Endocrinol. 2009; 7:101.
9. te Velde ER, Scheffer GJ, Dorland M, Broekmans FJ, Fauser BC. Developmental and endocrine aspects of normal ovarian aging. Mol Cell Endocrinol. 1998; 145:67-73.
10. Faddy MJ, Gosden RG, Gougeon A, Richardson SJ, Nelson JF. Accelerated disappearance of ovarian follicles in mid-life: Implications for forecasting menopause. Hum Reprod. 1992; 7:1342-1346.
11. Sohal RS. Role of oxidative stress and protein oxidation in the aging process. Free Radic Biol Med. 2002; 33:37-44.
12. Tarín JJ.. Aetiology of age–associated aneuploidy: A mechanism based on the 'free radical theory of ageing'. Hum Reprod. 1995; 10:1563-1565.
13. Tarín JJ. Potential effects of age-associated oxidative stress on mammalian oocytes/embryos. Mol Hum Reprod. 1996; 2:717-724.
14. Tamura H, Takasaki A, Miwa I, Taniguchi K, Maekawa R, Asada H, Taketani T, Matsuoka A, Yamagata Y, Shimamura K, Morioka H, Ishikawa H, Reiter RJ, Sugino N. Oxidative stress impairs oocyte quality and melatonin protects oocytes from free radical damage and improves fertilization rate. J Pineal Res. 2008; 44:280-287.
15. Liu L, Keefe DL. Cytoplasm mediates both development and oxidation-induced apoptotic cell death in mouse

zygotes. Biol Reprod. 2000; 62:1828-1834.

16. Liu L, Trimarchi JR, Keefe DL. Involvement of mitochondria in oxidative stress-induced cell death in mouse zygotes. Biol Reprod. 2000; 62:1745-1753.

17. Lass A, Skull J, McVeigh E, Margara R, Winston RM. Measurement of ovarian volume by transvaginal sonography before ovulation induction with human menopausal gonadotrophin for in-vitro fertilization can predict poor response. Hum Reprod. 1997; 12:294-297.

18. Nabhan SK, Bitencourt MA, Duval M, *et al*. Fertility recovery and pregnancy after allogeneic hematopoietic stem cell transplantation in Fanconi anemia patients. Haematologica. 2010; 95:1783-1787.

19. Nagano M, Kimura K, Yamashita T, Ohneda K, Nozawa D, Hamada H, Yoshikawa H, Ochiai N, Ohneda O. Hypoxia responsive mesenchymal stem cells derived from human umbilical cord blood are effective for bone repair. Stem Cells Dev. 2010;19:1195-1210.

20. Bieback K, Kern S, Klüter H, Eichler H. Critical parameters for the isolation of mesenchymal stem cells from umbilical cord blood. Stem Cells 2004 ;22:625-634.

21. Ciavarella S, Dominici M, Dammacco F, Silvestris F. Mesenchymal stem cells: A new promise in anticancer therapy. Stem Cells Dev. 2011;20:1-10.

22. Fong CY, Chak LL, Biswas A, Tan JH, Gauthaman K, Chan WK, Bongso A. Human Wharton's jelly stem cells have unique transcriptome profiles compared to human embryonic stem cells and other mesenchymal stem cells. Stem Cell Rev. 2011;7:1-16.

23. Wang S, Yu L, Sun M, Mu S, Wang C, Wang D, Yao Y. The therapeutic potential of umbilical cord mesenchymal stem cells in mice premature ovarian failure. Biomed Res Int. 2013; 2013:690491.

24. Liu T, Huang Y, Guo L, Cheng W, Zou G. CD44^{+}/CD105^{+} human amniotic fluid mesenchymal stem cells survive and proliferate in the ovary long-term in a mouse model of chemotherapy-induced premature ovarian failure. Int J Med Sci. 2012; 9:592-602.

25. Takehara Y, Yabuuchi A, Ezoe K, Kuroda T, Yamadera R, Sano C, Murata N, Aida T, Nakama K, Aono F, Aoyama N, Kato K, Kato O. The restorative effects of adipose-derived mesenchymal stem cells on damaged ovarian function. Lab Invest.. 2013; 93:181-193.

26. Liu T, Huang Y, Zhang J, Qin W, Chi H, Chen J, Yu Z, Chen C. Transplantation of human menstrual blood stem cells to treat premature ovarian failure in mouse model. Stem Cells Dev. 2014; 23:1548-1557.

27. Miyamoto K, Sato EF, Kasahara E, Jikumaru M, Hiramoto K, Tabata H, Katsuragi M, Odo S, Utsumi K, Inoue M. Effect of oxidative stress during repeated ovulation on the structure and functions of the ovary, oocytes, and their mitochondria. Free Radic Biol Med. 2010; 49:674-681.

28. Rivas-Arancibia S, Guevara-Guzman R, Lopez-Vidal Y, Rodriguez-Martinez E, Zanardo-Gomes M, Angoa-Perez M, Raisman-Vozari R. Oxidative stress caused by ozone exposure induces loss of brain repair in the hippocampus of adult rats. Toxicol Sci. 2010; 113:187-197.

29. Feng R, He W, Ochi H. A new murine oxidative stress model associated with senescence. Mech Ageing Dev. 2001; 122:547-559.

30. Qi S, Wu D. Bone marrow-derived mesenchymal stem cells protect against cisplatin-induced acute kidney injury in rats by inhibiting cell apoptosis. Int J Mol Med.

2013,32:1262-1272.

31. Park JH, Hwang I, Hwang SH, Han H, Ha H. Human umbilical cord blood-derived mesenchymal stem cells prevent diabetic renal injury through paracrine action. Diabetes Res Clin Pract. 2012;98:465-473.

32. Latifpour M, Nematollahi-Mahani SN, Deilamy M, Azimzadeh BS, Eftekhar-Vaghefi SH, Nabipour F, Najafipour H, Nakhaee N, Yaghoubi M, Eftekhar-Vaghefi R, Salehinejad P, Azizi H. Improvement in cardiac function following transplantation of human umbilical cord matrix-derived mesenchymal cells. Cardiology. 2011;120:9-18.

33. Chang YS, Choi SJ, Ahn SY, Sung DK, Sung SI, Yoo HS, Oh WI, Park WS. Timing of umbilical cord blood derived mesenchymal stem cells transplantation determines therapeutic efficacy in the neonatal hyperoxic lung injury. PLoS One. 2013;8:e52419.

34. Tilly JL. Ovarian follicle counts - not as simple as 1, 2, 3. Reprod Biol Endocrinol. 2003; 1:11.

35. Marcondes FK, Bianchi FJ, Tanno AP. Determination of the estrous cycle phases of rats some helpful considerations. Braz J Biol. 2002; 62:609-614.

36. Schedin P, Mitrenga T, Kaeck M. Estrous cycle regulation of mammary epithelial cell proliferation, differentiation, and death in the Sprague-Dawley rat: A model for investigating the role of estrous cycling in mammary carcinogenesis. J Mammary Gland Biol Neoplasia. 2000; 5:211-225.

37. Yang S, Wang S, Luo A, *et al*. Expression patterns and regulatory functions of microRNAs during the initiation of primordial follicle development in the neonatal mouse ovary. Biol Reprod. 2013; 89:126.

38. Aerts JL, Christiaens MR, Vandekerckhove P. Evaluation of progesterone receptor expression in eosinophils using real-time quantitative PCR. Biochim Biophys Acta. 2002; 1571:167-172.

39. Zhang J, Fang L, Lu Z, Xiong J, Wu M, Shi L, Luo A, Wang S. Are sirtuins markers of ovarian aging? Gene. 2016; 575:680-686.

40. Perheentupa A, Huhtaniemi I. Aging of the human ovary and testis. Mol Cell Endocrinol. 2009; 299:2-13.

41. Younis JS. Ovarian aging and implications for fertility female health. Minerva Endocrinol. 2012; 37:41-57.

42. Mersereau JE, Evans ML, Moore DH, Liu JH, Thomas MA, Rebar RW, Pennington E, Cedars MI. Luteal phase estrogen is decreased in regularly menstruating older women compared with a reference population of younger women. Menopause. 2008; 15:482-486.

43. Lee SJ, Lenton EA, Sexton L, Cooke ID. The effect of age on the cyclical patterns of plasma LH, FSH, oestradiol and progesterone in women with regular menstrual cycles. Hum Reprod. 1988; 3:851-855.

44. Muttukrishna S, Child T, Lockwood GM, Groome NP, Barlow DH, Ledger WL. Serum concentrations of dimeric inhibins, activin A, gonadotrophins and ovarian steroids during the menstrual cycle in older women. Hum Reprod. 2000; 15:549-556.

45. Nelson JF, Gosden RG, Felicio LS. Effect of dietary restriction on estrous cyclicity and follicular reserves in aging C57BL/6J mice. Biol Reprod. 1985; 32:515-522.

46. Broekmans FJ, Soules MR, Fauser BC. Ovarian aging: Mechanisms and clinical consequences. Endocr Rev. 2009; 30:465-493.

47. Soules MR, Sherman S, Parrott E, Rebar R, Santoro N, Utian W, Woods N. Executive summary: Stages of

Reproductive Aging Workshop (STRAW). Climacteric. 2001; 4:267-272.

48. Souidi N SM, Seifert M. Ischemia-reperfusion injury: Beneficial effects of mesenchymal stromal cells. Curr Opin Organ Transplant. 2013;18:34-43.

49. Lin H, Xu R, Zhang Z, Chen L, Shi M, Wang FS. Implications of the immunoregulatory functions of mesenchymal stem cells in the treatment of human liver diseases. Cell Mol Immunol. 2011;8:19-22.

50. Yan Y, Xu W, Qian H, Si Y, Zhu W, Cao H, Zhou H, Mao F. Mesenchymal stem cells from human umbilical cords ameliorate mouse hepatic injury *in vivo*. Liver Int. 2009;29:356-365.

51. Harman D. The free radical theory of aging. Antioxid Redox Signal. 2003; 5:557-561.

52. Chen JM, Gao HY, Ding Y, Yuan X, Wang Q, Li Q, Jiang GH. Efficacy and safety investigation of Kuntai capsule for the add-back therapy of gonadotropin releasing hormone agonist administration to endometriosis patients: a randomized, double-blind, blank- and tibolone-controlled study. Chin Med J (Engl). 2015;128:427-432.

53. Liu, CQ, Qin ZX, Jiang FF, Hong T, Wang F. Kuntai capsule combined with gonadotropin releasing hormone agonist in treatment of moderate-severe endometriosis: A clinical observation. Zhongguo Zhong Xi Yi Jie He Za Zhi. 2014; 34:1288-1291. (in Chinese)

Original Article

DHEA prevents bone loss by suppressing the expansion of CD4^{+} T cells and TNFa production in the OVX-mouse model for postmenopausal osteoporosis

Na Zhang[1,2,3,*], Yuyan Gui[1,2,3,*], Xuemin Qiu[1,2,3], Wei Tang[4], Lisha Li[1,2,3], Hans-Jürgen Gober[5], Dajin Li[1,2], Ling Wang[1,2,3,**]

[1] *Laboratory for Reproductive Immunology, Hospital & Institute of Obstetrics and Gynecology, IBS, Fudan University Shanghai Medical College, Shanghai, China;*
[2] *The Academy of Integrative Medicine of Fudan University, Shanghai, China;*
[3] *Shanghai Key Laboratory of Female Reproductive Endocrine Related Diseases, Shanghai, China;*
[4] *Department of Surgery, Graduate School of Medicine, the University of Tokyo, Tokyo, Japan;*
[5] *Department of Pharmacy, Wagner Jauregg Hospital and Children's Hospital, Linz, Austria.*

Summary   **Recent studies have suggested that dehydroepiandrosterone (DHEA) might serve as a form of immunomodulatory therapy for postmenopausal osteoporosis (PMO). The current study investigated the effects of DHEA administration on ovariectomy (OVX)-induced bone loss and its corresponding immunological changes. Adult OVX mice were treated with DHEA or 17-β-estradiol (E2) for 12 weeks, with or without the aromatase inhibitor letrozole. DHEA improved bone mass after OVX and displayed action like that of E2 with regard to decreasing osteoclast-related parameters. DHEA also suppressed an OVX-induced increase in CD4^{+} T cell subsets and TNF-α production. However, DHEA elevated serum E2 levels to a lesser extent than E2. Although letrozole decreased serum E2 levels in OVX mice treated with DHEA, it did not alter DHEA's effects on corresponding immunological changes due to OVX. In conclusion, DHEA may prevent bone loss by suppressing the OVX-induced expansion of CD4^{+} T cells and TNF-α production in mice, independent of E2.**

Keywords: Dehydroepiandrosterone, postmenopausal osteoporosis, CD4^{+} T cells, TNF-α

1. Introduction

Several epidemiologic trials have revealed a strong inverse correlation between levels of sex steroid hormones, such as dehydroepiandrosterone (DHEA) and estrogen, and the occurrence of several well-known geriatric syndromes, such as osteoporosis and cardiovascular disease (*1,2*). DHEA and its sulfate ester, DHEA sulfate (DHEAS), are the most abundant circulating hormones produced by the adrenal gland, and levels of these hormones decrease with age, sometimes decreasing to 10-20% of the levels found in young individuals (*3*). This age-related decrease has been called the "adrenopause" phenomenon. The decrease in DHEA in the elderly is more marked than the decrease in other hormones.

DHEA and DHEAS are both pre-hormones (*4*). However, only DHEA can be converted into more potent androgens and estrogens in peripheral tissues, while DHEAS is maintained as a circulating stock (*3*). In premenopausal women, 50-75% of estrogens, and the majority of androgens, are produced from DHEA, while almost all androgens and estrogens are synthesized from it during postmenopause (*5*). Postmenopausal osteoporosis (PMO) is a well-known estrogen deficiency-induced geriatric syndrome and is also a worldwide health problem. It manifests as a progressive systemic skeletal disorder characterized by reduced bone mass that leads to increased bone fragility and fracture risk. DHEA levels may be associated with bone marker levels and DHEA treatment might increase

bone mass (*6,7*). An *in vitro* analysis of primary human osteoblasts indicated that aromatase converts DHEA into estrogen (*8*). Thus, the role of DHEA in regulating bone metabolism in PMO has garnered increasing attention.

Many studies have suggested a beneficial effect of DHEA administration on preventing trabecular bone mineral density (BMD) loss in women with an estrogen deficiency (*8,9*). The current authors have conducted a number of previous studies on the effect of DHEA on bone. DHEA improved bone mass in ovariectomized (OVX) mice and appeared to have greater potential clinical value for the prophylactic and therapeutic treatment of PMO than estrogen (E2) (*10*); DHEA improved murine osteoblast growth *via* the mitogen-activated protein kinase (MAPK) signaling pathway, independent of either androgen receptors or estrogen receptors (*11*); DHEA protected OVX rabbits from atherosclerosis by alleviating inflammatory injury in endothelial cells (*12*); and DHEA promoted osteoblast differentiation by regulating the expression of osteoblast-related genes and Foxp3^{+} regulatory T cells in mice (*13*). However, what is still unclear is how DHEA affects other immune cells that may play a role in bone metabolism and whether DHEA regulates the immune cells only through its hormonal end products or as a result of its direct action through certain receptors.

Recent studies have reported an association between pathogenetic changes due to PMO and disturbances in the endocrine-immune network. Some researchers have contended that PMO can be classified as an inflammatory condition (*14*). Skeletal system homeostasis is greatly influenced by endocrine as well as immune factors (*15*). After menopause, diminished ovarian function has a deleterious effect on bone metabolism. Estrogen has been also known to regulate the functions of the immune system and T cells. Increased proliferation of activated T cells, and their longer lifespan, in OVX mice results in an expansion of the T cell pool in bone marrow (*16*). Bone loss has been induced in nude mice by OVX and it has been restored by transferring wild-type T cells into nude mice (*17*), and depletion of T cells by treatment with anti-CD4/CD8 antibodies protects mice from bone loss due to OVX (*18*). These findings indicate that T cells may play an essential role in the development of PMO. Immunophenotypical analyses of peripheral blood lymphocytes in osteoporotic patients suggested an increase in several subsets of T lymphocytes, including CD4^{+} T cells (*19*). OVX may also up-regulate TNF-α production, which is the most potent stimulator of osteoclastogenesis when estrogen is depleted (*20*). Moreover, CD4^{+} T cells secrete TNF-α and receptor activator for nuclear factor-κ B ligand (RANKL), which is an osteoclastogenic mediator (*21*). Therefore, enhancing the endocrine-immune network appears to positively modulate bone metabolism in PMO.

Various positive immunologic actions of DHEA

have been noted in various human diseases and animal models (*22-24*). These findings, coupled with the fact that DHEA promotes additional factors that modulate BMD in postmenopausal women, emphasizes the need for more information concerning the potential beneficial impact of DHEA on the interplay between the immune and skeletal systems. The current study investigated the effects of DHEA administration, with or without an aromatase inhibitor, on bone morphometry, E2 levels, CD4^{+} T cell expansion, and TNF-α production in OVX mice in order to determine the potential value of DHEA as a therapy for PMO and its mechanism of action.

2. Materials and Methods

2.1. *Reagents and chemicals*

Mouse lymphocytes from bone marrow and the spleen were cultured in complete RPMI-1640 medium (Wisent Inc., St-Bruno, QC, Canada) supplemented with 10% fetal bovine serum (FBS), penicillin (500 U/mL), and streptomycin (500 mg/mL). Saline, DHEA, 17-β-estradiol, letrozole, calcein, hematoxylin and eosin, and a tartrate-resistant acid phosphatase (TRAP) staining kit and a von Kossa staining kit were purchased from Sigma-Aldrich (St. Louis, MO, USA). A toluidine blue staining solution was purchased from Leagene, Inc. (Beijing, China). An estradiol (E2) enzyme immunoassay (EIA) kit was purchased from BioCheck Inc. (Burlingame, CA, USA). A TNF-α enzyme-linked immunosorbent assay (ELISA) kit was purchased from R&D Systems (Minneapolis, MN, USA). FITC-conjugated anti-mouse CD3, PE-conjugated anti-mouse CD4, and PE-CY5-conjugated anti-mouse CD8a antibodies were purchased from BD Biosciences (Mississauga, ON, CA). Magnetic beads coated with anti-mouse CD4 antibody were supplied by Miltenyi Biotech (Auburn, CA, USA). Trizol was purchased from GIBCO-BRL, Invitrogen Corp. (Carlsbad, CA, USA). A Revert AidTM H Minus first strand cDNA synthesis kit was obtained from Fermentas (St. Leon-Rot, Germany). A Light Cycler 480 SYBER Green I Master was supplied by Roche Diagnostics Pvt., Ltd. (Mumbai, India).

2.2. *Creation of an animal model of PMO and in vivo experiments*

Animal experiments were performed in accordance with the Principles of Laboratory Animal Care (National Institutes of Health publication number 85-23, revised 1985). The animals used were 64 female BALB/c mice, 8 weeks old, with a body mass of between 20 and 30 g, that were purchased from the Laboratory Animal Facility of the Chinese Academy of Sciences (Shanghai, China).

In the first *in vivo* experiment, 24 mice were randomly divided into four groups. The sham group (5 mice) underwent surgery without an ovariectomy.

One week after surgery, the mice were treated with a vehicle (gum acacia in distilled water) daily. A bilateral oophorectomy was performed on 19 mice. During the experimental period, 4 mice died during the administration of anesthesia, but there were no deaths due to other causes. The mice that died were excluded from analysis. One week after OVX, the mice were then randomly divided into 3 groups (OVX, OVX + DHEA, and OVX + E2; n = 5 per group).

The OVX control group was intragastrically administered saline (n = 5), the OVX + DHEA group was intragastrically administered 5 mg/kg per day of DHEA (n = 5) (*10*), and the OVX + E2 group was intragastrically administered estrogen (17-β-estradiol, E2) (100 μg/kg per day, n = 5) (*10,11,21*) daily. Twelve weeks after treatment, all mice were weighed, sacrificed after the final treatment, and blood and tissue samples were harvested for further investigation. A successful ovariectomy was confirmed in all OVX animals by observing the lack of ovarian tissue and atrophied uterine horns.

An additional *in vivo* experiment was performed to determine whether DHEA acted *via* an estrogen derivative or metabolite. A bilateral oophorectomy was performed on 40 mice; 20 were then treated with saline while the other 20 were treated with DHEA. OVX mice treated with saline or OVX mice treated with DHEA were then divided into the following 4 treatment groups: a group receiving the carrier solvent, and 3 groups receiving a 0.04, 0.2, or 2-μg/d injection of the aromatase inhibitor letrozole for 3 months (n = 5, all groups). Letrozole was dissolved in 0.1 mL of 0.3% hydroxyl propyl cellulose and given as a subcutaneous injection. Letrozole doses were selected as previously described (*25*).

2.3. *Analysis of bone mineral density*

To determine bone mineral density, the left femur and lumbar vertebrae were isolated after dissection. Dual energy X-ray absorptiometry (DEXA) was performed using an animal PIXImus densitometer (Lunar; GE Copr.). A consistent region of interest (the distal 4 mm of the femur) was selected to maintain uniformity during the analysis of samples.

2.4. *Bone histomorphometric analysis*

All bone histomorphometric analyses were performed in accordance with a previously described protocol (*26*). Briefly, the left tibia was isolated from each mouse; later, the proximal end was trimmed off and fixed in PBS-buffered 3.7% formaldehyde for 18 hours at 4°C. After incubation in 70% ethanol for 24 h, the undecalcified left proximal tibia was dehydrated in ascending alcohol concentrations, cleared in xylene, and embedded in methyl methacrylate; later, the tibia

was sectioned (5 μm). These sections were stained with toluidine blue and the von Kossa procedure as indicated in a standard protocol (*27*).

The parameters for static and dynamic histomorphometry were quantified using undecalcified proximal tibia sections (5 μm). To evaluate the number of osteoclasts, the decalcified proximal tibia was embedded in paraffin. Serial sections were prepared from paraffin blocks (6 μm thickness) and sections were stained for TRAP activity. The bone volume (BV), osteoblast surface (Ob. S), osteoclast number (Oc. N), bone surface (BS), bone volume/tissue volume (%) (BV/TV), osteoblast surface/bone surface (%) (Ob. S/BS), osteoid surface/bone surface (%) (OS/BS), osteoclast surface/bone surface (%) (Oc. S/BS), osteoclast number/bone perimeter (1/mm) (Oc. N/BP), and eroded surface/bone surface (%) (ES/BS) were measured using the Osteo-Measure Histomorphometry System (Osteometrics, Atlanta, GA, USA) according to standardized protocols. All of these parameters were in accordance with the histomorphometric nomenclature and definitions of the American Society of Bone Mineral Research.

2.5. *Calcein labeling*

To label the sites of active bone formation in mice, double labeling was used, with calcein as a marker (*28*). First, 2.5 mg/mL of calcein was prepared in a 2% solution of sodium bicarbonate. The mice were weighed and injected twice, intraperitoneally, with calcein at a dose of 10 mg/kg body weight at 3-day intervals (*29*). The mice were sacrificed 2 days after the second injection.

Calcein double labeling was verified with fluorescence microscope measurements to determine the mineral apposition rate (MAR) and bone formation rate (BFR), which were evaluated on two nonconsecutive sections for each animal. The double calcein-green labels were measured on bone trabeculae using fluorescence microscopy (Olympus BX-60) with an excitation wavelength of 485 nm and emission wavelength of 510 nm. The mineralizing surface/BS (%) (MS/BS), MAR (μm/day), and BFR ($\mu m^3/\mu m^2$ per year) were measured using the Osteo-Measure Histomorphometry System (Osteometrics, Atlanta, GA, USA) according to standardized protocols. All of these parameters were in accordance with the histomorphometric nomenclature and definitions of the American Society of Bone Mineral Research.

2.6. *Flow cytometry*

After autopsy, bones and spleens were collected and placed in PBS. Bone marrow was flushed out and labeled with fluorescent antibodies for analysis of CD4^{+} T cells. In brief, total lymphocytes were isolated from bone marrow with Hisep LSM 1084 (Himedia) by

means of the density (1.084 ± 0.0010 g/mL) gradient centrifugation technique.

Cells from bone marrow or the spleen were labelled with anti-CD3, CD4, and CD8a antibodies, FITC-conjugated anti-mouse CD3, PE-conjugated anti-mouse CD4, and PE-CY5 conjugated anti-mouse CD8a antibodies to assess the percentage of CD4$^+$ in CD3$^+$ cells. The specificity of immunostaining was ascertained based on the background fluorescence of cells incubated with Ig isotype controls. Fluorescence data from at least 10,000 cells were collected from each sample. Immunostaining was done according to the manufacturer's instructions. FACS Caliber and FACS Arya (BD Biosciences Mississauga, ON, CA) were used to quantify the percentage of CD4$^+$ in CD3$^+$ cells in all groups.

2.7. Isolation of CD4$^+$ T cells from the spleen or bone marrow

Single cell suspensions were obtained from the spleen or bone marrow and incubated with magnetic beads coated with anti-mouse CD4 antibody. CD4$^+$ T cells were isolated according to the manufacturer's instructions. These purified cells were then collected in Trizol for real-time PCR.

2.8. Quantitative real-time PCR

Total RNA was extracted from isolated CD4$^+$ T cells using Trizol. cDNA was synthesized from 1 μg of total RNA with the Revert AidTM H Minus first strand cDNA synthesis kit. SYBR green chemistry was used for quantitative determination of TNF-α and GAPDH mRNAs according to an optimized protocol. The design of the sense and antisense oligonucleotide primers was based on published cDNA sequences using the Universal Probe Library (Roche Diagnostics, USA). The resulting cDNA was used in a PCR reaction using gene-specific primers for TNF-α (5'-TCTTCTCATTCCTGCTTGTGG-3' and 5'-GGTCTGGGCCATAGAACTGA-3') and GAPDH (5'- AGCTTGTCATCAACGGGAAG -3' and 5'- TTTGATGTTAGTGGGGTCTCG -3'). For real-time PCR, the cDNA was amplified with Light Cycler 480 (Roche Diagnostics Pvt., Ltd.). Double-stranded DNA-specific dye SYBR Green I was incorporated into the PCR buffer provided in the Light Cycler 480 SYBER Green I Master to allow for quantitative detection of PCR products in a 20-μL reaction volume. The temperature protocol for the reaction was 95°C for 5 min, 40 cycles of denaturation at 94°C for 2 minutes, annealing and extension at 62°C for 30 seconds, and extension at 72°C for 30 seconds. GAPDH was used to control for differences in RNA isolation, RNA degradation, and the efficiency of reverse transcription.

2.9. Measurement of serum E2 and TNF-α levels

At the end of the experiment, mice were anesthetized and sacrificed. A blood sample was quickly obtained by cardiac puncture. Blood volumes up to 1 mL have frequently been obtained from mice *via* this method. Serum samples were prepared by centrifugation. The serum samples were inactivated at 56°C for 30 minutes and filtered with a 0.2 -μm filter and then stored at -20°C for determination of the levels of E2 and TNF-α. Furthermore, the E2 level in serum samples was measured using an E2 ELISA kit according to the manufacturer's protocol. Serum TNF-α was also measured in all groups using an ELISA kit according to the manufacturer's instructions.

2.10. Statistical analysis

All values are expressed as the mean ± SD. Data were analyzed with aid of the software SPSS, and variance was evaluated using one-way ANOVA. Differences were accepted as significant at $p < 0.05$.

3. Results

3.1. Both DHEA and E2 administration increased BMD in OVX mice

As shown in Figure 1A, a significant decrease in femur and vertebra BMD was noted in OVX mice compared to sham-treated mice ($p < 0.01$, Figure 1). The OVX animals that were administered DHEA or E2 had a significantly higher femur and vertebra BMD compared to the OVX group ($p < 0.01$, Figure 1). Femur and vertebra BMD did not differ significantly in the OVX + DHEA group and the OVX + E2 group ($p > 0.05$, Figure 1).
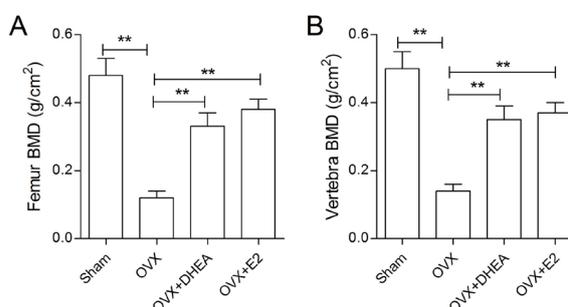
Figure 1. DHEA treatment improved BMD in OVX mice. (A) The sham group ($n = 5$) underwent surgery without an ovariectomy (OVX). OVX mice were treated with saline including 0.1% ethanol daily, 5 mg/kg per day of DHEA, or 100 μg/kg per day of E2 ($n = 5$). All treatments were administered to mice intragastrically. **(A)** Analysis of the BMD of the left femur in different groups. **(B)** Analysis of the BMD of the lumbar vertebrae. Data are expressed as the mean ± SD. *$p < 0.05$, **$p < 0.01$.

3.2. *DHEA reduced the OVX-induced enhancement of osteoclast-mediated bone resorption and improved osteoblast-mediated bone formation*

As expected, OVX significantly increased bone resorption in combination with enhanced bone formation. However, increased bone resorption is superior to enhanced bone formation. Thus, an imbalance in bone transition led to the loss of bone microarchitecture in the OVX group in comparison to the sham-treated group (Figures 2A and 3A). Analysis of dynamic and static bone histomorphometric parameters (*i.e.* Ob. S/BS, OS/BS, MS/BS, MAR, and BFR) indicated an increase in bone formation in the OVX group in comparison to bone formation in the sham group ($p < 0.01$ or $p < 0.05$, Figures 2B and 3B). Twelve weeks of treatment with DHEA increased bone mass and formation (*i.e.* BV/TV, Ob. S/BS, OS/BS, MS/BS, and BFR, $p < 0.01$ for all, Figures 2B and 3B) in comparison to bone mass and formation in the OVX group, thus indicating further
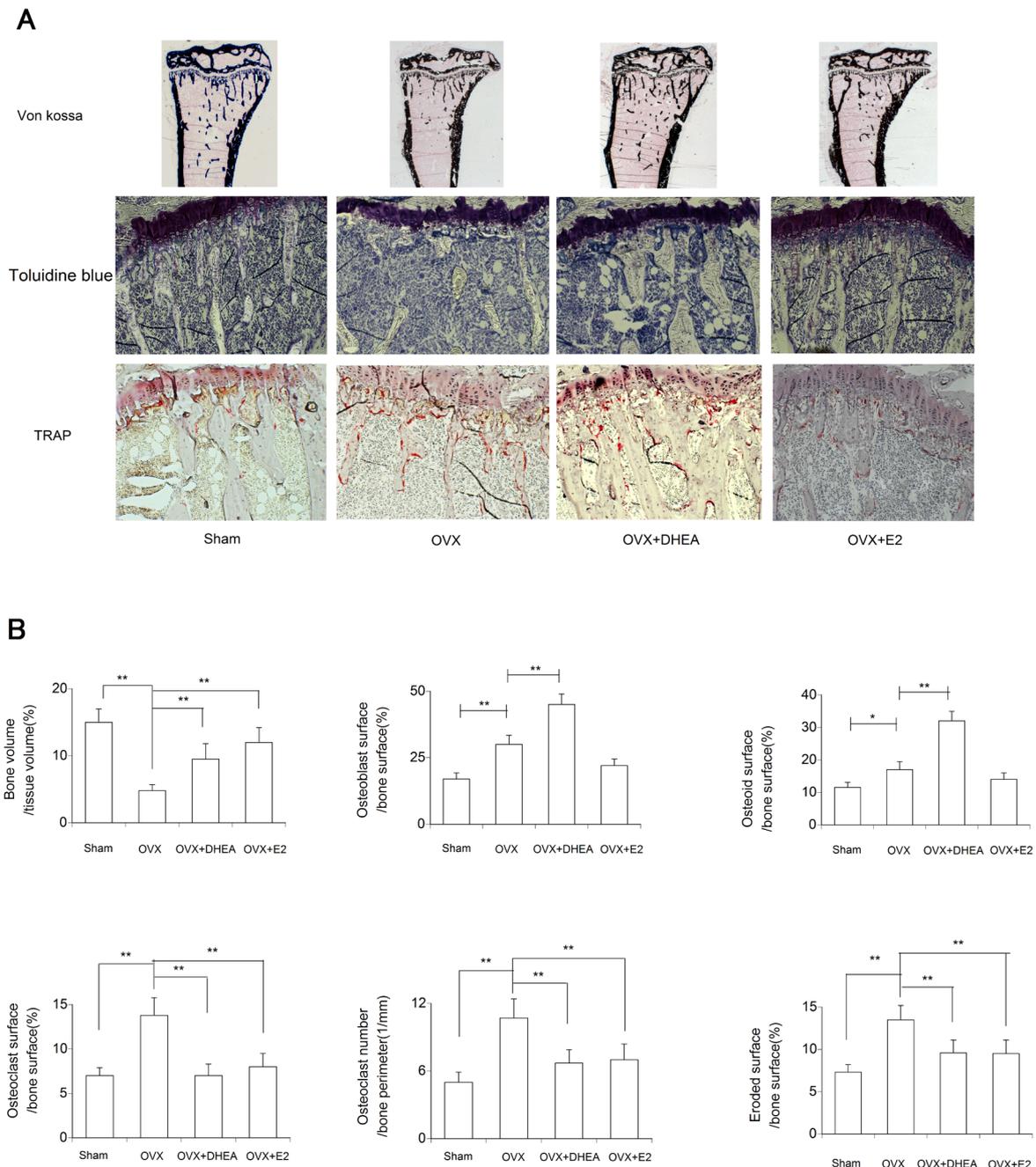
Figure 2. DHEA improved the bone phenotype of OVX mice. Static histological analysis of the proximal tibia in each group. **(A)** The first panels are von Kossa staining, the middle panels are toluidine blue staining, and the panels on the far right are TRAP staining. **(B)** The bone volume/tissue volume (%), osteoblast surface/bone surface (%), osteoid surface/bone surface (%), osteoclast surface/bone surface (%), osteoclast number/bone perimeter (1/mm), and eroded surface/bone surface (%) were measured according to standardized protocols using the Osteo-Measure Histomorphometry System. Data are expressed as the mean ± SD. *$p < 0.05$, **$p < 0.01$.

enhancement of osteoblast differentiation. However, E2 administration did not significantly affect osteoblast-related dynamic bone histomorphometric parameters in comparison to those parameters in the OVX group ($p >$ 0.05, Figures 2B and 3B).

Static histomorphometry confirmed the loss of bone microarchitecture in OVX mice in comparison to sham-treated mice (Figure 2A). Specifically, OVX significantly increased osteoclast-related parameters (*i.e.* Oc. S/BS, Oc. N/BP, and ES/BS) in comparison to

sham treatment ($p < 0.01$ for all, Figure 2B). After 12 weeks of treatment, both DHEA and E2 administration significantly decreased those parameters in comparison to parameters in the OVX group ($p < 0.01$ for all, Figure 2B). Dynamic bone histomorphometry parameters related to bone resorption did not differ significantly in the OVX + DHEA group and the OVX + E2 group ($p >$ 0.05 for all, Figure 2B).

In other words, E2 primarily reduced osteopenia after OVX by decreasing osteoclast-related parameters,
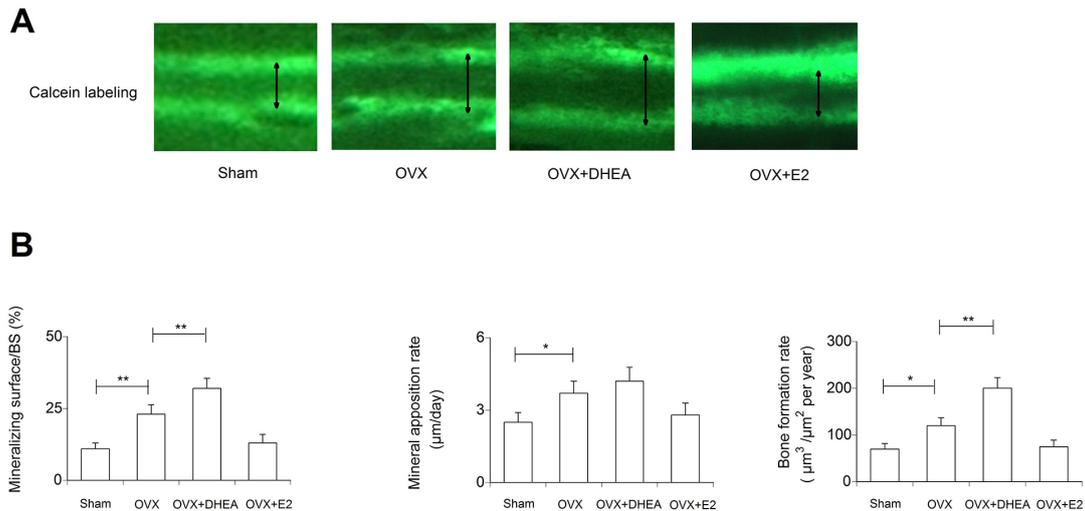
Figure 3. Bone dynamic histomorphometry of the proximal tibia. (A) Calcein double labels were measured on bone trabeculae by fluorescence microscope measurements with an excitation wavelength of 485 nm and emission wavelength of 510 nm for each group. **(B)** To determine the mineralizing surface/BS, mineral apposition rate and bone formation rate, calcein double labeling was analyzed with the Osteo-Measure Histomorphometry System. Data are expressed as the mean ± SD. *$p < 0.05$, **$p < 0.01$.
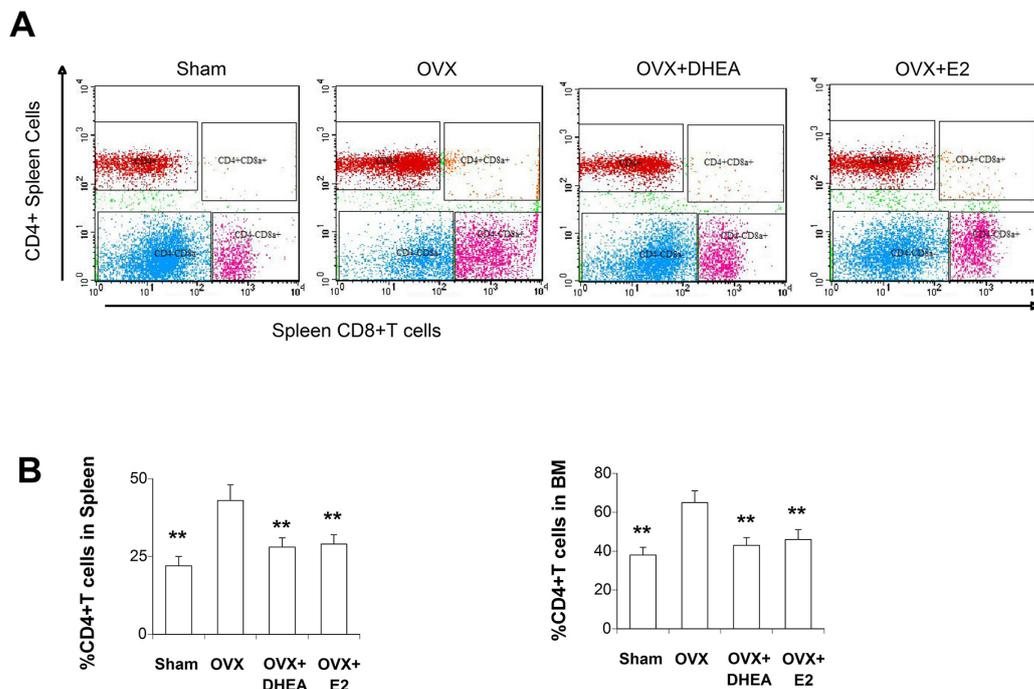
Figure 4. DHEA treatment significantly decreased OVX-induced increases in CD4^{+} T cells subsets in bone marrow and the spleen. Mice were treated as described in Figure 1. **(A)** CD4^{+} T cells in the spleen were quantified using flow cytometry. **(B)** Bar graphs indicate the percentage of CD4^{+} T cells in the spleen or in bone marrow. Data are expressed as the mean ± SD; **$p < 0.01$ compared to the OVX group.

while DHEA alleviated OVX-induced bone loss by inhibiting osteoclast-mediated bone resorption and by improving osteoblast-mediated bone formation. Moreover, DHEA and E2 did not differ significantly in terms of their decreasing osteoclast-related parameters.

3.3. Enhanced TNF-α-production of CD4+ T cells in OVX mice is restored by treatment with either DHEA or E2

To determine whether DHEA treatment affected the endocrine-immune network in PMO, the effects of DHEA on the CD4+ T cells and its production of TNF-α were analyzed. OVX mice treated for 12 weeks had a greater number of CD4+ T cells in bone marrow or the spleen in comparison to the sham group. Treatment of OVX mice with either DHEA or E2 resulted in a significant reduction in the OVX-induced expansion of CD4+ T cells in bone marrow or the spleen in comparison that in the OVX group ($p < 0.01$, Figure 4). However, the OVX-induced expansion of CD4+ T cells did not differ significantly in the OVX + DHEA group and OVX + E2 group ($p > 0.05$, Figure 4).

E2 deficiency is known to increase levels of circulating TNF-α (17,30). The current findings indicated that OVX led to a significant increase in levels of circulating TNF-α ($p < 0.01$, Figure 5A) and levels of TNF-α mRNA in bone marrow CD4+ T cells ($p < 0.01$, Figure 5B) in comparison to levels in the sham group. However, treatment with DHEA or E2 led to a significant reduction in TNF-α production ($p < 0.01$, Figure 5). Results indicated that TNF-α production did not differ significantly in the OVX + DHEA group and the OVX + E2 group ($p > 0.05$, Figure 5).

3.4. DHEA led to a slight elevation of serum E2 levels that was eliminated by the aromatase inhibitor letrozole

The findings above indicated that both DHEA and E2 can prevent bone loss and suppress the OVX-induced expansion of CD4+ T cells and TNF-α production. Given
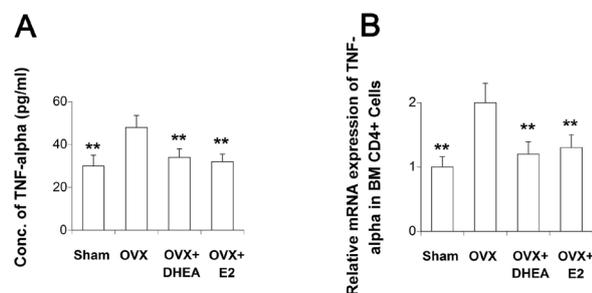
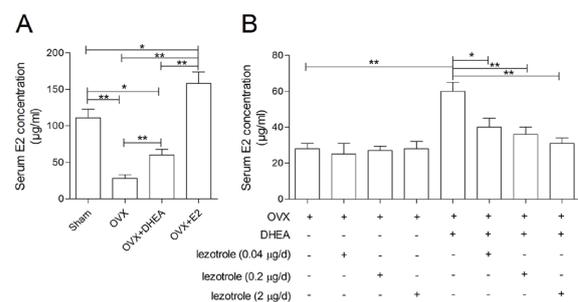that DHEA is the pre-hormone for E2, the serum E2 level was measured to determine if DHEA improved bone mass *via* its end metabolites.

As expected, the serum level of estrogen decreased significantly in the OVX group in comparison to that in the sham-treated group ($P < 0.01$, Figure 6A). An increase in the E2 level was noted in both OVX + DHEA mice and OVX + E2 mice in comparison to OVX mice ($p < 0.05$, $p < 0.01$, respectively, Figure 6A). However, DHEA had less of an effect on the elevation of serum estrogen levels ($p < 0.01$, Figure 6A) than E2 did. Serum estrogen levels in the OVX + DHEA group were lower than those in the sham-treated group ($p < 0.05$, Figure 6A) while serum estrogen levels in the OVX + E2 group were higher than those in the sham-treated group ($p < 0.05$, Figure 6A). The *in vivo* experiment (DHEA plus letrozole) indicated that a DHEA-induced increase in E2 was suppressed by injection of the aromatase inhibitor letrozole (0.04, 0.2, 2 μg/d) ($p < 0.05$, $p < 0.01$, Figure 6B). However, letrozole did not affect E2 levels in OVX mice ($p > 0.05$, Figure 6B). The findings above indicate that conversion of DHEA into estrogen might be one way in which DHEA can be used to prevent PMO.

3.5. The DHEA-mediated suppression of the OVX-induced expansion of CD4+ T cells and TNF-α production was not eliminated by the aromatase inhibitor letrozole

Although DHEA and E2 have almost the same action with regard to decreasing osteoclast-related parameters and modulating TNF-α-producing CD4+ T cells, DHEA only moderately elevated the serum estrogen level. Thus, DHEA was hypothesized to inhibit TNF-α-producing CD4+ T cells in OVX mice *via* its conversion into metabolites, such as E2. To confirm this hypothesis, the effects of DHEA plus letrozole on CD4+ T cells and

Figure 5. DHEA treatment significantly decreased OVX-induced increases in TNF-α production. (A) Circulating levels of TNF-α were measured in different groups using ELISA. **(B)** Levels of TNF-α mRNA in bone marrow CD4+ T cells were measured in different groups using qPCR. Data are expressed as the mean ± SD; **$p < 0.01$ compared to the OVX group.

Figure 6. DHEA led to a slight elevation of serum E2 levels and this effect was eliminated by the aromatase inhibitor letrozole in OVX mice. (A) E2 levels in different group of mice treated as described in Figure 1. **(B)** OVX mice were intragastrically administered saline or DHEA ($n = 20$), and then both OVX mice treated with saline ($n = 20$) and OVX mice treated with DHEA ($n = 20$) were divided into thew following 4 treatment groups: a group receiving the carrier solvent, and 3 groups receiving a 0.04, 0.2, or 2-μg/d letrozole injection for 3 months ($n = 5$ for each group). After the experiment, mice were sacrificed and serum was collected to measure E2 levels. E2 levels in sera were measured with ELISA. Data are expressed as the mean ± SD. *$p < 0.05$, **$p < 0.01$.
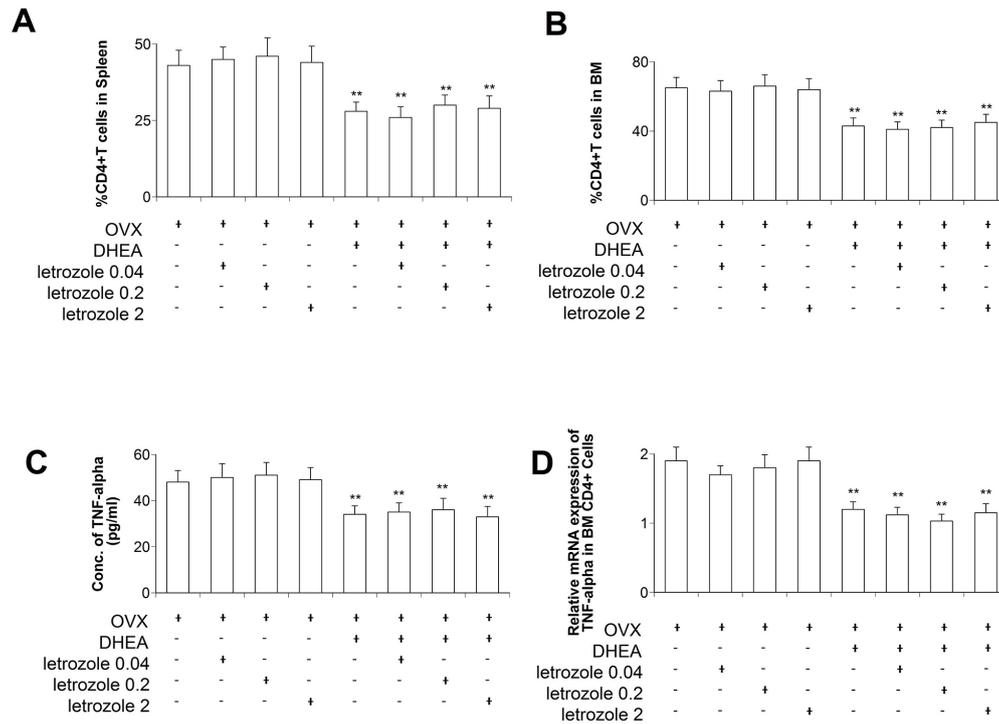
Figure 7. The aromatase inhibitor letrozole did not affect suppression of OVX-induced expansion of CD4+ T cells and TNF-α production by DHEA. OVX mice were intragastrically administered saline or DHEA (*n* = 20), and then both OVX mice treated with saline (*n* = 20) and OVX mice treated with DHEA (*n* = 20) were divided into the following 4 treatment groups: a group receiving the carrier solvent, and 3 groups receiving a 0.04, 0.2, or 2-μg/d letrozole injection for 3 months (*n* = 5 for each group). **(A)** CD4+ T cells in the spleen and **(B)** CD4+ T cells in bone marrow were quantified using flow cytometry. **(C)** Circulating levels of TNF-α were measured in different groups using ELISA. **(D)** Levels of TNF-α mRNA in bone marrow CD4+ T cells were measured in different groups using qPCR. Data are expressed as the mean ± SD; **$p < 0.01$ compared to the OVX group.

TNF-α production were analyzed in OVX mice.

Compared to the OVX group, each group of mice treated with DHEA had fewer CD4+ T cells in bone marrow or the spleen ($p < 0.01$, Figures 7A and 7B). However, in both OVX mice and mice treated with DHEA, treatment with serial concentrations of letrozole did not result in significant changes in the OVX-induced expansion of CD4+ T cells in either bone marrow or the spleen ($p > 0.05$, Figures. 7A and 7B). Furthermore, both DHEA administered alone and DHEA plus letrozole administration led to a significant increase in levels of circulating TNF-α ($p < 0.01$, Figure 7C) and levels of TNF-α mRNA in bone marrow CD4+ T cells ($p < 0.01$, Figure 7D) in comparison to levels in the OVX group. In addition, treatment with letrozole did not affect the production of TNF-α in OVX mice treated with DHEA ($p > 0.05$, Figures 7C and 7D). However, when OVX mice treated with E2 were subsequently treated with letrozole, both the increases in levels of circulating TNF-α and levels of TNF-α mRNA in bone marrow CD4+ T cells were inhibited (data not shown). Thus, suppression of the OVX-induced expansion of CD4+ T cells and TNF-α production by DHEA was not *via* its conversion into E2.

4. Discussion

DHEA has been known to function as an inert precursor

of sex steroids such as E2 and testosterone (*4*). However, the identification of DHEA receptors in the liver, kidneys, and testes of rats suggests that DHEA has specific physiologic actions of its own (*4,31-33*). As far as existing studies are concerned, DHEA may prevent PMO *via* an indirect or direct pathway. In the indirect pathway, DHEA may be converted to estrogen locally or systematically (*4,8*). In the direct pathway, DHEA may regulate the function of osteoblasts and osteoclasts *via* its own specific physiologic actions (*10,11,34,35*). The current results revealed the following: (*i*) DHEA treatment improved the bone phenotype of OVX mice *via* its action on osteoclast-related parameters (Figures 1-3), it reduced the OVX-induced enhancement of osteoclast-mediated bone resorption, and it improved osteoblast-mediated bone formation (Figures 2 and 3) while E2 only reduced the OVX-induced increase in osteoclast parameters (Figures 2 and 3). (*ii*) DHEA restored the enhanced TNF-α-production of CD4+ T cells in OVX mice (Figures 4 and 5). (*iii*) DHEA elevated the serum E2 level, but the effect was moderate and was eliminated by the aromatase inhibitor letrozole (Figure 6). (*iv*) Although letrozole suppressed a DHEA-induced elevation of E2 levels, it did not affect the suppression of the OVX-induced expansion of CD4+ T cells and TNF-α production by DHEA (Figure 7).

Many studies have suggested a beneficial effect of

DHEA administration on the prevention of trabecular BMD loss in postmenopausal women (8,9). DHEA levels in blood fall following OVX in rats and DHEA replacement counters the skeletal effects of OVX (36). These results coincide with the current findings. The current results indicated that DHEA treatment improves the bone phenotype of OVX mice by limiting osteoclast-mediated bone resorption and by improving osteoblast-mediated bone formation (Figures 1-3). However, E2 primarily increases bone mass after OVX by decreasing osteoclast-related parameters (Figures 1-3). A previous study by the current authors also noted DHEA's preferential stimulatory effect on bone, thus supporting DHEA's potential clinical value over estrogen in the prophylactic and therapeutic treatment of PMO (10). Furthermore, DHEA and E2 did not differ significantly in terms of the extent to which they decreased osteoclast-related parameters (Figure 2).

Researchers have begun to recognize the fact that the skeletal and immune systems mutually regulate one another to a much greater degree than previously believed, and "osteoimmunology", an interdisciplinary research principle, plays many roles in the cross-talk between the bone and immune systems (37). PMO is known to be associated with a variety of endocrine and immune alterations (38). Researchers have contended that positive effects on immune status can be achieved by altering the hormonal milieu (39). Such cross-talk between the endocrine and immune systems might be exploited to treat PMO. Various positive immunologic actions of DHEA have been noted in various human diseases and animal models, *e.g.* it influences the systemic concentrations of inflammatory cytokines, it promotes the proliferation of T-lymphocytes, and it alters subsets of T-lymphocytes, thus improving immune functions (40-44). The current findings indicated that OVX caused an expansion of the CD4^{+} T cell pool in bone marrow and the spleen, which may occur as a result of increased proliferation of CD4^{+} T cells and cells with a longer lifespan (Figure 5). DHEA and E2 reduced the proportion of the OVX-induced increase in bone marrow and spleen CD4^{+} T cells (Figure 4). The current findings also indicated that OVX led to a significant increase in levels of circulating TNF-α and levels of TNF-α mRNA of bone marrow CD4^{+} T cells in OVX mice in comparison to levels in sham-treated mice (Figure 5). This finding coincides with previous results (30). Additionally, treatment with DHEA or E2 inhibited OVX induced production of TNF-α (Figure 5). Together, the current findings suggest that both DHEA and E2 limit expansion of the CD4^{+} T cell pool and the systemic and local (*via* bone marrow T cells) increase in TNF-α caused by a deficiency of E2.

RANKL is an osteoclastogenic mediator that is mainly expressed in bone by cells of mesenchymal origin (37). However, T cells can also be an important source of RANKL under certain conditions, such as

PMO (37). CD4^{+} T cells have the potential to both positively and negatively impact osteoclastogenesis by secreting pro-osteoclastogenic cytokines like RANKL and by secreting cytokines to induce anti-osteoclastogenic cytokine OPG expression (45,46). RANKL/RANK/OPG represents the primary triad in the cross-talk between osteoblasts and osteoclasts that regulates osteoclastogenesis. Upregulating TNF-α directly, or by augmenting RANKL secretion, may lead to enhanced osteoclastogenesis (47).

DHEA is a pre-hormone for estrogen. *In vitro* analysis indicated that primary human osteoblasts exhibit aromatase activity that converts DHEA into estrogen (8). The current study also indicated that DHEA elevated the serum E2 level in OVX mice (Figure 6A), and this phenomenon was eliminated by the aromatase inhibitor letrozole (Figure 6B). However, the current results indicated that DHEA suppresses OVX-induced expansion of CD4^{+} T cells and TNF-α-production but not *via* the conversion of DHEA into E2. Moreover, DHEA has specific physiologic actions of its own. A previous study by the current authors indicated that DHEA inhibited osteoclastogenesis *via* an estrogen receptor α-dependent pathway (48). Furthermore, another study by the current authors suggested that DHEA improved murine osteoblast growth *via* the MAPK signaling pathway, independent of either androgen receptors or estrogen receptors (11). Although DHEA and E2 did not differ significantly in terms of their suppression of OVX-induced expansion of TNF-α-producing CD4^{+} T cells and their decreasing osteoclast-related parameters, serum estrogen levels in the OVX + DHEA group were only slightly elevated. Those levels were lower than physiological levels in the sham-treated group and they were markedly lower than levels in the OVX + E2 group. Moreover, the aromatase inhibitor letrozole suppressed a DHEA-induced elevation of E2 levels in OVX mice but it did not affect the suppression of the OVX-induced expansion of CD4^{+} T cells and TNF-α production by DHEA (Figure 7). This suggested that suppression of the OVX-induced expansion of CD4^{+} T cells and TNF-α production by DHEA is not *via* its conversion into a metabolite. Thus, the conversion of DHEA into E2 might be one way in which DHEA prevents OVX-induced bone loss, but not the only way. Another mechanism might account for DHEA's ability to modulate immunity and improve the bone phenotype after OVX. Further work should be done to establish the causal relationship between changes in T-cells and bone-preserving effects of DHEA in OVX mice.

In conclusion, immune function is disrupted in OVX mice. DHEA reversed detrimental immunological changes due to OVX and it provided protection against bone loss. Moreover, these effects were not eliminated by the aromatase inhibitor letrozole. Based on the current findings, DHEA may prevent bone loss by suppressing the OVX-induced expansion of CD4^{+} T

cells and TNF-α production instead of its conversion into estrogen, its end metabolite.

Acknowledgements

References

1. Mannic T, Viguie J, Rossier MF. *In vivo* and *in vitro* evidences of dehydroepiandrosterone protective role on the cardiovascular system. Int J Endocrinol Metab. 2015; 13:e24660.
2. Samaras N, Samaras D, Lang PO, Forster A, Pichard C, Frangos E, Meyer P. A view of geriatrics through hormones. What is the relation between andropause and well-known geriatric syndromes? Maturitas. 2013; 74:213-219.
3. Genazzani AD, Lanzoni C, Genazzani AR. Might DHEA be considered a beneficial replacement therapy in the elderly? Drugs Aging. 2007; 24:173-185.
4. Traish AM, Kang HP, Saad F, Guay AT. Dehydroepiandrosterone (DHEA) – a precursor steroid or an active hormone in human physiology. J Sex Med. 2011; 8:2960-2982; quiz 2983.
5. Samaras N, Samaras D, Frangos E, Forster A, Philippe J. A review of age-related dehydroepiandrosterone decline and its association with well-known geriatric syndromes: Is treatment beneficial? Rejuvenation Res. 2013; 16:285-294.
6. Ostrowska Z, Ziora K, Oswiecimska J, Swietochowska E, Wolkowska-Pokrywa K. Dehydroepiandrosterone sulfate, osteoprotegerin and its soluble ligand sRANKL and bone metabolism in girls with anorexia nervosa. Postepy Hig Med Dosw (Online). 2012; 66:655-662.
7. Park J, Aizawa K, Akimoto T, Iemitsu M, Agata U, Maeda S, Lim K, Omi N. Dehydroepiandrosterone administration increased trabecular mass and dihydrotestosterone levels in the cancellous region of the tibia in young female rats. Horm Metab Res. 2014; 46:651-655.
8. Nawata H, Tanaka S, Tanaka S, Takayanagi R, Sakai Y, Yanase T, Ikuyama S, Haji M. Aromatase in bone cell: Association with osteoporosis in postmenopausal women. J Steroid Biochem Mol Biol. 1995; 53:165-174.
9. Clarke BL, Ebeling PR, Jones JD, Wahner HW, O'Fallon WM, Riggs BL, Fitzpatrick LA. Predictors of bone mineral density in aging healthy men varies by skeletal site. Calcif Tissue Int. 2002; 70:137-145.
10. Wang L, Wang YD, Wang WJ, Li DJ. Differential regulation of dehydroepiandrosterone and estrogen on bone and uterus in ovariectomized mice. Osteoporos Int. 2009; 20:79-92.
11. Wang L, Wang YD, Wang WJ, Zhu Y, Li DJ. Dehydroepiandrosterone improves murine osteoblast growth and bone tissue morphometry *via* mitogen-activated protein kinase signaling pathway independent of either androgen receptor or estrogen receptor. J Mol Endocrinol. 2007; 38:467-479.
12. Wang L, Hao Q, Wang YD, Wang WJ, Li DJ. Protective effects of dehydroepiandrosterone on atherosclerosis in ovariectomized rabbits *via* alleviating inflammatory injury in endothelial cells. Atherosclerosis. 2011; 214:47-57.
13. Qiu X, Gui Y, Xu Y, Li D, Wang L. DHEA promotes osteoblast differentiation by regulating the expression of osteoblast-related genes and Foxp3$^+$ regulatory T cells. Biosci Trends. 2015; 9:307-314.
14. Weitzmann MN, Pacifici R. Estrogen regulation of immune cell bone interactions. Ann N Y Acad Sci. 2006; 1068:256-274.
15. Zallone A. Direct and indirect estrogen actions on osteoblasts and osteoclasts. Ann N Y Acad Sci. 2006; 1068:173-179.
16. Cenci S, Weitzmann MN, Roggia C, Namba N, Novack D, Woodring J, Pacifici R. Estrogen deficiency induces bone loss by enhancing T-cell production of TNF-alpha. J Clin Invest. 2000; 106:1229-1237.
17. Roggia C, Gao Y, Cenci S, Weitzmann MN, Toraldo G, Isaia G, Pacifici R. Up-regulation of TNF-producing T cells in the bone marrow: A key mechanism by which estrogen deficiency induces bone loss *in vivo*. Proc Natl Acad Sci U S A. 2001; 98:13960-13965.
18. Li JY, Tawfeek H, Bedi B, Yang X, Adams J, Gao KY, Zayzafoon M, Weitzmann MN, Pacifici R. Ovariectomy disregulates osteoblast and osteoclast formation through the T-cell receptor CD40 ligand. Proc Natl Acad Sci U S A. 2011; 108:768-773.
19. D'Amelio P, Grimaldi A, Di Bella S, Brianza SZ, Cristofaro MA, Tamone C, Giribaldi G, Ulliers D, Pescarmona GP, Isaia G. Estrogen deficiency increases osteoclastogenesis up-regulating T cells activity: A key mechanism in osteoporosis. Bone. 2008; 43:92-100.
20. Weitzmann MN, Pacifici R. T cells: Unexpected players in the bone loss induced by estrogen deficiency and in basal bone homeostasis. Ann N Y Acad Sci. 2007; 1116:360-375.
21. Tyagi AM, Srivastava K, Kureel J, Kumar A, Raghuvanshi A, Yadav D, Maurya R, Goel A, Singh D. Premature T cell senescence in Ovx mice is inhibited by repletion of estrogen and medicarpin: A possible mechanism for alleviating bone loss. Osteoporos Int. 2012; 23:1151-1161.
22. Prall SP, Muehlenbein MP. Dehydroepiandrosterone and multiple measures of functional immunity in young adults. Am J Hum Biol. 2015;27:877-880.
23. Pinto A, Malacrida B, Oieni J, Serafini MM, Davin A, Galbiati V, Corsini E, Racchi M. DHEA modulates the effect of cortisol on RACK1 expression *via* interference with the splicing of the glucocorticoid receptor. Br J Pharmaco. 2015; 172:2918-2927.
24. Al-Banna N, Pavlovic D, Sharawi N, Bac VH, Jaskulski M, Balzer C, Weber S, Nedeljkov V, Lehmann C. Combination of dehydroepiandrosterone and

25. Li F, Chow S, Cheung WH, Chan FL, Chen S, Leung LK. The citrus flavonone hesperetin prevents letrozole-induced bone loss in a mouse model of breast cancer. J Nutr Biochem. 2013; 24:1112-1116.

26. Abdallah BM, Ditzel N, Mahmood A, Isa A, Traustadottir GA, Schilling AF, Ruiz-Hidalgo MJ, Laborda J, Amling M, Kassem M. DLK1 is a novel regulator of bone mass that mediates estrogen deficiency-induced bone loss in mice. J Bone Miner Res. 2011; 26:1457-1471.

27. Yang JY, Cho SW, An JH, Jung JY, Kim SW, Kim SY, Kim JE, Shin CS. Osteoblast-Targeted Overexpression of TAZ Increases Bone Mass In Vivo. PLoS One. 2013; 8:e56585.

28. Zhou X, Pu D, Liu R, Li X, Wen X, Zhang L, Chen L, Deng M, Liu L. The Fgfr2 mutation in mice retards mandible formation and reduces bone mass as in human Apert syndrome. Am J Med Genet A. 2013;161a:983-992.

29. Zhao B, Takami M, Yamada A, Wang X, Koga T, Hu X, Tamura T, Ozato K, Choi Y, Ivashkiv LB, Takayanagi H, Kamijo R. Interferon regulatory factor-8 regulates bone metabolism by suppressing osteoclastogenesis. Nat Med. 2009; 15:1066-1071.

30. Tyagi AM, Srivastava K, Sharan K, Yadav D, Maurya R, Singh D. Daidzein prevents the increase in CD4$^+$CD28null T cells and B lymphopoesis in ovariectomized mice: A key mechanism for anti-osteoclastogenic effect. PLoS One. 2011; 6:e21216.

31. Magyar Z, Bekesi G, Racz K, et al. Increased total scavenger capacity and decreased liver fat content in rats fed dehydroepiandrosterone and its sulphate on a high-fat diet. Gerontology. 2011; 57:343-349.

32. Jahn MP, Gomes LF, Jacob MH, da Rocha Janner D, Araujo AS, Bello-Klein A, Ribeiro MF, Kucharski LC. The effect of dehydroepiandrosterone (DHEA) on renal function and metabolism in diabetic rats. Steroids. 2011; 76:564-570.

33. Sah C, Aridogan IA, Izol V, Erdogan S, Doran S. Effects of Long-term Administration of the Antiaging Hormone Dehydroepiandrosterone Sulfate on Rat Prostates and Testes as Androgen-Dependent Organs. Korean J Urol. 2013; 54:199-203.

34. Wang YD, Tao MF, Cheng WW, Liu XH, Wan XP, Cui K. Dehydroepiandrosterone indirectly inhibits human osteoclastic resorption via activating osteoblastic viability by the MAPK pathway. Chin Med J (Engl). 2012; 125:1230-1235.

35. Wang YD, Tao MF, Wang L, Cheng WW, Wan XP. Selective regulation of osteoblastic OPG and RANKL by dehydroepiandrosterone through activation of the estrogen receptor beta-mediated MAPK signaling pathway. Horm Metab Res. 2012; 44:494-500.

36. Turner RT, Lifrak ET, Beckner M, Wakley GK, Hannon KS, Parker LN. Dehydroepiandrosterone reduces cancellous bone osteopenia in ovariectomized rats. Am J Physiol. 1990; 258:E673-677.

37. Guerrini MM, Takayanagi H. The immune system, bone and RANKL. Arch Biochem Biophys. 2014; 561:118-123.

38. Fan XL, Duan XB, Chen ZH, Li M, Xu JS, Ding GM. Lack of estrogen down-regulates CXCR4 expression on Treg cells and reduces Treg cell population in bone marrow in OVX mice. Cell Mol Biol (Noisy-le-grand). 2015; 61:13-17.

39. Nadkarni S, McArthur S. Oestrogen and immunomodulation: New mechanisms that impact on peripheral and central immunity. Curr Opin Pharmacol. 2013; 13:576-581.

40. Pratschke S, von Dossow-Hanfstingl V, Dietz J, Schneider CP, Tufman A, Albertsmeier M, Winter H, Angele MK. Dehydroepiandrosterone modulates T-cell response after major abdominal surgery. J Surg Res. 2014; 189:117-125.

41. Moynihan JA, Callahan TA, Kelley SP, Campbell LM. Adrenal hormone modulation of type 1 and type 2 cytokine production by spleen cells: Dexamethasone and dehydroepiandrosterone suppress interleukin-2, interleukin-4, and interferon-gamma production in vitro. Cell Immunol. 1998; 184:58-64.

42. Lichte P, Pfeifer R, Werner BE, Ewers P, Tohidnezhad M, Pufe T, Hildebrand F, Pape HC, Kobbe P. Dehydroepiandrosterone modulates the inflammatory response in a bilateral femoral shaft fracture model. Eur J Med Res. 2014; 19:27.

43. Brazao V, Santello FH, Caetano LC, Del Vecchio Filipin M, Toldo MP, do Prado JC, Jr. Immunomodulatory effects of zinc and DHEA on the Th-1 immune response in rats infected with Trypanosoma cruzi. Immunobiology. 2010; 215:427-434.

44. Casson PR, Andersen RN, Herrod HG, Stentz FB, Straughn AB, Abraham GE, Buster JE. Oral dehydroepiandrosterone in physiologic doses modulates immune function in postmenopausal women. Am J Obstet Gynecol. 1993; 169:1536-1539.

45. Kim HR, Kim KW, Kim BM, Jung HG, Cho ML, Lee SH. Reciprocal activation of CD4$^+$ T cells and synovial fibroblasts by stromal cell-derived factor 1 promotes RANKL expression and osteoclastogenesis in rheumatoid arthritis. Arthritis Rheumatol. 2014; 66:538-548.

46. Stein NC, Kreutzmann C, Zimmermann SP, Niebergall U, Hellmeyer L, Goettsch C, Schoppet M, Hofbauer LC. Interleukin-4 and interleukin-13 stimulate the osteoclast inhibitor osteoprotegerin by human endothelial cells through the STAT6 pathway. J Bone Miner Res. 2008; 23:750-758.

47. Matuszewska A, Szechinski J. [Mechanisms of osteoporosis development in patients with rheumatoid arthritis]. Postepy Hig Med Dosw (Online). 2014; 68:145-152.

48. Gui Y, Qiu X, Xu Y, Li D, Wang L. Bu-Shen-Ning-Xin decoction suppresses osteoclastogenesis via increasing dehydroepiandrosterone to prevent postmenopausal osteoporosis. Biosci Trends. 2015; 9:169-181.

Original Article

Effect of lycopene on the blood-spinal cord barrier after spinal cord injury in mice

Qian Zhang[1,*], Jianbo Wang[1,*], Zhengsong Gu[2], Qing Zhang[1], Hong Zheng[1,**]

[1] *Department of Anesthesia, Tianjin Central Hospital of Gynecology & Obstetrics, Tianjin, China;*
[2] *Department of Anesthesia, Zhenjiang Hospital of Traditional Chinese Medicine, Jiangsu, China.*

Summary	The current study aimed to investigate the effect of lycopene on the blood-spinal cord barrier (BSCB) after spinal cord injury (SCI) in a mouse model. Lycopene inhibited lipid peroxidation and oxidative DNA damage as a highly efficient antioxidant and free radical scavenger. Lycopene (4 mg/kg/d) was administrated immediately following SCI. The permeability of the BSCB and water content in the spinal cord tissue were evaluated. Additionally, levels of expression of tight junction proteins and heme oxygenase-1 (HO-1) were determined with Western blotting. An enzyme-linked immunosorbent assay analysis of spinal cord tissue homogenates was performed 48 h after SCI to evaluate the expression of inflammation-related cytokines. In addition, recovery of motor function was assessed 1 d, 2 d, 5 d, 10 d, and 15 d after SCI using the Basso Mouse Scale to score locomotion. Compared to the group with an untreated SCI, mice with an SCI treated with lycopene had significantly reduced spinal cord tissue water content and BSCB permeability. Furthermore, motor function of mice with an SCI was also greatly improved by lycopene administration. The expression of the proinflammatory factors TNF-α and NF-kB increased markedly 48 h after SCI, and their upregulation was significantly attenuated by lycopene treatment. The expression of molecules that protect tight junctions, zonula occluden-1 and claudin-5, was upregulated by lycopene treatment after SCI. Taken together, these results clearly indicate that lycopene attenuated SCI by promoting repair of the damaged BSCB, so lycopene is a novel and promising treatment for SCI in humans.

Keywords: Lycopene, spinal cord injury, blood-spinal cord barrier, tight junction

1. Introduction

Spinal cord injury (SCI) is a severe trauma of the central nervous system (CNS) that results in loss of blood vessels and disruption of the blood-spinal cord barrier (BSCB) (*1,2*). Previous studies focused largely on alleviating neurological manifestations of the injury while ignoring pathological changes in the spinal cord (*3*). The compression forces induced by SCI can rupture

blood vessels, destroy endothelial cells and pericytes, disrupt the BSCB, and cause production of numerous molecules that result in vascular disruption (*4,5*).

Maintaining spinal cord microcirculation in required to sustain the normal functioning of spinal cord nerve cells. After injury, damaged blood vessels allow an influx of blood cells including leucocytes, monocytes, and macrophages, contributing to additional loss of nervous tissue in some way. Blood is toxic to nervous tissue probably because degradation of hemoglobin releases catalytic metal ions, it produces free radicals, and it thereby leads to lipid peroxidation. Previous researchers focused on improving sensory motor function. However, they ignored the microvascular reaction of the spinal cord or alterations to the properties of the BSCB. Pharmaceuticals may have a considerable effect on microcirculation (*6*). Lycopene, a carotenoid mostly

found in tomatoes and tomato products, possesses potent neuroprotective (*7*), antiproliferative, anticancer (*8*), and hypocholesterolemic activity (*9*). Lycopene reduces proinflammatory cytokine and chemokine-expressing macrophages (*10*), it protects cultured hippocampal neurons against Aβ and glutamate toxicity (*11*), it protects against microglial activation in focal cerebral ischemia in rats (*7*), and it attenuates cognition impairment in the elderly (*12*). Lycopene is an agent that may prove useful in managing neurodegenerative disorders because of its ability to cross the blood-brain barrier (BBB) (13) and its strong antioxidant properties (*14*). Furthermore, lycopene has been shown to reverse neurobehavioral deficits in rats (*15*). However, the mechanism by which lycopene affects the integrity of the BSCB after SCI remains unclear. The current study used a mouse model of SCI due to impact to investigate the mechanism by which lycopene acts on the BSCB.

2. Materials and Methods

2.1. *Animals*

Male C57BL mice weighing 22-25 g (Vital River Laboratory Animal Technology Co. Ltd, Beijing, China) were housed under standard 12-h light/dark conditions and received food *ad libitum*. All procedures involving experimental animals were approved by the Laboratory Animal Care and Ethics Committee of Tianjin Central Hospital.

2.2. *Induction of an SCI*

Mice were anesthetized using pentobarbital sodium (80 mg/kg body weight). The modified weight-drop model was used to produce an SCI (*16*). A longitudinal incision was made along the midline of the back to expose the paravertebral muscles, which were dissected away to expose the T10 vertebra. The laminae were removed. The animal was subjected to an impact of 50 g/mm (a 5-g weight dropped from a height of 10 mm) to the dorsal surface of the spinal cord. Afterwards, the muscles were sutured and the incision was closed. Following the surgical procedure, the rats were placed in a warming chamber. In the SCI groups, the cord was compressed for 1 min. Following surgery, 0.2 mL of saline was administered subcutaneously in order to replace the blood volume lost during surgery. The mice were singly housed at 25°C in a temperature-controlled room for 48 h. During this period, the animals' bladders were manually voided twice a day. Sham-injured animals were only subjected to laminectomy.

2.3. *Experimental design*

Mice were randomly divided into three groups: (a) A sham group in which the T10 vertebra was removed but

no impact was applied and that was treated with saline containing 5% ethanol (*n* = 29); (b) A group in which an SCI was produced and treated with saline containing 5% ethanol (*n* = 29); and (c) A group in which an SCI was produced and treated with lycopene (*n* = 29) at a dose of 4 mg/kg/d (*17*).

2.4. *Evaluation of the permeability of the BSCB*

Evans blue (EB) leakage was assessed using an established protocol (*18*). EB (Sigma-Aldrich, USA, 2% w/v in saline) was injected intraperitoneally. Mice were perfused transcardially with saline and rinsed thoroughly until no more blue dye flowed out of the right atrium 3 h after the injection. The tissues (epicenter ± 0.5 cm) were dehydrated at 60°C for 48 h. Afterwards, they were weighed and extracted in 60% trichloroacetic acid for 72 h. To measure EB dye, the tissues were then centrifuged at 14000× g for 8 min. A standard curve with EB dye was plotted and fluorescence intensity was measured in the supernatant using a spectrophotometer at an excitation wavelength of 620 nm and an emission wavelength of 680 nm. All measurements were within the range of detection established by the standard curve. R^2 of the standard curve was 0.99. The concentration of dye was calculated as the ratio of absorbance relative to the tissue volume.

2.5. *Evaluation of the water content in spinal cord tissue*

Lycopene treatment (4 mg/kg/d) was administered within 30 min of surgery and then every 24 h. Forty-eight h after SCI, the injured spinal cord (epicenter ± 0.5 cm) was extracted and dried at 80°C for 48 h. Water content in spinal cord tissue was calculated according to the following formula: spinal cord water content (%) = (wet weight-dry weight)/wet weight × 100%.

2.6. *Functional testing*

Functional recovery after SCI was assessed using Basso Mouse Scale (BMS) (*19*). Mice with an SCI were tested 1 d, 2 d, 5 d, 10 d, and 15 d after SCI, and they were scored in an open-field environment by trained investigators.

2.7. *Enzyme-linked immunosorbent assay*

To detect the levels of inflammation-related cytokines, the rats were sacrificed 48 h after SCI and the injured spinal cord was used to prepare spinal cord tissue homogenates (epicenter ± 0.5 cm). Levels of TNF-α and NF-kB were determined using specific enzyme-linked immunosorbent assay (ELISA) kits according to the manufacturer's instructions (Beyotime Institute of Biotechnology, Shanghai, China).

2.8. Western blotting

Spinal cord samples (epicenter ± 0.5 cm) were collected and total protein was prepared with a lysis buffer (Beyotime Institute of Biotechnology, Shanghai, China). Protein levels were determined using a protein assay kit (BCA, Pierce, Rockford, USA). Protein was separated with 10% SDS-PAGE and transferred onto PVDF membranes. The membranes, blocked with 5% BSA for 1 h, were incubated with antibodies against heme oxygenase-1 (HO-1) (1:100, Santa Cruz, USA), zonula occluden-1 (ZO-1) (1:100, Santa Cruz, USA) and claudin-5 (1:100, Santa Cruz, USA). The primary antibodies were detected using horseradish peroxidase-conjugated rat anti-rabbit, rat anti-mouse, or rabbit anti-goat IgG secondary antibodies (1:500, Santa Cruz, USA). The bands were visualized using enhanced chemiluminescence and relative band intensities were quantified using Image Pro Plus 7.0 (Media Cybernetics, Silver Spring, MD).

2.9. Statistical analysis

All data are presented as the mean ± SD. Data on the two groups were compared using a paired student's *t* test. One-way analysis of variance and Tukey's post-hoc tests were used to compare groups. $p < 0.05$ was considered statistically significant.

3. Results

3.1. Effect of lycopene on motor function

Functional recovery of overground locomotion was observed 2 d, 5 d, 10 d, and 15 d after SCI in all groups, and observations indicated that motor function of the group with an SCI treated with lycopene improved significantly compared to that of the group with an untreated SCI ($p < 0.05$). At 24 h, there were no significant differences in the motor function of the group with an untreated SCI and the group with an SCI treated
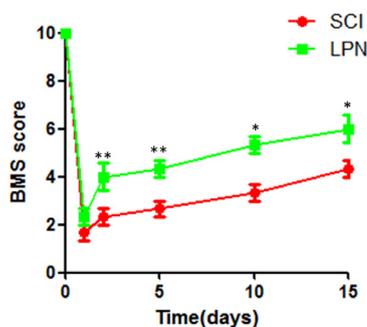
Figure 1. Lycopene improved functional recovery. Motor function of the group with an untreated SCI and the group with an SCI treated with lycopene was assessed using the BMS score ($n = 8$). Two d, 5 d, 10 d, and 15 d after SCI, motor function of the group with an SCI treated with lycopene was better than that of the group with an untreated SCI. *$p < 0.05$, **$p < 0.01$.

with lycopene (Figure 1).

3.2. Effect of lycopene on the water content in the spinal cord

Water content in the spinal cord was detected to evaluate whether lycopene has protective action by reducing the level of edema. Water content in the spinal cord after injury increased significantly in the group with an untreated SCI compared to that in the sham group (untreated SCI: 0.72 ± 0.02 *vs.* sham: 0.47 ± 0.04, $p < 0.001$). Water content in the spinal cord decreased in the group with an SCI treated with lycopene in comparison to that in the group with an untreated SCI (untreated SCI: 0.72 ± 0.02 *vs.* SCI treated with lycopene: 0.62 ± 0.06, $p < 0.05$) (Figure 2).

3.3. Effect of lycopene on the permeability of the BSCB

To determine whether lycopene reduced the increase in permeability induced by compression injury, the level of EB in injured tissue was determined. The level of EB in the group with an untreated SCI increased significantly compared to that in the sham group (SCI: 0.48 ± 0.15 μg/mg *vs.* sham: 0.01 ± 0.03 μg/mg, $p < 0.001$). After lycopene treatment, the level of EB in the spinal cord tissue decreased significantly compared to that in the group with an untreated SCI (untreated SCI: 0.48±0.15 μg/mg *vs.* SCI treated with lycopene: 0.25 ± 0.10 μg/mg, $p < 0.05$) (Figure 3).
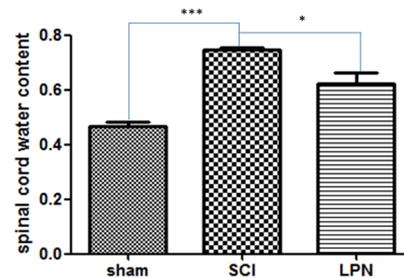
Figure 2. Lycopene reduced edema of the spinal cord after SCI. Water content in the spinal cord was determined ($n = 6$). *$p < 0.05$, ***$p < 0.001$.
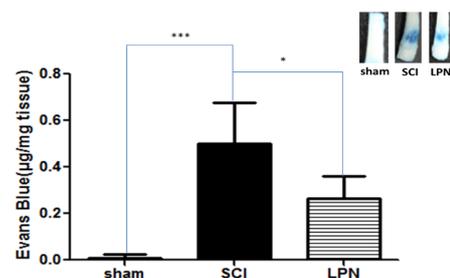

Figure 3. As indicated by EB levels, lycopene reduced the permeability of the BSCB. Shown here are photographs of the sham group, the group with an untreated SCI, and the group with an SCI treated with lycopene. The length of each tissue specimen was 1 cm. The fluorescence intensity of EB in the three groups was quantified ($n = 6$). *$p < 0.05$, **$p < 0.01$.

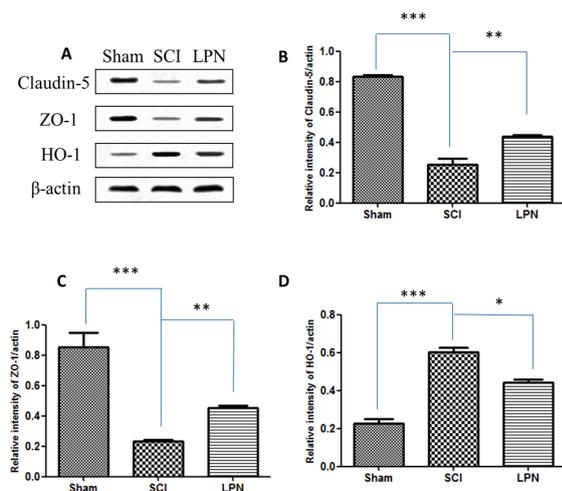### 3.4. *Effect of lycopene on the expression of pro-inflammatory cytokines after SCI*

Changes in levels of TNF-α and NF-kB in the spinal cord were detected with ELISA. Compared to the sham group, the group with an untreated SCI had marked increased levels of expression of TNF-α (untreated SCI: 14.03 ± 0.60 pg/mg *vs.* sham: 9.94 ± 0.05 pg/mg, $p < 0.001$) and NF-kB (untreated SCI: 24.03 ± 0.55 pg/mg *vs.* sham: 11.26 ± 0.38 pg/mg, $p < 0.001$). Compared to the group with an untreated SCI, the group with an SCI treated with lycopene had markedly decreased levels of expression of TNF-α (untreated SCI: 14.03 ± 0.60 pg/mg, lycopene: 11.59 ± 0.51 pg/mg, $p < 0.05$) and NF-kB (untreated SCI: 24.03 ± 0.55 pg/mg, SCI treated with lycopene: 14.92 ± 0.88 pg/mg, $p < 0.001$) (Figure 4).

3.5. *Effect of lycopene on expression of tight junction (TJ) proteins and the protein HO-1*

Proteins related to the BSCB, *i.e.* ZO-1, claudin-5, and HO-1, were detected. Expression of TJ proteins was
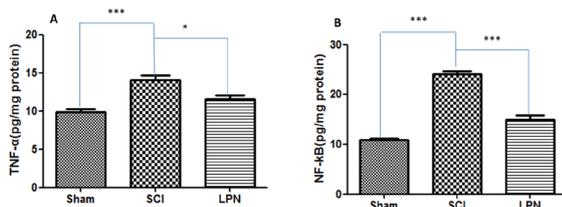
Figure 4. Effect of lycopene on the concentrations of inflammation cytokines after SCI. Injured spinal cord tissue was used to prepare spinal cord tissue homogenates (epicenter $\pm$ 5 mm) 48 h after SCI, and levels of TNF-α **(A)** and NF-kB **(B)** were determined using ELISA (n = 6). ***$p < 0.001$.

Figure 5. Effect of lycopene on expression of the proteins ZO-1, claudin-5, and HO-1 at the injured spinal cord 48 h after SCI (n = 3). (A) Expression of claudin-5, ZO-1, and HO-1 in the three groups. **(B-D)** The relative intensity of claudin-5, ZO-1, and HO-1 expression in the three groups. *$p < 0.05$, **$p < 0.01$, and ***$p < 0.001$.

upregulated by lycopene 48 h after SCI. The levels of expression of the proteins ZO-1 and claudin-5 were much lower in the group with an untreated SCI than those in the sham group 48 h after SCI. However, lycopene alleviated the abnormal disruption of ZO-1 and claudin-5 in the group with an SCI treated with lycopene. The group with a treated SCI had a significantly increased level of HO-1 protein 48 h after SCI compared to the sham group ($p < 0.001$). The level of HO-1 decreased in the group with an SCI treated with lycopene in comparison to that in the group with an untreated SCI ($p < 0.05$) (Figure 5).

4. Discussion

As a member of the carotenoid family, lycopene has numerous potential health benefits, most of which are based on its antioxidant properties. Previous researchers focused on improving sensory motor function, but microvascular reactions of the spinal cord or alterations to the properties of the BSCB were neglected. Any alterations to the BSCB may change the spinal cord microfluid environment, leading to functional disturbance. Reducing the breakdown of the BSCB may protect the nervous system. However, how lycopene acts on the integrity of the BSCB and microcirculation after SCI remains unclear.

Spinal cord edema largely explains the morbidity and mortality of SCI (*20*). Spinal cord edema induces openings in the BSCB, leading to an exchange of harmful substances between blood and tissue. Disruption of the BSCB elicits marked local inflammation with the infiltration of neutrophils and macrophages, leading to cell death and permanent neurological disability (*21,22*). The current study found that lycopene significantly reduced the level of edema after SCI.

TJs are located at the apical end of the inter-endothelial space and are connected to adherens junctions near the basal end of the inter-endothelial space (*23*). TJ proteins, such as transmembrane proteins claudin-5 and the peripheral membrane protein ZO-1, are essential to the normal functioning of TJs (*24*). Changes in the distribution and expression of TJ-associated proteins are reported to be closely related to the permeability of the BSCB after an SCI (*25,26*). In the current study, expression of ZO-1 and claudin-5 was detected and lycopene treatment significantly increased the expression of ZO-1 and claudin-5 compared to levels in the group with an untreated SCI. This indicated that lycopene treatment increased the integrity of the BSCB after SCI by regulating ZO-1 and claudin-5.

Neuroinflammation leads to breakdown of the BSCB, which is implicated in the pathogenesis of CNS disease. The expression of proinflammatory cytokines, including TNF-α and NF-kB, at the site of injury has been found to regulate the permeability of the BSCB following SCI (*27,28*). Exposure of the endothelium

to proinflammatory cytokines interrupts the BBB by disorganizing cell-cell junctions (*29*). In the current study, the effect of lycopene on the inflammatory mediator TNF-α and its regulatory factor NF-kB was investigated. Results revealed that lycopene treatment significantly decreased the activation of TNF-α and NF-kB compared to levels in the group with an untreated SCI. These results indicate that lycopene inhibited the generation of inflammatory mediators, thereby limiting disruption of the BSCB and eventually resulting in amelioration of pathological changes caused by SCI.

HO-1 is involved in the rate-limiting step in the oxidative degradation of heme. HO-1 expression is upregulated in response to oxidative stress, which catalyzes the degradation of pro-oxidant heme to carbon monoxide, iron, and bilirubin (*30*). HO-1 expression is an adaptive and protective response to oxidative stress. HO-1 can be induced by a variety of stimuli and various agents that cause oxidative stress, and it protects cells from the oxidative damage caused by reactive oxygen species (*31*). Lycopene has been found to protect against oxidation of lipids, proteins, and DNA *in vivo*. Therefore, the current study used lycopene to detect an anti-oxidant effect after SCI, and the results indicated that lycopene significantly decreased the expression of HO-1.

In conclusion, the current findings indicate that lycopene could potentially serve as a treatment to reduce the severity of SCI. These results should help in studying the mechanism and treatment of SCI in humans. This study found that lycopene acts on the BSCB after SCI. Lycopene improved motor function, it reduced the permeability of the BSCB, it increased the number of tight junctions, and it reduced inflammatory factors. However, how lycopene acts on the components of the BSCB (endothelial cells, pericytes, and astrocytes) remains unclear. Future studies should concentrate on the key molecules mediating neurovascular links among the various types of cells of the BSCB and pharmaceuticals should be developed to treat SCI and other CNS conditions.

Acknowledgements

References

1. Bilgen M, Dogan B, Narayana PA. *In vivo* assessment of blood-spinal cord barrier permeability: Serial dynamic contrast enhanced MRI of spinal cord injury. Magn Reson Imaging. 2002; 20:337-341.
2. Fan ZK, Lv G, Wang YF, Li G, Yu DS, Wang YS, Zhang YQ, Mei XF, Cao Y. The protective effect of salvianolic acid B on blood-spinal cord barrier after compression spinal cord injury in rats. J Mol Neurosci. 2013; 51:986-993.
3. Sharma HS. Early microvascular reactions and blood-spinal cord barrier disruption are instrumental in pathophysiology of spinal cord injury and repair: Novel therapeutic strategies including nanowired drug delivery to enhance neuroprotection. J Neural Transm (Vienna). 2011; 118:155-176.
4. Casella GT, Bunge MB, Wood PM. Endothelial cell loss is not a major cause of neuronal and glial cell death following contusion injury of the spinal cord. Exp Neurol. 2006; 202:8-20.
5. Dulmovits BM, Herman IM. Microvascular remodeling and wound healing: A role for pericytes. Int J Biochem Cell Biol. 2012; 44:1800-1812.
6. Jung F. From hemorheology to microcirculation and regenerative medicine: Fahraeus Lecture 2009. Clin Hemorheol Microcirc. 2010; 45:79-99.
7. Hsiao G, Fong TH, Tzu NH, Lin KH, Chou DS, Sheu JR. A potent antioxidant, lycopene, affords neuroprotection against microglia activation and focal cerebral ischemia in rats. *In Vivo*. 2004; 18:351-356.
8. Gunasekera RS, Sewgobind K, Desai S, Dunn L, Black HS, McKeehan WL, Patil B. Lycopene and lutein inhibit proliferation in rat prostate carcinoma cells. Nutr Cancer. 2007; 58:171-177.
9. Riso P, Visioli F, Grande S, Guarnieri S, Gardana C, Simonetti P, Porrini M. Effect of a tomato-based drink on markers of inflammation, immunomodulation, and oxidative stress. J Agric Food Chem. 2006; 54:2563-2566.
10. Lee W, Ku SK, Bae JW, Bae JS. Inhibitory effects of lycopene on HMGB1-mediated pro-inflammatory responses in both cellular and animal models. Food Chem Toxicol. 2012; 50:1826-1833.
11. Mattson MP, Chan SL, Duan W. Modification of brain aging and neurodegenerative disorders by genes, diet, and behavior. Physiol Rev. 2002; 82:637-672.
12. Akbaraly NT, Faure H, Gourlet V, Favier A, Berr C. Plasma carotenoid levels and cognitive performance in an elderly population: Results of the EVA Study. J Gerontol A Biol Sci Med Sci. 2007; 62:308-316.
13. Khachik F, Carvalho L, Bernstein PS, Muir GJ, Zhao DY, Katz NB. Chemistry, distribution, and metabolism of tomato carotenoids and their impact on human health. Exp Biol Med (Maywood). 2002; 227:845-851.
14. Rafi MM, Yadav PN, Reyes M. Lycopene inhibits LPS-induced proinflammatory mediator inducible nitric oxide synthase in mouse macrophage cells. J Food Sci. 2007; 72:S069-074.
15. Rao AV, Balachandran B. Role of oxidative stress and antioxidants in neurodegenerative diseases. Nutr Neurosci. 2002; 5:291-309.
16. ALLEN A. Surgery of experimental lesion of spinal cord equivalent to crush injury of fracture dislocation of spinal column. A preliminary report. JAMA. 1911; 57:878-880.
17. Wu A, Liu R, Dai W, Jie Y, Yu G, Fan X, Huang Q. Lycopene attenuates early brain injury and inflammation following subarachnoid hemorrhage in rats. Int J Clin Exp Med. 2015; 8:14316-14322.
18. Echeverry S, Shi XQ, Rivest S, Zhang J. Peripheral nerve injury alters blood-spinal cord barrier functional and molecular integrity through a selective inflammatory pathway. J Neurosci. 2011; 31:10819-10828.
19. Basso DM, Fisher LC, Anderson AJ, Jakeman LB,

McTigue DM, Popovich PG. Basso Mouse Scale for locomotion detects differences in recovery after spinal cord injury in five common mouse strains. J Neurotrauma. 2006; 23:635-659.

20. Goldberg AL, Kershah SM. Advances in imaging of vertebral and spinal cord injury. J Spinal Cord Med. 2010; 33:105-116.

21. Lee JY, Kim HS, Choi HY, Oh TH, Ju BG, Yune TY. Valproic acid attenuates blood-spinal cord barrier disruption by inhibiting matrix metalloprotease-9 activity and improves functional recovery after spinal cord injury. J Neurochem. 2012; 121:818-829.

22. Fan ZK, Cao Y, Lv G, Wang YS, Guo ZP. The effect of cigarette smoke exposure on spinal cord injury in rats. J Neurotrauma. 2013; 30:473-479.

23. Oudega M. Molecular and cellular mechanisms underlying the role of blood vessels in spinal cord injury and repair. Cell Tissue Res. 2012; 349:269-288.

24. Luissint AC, Artus C, Glacial F, Ganeshamoorthy K, Couraud PO. Tight junctions at the blood brain barrier: Physiological architecture and disease-associated dysregulation. Fluids Barriers CNS. 2012; 9:23.

25. Liebner S, Czupalla CJ, Wolburg H. Current concepts of blood-brain barrier development. Int J Dev Biol. 2011; 55:467-476.

26. Wu Q, Jing Y, Yuan X, Zhang X, Li B, Liu M, Wang B, Li H, Liu S, Xiu R. Melatonin treatment protects against acute spinal cord injury-induced disruption of blood spinal cord barrier in mice. J Mol Neurosci. 2014; 54:714-722.

27. Esposito E, Cuzzocrea S. Anti-TNF therapy in the injured spinal cord. Trends Pharmacol Sci. 2011; 32:107-115.

28. Beattie MS, Hermann GE, Rogers RC, Bresnahan JC. Cell death in models of spinal cord injury. Prog Brain Res. 2002; 137:37-47.

29. Kniesel U, Wolburg H. Tight junctions of the blood-brain barrier. Cell Mol Neurobiol. 2000; 20:57-76.

30. Bhaskaran N, Shukla S, Kanwal R, Srivastava JK, Gupta S. Induction of heme oxygenase-1 by chamomile protects murine macrophages against oxidative stress. Life Sci. 2012; 90:1027-1033.

31. Castilho A, Aveleira CA, Leal EC, Simoes NF, Fernandes CR, Meirinhos RI, Baptista FI, Ambrosio AF. Heme oxygenase-1 protects retinal endothelial cells against high glucose- and oxidative/nitrosative stress-induced toxicity. PLoS One. 2012; 7:e42428.

Serum levels of RIPK3 and troponin I as potential biomarkers for predicting impaired left ventricular function in patients with myocardial infarction with ST segment elevation and normal troponin I levels prior percutaneous coronary intervention

Javor K Kashlov[1,2], **Ivan S Donev**[1,3,*], **Jordanka G Doneva**[1,2], **Veselin D Valkov**[1,4], **Arpine D Kirkorova**[1,2], **Peter I Ghenev**[5,6], **Nikolay V Conev**[1,3], **Temenuzhka R Radeva**[7], **Borislav D Ivanov**[8], **Zhaneta T Georgieva**[1,2]

[1] *Department of Propedeutics of Internal Medicine, Medical University of Varna, Bulgaria;*
[2] *Department of Internal Medicine, St. Marina UMHAT, Varna, Bulgaria;*
[3] *Clinic of Medical Oncology, St. Marina UMHAT, Varna, Bulgaria;*
[4] *Department of Cardiology, St. Marina UMHAT, Varna, Bulgaria;*
[5] *Department of General and Clinical Pathology, Forensic Medicine and Deontology, Faculty of Medicine, Medical University of Varna, St. Marina UMHAT, Varna, Bulgaria;*
[6] *Center of Clinical Pathology, St. Marina UMHAT, Varna, Bulgaria;*
[7] *Department of Radiation Oncology and Imaging Diagnostic, St. Marina UMHAT, Varna Bulgaria;*
[8] *Department of Clinical Medical Sciences, Medical University of Varna, Bulgaria.*

Summary   The current study examined the serum levels of receptor-interacting protein kinase 3 (RIPK3) in 51 patients with New York Heart Association (NYHA) class III-IV heart failure, 53 patients with myocardial infarction with ST elevation (STEMI), and 19 healthy subjects serving as a control group. An enzyme-linked immunoadsorbent assay (ELISA) was used to measure the levels of RIPK3 expression in serum. The area under the receiver operating characteristic curve (AUC) was then used to evaluate the predictive performance of RIPK3 and troponin I in patients with STEMI. In patients with normal levels of troponin I prior to percutaneous coronary intervention (PCI), serum levels of RIPK3 and troponin I after PCI were sufficient to differentiate patients with a preserved left ventricular ejection fraction (LVEF) from those with impaired left ventricular function after PCI (AUC = 0.780 (95% CI: 0.565-0.995, p = 0.043) with a sensitivity of 76.9% and a specificity of 71.4% *vs.* AUC = 0.735 (95% CI: 0.530-0.941, p = 0.038) with a sensitivity of 88.2% and a specificity of 63.6% at the optimal cutoff values, respectively). Moreover, elevated levels of troponin I after PCI were associated with an increased risk of an LVEF < 50% prior to discharge (odds ratio, 1.014; 95 % CI, 1.001 to 1.027; p = 0.03), while elevated levels of RIPK3 were not associated with such a risk. The current findings suggest that in patients with normal levels of troponin I prior to PCI, serum levels of RIPK3 and troponin I can serve as a potential marker to identify patients with a decreased LVEF, thus possibly allowing an early shift to more intensive therapy.

Keywords: Receptor-interacting protein kinase 3 (RIPK3), marker, percutaneous coronary intervention (PCI), left ventricular ejection fraction (LVEF)

---

1. Introduction

The prevalence of acute and chronic ischemic heart disease and heart failure is as high as 8% in Western countries; these conditions account for more than one-third of all human mortality and remain the leading causes of death worldwide (*1*). The myocardium consists

of differentiated cardiomyocytes that are responsible for its contractile function. The heart is an organ with limited capacity for regeneration and repair. In cardiovascular diseases such as myocardial infarction and congestive heart failure, there is a significant loss of cardiomyocytes (2). Hence, new biomarkers that indicate early cardiac cell death need to be found. Much attention has been focused on understanding the mechanism of cell death in acute and chronic heart diseases in order to improve patient outcomes. All types of cell death - autophagy, apoptosis and necrosis - participate in the progression of heart diseases - with a great uncertainty as to which of them prevails (3,4).

Recently, a novel type of cell death called "programmed necrosis" or necroptosis has been reported to be involved in the pathogenesis of heart disease (5). Similar to apoptosis, this process is tightly regulated by distinct molecules and has morphological features of both necrosis and inflammation (3,6-9). Nevertheless, the exact pathways activating this programmed necrosis are not fully understood (10). A study has shown that tumor necrosis factor alpha (TNF-α) is a factor that triggers the formation of a complex, called necrosome, in the cytoplasm between receptor-interacting protein kinase 1 (RIPK1) and receptor-interacting protein kinase 3 (RIPK3) (7). In the process of the formation of this complex, RIPK3 phosphorylates RIPK1, which is an essential step in inducing necroptosis (11).

The current study examined the serum levels of RIPK3 in 51 patients with New York Heart Association (NYHA) class III-IV heart failure, 53 patients with myocardial infarction with ST elevation (STEMI), and 19 healthy subjects. This study sought to determine the dynamics of the release of RIPK3 after myocyte injury within 48 hours after the onset of symptoms in all patients with STEMI. This study examined the association between serum levels of RIPK3 and patient outcomes like a decreased left ventricular ejection fraction (LVEF), mortality, and further hospitalization.

2. Materials and Methods

2.1. Ethics Statement

All procedures were approved by the Scientific Research Ethics Committee of the Prof. Dr. Paraskev Stoyanov Medical University of Varna. Blood samples were collected from 53 patients with STEMI (myocardial infarction with ST elevation), 51 patients with NYHA class III-IV heart failure, and 19 healthy individuals at St. Marina University Hospital, Varna after an informed consent form (ICF) was obtained from all study participants.

2.2. Patient selection

From October 2014 to April 2016, 123 subjects were

enrolled - 51 with NYHA class III-IV heart failure, 53 with STEMI, and 19 healthy individuals serving as controls. Every possible attempt was made to ensure that selected groups, including healthy controls, were matched by age and sex. Patients with STEMI were treated with percutaneous coronary intervention (PCI). All patients with STEMI had a post-procedure Thrombolysis in Myocardial Infarction (TIMI) flow grade of 3. Serum levels of RIPK3 were measured upon admission on Day 0 (< 12 hours of the onset of symptoms) and on Day 1 (24-48 hours after the onset of symptoms). Serum levels of RIPK3 were not evaluated on Day 2 or later after PCI. Inclusion criteria for patients with myocardial infarction were: chest pain with significant (minimum 2-mm) ST segment elevation according to at least 2 contiguous electrocardiogram (ECG) leads, a significant increase in cardiac markers (troponin I > 0.2 ng/mL), and < 12 hours of the onset of symptoms to primary PCI. All of the patients with myocardial infarction underwent cardiac catheterization and were treated with primary angioplasty and stent replacement.

Serum from 51 hospitalized patients with NYHA class III-IV heart failure was collected to measure RIPK3. The current study defined heart failure in accordance with the definition of the European Society of Cardiology (12), which defines heart failure as a clinical syndrome characterized by typical symptoms (*e.g.* breathlessness, ankle swelling, and fatigue) that may be accompanied by signs (*e.g.* elevated jugular venous pressure, pulmonary crackles, and peripheral oedema) caused by a structural abnormality resulting in a reduced cardiac output and/or elevated intracardiac pressures at rest or during stress. Seven (13.7%) of the 51 patients had NYHA class IV heart failure. For most patients (34/51, 66.7%), symptoms of heart failure were due to ischemic heart disease or previous myocardial infarction. In 9/51 patients (17.6%), heart failure was due to idiopathic dilated cardiomyopathy, and in 8/51 patients (15.6%) heart failure was due to some other reason – *e.g.* heart valve disease or arrhythmia. All patients had a decreased LVEF (mean 34.4% ± 8.07). Exclusion criteria for all groups were: a current infection, an inflammatory disease, or an oncological disease.

2.3. Echocardiography

LVEF was measured using the biplane method of disks (Simpson's rule) in accordance with the European Association of Cardiovascular Imaging (13). LVEF was evaluated prior to PCI and upon discharge. The LVEF upon discharge (49.5% ± 9.5) improved significantly compared to the LVEF prior to PCI (47.3% ± 11.6).

2.4. Measurement of RIPK3 and troponin I in serum

For patients with STEMI, peripheral venous blood was drawn at the beginning of the procedure and then again

Table 1. Baseline characteristics of patients with STEMI, patients with heart failure, and healthy control subjects

Demographic characteristics	Patients with heart failure	Patients with STEMI	Significance	Healthy control subjects	Significance
Age; yrs.	67.2 ± 9.3	63.9 ± 12.9	$p = 0.32$	59.5 ± 10.5	$p = 0.11$
Male, %	72.9	57.4	$p = 0.43$	73.7	$p = 0.12$
Hypertension, %	100	100	-	-	-
Diabetes, %	18.6	15.7	$p = 0.68$	-	-
Hypercholesterolemia, %	64.8	70.2	$p = 0.13$	-	-

STEMI: myocardial infarction with ST elevation.

between 24-48 hours after the onset of symptoms. For patients with heart failure, peripheral blood was drawn once during hospitalization. From healthy subjects, samples were collected once from 8-12 AM. Blood was collected in 5-mL containers and no more than 15 min later it was centrifuged at 2,500 g for 20 min. Serum was stored at -80°C. Samples were analyzed for RIPK3 using an ELISA kit (CUSABIO, Wuhan, China) according to the manufacturer's instructions. RIPK3 levels were not used to render clinical decisions about patients. Levels of troponin I in serum were measured with Immulite 2000 (Siemens, Erlangen, Germany).

2.5. Statistical analysis

Statistical analysis was performed with SPSS Statistics v.23 using descriptive statistics. Categorical variables were summarized with frequencies and percentages. Variables are expressed as the mean ± standard deviation (SD). The Mann-Whitney U test, Wilcoxon paired test, Pearson correlation, and χ^2 test were used to compare and estimate correlations between serum levels of RIPK3 and troponin I and demographic and clinical characteristics such as gender and age. The specificity and sensitivity with which serum levels of RIPK3 and troponin I were able to differentiate patients with a preserved LVEF ($\geq 50\%$) from patients with impaired left ventricular function after STEMI upon discharge were evaluated with receiver operating curve (ROC) analysis. The diagnostic accuracy of biomarkers was also determined by obtaining the largest possible area under the curve (AUC) in ROC analysis. Simple logistic regression was used to estimate the odds ratios with which to predict a decreased LVEF after PCI and prior to discharge. Two-tailed p-values (< 0.05) were considered significant.

3. Results

3.1. Patient characteristics and outcomes

Demographic characteristics of patients with STEMI ($n = 53$) and heart failure ($n = 51$) are shown in Table 1. There were no significant differences between healthy control subjects and patients with STEMI in terms of age. There were no significant differences between patients with heart failure and STEMI in terms
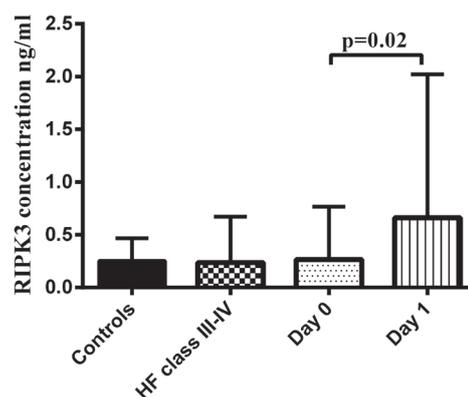
Figure 1. Bar graph, representing serum levels of RIPK3 in healthy controls, patients with class III-IV NYHA heart failure (HF), and patients with STEMI. The Wilcoxon paired test was used to detect significant differences in serum levels of RIPK3 in patients with STEMI on Day 0 and Day 1. Two-tailed p-values (< 0.05) were considered significant. (RIPK3: receptor-interacting protein kinase 3; STEMI: myocardial infarction with ST elevation.)

of demographic variables. Median follow-up was 10 months for patients with STEMI and patients with heart failure. After the follow-up, 5 patients with STEMI and 5 patients with heart failure died due to cardiac causes. Four patients with STEMI were hospitalized again during follow-up due to symptoms of heart failure.

3.2. RIPK3 levels in patients with heart failure or STEMI and its predictive value

The current study sought to determine if RIPK3 is released extracellularly and if it could serve as a marker of necroptosis and cellular injury. RIPK3 was measured in 51 patients with NYHA class III-IV heart failure and 19 healthy subjects. Serum levels of RIPK3 did not differ significantly in healthy persons (mean 0,253 ng/mL ± 0.2) and patients with NYHA class III-IV heart failure (mean 0,236 ng/mL ± 0.4) (Figure 1). Patients with NYHA class III-IV heart failure who died during the follow-up ($n = 5$) had RIPK3 levels that were not significantly higher than those in patients who did not die. Linear and logistic regression were used to evaluate the potential association between baseline variables such as the number of previous hospitalizations due to heart failure, the decrease in the LVEF, and the serum level of RIPK3. No significant associations were noted.

Serum levels of RIPK3 and troponin I were measured

Table 2. Dynamic changes in serum levels of troponin I and RIPK3 in patients with STEMI

Items	Up to 12 hours after the onset of symptoms	24 hours after the onset of symptoms	Significance
Troponin I (ng/mL)	7.6 ± 14.8	42.7 ± 32.1	$p < 0.001$
RIPK3 (ng/mL)	0.264 ± 0.5	0.660 ± 1.3	$p = 0.02$

RIPK3: receptor-interacting protein kinase 3; STEMI: myocardial infarction with ST elevation.

in 53 patients with STEMI on Day 0 following admission to the intensive care unit. All patients underwent PCI and a blood sample was collected on Day 1 to measure levels of RIPK3 and troponin I (Table 2). Serum levels of RIPK3 on Day 0 did not differ significantly from those in patients with NYHA class III-IV heart failure. However, serum levels of RIPK3 on Day 0 (mean 0,264 ng/mL ± 0.5) and Day 1 (mean 0.660 ng/mL ± 1.3) did differ significantly (Figure 1). Troponin I was more sensitive than RIPK3 at detecting early biochemical evidence of cardiac myocyte death. The ROC curve was plotted for highest levels of troponin I and RIPK3 and the LVEF prior to discharge. Neither serum levels of RIPK3 nor troponin I were sufficient to differentiate patients with a preserved LVEF from those with impaired left ventricular function after STEMI. Patients with STEMI who died ($n = 5$) or were hospitalized again ($n = 4$) during follow-up had RIPK3 or troponin I levels that were not significantly higher than those in surviving patients with STEMI.

The current study divided patients with STEMI ($n = 53$) into two groups - one with increased troponin I levels ($n = 25$) and another with normal troponin I levels ($n = 28$) prior to PCI. In patients with normal levels of troponin I prior to PCI, serum levels of RIPK3 and troponin I after PCI were sufficient to differentiate patients with a preserved LVEF and those with impaired left ventricular function after PCI (AUC = 0.780 (95% CI: 0.565-0.995, $p = 0.043$) with a sensitivity of 76.9% and a specificity of 71.4% *vs*. AUC = 0.735 (95% CI: 0.530-0.941, $p = 0.038$) a sensitivity of 88.2% and a specificity of 63.6% at the optimal cutoff values, respectively) (Figure 2). Upon discharge, serum levels of RIPK3 (mean 0.860 ng/mL ± 1.6) and troponin I (mean 139.1 ng/mL ± 55.8) in the patients with an LVEF < 50% were significantly higher than those in patients with a preserved LVEF (Figure 3). Simple logistic regression analysis showed that elevated levels of troponin I after PCI were associated with an increased risk of an LVEF < 50% prior to discharge (odds ratio, 1.014; 95% CI, 1.001 to 1.027; $p = 0.03$), while elevated levels of RIPK3 were not associated with such a risk. There was a weak correlation between serum levels of troponin I and RIPK3, but that correlation was not significant.

4. Discussion

Cell death plays a critical role in the pathogenesis of the major syndromes that affect the heart: heart failure and myocardial infarction. The magnitude and time of cell
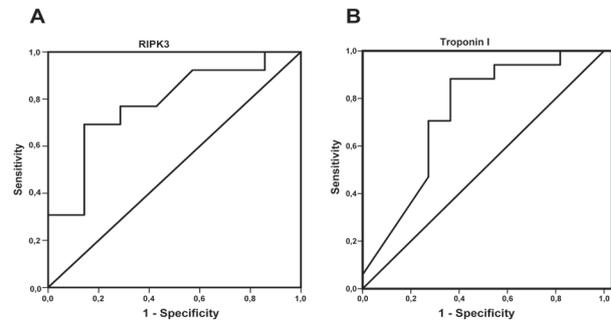
Figure 2. Receiver operating curve (ROC) analysis, using serum levels of RIPK3 and troponin I to differentiate patients with a preserved left ventricular ejection fraction (LVEF) and those with impaired left ventricular function after PCI. All patients included in this analysis had normal troponin I levels prior to percutaneous coronary intervention (PCI). Diagnostic accuracy of biomarkers was determined by obtaining the largest possible area under the curve (AUC) in ROC analysis. **(A)**. RIPK3 AUC = 0.780, **(B)**. Troponin I AUC = 0.735
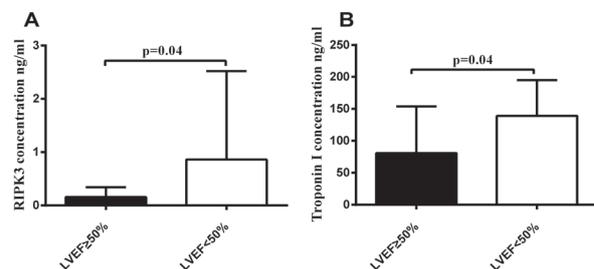
Figure 3. Bar graph, representing serum levels of RIPK3 and troponin I in patients with STEMI and normal troponin I levels prior to percutaneous coronary intervention (PCI) according to the left ventricular ejection fraction (LVEF) prior to discharge. The Mann-Whitney U test was used to detect significant differences in patients' serum levels. Two-tailed p-values (< 0.05) were considered significant. **(A)**. RIPK3, **(B)**. Troponin I

death in these syndromes differ significantly. Patients with heart failure exhibit ongoing myocyte death over months, but patients with myocardial infarction have a spike in cell death for several hours only (*14*).

RIPK3 is a novel regulator of programmed cell death. The goal of the current study was to examine the serum levels of RIPK3 expression in patients with NYHA class III-IV heart failure and patients with STEMI in comparison to levels in healthy control subjects. There were no significant differences in the serum levels of RIPK3 in patients with NYHA class III-IV heart failure and patients with STEMI up to 12 hours after the onset of symptoms in comparison to levels in healthy controls. However, RIPK3 and troponin I were

found to have a potential role in differentiating patients with preserved left ventricular function from patients with impaired left ventricular function after STEMI among patients with normal serum levels of troponin I prior to PCI.

Programmed necrosis mediated by RIPK3 has recently been defined as a novel mechanism of cell death with major functional importance in several organs, including the heart (15). Cell culture experiments in human cell lines have shown that an association between RIPK1 and RIPK3 in response to TNF-α stimulation represents the crucial initial step in programmed necrosis (5). Although the exact mechanisms of necroptosis remain unknown, necroptosis is believed to lead to rapid plasma membrane permeabilization, release of cell contents, and exposure of damage-associated molecular pattern molecules (16). This provokes a strong inflammatory response, resulting in impaired left ventricular function (17). RIPK3 is also responsible for generation of reactive oxygen species, which may be another mechanism for organ damage due to myocardial ischemia (5).

In a study using an *in vivo* model of myocardial infarction 24 hours after permanent ligation of the left anterior descending coronary artery, overexpression of RIPK3 was detected via an immunoblot test in mouse hearts (10). In that study, RIPK3-deficient mice had a significantly better ejection fraction and less hypertrophy in magnetic resonance imaging (MRI) studies 30 days after experimental infarction in comparison to wild-type mice. Moreover, the hearts of RIPK3-deficient mice were found to have lower levels of B-type natriuretic peptide (BNP) and those mice were found to have lower serum levels of troponin T (10). Another *in vivo* study found that pharmacological inhibition of necroptosis reduces infarct size 24 hours after induction of ischemia (18).

The widespread use of PCI has hampered the diagnosis of myocardial necrosis and infarction. Given these circumstances, whether a biomarker alone is sufficient to define myocardial infarction without angiographic evidence of ischemia is still uncertain (19). After PCI, levels of troponin are often elevated without clinical symptoms. Several mechanisms, such as distal embolization of plaques disrupted by a stent or balloon, platelet-rich microthrombi, and vasospasms, have been proposed as an explanation (20). Restoring blood flow can paradoxically induce cardiac injury, but PCI is nonetheless the most effective strategy for improving clinical outcomes. Recently, important differences in the underlying mechanism of myocardial ischemia and reperfusion injury after PCI have been noted (21). The current results suggest that RIPK3 is at least partially involved in this post-procedure injury. This is consistent with previous studies that reported that a deficiency in RIPK3 provides profound protection against cardiac injury induced by reperfusion (22). Several studies in patients with normal levels of troponin prior to PCI have found that an increase in troponin levels after PCI is associated with myocardial necrosis according to MRI and a poor outcome (23-25). The current results suggest that in patients with normal levels of troponin prior to PCI, serum levels of RIPK3 and troponin I after PCI can differentiate patients with preserved left ventricular function and impaired left ventricular function (AUC = 0.780 (95% CI: 0.565-0.995, p = 0.043) with a sensitivity of 76.9% and a specificity of 71.4% vs. AUC = 0.735 (95% CI: 0.530-0.941, p = 0.038) with a sensitivity of 88.2% and a specificity of 63.6% at the optimal cutoff values, respectively) (Figure 2). RIPK3 is not specific to the heart, so other reasons besides myocardial infarction for elevated levels of RIPK3 on Day 1 cannot be ruled out. Only a few studies of human pathology have examined levels of RIPK3 expression and their association with clinical outcomes (26,27). The current results suggest that the serum level of RIPK3 increased significantly 24 hours after the onset of symptoms. Unfortunately, the current results provide no direct evidence that necroptosis is the dominant form of cell death in myocardial damage after PCI. Troponin I is a more specific and sensitive marker than RIPK3 in detecting the level of cardiomyocyte death, but whether existing biomarkers alone and to what extent they are sufficient enough to define PCI-related myocardial injury without the presence of angiographic ischemia is uncertain (24). Significantly elevated serum levels of RIPK3 on Day 1 (after PCI) may indicate myocardial injury after PCI. Therefore, RIPK3 may have the potential to be specific marker for myocardial injury after PCI. However, larger studies are necessary to determine whether RIPK3 can serve as a specific marker of necroptosis and to define its role as a biomarker in patients with myocardial infarction.

A study has indicated that apoptosis is a key factor in the pathogenesis of heart failure (28). The prevalence of necrosis in heart failure has not been studied intensively. Several mice models suggested that necrosis plays a role in the progression of heart failure (29,30). A limitation of the current study, besides its relative small sample, is that most patients had serum levels of RIPK3 close to the minimum detection limits of the assay used. The expected difference in the serum levels of RIPK3 in patients with heart failure and healthy controls was in a very low range that the assay was able to detect. This means that the sensitivity issue is unresolved (31).

In summary, the current results suggest that RIPK3 is significantly elevated in patients with STEMI after PCI, implying that RIPK3 may be involved in post-procedure injury. In patients with normal troponin I levels prior to PCI, elevated levels of RIPK3 and troponin I can serve as a potential marker with which to identify patients with a decreased LVEF prior to discharge. This may allow an early shift to more intensive therapy to improve clinical outcomes.

References

1. Gaziano T, Reddy KS, Paccaud F, Horton S, Chaturvedi V. Cardiovascular Disease. In: Disease Control Priorities in Developing Countries (Jamison DT, Breman JG, Measham AR, Alleyne G, Claeson M, Evans DB, Jha P, Mills A, Musgrove P, eds.). Washington (DC), USA, 2006; pp. 645-662.
2. Orogo AM, Gustafsson AB. Cell death in the myocardium: My heart won't go on. IUBMB Life. 2013; 65:651-656.
3. Kung G, Konstantinidis K, Kitsis RN. Programmed necrosis, not apoptosis, in the heart. Circ Res. 2011; 108:1017-1036.
4. Chiong M, Wang ZV, Pedrozo Z, Cao DJ, Troncoso R, Ibacache M, Criollo A, Nemchenko A, Hill JA, Lavandero S. Cardiomyocyte death: Mechanisms and translational implications. Cell Death Dis. 2011; 2:e244.
5. Zhao H, Jaffer T, Eguchi S, Wang Z, Linkermann A, Ma D. Role of necroptosis in the pathogenesis of solid organ injury. Cell Death Dis. 2015; 6:e1975.
6. Declercq W, Vanden Berghe T, Vandenabeele P. RIP kinases at the crossroads of cell death and survival. Cell. 2009; 138:229-232.
7. He S, Wang L, Miao L, Wang T, Du F, Zhao L, Wang X. Receptor interacting protein kinase-3 determines cellular necrotic response to TNF-alpha. Cell. 2009; 137:1100-1111.
8. Christofferson DE, Yuan J. Necroptosis as an alternative form of programmed cell death. Curr Opin Cell Biol. 2010; 22:263-268.
9. Zhang DW, Shao J, Lin J, Zhang N, Lu BJ, Lin SC, Dong MQ, Han J. RIP3, an energy metabolism regulator that switches TNF-induced cell death from apoptosis to necrosis. Science. 2009; 325:332-336.
10. Luedde M, Lutz M, Carter N, *et al*. RIP3, a kinase promoting necroptotic cell death, mediates adverse remodelling after myocardial infarction. Cardiovasc Res. 2014; 103:206-216.
11. Cho YS, Challa S, Moquin D, Genga R, Ray TD, Guildford M, Chan FK. Phosphorylation-driven assembly of the RIP1-RIP3 complex regulates programmed necrosis and virus-induced inflammation. Cell. 2009; 137:1112-1123.
12. Ponikowski P, Voors AA, Anker SD, *et al*. 2016 ESC Guidelines for the diagnosis and treatment of acute and chronic heart failure: The Task Force for the diagnosis and treatment of acute and chronic heart failure of the European Society of Cardiology (ESC). Developed with the special contribution of the Heart Failure Association (HFA) of the ESC. Eur J Heart Fail. 2016. doi: 10.1002/ejhf.592.
13. Lang RM, Badano LP, Mor-Avi V, *et al*. Recommendations for cardiac chamber quantification by echocardiography in adults: An update from the American Society of Echocardiography and the European Association of Cardiovascular Imaging. Eur Heart J Cardiovasc Imaging. 2015; 16:233-270.
14. Kajstura J, Cheng W, Reiss K, Clark WA, Sonnenblick EH, Krajewski S, Reed JC, Olivetti G, Anversa P. Apoptotic and necrotic myocyte cell deaths are independent contributing variables of infarct size in rats. Lab Invest. 1996; 74:86-107.
15. Linkermann A, Green DR. Necroptosis. N Engl J Med. 2014; 370:455-465.
16. Kanduc D, Mittelman A, Serpico R, *et al*. Cell death: Apoptosis versus necrosis (review). Int J Oncol. 2002; 21:165-170.
17. Kaczmarek A, Vandenabeele P, Krysko DV. Necroptosis: The release of damage-associated molecular patterns and its physiological relevance. Immunity. 2013; 38:209-223.
18. Oerlemans MI, Liu J, Arslan F, den Ouden K, van Middelaar BJ, Doevendans PA, Sluijter JP. Inhibition of RIP1-dependent necrosis prevents adverse cardiac remodeling after myocardial ischemia-reperfusion *in vivo*. Basic Res Cardiol. 2012; 107:270.
19. Prasad A, Herrmann J. Myocardial infarction due to percutaneous coronary intervention. N Engl J Med. 2011; 364:453-464.
20. Thygesen K, Alpert JS, Jaffe AS, *et al*. Third universal definition of myocardial infarction. Circ J. 2012; 126:2020-2035.
21. Buja LM. Myocardial ischemia and reperfusion injury. Cardiovasc Pathol. 2005; 14:170-175.
22. Zhang T, Zhang Y, Cui M, *et al*. CaMKII is a RIP3 substrate mediating ischemia- and oxidative stress-induced myocardial necroptosis. Nat Med. 2016; 22:175-182.
23. Tricoci P, Leonardi S. Determining myocardial infarction after PCI: CK-MB, troponin, both, or neither? MLO Med Lab Obs. 2015; 47:14, 16.
24. Tricoci P, Leonardi S, White J, White HD, Armstrong PW, Montalescot G, Giugliano RP, Gibson CM, Van de Werf F, Califf RM, Harrington RA, Braunwald E, Mahaffey KW, Newby LK. Cardiac troponin after percutaneous coronary intervention and 1-year mortality in non-ST-segment elevation acute coronary syndrome using systematic evaluation of biomarker trends. J Am Coll Cardiol. 2013; 62:242-251.
25. Herrmann J. Peri-procedural myocardial injury: 2005 update. Eur Heart J. 2005; 26:2493-2519.
26. Qing DY, Conegliano D, Shashaty MG, Seo J, Reilly JP, Worthen GS, Huh D, Meyer NJ, Mangalmurti NS. Red blood cells induce necroptosis of lung endothelial cells and increase susceptibility to lung inflammation. Am J Respir Crit Care Med. 2014; 190:1243-1254.
27. Roychowdhury S, McMullen MR, Pisano SG, Liu X, Nagy LE. Absence of receptor interacting protein kinase 3 prevents ethanol-induced liver injury. Hepatology. 2013; 57:1773-1783.
28. Whelan RS, Kaplinskiy V, Kitsis RN. Cell death in the pathogenesis of heart disease: Mechanisms and significance. Annu Rev Physiol . 2010; 72:19-44.
29. Nakayama H, Chen X, Baines CP, Klevitsky R, Zhang X, Zhang H, Jaleel N, Chua BH, Hewett TE, Robbins J, Houser SR, Molkentin JD. Ca2+- and mitochondrial-dependent cardiomyocyte necrosis as a primary mediator of heart failure. J Clin Invest. 2007; 117:2431-2444.
30. Elrod JW, Wong R, Mishra S, Vagnozzi RJ, Sakthievel B, Goonasekera SA, Karch J, Gabel S, Farber J, Force T, Brown JH, Murphy E, Molkentin JD. Cyclophilin D controls mitochondrial pore-dependent Ca(2+) exchange, metabolic flexibility, and propensity for heart failure in mice. J Clin Invest. 2010; 120:3680-3687.
31. Leng SX, McElhaney JE, Walston JD, Xie D, Fedarko NS, Kuchel GA. ELISA and multiplex technologies for cytokine measurement in inflammation and aging research. J Gerontol A Biol Sci Med Sci. 2008; 63:879-884.

Original Article

Age does not affect complications and overall survival rate after pancreaticoduodenectomy: Single-center experience and systematic review of literature

Yoshihiro Miyazaki[1,*], Takashi Kokudo[1,*], Katsumi Amikura[1], Yumiko Kageyama[1], Amane Takahashi[1], Nobuhiro Ohkohchi[2], Hirohiko Sakamoto[1]

[1] *Division of Gastroenterological Surgery, Saitama Cancer Center, Saitama, Japan;*
[2] *Department of Surgery, Clinical Sciences, Faculty of Medicine, University of Tsukuba, Tsukuba, Ibaraki, Japan.*

Summary   We aimed to evaluate the feasibility of pancreaticoduodenectomy (PD) in elderly patients. We retrospectively analyzed data from 206 patients who underwent PD between 2008 and 2015. The patients were divided into two groups: patients aged < 70 years ($n = 117$) and those aged ≥ 70 years ($n = 89$). To update the outcome of PD in elderly patients, we performed a systematic review of published work. The preoperative patient characteristics were similar between the two groups except for hypertension, which was significantly more frequent in the older group (25% *vs.* 52%; $p < 0.001$). There was no difference in the mortality (0% *vs.* 1%; $p = 0.43$) or morbidity (26% *vs.* 20%; $p = 0.41$) rates between the two groups. The overall survival rate in patients with pancreatic cancer between the two groups did not differ ($p = 0.40$). Twenty-one studies, including our own, were identified in the published work. The overall median morbidity and mortality rates of the elderly patients were 41.5% (range, 20-78%) and 5.8% (range, 0-10.5%), respectively. PD is feasible in elderly patients with acceptable morbidity and mortality rates.

Keywords: Pancreaticoduodenectomy, elderly, complication, mortality, pancreatic neoplasm

1. Introduction

In the early 1990s, pancreaticoduodenectomy (PD) was rarely performed in elderly patients because of the high postoperative morbidity and mortality rates, even in young patients. During the last two decades, the mortality rates after pancreatic resection have decreased to no more than 2% in experienced centers (*1,2*), with an acceptable morbidity rate.

Several reports have shown that postoperative complication rates of surgical resection in elderly patients are similar to those in younger patients, and the overall survival is comparable (*3-5*). Others have shown

the contrary, *i.e.*, elderly patients have a higher mortality rate, have a tendency to stay longer in the intensive care unit, have higher incidences of postoperative cardiac events, experience more nutritional and functional difficulties, and show a higher rate of readmission compared to younger patients (*6-8*).

The aim of the present study was to compare the postoperative complication rate and overall survival between patients younger and older than 70 years old who underwent PD. Moreover, we performed a systematic review of the literature related to complications of PD in elderly patients.

2. Materials and Methods

2.1. Patients

A prospectively collected database of 206 patients who underwent PD from January 2008 to December 2015 in our department was retrospectively analyzed. The patients who had a performance status of 2 or more,

symptomatic cardiac or pulmonary insufficiency, renal failure with dialysis, or dementia were considered as contraindicated for PD regardless of age in our department. Neoadjuvant chemotherapy or radiotherapy was not performed.

Patients who underwent PD were divided into two groups: patients aged < 70 years (young group) and patients aged ≥ 70 years (old group). The two groups were compared in terms of preoperative demographic features, comorbidities, surgical procedures, postoperative outcomes, nutritional status, and survival. Preoperative comorbidities included diabetes mellitus, chronic obstructive pulmonary disease, hypertension, coronary artery disease, cardiac insufficiency, renal insufficiency, and cerebrovascular disease.

The surgical procedure included exploration, tumor resection and regional lymph node dissection. Subtotal stomach-preserving PD with reconstruction through pancreaticojejunostomy or pancreaticogastrostomy was performed. Pancreaticogastrostomy was performed in patients with soft pancreatic texture or a small pancreatic duct. In patients with portal vein invasion, portal vein resection was associated with PD. One of the two staff surgeons in our institution always participated in the operation as either the operator or instructor, and PD was performed in the same manner for all patients.

Postoperative mortality was defined as death within 30 days after the operation or during hospitalization. A postoperative pancreatic fistula (POPF) was defined according to the criteria of the International Study Group of Pancreatic Fistula (ISGPF) (*9*); postoperative pancreatic hemorrhage (PPH) according to the criteria of International Study Group of Pancreatic Surgery (ISGPS) (*10*); bile leakage according to the International Study Group of Liver Surgery (ISGLS) (*11*), delayed gastric emptying (DGE) according to the ISGPS criteria (*12*). Postoperative abdominal complications were recorded and graded according to the Dindo-Clavien classification (*13*). Grade III or IV complications were categorized as severe complications. Nutritional status was evaluated using prognostic nutritional index (PNI) (*14*). PNI was calculated by the following formula: 10 × serum albumin level (g/dL) × absolute lymphocyte count (number/mm^2). PNI was evaluated preoperatively and 6 months postoperatively.

2.2. Review of literature

To understand the outcomes of PD in elderly patients, we performed a systematic review of published work on this topic based on the data available on PubMed (1976-2015). The search strategy used the following terms: "pancreaticoduodenectomy, complication, aged, and 70." Related citations in the retrieved articles were also reviewed. Postoperative mortality and morbidity rates and the length of hospital stay were analyzed.

2.3. Statistical analysis

Statistical analysis was performed using JMP 11 software (SAS Institute Inc., Cary, NC). Categorical variables were analyzed using Chi-square or Fisher's exact test, as appropriate. Continuous variables were analyzed using the Wilcoxon rank-sum test. The overall survival curves were determined using the Kaplan-Meier method and compared using the log-rank test. All statistical analyses were two-tailed and *p*-values < 0.05 were considered to indicate statistical significance.

3. Results

3.1. Patient characteristics

During the study period, 206 patients underwent PD in our department: 117 patients belonged to the young group and 89 patients belonged to the old group. Patients underwent PD for pancreatic cancer (47%), bile duct cancer (26%), intraductal papillary mucinous neoplasm (13%), ampullary cancer (8%), and other diseases (6%). The preoperative patients characteristics were similar between the two groups except for hypertension, which was significantly more frequent in the old group (25% *vs.* 52%; *p* < 0.001), and the preoperative hemoglobin level, which was significantly lower in the old group [12.3 g/dL (interquartile range: 11.4-13.6) *vs.* 11.7 g/dL (interquartile range: 10.7-12.6); *p* = 0.005] (Table 1).

There were no differences in the operative time, pancreatic texture, anastomosis, concomitant other procedures (*e.g.*, colectomy and hepatectomy), or the vascular resection frequency between the two groups (Table 2). However, intraoperative blood loss was larger [823 mL (interquartile range, 548-1269 ml) *vs.* 1020 mL (interquartile range, 655-1564 mL); *p* = 0.04] and the red blood cell transfusion rate was higher in the old group (20% *vs.* 33%; *p* = 0.04).

3.2. Short-term outcomes

Of the 206 patients, only one patient died of postoperative pancreatic fistula. There was no difference in the mortality rate (0% *vs.* 1%; *p* = 0.43) and complication rates (26% *vs.* 20% *p* = 0.41) between the two groups (Table 3). The most frequent complication in both groups was pancreatic fistula: grade A [6/117 (5%) *vs.* 2/89 (2%); *p* = 0.47], grade B [24/117 (21%) *vs.* 13/89 (15%); *p* = 0.35] grade C [1/117 (1%) *vs.* 2/89 (2%); *p* = 0.57]. There were no differences in the postoperative length of hospital stay: 23 days (interquartile range, 18-29 days) *vs.* 23 days (interquartile range, 19-31 days); *p* = 0.95.

There were no differences in the mortality rate [0/101 (0%) *vs.* 1/83 (1%); *p* = 0.45] and complication rate [23/101 (26%) *vs.* 17/83 (20%); *p* = 0.72] between the two groups in the malignancy patients sub-group.

Table 1. Preoperative baseline characteristics of the younger (age < 70) and the elderly (age ≥ 70) groups

Items	Age < 70, n = 117	Age ≥ 70, n = 89	p-value
Age (median (range), y)	63 (40-69)	75 (70-86)	< 0.001
Sex (Male/Female)	70/47 (60/40)	51/38 (57/43)	0.77
Body mass index (median (range), kg/m^2)	21.5 (14-34.3)	21.6 (15.6-31.2)	0.78
ASA score			
1-2	107 (91%)	76 (85%)	0.19
3-4	10 (9%)	13 (15%)	
Comorbidities			
Diabetes mellitus	29 (25%)	24 (27%)	0.75
COPD	23 (20%)	23 (26%)	0.31
Hypertension	29 (25%)	46 (52%)	< 0.001
Coronary artery disease	6 (5%)	8 (9%)	0.40
Cardiac insufficiency	1 (1%)	4 (5%)	0.17
Renal insufficiency	4 (3%)	4 (5%)	0.73
Cerebrovascular disease	5 (4%)	6 (7%)	0.54
Tabacco use	58 (50%)	32 (36%)	0.07
Ethanol use	39 (33%)	33 (37%)	0.66
Hemoglobin level (median (IQR), g/dL)	12.3 (11.4-13.6)	11.7 (10.7-12.6)	0.005
Malignancy	101 (86%)	83 (93%)	0.17
Pancreatic cancer	56 (48%)	42 (47%)	0.92
Bile duct cancer	30 (26%)	25 (28%)	0.69
Ampullary cancer	8 (7%)	9 (10%)	0.40
Other	7 (6%)	7 (8%)	0.59

ASA, American society of anesthesiologist; COPD, chronic obstructive pulmonary disease; IQR, interquartile range.

Table 2. Intraoperative data of the younger (age < 70) and the elderly (age ≥ 70) groups

Items	Age < 70, n = 117	Age ≥ 70, n = 89	p-value
Operative time (median (IQR), min)	435 (IQR, 385-500)	440 (IQR, 378-525)	0.48
Portal vein resection	20 (17%)	21 (24%)	0.29
Pancreatic texture			0.12
Hard	100 (85%)	83 (93%)	
Soft	17 (15%)	6 (7%)	
Anastmosis			1.00
Pancreaticogastrostomy	5 (4.3%)	3 (3.4%)	
Pancreaticojejunostomy	112 (95.7%)	86 (96.6%)	
Additional procedure	18 (15%)	11 (12%)	0.69
Blood loss (median (IQR), mL)	823 (IQR, 548-1269)	1020 (IQR, 655-1564)	0.04
Patients requiring RBC transfusion	23 (20%)	29 (33%)	0.04
Patients requiring FFP transfusion	8 (7%)	12 (13%)	0.15

IQR, interquartile range; RBC, red blood cells; FFP, fresh frozen plasma.

Table 3. Short-term outcomes of the younger (age < 70) and the elderly (age ≥ 70) groups

Items	Age < 70, n = 117	Age ≥ 70, n = 89	p-value
Postoperative complication			
Pancreatic fistula*			
Grade A	6 (5%)	2 (2%)	0.47
Grade B	24 (21%)	13 (15%)	0.35
Grade C	1 (1%)	2 (2%)	0.57
Delayed gastric emptying	1 (1%)	0	1
Hemorrhage	0	0	0
Bile leakage	1 (1%)	0	1
Cholangitis	0	1 (1%)	0.43
Heart failure	0	1 (1%)	0.43
Pneumonia	0	0	0
Overall complication	30 (26%)	18 (20%)	0.41
Postoperative length of stay (median (IQR), d)	23 (IQR, 18–29)	23 (IQR, 19–31)	0.95
Mortality	0 (0%)	1 (1%)	0.43

Grade III to IV according to Dindo *et al*. Classification; *according to the criteria from the International Study Group of Pancreatic Fistula; IQR, interquartile range.
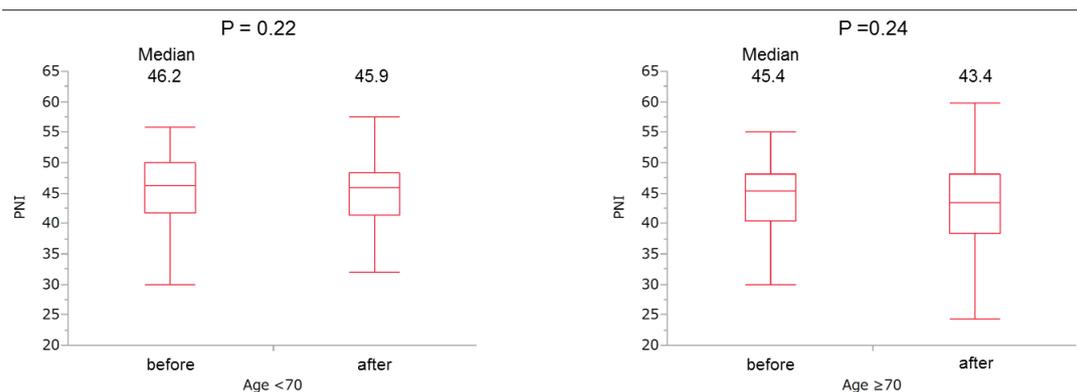
Figure 1. The prognostic nutritional index (PNI) before and after surgery of the younger (age < 70) and the elderly (age ≥ 70) groups.
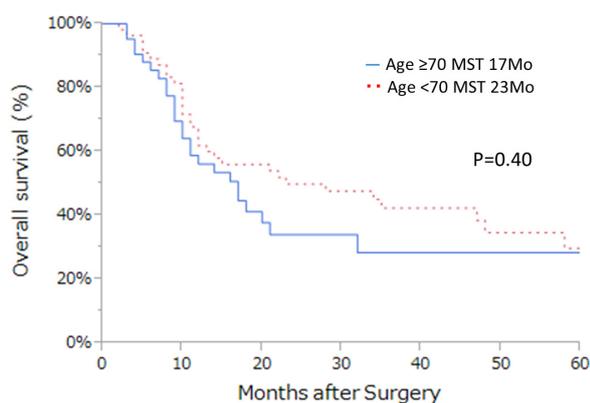
Figure 2. Overall survival of pancreatic cancer patients in the younger (age < 70) and the elderly (age ≥ 70) groups.

3.3. *Long-term outcomes*

Adjuvant chemotherapy was performed in 90 patients. There was no difference in the frequencies of adjuvant chemotherapy between the two groups (54% *vs.* 42%; *p* = 0.102). The preoperative and postoperative PNIs were not different in both groups (Figure 1).

Of the 206 patients, 98 patients underwent PD for pancreatic cancer. Among the 98 patients, there were no differences in the frequencies of R0 resection [45/56 (80%) *vs.* 27/42 (64%); *p* = 0.11], histological papillary or well differentiated adenocarcinoma [16/56 (29%) *vs.* 8/42 (19%); *p* = 0.35], and the Union for International Cancer Control (UICC) cancer stage I or II [5/56 (9%) *vs.* 3/42 (7%); *p* = 1.00] between the two groups.

The median survival time of the young group and old group was 23 and 17 months, respectively (Figure 2). The overall survival between the two groups did not differ (*p* = 0.40). The overall 1-, 3-, and 5-year survival rates of the young group were 62%, 42%, and 25%, respectively, and those of the old group were 56%, 28%, and 28%, respectively.

3.4. *Systematic review*

A review of the published work on the complications of PD in the elderly is shown in Table 4. A total of 21 studies were identified (*15-34*). A total of 6,933 PDs were collected, and of these, 1,931 PDs (27.9%) were performed in elderly patients. The overall median morbidity and mortality rates of the elderly patients were 41.5% (range, 20-78%) and 5.8% (range, 0-10.5%), respectively. Fourteen studies showed that the outcome after PD was not different between the young and old groups. Two studies showed that morbidity and mortality of elderly patients were worse than those of younger patients. Five studies showed that either the morbidity or the mortality of the old group was worse than that of the young group.

4. Discussion

In the present study, patients aged ≥ 70 years had similar outcomes compared to those aged < 70 years, with no differences in the morbidity, mortality, or pancreatic fistula rates. The older group also had lengths of hospital stay similar to that of the young group. There was no difference in the postoperative nutritional state or tolerance of adjuvant chemotherapy between the two groups. Overall survival after the resection of pancreatic cancer was similar between the two groups. Therefore, PD is feasible and can be safely performed in elderly patients with acceptable postoperative survival.

We set 70 years as the cut-off value, because it was the most frequent value used in the literature. Several papers showed that age is one of the risk factors for postoperative complications. Kimura *et al.* reported that age was a risk factor for mortality using the Japanese national clinical database (*6*). However, the indication of PD in the elderly differs among institutions. One of the reasons why there was no difference in the morbidity rate in the present study may be the appropriate patient selection criteria in our department. The patients who had a performance status of 2 or more, symptomatic cardiac or pulmonary insufficiency, renal failure with dialysis, or dementia were considered as contraindications for PD regardless of age in our department, similar to the criteria proposed by Tzeng

Table 4. Postoperative outcome of pancreaticoduodenectomy for elderly patients published in the English literature

Author	Year	*n*	Mortality (%)	*p*-value	Morbidity (%)	*p*-value	Postoperative hospital stay (d)	*p*-value
Fong (*15*)	1995	350 *vs.* 138	4 *vs.* 6	NS	39 *vs.* 45	NS	20 *vs.* 20	NS
Richter (*16*)	1996	293 *vs.* 45	1.9 *vs.* 4.3	Not reported	22 *vs.* 39	Not reported	Not reported	Not reported
Dicarlo (*17*)	1998	85 *vs.* 33	4 *vs.* 6	NS	33 *vs.* 39	NS	17 *vs.* 17	NS
Bottger (*18*)	1999	300 (total)	3.2 *vs.* 2.3	NS	22.1 *vs.* 30.2	Not reported	Not reported	Not reported
al-Sharaf (*19*)	1999	47 *vs.* 27	4 *vs.* 7	NS	46 *vs.* 45	NS	16 *vs.* 13	NS
Hodul (*20*)	2001	74 *vs.* 48	1.4 *vs.* 0	NS	35 *vs.* 40	NS	11 *vs.* 12	NS
Muscari (*21*)	2006	248 *vs.* 52	8 *vs.* 17	< 0.03	38 *vs.* 42	NS	Not reported	Not reported
Brozetti (*22*)	2006	109 *vs.* 57	3.7 *vs.* 10.5	NS	46 *vs.* 49	NS	16 *vs.* 16	NS
Kang (*23*)	2007	66 *vs.* 11	1.5 *vs.* 0	NS	38 *vs.* 73	0.049	23 *vs.* 29	NS
Ouaissi (*24*)	2008	150 (total)	0 *vs.* 16	Not reported	36 *vs.* 56	NS	19 *vs.* 21	NS
Shin (*25*)	2011	36 *vs.* 19	2.7 *vs.* 0	NS	52.8 *vs.* 57.9	NS	30.2 *vs.* 37.8	0.148
de Franco (*26*)	2011	41 *vs.* 41	2.5 *vs.* 5	NS	78 *vs.* 71	NS	29 *vs.* 30	NS
Haigh (*27*)	2011	1633 *vs.* 977	1.7 *vs.* 4.3	< 0.001	34 *vs.* 41	0.001	Not reported	Not reported
Lahat (*28*)	2011	173 *vs.* 120	2.3 *vs.* 5.8	0.02	29 *vs.* 41	0.01	20 *vs.* 28	< 0.0001
Brachet (*29*)	2012	173 (total)	4.1 *vs.* 12	NS	Not available	0.002	Not available	Not available
Kanda (*30*)	2014	272 (total)	0 *vs.* 0	NS	40 *vs.* 35	NS	Not reported	Not reported
Sun (*31*)	2014	208 *vs.* 88	1.0 *vs.* 1.1	NS	61 *vs.* 78	0.003	28 *vs.* 30	NS
Adham (*32*)	2014	228 *vs.* 116	3.9 *vs.* 13	0.003	68 *vs.* 72	NS	23 *vs.* 25	NS
Zhang (*33*)	2015	148 *vs.* 70	3.4 *vs.* 8.8	NS	54 *vs.* 41	NS	20 *vs.* 25	0.013
Urbonas (*34*)	2015	251 (total)	2.8 *vs.* 8.3	NS	22.4 *vs.* 29.6	NS	Not reported	Not reported
Present case	2016	117 *vs.* 89	0 *vs.* 1	NS	26 *vs.* 20	NS	23 *vs.* 23	NS

NS, not significant.

et al. (*35*). Postoperative hemorrhage, pancreatic fistula and delayed gastric emptying are the three most common surgical complications after PD. The incidence of these complications varies among studies. DiCarlo *et al.* (*17*) reported that patients aged ≥ 70 years had more relaparotomies and hemorrhagic complications following pancreatic resection. A French study by Scurtu *et al.* (*36*) demonstrated a statistically higher incidence of delayed gastric emptying in the old group. However, our study showed that there were no significant differences in these three complications between the two groups with similar postoperative length of hospital stay; this result was similar to that reported by Kanda *et al.* (*30*), Usuba *et al.* (*37*), and Hatzaras *et al.* (*38*). However, in our study, the red blood cell transfusion rate was higher in the old group. This may be due to the fact that elderly patients had preoperative anemia more frequently and more intraoperative blood loss than the young patients.

A literature review concerning PD in elderly patients is summarized in Table 4. In the vast majority of studies, the reported postoperative mortality and complication rates after PD were slightly higher in the group defined as elderly, but the difference was not statistically significant (Table 4) (*15-34*). Many of these series concluded that PD is feasible in elderly patients with acceptable morbidity and mortality rates, which is consistent with our conclusion.

Several single-institution studies have described long-term survival following PD in elderly patients for malignancy. The reported median overall survival ranged from 14-38 months and 5-year survival rates ranged from 12-31% (*15,17,27,39*). In the present study, the median survival time of the two groups were

17 months in the old group and 23 months in the young group. Furthermore, the 5-year survival rate was 28.3% and 24.7%, respectively. One of the reasons that the older patients exhibited a good long-term outcome, as well as the younger patients is patient selection. We performed PD for selected patients who were in good condition, without cardio-pulmonary disease and severe renal insufficiency. Thus, the older patients in this study had a good long-term outcome. These results are comparable with the previous reports and justify PD in elderly patients with pancreatic cancer.

A limitation of our study is the relatively small number of elderly patients and the retrospective nature of the study. Therefore, we attempted to overcome this limitation by adding a systematic review of the published work. There may be a selection bias (*i.e.*, all subjects were a selected subset of relatively fit patients in the old group): however, the preoperative characteristics were similar between the two groups. As shown in the recent evidence (*33,40*), PD is certainly a feasible procedure in selected elderly patients.

Several studies have shown that age is a risk factor for postoperative morbidity and mortality following PD (*27,41*). However, others (including ours) have demonstrated that there are no differences in the incidence of postoperative complications between the two groups (*3-5*). These results may indicate that the patient selection and preoperative recognition of high-risk patients are important in elderly patients before PD. Several methods for assessing the surgical risk of the old group have been introduced in clinical practice: Charlson comorbidity index (*42*), G8 geriatric screening tool (*43*), and Adult Comorbidity Evaluation-27 (*44*). These scoring systems may be helpful in selecting

elderly patients before PD.

In conclusion, PD is feasible in elderly patients with acceptable morbidity and mortality rates. Moreover, the overall survival rate in patients with pancreatic cancer did not differ between the old and young groups.

References

1.	Winter JM, Cameron JL, Campbell KA, Arnold MA, Chang DC, Coleman J, Hodgin MB, Sauter PK, Hruban RH, Riall TS, Schulick RD, Choti MA, Lillemoe KD, Yeo CJ. 1423 pancreaticoduodenectomies for pancreatic cancer: A single institution experience. J Gastrointest Surg. 2006; 10:1199-1210.

2.	Fernández-del Castillo C, Morales-Oyarvide V, McGrath D, Wargo JA, Ferrone CR, Thayer SP, Lillemoe KD, Warshaw AL. Evolution of Whipple procedure at the Massachusetts General Hospital. Surgery. 2012; 152:s56-s63.

3.	Stauffer JA, Grewal MS, Martin JK, Nguyen JH, Asbun HJ. Pancreas surgery is safe for octogenarians. J Am Geriatr Soc. 2011; 59:184-186.

4.	Lee MK, Dinorcia J, Reavey PL, Nguyen JH, Asbun HJ. Pancreaticoduodenectomy can be performed safely in patients aged 80 years and older. J Gastrointest Surg. 2010; 14:1838-1846.

5.	Oliverius M, Kala Z, Varga M, Gürlich R, Lanska V, Kubesova H. Radical surgery for pancreatic malignancy in the elderly. Pancreatology. 2010; 10:499-502.

6.	Kimura W, Miyata H, Gotoh M, Hirai I, Kenjo A, Kitagawa Y, Shimada M, Baba H, Tomita N, Nakagoe T, Sugihara K, Mori M. A pancreaticoduodenectomy risk model derived from 8575 cases from a national single-race population (Japanese) using a web-based data entry system: The 30-day and in-hospital mortality rates for pancreaticoduodenectomy. Ann Surg. 2014; 259:773-80.

7.	Lightner AM, Glasgow RE, Jordan TH, Krassner AD, Way LW, Mulvihill SJ, Kirkwood KS. Pancreatic resection in the elderly. J Am col Surg. 2004; 198:697-706.

8.	Yermilov I, Bentrem D, Sekeris E, Jain S, Maggard MA, Ko CY, Tomlinson JS.Readmissions following pancreaticoduodenectomy for pancreas cancer: A population-based appraisal. Ann Surg Oncol. 2009; 16:554-561.

9.	Bassi C, Dervenis C, Butturini G, Fingerhut A, Yeo C, Izbicki J, Neoptolemos J, Sarr M, Traverso W, Buchler M; International Study Group on Pancreatic Fistula Definition. Postoperative pancreatic fistula: An international study group (ISGPF) definition. Surgery. 2005; 138:8-13.

10.	Wente MN, Veit JA, Bassi C, Dervenis C, Fingerhut A, Gouma DJ, Izbicki JR, Neoptolemos JP, Padbury RT, Sarr MG, Yeo CJ, Büchler MW. Postpancreatectomy hemorrhage (PPH): An International Study Group of Pancreatic Surgery (ISGPS) definition. Surgery. 2007; 142:20-25.

11.	Koch M, Garden OJ, Padbury R, et al. Bile leakage after hepatobiliary and pancreatic surgery: A definition and grading of severity by the International Study Group of Liver Surgery. Surgery. 2011; 149:680-688.

12.	Wente MN, Bassi C, Dervenis C, Fingerhut A, Gouma DJ, Izbicki JR, Neoptolemos JP, Padbury RT, Sarr MG, Traverso LW, Yeo CJ, Büchler MW. Delayed gastric emptying (DGE) after pancreatic surgery: A suggested definition by the International Study Group of Pancreatic Surgery (ISGPS). Surgery. 2007; 142:761-768.

13.	Clavien PA, Barkun J, de Oliveira ML, Vauthey JN, Dindo D, Schulick RD, de Santibañes E, Pekolj J, Slankamenac K, Bassi C, Graf R, Vonlanthen R, Padbury R, Cameron JL, Makuuchi M. The Clavien-Dindo classification of surgical complications: Five-year experience. Ann Surg. 2009; 250:187-196.

14.	Onodera T, Goseki N, Kosaki G. Prognostic nutritional index in gastrointestinal surgery of malnourished cancer patients. Nihon Geka Gakkai Zasshi. 1984; 85:1001-1005.

15.	Fong Y, Blumgart LH, Fortner JG, Brennan MF. Pancreatic or liver resection for malignancy is safe and effective for the elderly. Ann Surg. 1995; 222:426-434.

16.	Richiter A, Schwab M, Lorenz D, Rumstadt B, Trede M. Surgical therapy of pancreatic carcinoma in elderly patients over 70. Langenbecks Arch Chir Suppl Kongressbd. 1996; 113:492-494.

17.	DiCarlo V, Balzano G, Zerbi A, Villa E. Pancreatic cancer resection in elderly patients. Br J Surg. 1998; 85:607-610.

18.	Bottger TC, Engelmann R, JunGinger T. Is age a risk for major pancreatic surgery? An analysis of 300 resections. Hepatogastroenterology. 1999; 46:2589-2598

19.	al-Sharaf K, Andren-Sandberg A, Ihse I. Subtotal pancreatomy for cancer can be safe in the elderly. Eur J Surg. 1999; 165:230-235.

20.	Hodul P, Tansey J, Golts E, Oh D, Pickleman J, Aranha GV. Age is not a contraindication to pancreatico-duodenectomy. Am Surg. 2001; 67:270-275.

21.	Muscari F, Suc B, Kirzin S, Hay JM, Fourtanier G, Fingerhut A, Sastre B, Chipponi J, Fagniez PL, Radovanovic A; French Associations for Surgical Research. Risk factors for mortality and intra-abdominal complications after pancreatoduodenectomy: Multivariate analysis in 300 patients. Surgery. 2006; 139:591-598.

22.	Brozzetti S, Mazzoni G, Miccini M, Puma F, De Angelis M, Cassini D, Bettelli E, Tocchi A, Cavallaro A. Surgical treatment of pancreatic head carcinoma in elderly patients. Arch Surg. 2006; 141:137-142.

23.	Kang CM, Kim JY, Choi GH, Kim KS, Choi JS, Lee WJ, Kim BR. Pancreaticoduodenectomy of pancreatic ductal adenocarcinoma in the elderly. Yonsei Med J. 2007; 48:488-494.

24.	Ouaïssi M, Sielezneff I, Pirrò N, Merad A, Loundou A, Chaix JB, Dahan L, Ries P, Seitz JF, Payan MJ, Consentino B, Sastre B. Pancreatic cancer and pancreaticoduodenectomy in elderly patient: Morbidity and mortality are increased. Is it the real life? Hepatogastroenterology. 2008; 55:2242-2246.

25.	Shin JW, Ahn KS, Kim YH, Kang KJ, Lim TJ. The impact of old age on surgical outcomes after pancreaticoduodenectomy for distal bile duct cancer. Korean J Hepatobiliary Pancreat Surg. 2011; 15:248-253.

26.	de Franco V, Frampas E, Wong M, Meurette G, Charvin M, Leborgne J, Regenet N. Safety and feasibility of pancreaticoduodenectomy in the elderly: A matched study. Pancreas. 2011; 40:920-924.

27.	Haigh PI, Bilimoria KY, DiFronzo LA. Early postoperative outcomes after pancreaticoduodenectomy in the elderly. Arch Surg. 2011; 146:715-723.

28.	Lahat G, Sever R, Lubezky N, Nachmany I, Gerstenhaber F, Ben-Haim M, Nakache R, Koriansky J, Klausner JM. Pancreatic cancer: Surgery is a feasible therapeutic option for elderly patients. World J Surg Oncol. 2011; 9:10.

29. Brachet D, Lermite E, Vychnevskaia-Bressollette K, Mucci S, Hamy A, Arnaud JP. Should pancreaticoduodenectomy be performed in the elderly? Hepatogastroenterology. 2012; 59:266-271.

30. Kanda M, Fujii T, Suenaga M, Takami H, Inokawa Y, Yamada S, Kobayashi D, Tanaka C, Sugimoto H, Nomoto S, Fujiwara M, Kodera Y. Pancreatoduodenectomy with portal vein resection is feasible and potentially beneficial for elderly patients with pancreatic cancer. Pancreas. 2014; 43:951-958.

31. Sun JW, Zhang PP, Ren H, Hao JH. Pancreatico-duodenectomy and pancreaticoduodenectomy combined with superior mesenteric-portal vein resection for elderly cancer patients. Hepatobiliary Pancreat Dis Int. 2014; 13:428-434.

32. Adham M, Bredt LC, Robert M, Perinel J, Lombard-Bohas C, Ponchon T, Valette PJ. Pancreatic resection in elderly patients: Should it be denied? Langenbecks Arch Surg. 2014; 399:449-459.

33. Zhang D, Gao J, Li S, Wang F, Zhu J, Leng X. Outcome after pancreaticoduodenectomy for malignancy in elderly patients. Hepatogastroenterology. 2015; 62:451-454.

34. Urbonas K, Gulbinas A, Smailyte G, Pranys D, Jakstaite A, Pundzius J, Barauskas G. Factors influencing survival after pancreatoduodenectomy for ductal adenocarcinoma depend on patients' age. Dig Surg. 2015; 32:60-67.

35. Tzeng CW, Katz MH, Fleming JB, Lee JE, Pisters PW, Holmes HM, Varadhachary GR, Wolff RA, Abbruzzese JL, Vauthey JN, Aloia TA. Morbidity and mortality after pancreaticoduodenectomy in patients with borderline resectable type C clinical classification. J Gastrointest Surg. 2014; 18:146-155.

36. Scurtu R, Bachellier P, Oussoultzoglou E, Rosso E, Maroni R, Jaeck D. Outcome after pancreatico-duodenectomy for cancer in elderly patients. J Gastrointest Surg. 2006; 10:813-822.

37. Usuba T, Takeda Y, Murakami K, Tanaka Y, Hanyu N. Clinical outcomes after pancreaticoduodenectomy in elderly patients at middle-volume center. Hepatogastroenterology. 2014; 61:1762-1766.

38. Hatzaras I, Schmidt C, Klemanski D, Muscarella P, Melvin WS, Ellison EC, Bloomston M. Pancreatic resection in the octogenarian: A safe option for pancreatic malignancy. J Am Coll Surg. 2011; 212:373-377.

39. Bathe OF, Levi D, Caldera H, Franceschi D, Raez L, Patel A, Raub WA Jr, Benedetto P, Reddy R, Hutson D, Sleeman D, Livingstone AS, Levi JU. Radical resection of periampullary tumors in the elderly: Evaluation of long-term results. World J Surg. 2000; 24:353-358.

40. Beltrame V, Gruppo M, Pastorelli D, Pedrazzoli S, Merigliano S, Sperti C. Outcome of pancreatico-duodenectomy in octogenarians: Single institution's experience and review of the literature. J Visc Surg. 2015; 152:279-284.

41. de la Fuente SG, Bennett KM, Pappas TN, Scarborough JE. Pre- and intraoperative variables affecting early outcomes in elderly patients undergoing pancreatico-duodenectomy. HPB. 2011; 13:887-892.

42. Charlson ME, Pompei P, Ales KL, MacKenzie CR. A new method of classifying prognostic comorbidity in longitudinal studies: Development and validation. J Chronic Dis. 1987; 40:373-383.

43. Bellera CA, Rainfray M, Mathoulin-Pélissier S, Mertens C, Delva F, Fonck M, Soubeyran PL. Screeing older cancer patients: First evaluation of the G-8 geriatirc screening tool. Ann Oncol. 2012; 23:2166-2172.

44. Kallogjeri D, Piccirillo JF, Spitznagel EL, Steyerberg EW. Comparison of scoring methods for ACE-27: Simpler is better. J Geriatr Oncol. 2012; 3:238-245.

Original Article

The preliminary clinical observation and analysis of childbearing-age women with a history of iodine-131 treatment for Graves' disease

Liang Guan[1,2], Gang Chen[1,2], Jiali Zhang[3,4,5], Ling Wang[3,4,5,*]

[1] *Department of Nuclear Medicine, Ruijin Hospital, School of Medicine, Shanghai Jiaotong University, Shanghai, China;*
[2] *Department of Nuclear Medicine, Ruijin Hospital North, School of Medicine, Shanghai Jiaotong University, Shanghai, China;*
[3] *Laboratory for Reproductive Immunology, Hospital & Institute of Obstetrics and Gynecology, IBS, Shanghai Medical College, Fudan University, Shanghai, China;*
[4] *The Academy of Intergrative Medicine of Fudan University;*
[5] *Shanghai Key Laboratory of Female Reproductive Endocrine Related Diseases, Shanghai, China.*

Summary   Whether radioactive iodine treatment of Graves' disease (GD) during pregnancy will increase pregnancy loss and affect fetal development is still a matter of concern. From May 2005 to December 2015, 2,276 childbearing-age women with GD received iodine-131 treatment in our departments and were retrospectively enrolled in our study. When some of them were found to have been pregnant, their thyroid functions were measured every 4 weeks, in addition, thyroid-stimulating hormone (TSH) was measured 6 weeks after delivery. When necessary, levothyroxine or propylthiouracil (PTU) was given in order to control their TSH levels during pregnancy. Finally, 69 pregnant women (29 ± 3.5 years old) and 1346 women who were not pregnant during the follow-up period were enrolled into this study. They were all hyperthyroid before or during pregnancy. Among 69 pregnant women, the administrated amount of iodine-131 was 254.9 ± 99.9 MBq. Fifty patients became subclinically hypothyroid after treatment and were administrated levothyroxine (55 ± 25 µg/d). Seven patients were diagnosed with subclinical hyperthyroidism during pregnancy and they received PTU (25 ± 12.5 mg/d). Twelve patients with normal thyroid function were also clinically followed. Among 69 women, 63 had a single birth, 3 had dizygotic twins, 2 had two pregnancies and 1 had a single twin birth. Sixty five babies were born full-term, while 9 were premature (4 ± 1 weeks early) with birth weight 3.2 ± 0.5 kg. Six new born babies were considered to be low birth weight infants (< 2.5 kg) while 5 were high birth weight (> 4 kg), but the weights of all the infants were within the normal range. During the period of observation to December 2015, all the infants were found to grow and develop normally. Among 1346 women who were not pregnant were in the further follow-up. Our study found no detrimental effects of the iodine-131 treatment in the pregnant women or their offspring so far.

Keywords: Graves' disease, pregnancy, iodine-131

1. Introduction

Graves' disease (GD) is one of the most common causes of hyperthyroidism worldwide, especially in iodine-

Address correspondence to:
Dr. Ling Wang, Obstetrics & Gynecology Hospital of Fudan University,413 Zhaozhou Road, Shanghai 200011, China.
E-mail: Dr.wangling@fudan.edu.cn

sufficient areas. GD accounts for nearly 90% of all cases and the incidence rate is about 1 in 1,000 per year (*1*). In China, the prevalence of hyperthyroidism is about 3%, with 88% to 90% being caused by GD (*2*). The treatment strategy varies around the world. In the United States and Europe, radioactive iodine-131 treatment is the first therapeutic choice and is widely accepted by physicians and patients (*3*). After more than 60 years of experience with iodine-131, it has been shown to be an inexpensive, safe, and effective treatment for hyperthyroidism (*4,5*). However, despite a high rate of recurrence, anti-thyroid

drugs (ATDs) such as methimazole and propylthiouracil (PTU) were still used as the preferred treatment for GD in China and other countries in Asia. The main concern among general practitioners is iodine-131 induced hypothyroidism, because many rural patients do not comply with lifelong regular levothyroxine (L-T4) replacement (*2*). Nevertheless, changing economic factors and high relapse rates observed after discontinuation of ATD treatment, the use of iodine-131 has dramatically increased.

Although iodine-131 therapy is generally well tolerated, potential side effects may occur, such as radiation-induced thyroiditis, sialadenitis, bone marrow depression, pulmonary fibrosis, and rarely induction of a second primary malignancy (*6-8*). Besides, transient or chronic hypospermia can be detected (*9,10*), as well as possible early onset of menopause (*11*) and menstrual cycle abnormalities (*12*). The mentioned severe side effects were all observed in those who receive high dose iodine-131 treatment in thyroid cancer instead of the lower doses used in the treatment of GD. Considering the much lower dose of iondine-131 administrated in GD than in cancer, we investigated whether iodine-131 treatment in GD would increase pregnancy loss and alter fetal development. Here, we aimed to investigate the pregnancy outcomes of childbearing-age women with GD who inadvertently received iodine-131 treatment in our hospitals.

2. Materials and Methods

2.1. *Patients*

From May 2005 to December 2015, 2,276 childbearing-age (from 20 to 40 years old) women with GD received iodine-131 treatment in Ruijin Hospital and Ruijin Hospital North (Shanghai Jiaotong University, School of Medicine, Shanghai, China) and were retrospectively enrolled. We excluded patients who delivered before iodine-131 treatment, and were unwilling to participate or failed to appear for follow-up for this study. Eventually, we enrolled 69 pregnant women and 1346 women who were not pregnant during the whole treatment and follow-up period.

2.2. *Hyperthyroidism Treatment*

The diagnoses of hyperthyroidism were based on serum free triiodothyronine (FT3), free thyroxine (FT4) and thyroid-stimulating hormone (TSH) levels, 24 hours thyroid radioactive iodine uptake (RAIU). Thyroid weight was based on color Doppler ultrasonography inspection and palpation. Accordingly, nuclear medicine physicians calculated and checked the required activity of iodine-131 (Shanghai Anshengkexing Pharmaceutical Co. Ltd., Shanghai, China) for individual patients. When necessary, repeated treatments were performed

as needed in other studies (*13*). Before iodine-131 treatment, women of childbearing age underwent routine detection of serum β-HCG, which was an endocrine indicator of pregnancy. If the pregnant woman was found to have severe hyperthyroidism, she was advised to interrupt the pregnancy and receive treatment two months later. If the woman became pregnant within 6 months after iodine-131 treatment, and her hyperthyroid symptoms persisted unabated, the patient was recommended for therapeutic abortion in accord with the maternal condition and fetal development status.

Patients were informed of radiation safety guidelines before iodine-131 treatment, and they all agreed and signed informed consents.

2.3. *Follow-up*

The follow-up was divided into two parts. One was regular follow-up after iodine-131 treatment for all women enrolled in our study, the other was specific for pregnancy and birth follow-up after iodine-131 for 69 pregnant women. Regular follow-up observation after iodine-131 treatment was conducted at 1 month, 3 months, 6 months and 1 year after iodine-131 treatment. Measurements of serum FT3, FT4 and TSH levels of the treated patients were performed to indicate thyroid functional restoration and measurement of the volume of thyroid was conducted at the same time. During the follow-up, if women had significantly increased FT3 or FT4, and goiter (over I degree goiter) after treatment, they had another iodine-131 treatment (3~6 months after previous treatment) as an outpatient. If women had slightly increased FT3, FT4 or TSH without goiter, they received moderate anti-thyroid drugs (ATDs) or levothyroxine (L-T4), or continued observation as an ordinary outpatient. As for 69 pregnant women, they first had serum β- Human chorionic gonadotropin (hCG) and mode-B ultrasonography for baby at 4 to 8 gestational weeks to confirm pregnancy. The thyroid functions of pregnant women were monitored every 4 weeks. The thyroid function was measured at 6 months postpartum, and the height, weight and intelligence development of babies were also monitored at the same time.

2.4. *Pregnancy management*

Management of thyroid function during pregnancy: *i*) According to the follow-up measurements of thyroid function and related hormones at 1 months, 3 months, 6 months and 1 year after iodine-131 treatment, the treated patients were classified in three thyroid function states: euthyroid, subclinical hyperthyroid and subclinical hypothyroid; *ii*) The treated women patients were administered adjustable doses of L-T4 as needed, depending on the serum TSH level; *iii*) The treated

women were recommended to avoid pregnancy until more than 6 months after iodine-131 treatment. L-T4 for hypothyroid patients was administered and PTU was prescribed for hyperthyroid patients to control the serum TSH level below 2.5 mU/L. The objective serum TSH level in pregnancy ranges from 0.1 to 2.5 mU/L in early stage, from 0.2 to 3.0 mU/L in middle stage and from 0.3 to 3.0 mU/L in late stage.

Those pregnant women enrolled in our study underwent antenatal care regularly in order to monitor the normal growth and development status of the fetuses, and healthy condition of mothers, mainly including fetal malformation screening, periodic mode-B ultrasonography, and amniotic cell karyotype analysis would be done if it was necessary to further confirm numerical and structural fetal chromosomal aberrations.

2.5. Statistical analysis

Statistical analysis was carried out using software package SPSS17.0, and statistically significant differences were assessed by one-way ANOVA followed by Tukey's test. A p value of less than 0.05 was considered to be statistically significant. All descriptive data was reported as median ± standard deviation ($\bar{x} \pm s$).

3. Results

Among 2,276 childbearing-age women with GD who received iodine-131 treatment during May 2005 to December 2015, 769 women delivered before iodine-131 treatment, 92 women were unwilling to participate or failed to appear for follow-up for this study for individual reasons except for healthy problems. The reasons we failed to follow-up were mainly that patients came from all around China often went back to their hometown after treatment, and thus it was hard to follow when they changed their contact information. It was also hard to look for their information in researching birth registries in the region because it didn't cover all distant places around China. Those women were excluded from our study. Finally, 1,346 women did not become pregnant after therapy and 69 successfully pregnant women were enrolled for further analysis. They were all hyperthyroid before pregnancy, and received iodine-131 treatment in our hospital. Some patients received treatment several times, and the earliest treatment started from May 3nd, 2005. The circulating thyroid hormone hormones levels were measured by chemiluminescent immunoassay, and the results showed the FT3 levels of these patients before treatment were all above 5.7 pmol/L (reference value range: 2.63-5.70 pmol/L), FT4 levels were all above 19 pmol/L (reference value range: 9.01-19.04 pmol/L), and TSH levels were less than 0.3 mU/

L (reference value range: 0.35-4.94 mU/L). Before treatment, each individual's 24 hour thyroid RAIU was more than 50%. Accordingly, the nuclear medicine physicians calculated and checked the required activity of iodine-131 for individuals, and considered much concern about hypothyroidism after treatment. The administered patient-specific doses were conservatively among low and medium dosage, most ranged from 111 to 333 MBq (average 222 MBq).

3.1. Analysis of the 69 pregnant women

The nuclear medicine physicians calculated and checked the required activity of iodine-131 for individuals, 254.9 ± 99.9 MBq (range from 92.5-740 MBq) of iodine-131 (Table 1, Figure 1A). Before pregnancy, 55 patients received one single dosage, 11 patients received two treatments, 1 patient was treated three times (No.67) and the other 2 had four treatments (No. 68 and No. 69). The interval between first and second iodine-131 treatment was 7 ± 6 months, interval between second and third iodine-131 treatment was 6 ± 2 months, and interval between second and third iodine-131treatment was 6 ± 1 months (Figure 1B).

On the other hand, the interval between pregnancy and iodine-131 treatment was 22 ± 16 months (range from 4-76 months) in all 69 participants. Because an increased risk of miscarriage, fetal or neonatal death is correlated with higher maternal TSH levels in pregnancy (*14*), the mothers' serum TSH levels should be manipulated to lower levels before they become pregnant. After iodine-131 treatment, 50 women patients were subclinically hypothyroid, and they needed L-T4 to control TSH and circulating thyroid hormones to maintain normal thyroid function. The administration doses were 55 ± 25 μg/d. Pregnant women were administered adjusted doses of L-T4 depending on TSH levels measured every 4 weeks to control TSH levels below 2.5 mU/L. The administered doses during pregnancy were changed from 12.5-25μg/d. 7 patients were subclinically hyperthyroid after iodine-131 treatment, and their administered PTU doses were 25 ± 12.5 mg/d. While the other 12 euthyroid patients had normal thyroid function test results.

A retrospective analysis showed that the morbidity of birth disorders in the region was 1.06% in the recent year and congenital heart disease, multi finger (toe), hypospadias, cleft lip, and palate and deformity of external ear were the 5 top birth defects. Compared to infants born with no birth defects, male, low birth weight, twins and multiple births were statistically higher in infants (*15*). Complication of labor and pregnancy, pregnant infection, fetal growth restriction (FGR), birth disorders can be the first five reasons related to stillbirth (*16*). In the 8th and 16th gestational weeks, the 69 pregnant women received mode-B ultrasonography studies to detect their fetal

Table 1. Iodine-131 treatment and pregnancy outcomes of 69 cases of hyperthyroid women patients (until 12-30-2015)

Treatment times	No.	I-131 dose (MBq)	Thyroid function management		Interval between pregnancy and treatment (month)	Infant age (years)	Infant gender (M/F)	Birth-weight (kg)
			L-T4 (µg)	PTU (mg)				
1	1	111			16	2.7	F	3
	2	111			9	3.0	F	3
	3	111	75		5	4.1	M	3.8
	4	111	50		33	2.6	M	3.8
	5	111	62.5		30	1.9	F	3.5
	6	111	50		15	1.2	M	3.3
	7	111	125		5	1.1	M	3.3
	8	111		25	11	1.4	M	4.1
	9	129.5	50		9	5.6	M	3.4
	10	129.5	25		41	2.7	F	3.5
	11	148			13	7.4	F	2.6
	12	148	25		8	0.2	F	3.05
	13	162.8	100		15	4.7	F	2.85
	14	185			22	1.1	M	3.9
	15	185	25		12	5.9	M	3.4
	16	185	75		14	5.4	F	3.3
	17	185	25		38	0.6	F	4
	18	203.5	25		16	3.9	M	3.05
	19	203.5	50		31	3	M	2.8
	20	203.5	37.5		69	1.3	F	3.05
	21	214.6			25	4.1	F	3.45
	22	222	100		13	5.9	M	3.2
	23	222	75		29	4.5	F	2.85
	24	222	37.5		8	2.2	F	3.3
	25	222	25		49	1.4	F	4.01
	26	222	50		48	1.2	M	3.5
	27	222	12.5		22	1.2	F	2.45
	28	222		25	8	3.0	M	2.75
	29	240.5	50		10	6.0	M	2.85
	30	240.5	50		16	3	M	3.3
	31	259			7	4.9	M	3.5
	32	259	50		21	5	M	3.3
	33	259	62.5		32	2.1	M	3.1
	34	259	50		53	1.8	M	3.3
	35	259	50		11	1.7	M	2.8
	36	259	75		35	2/2	MT:M/M	2.5/2.5
	37	259	75		10	7.4/7.4	DT:M/F	3/2.9
	38	259	50		75	0.7	F	3.5
	39	259		12.5	6	4.2	M	4.2
	40	259		25	14	0.8	F	3.3
	41	277.5	75		34	3.0	F	2.75
	42	277.5	100		32	2.2	F	2.3
	43	277.5	50		22	3.7/3.7	DT:F/M	2.2/2.3
	44	296			55	1.7	M	3.3
	45	296	50		10	6.0	F	2.8
	46	296	50		16	5.1	M	3.35
	47	296	50		13	3.1	M	3.5
	48	296	50		35	0.4	F	3.35
	49	333			19	3.2	F	2.4
	50	333	25		10	6.7	F	3.6
	51	333	100		36	3.8	M	3.9
	52	333	50		11	3.6	M	4.25
	53	333	100		18	2.7	F	3
	54	351.5	50		11	5.9	M	3.6
	55	351.5	50		13	3.3	F	2.5
2	56	185/222	50		28	4.3	F	2.9
	57	259/166.5			20	1.5	M	3.6
	58	259/203.5	3.75		12/31	4.8/3.2	F/M	3/3
	59	259/222			14	6	F	3.5
	60	259/222	25		10	4.4	M	3.5
	61	259/92.5			11	0.4	F	3
	62	277.5/277.5		25	11	4.2	M	3.25
	63	296/240.5			14	3.8	F	3.25
	64	314.5/203.5	50		10	4.5	F	3.2
	65	333/370		12.5	7	3.7	F	3.9
	66	481/296	87.5/85		7/64	5.8/1	M/M	2.7/3.25
3	67	259/296/259	100		4	5.1/5.1	DT:M/F	2.5/2.6
4	68	333/370/370/203.5		50	14	2.1	F	3.3
	69	333/555/740/370			6	4.7	M	2.35

Abbreviation: L-T4, levo thyroxine; PTU, propylthiouracil; M, male; F, female; MT, monozygotic twins; DT, dizygotic twin.
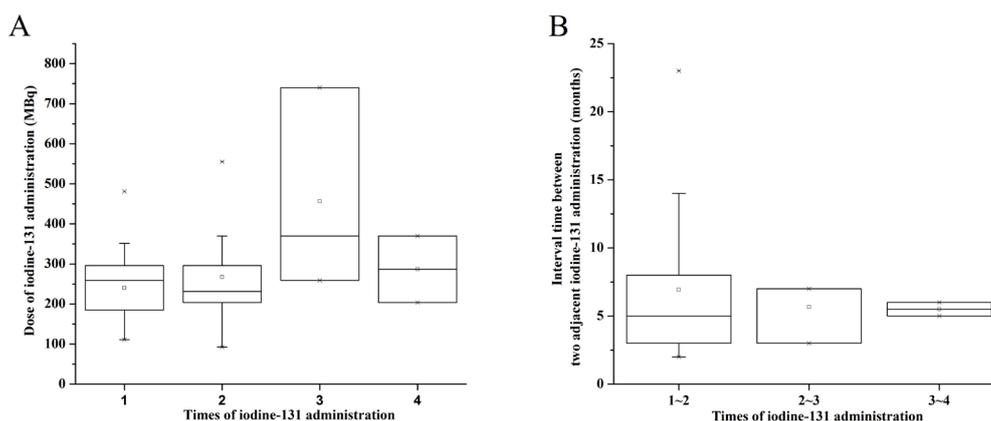
Figure 1. Administration of Iodine-131 in 69 pregnant women (till 2015-12-30). (A) 69 pregnant women with hyperthyroid were administrated iodine-131 at different times, the administered amount was 242.8 ± 79.5 MBq in all 69 women for the first time, 266.9 ± 111.4 MBq in 14 women for the second time, 456.3 ± 205.6 MBq in 3 women for the third time, and 286.8 ± 117.7 MBq in 2 women for the fourth time. **(B)** Among 69 pregnant women, 14 women had a second administration, the interval time between first and second time was 7±6 months, 3 women had a third administration, the interval time between second and third time was 6 ± 2 months, 2 women had a fourth administration, the interval time between third and fourth time was 6 ± 1 months. *Abbreviation*: 1~2, between the first and second iodine-131 administration; 2~3, between the second and third iodine-131 administration; 3~4, between the third and forth iodine-131 administration.

development stage. The inspections showed normal growth and development status of the fetuses. The predictive analysis of prenatal screening in the 16th gestational week indicated the mothers were at low risk for fetuses with Down's syndrome. Two of these mothers received amniotic cell karyotype analysis in the 20th gestational week to diagnose whether their fetus' chromosomes were indicative of a malformation abnormality, and the results showed no structural change in these cases. Fetal quickening, heart monitoring and mode-B ultrasonography inspections were performed once every 4 weeks after the 24th gestational week to monitor the fetuses developmental status, and to assess whether the fetuses were all in normal condition. One treated patient became pregnant 4th months after iodine-131 treatment (No.67), and mode-B ultrasonography inspection showed the mother conceived dizygotic twins. All inspection parameters of both twins remained normal during pregnancy. The treating physicians discussed in detail and deliberatively reached an agreement to continue the pregnancy with approval of the patient's family.

Among these 69 pregnant patients with successful childbirth, 63 mothers had singleton pregnancies, and 3 had dizygotic twin pregnancies (No. 37, 43 and 67), and among 2 two singleton pregnancies, one successively (No. 66) gave birth to two baby boys, while the other (No. 58) had a baby girl and a baby boy, and 1 had monozygotic twins (No. 36) with two identical baby boys.

The sex ratio of 75 newborn infants was 41 boys *vs.* 34 girls (Figure 2). In all 75 babies, 65 babies were full-term birth while only 9 were premature (4 ± 1 weeks early). Their birth weight was 3.2 ± 0.5 kg; 6 new-birth babies (No. 27, 42, 43, 49, 69) were considered to be low birth weight infants (< 2.5 kg) while the other
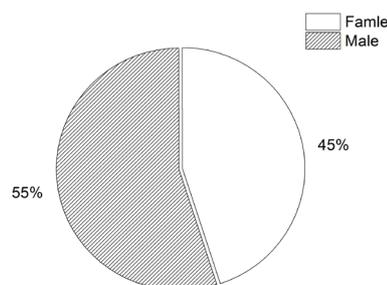
Figure 2. Birth sex ratio of 75 newborn infants. 69 pregnant patients has 75 babies with successful childbirth, the sex ratio of 75 newborn infants was 41 boys *vs.* 34 girls. The male proportion was 55%, and the female proportion was 45%.
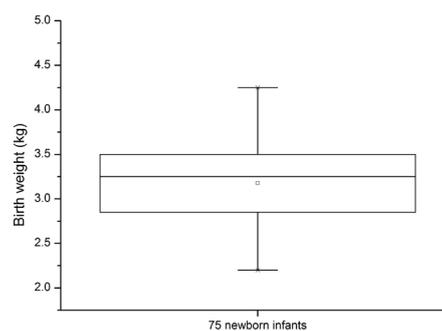
Figure 3. Birth weight of 75 newborn infants. 69 pregnant patients has 75 babies with successful childbirth, the birth weight of 75 newborn infants was 3.2 ± 0.5 kg.

5 babies' (No. 8, 17, 25, 39, 52) were high birth weight (> 4 kg) (Figure 3).

Of 75 newborn infants, screening for evidence of neonatal diseases, done by analysis of blood samples collected from their heels, showed normal blood physiological and biochemical indices and TSH levels (0-10 mU/L) in the normal range.

To date, the infants of iodine-131-treated mothers show
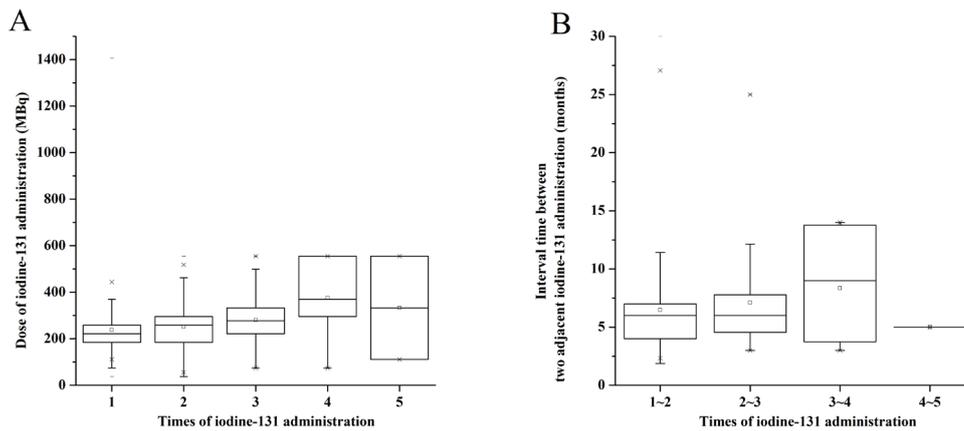
Figure 4 Administration of Iodine-131 in 1346 women with Grave's disease (until 12-30- 2015). (A) 1346 hyperthyroid women were administrated iodine-131 at different times, the administered amount was 237.7 ± 87.3 MBq in all 1346 women for the first time, 251.83±89.82 MBq in 289 women for the second time, 280.0 ± 110.2 MBq in 44 women for the third time, 375.3 ± 167.4 MBq in 7 women for the fourth time, and 333.0 ± 314.0 MBq in 2 women for the fifth time. **(B)** Among 1346 pregnant women, 289 women had a second administration, the interval time between first and second time was 6.5 ± 3.9 months, 44 women had a third administration, the interval time between second and third time was 7.1 ± 4.6 months, 7 women had a forth administration, the interval time between third and fourth time was 8.3 ± 4.6 months, 2 women had a fifth administration, the interval time between fourth and fifth time was 5.0 ± 0 months.

Table 2. Thyroid function after iodine-131 treatment and pregnancy outcomes of 1346 women with Grave's disease (until 12-30-2015)

Items	Percent of different thyroid function states	Number of women under pregnancy	Pregnancy outcome
Subclinically hypothyroid	70%	3	2 had full-term delivery and neonatal death, 2 chose to take PTU to
Subclinically hyperthyroid	20%	1	control the hyperthyroidism and put off the iodine-131 treatment.
Euthyroid	10%	1	-

the same developmental progression as do the children of untreated euthyroid mothers with respect to when they sit, crawl, stand, walk, run and talk. The oldest child is now 7.4 years old, and this child's thyroid function, developmental status and intelligence does not show any difference compared to children of the same age. One premature infant of low birth-weight is now 4.7 years old, and his weight at 2 years' old is lighter than children of the same age, but thyroid function and intelligence is the same as his peers.

3.2. Analysis of the 1346 women who were not pregnant

The times of iodine-131 treatment in 1346 women who were not pregnant range from 1 to 5. These 1346 women that were hyperthyroid were administrated iodine-131 at different times, the administered amount was 237.7 ± 87.3 MBq in all 1346 women for the first time, 251.83 ± 89.82 MBq in 289 women for the second time, 280.0 ± 110.2 MBq in 44 women for the third time, 375.3 ± 167.4 MBq in 7 women for the fourth time, and 333.0 ± 314.0 MBq in 2 women for the fifth time (Figure 4A). Among 1346 pregnant women, 289 women who had a second administration, the interval time between first and second time was 6.5 ± 3.9 months, 44 women who had a third administration, the interval time between second and third time was 7.1

± 4.6 months, 7 women who had a forth administration, the interval time between third and fourth time was 8.3 ± 4.6 months, 2 women who had a fifth administration, the interval time between fourth and fifth time was 5.0 ± 0 (Figure 4B). After iodine-131 treatment, 70% of women turned to subclinical hypothyroid and administered LT-4 (dose ranges from 50 to 100 mg), 20% of women turned to subclinical hyperthyroid and administered PTU (dose ranges from 12.5 to 50 mg). While the other 10% of euthyroid patients had normal thyroid function test results. All patients had no other special side reactions reported so far. Until December, 12th, 2015, 5 were found pregnant among the 1346 patients (gestational weeks ranged from 6 to 9 months). 3 of them were subclinically hypothyroid and administered LT-4, 1 of them turned to subclinical hyperthyroid and administered PTU and of them 1 had normal thyroid function test results. We had further follow-up and observed 2 of them had full-term delivery, however one of newborn babies died after birth because of congenital heart disease and the other died 3 days after birth because of cerebral hemorrhage. These two babies did not undergo an autopsy. Two patients were found pregnant among the 1346 patients who took the iodine-131 treatment, thus they chose to take PTU to control the hyperthyroidism and put off the iodine-131 treatment until after delivery (Table 2)

4. Discussion

Although iodine-131 treatment of hyperthyroidism has been used in clinical practice for over half a century, data about possible damage to the female gonads after administration for therapeutic purposes are still inconclusive. There are only a few literature reports dealing with this issue and the majority of them deal with high dose treatment for thyroid cancer (*17*). For women patients, the effects of iodine-131 therapy on gonadal function are a critical consideration because many are of childbearing-age and wish to have healthy children. Female gonads may be affected during iodine-131 therapy from circulating radioiodine in the blood, as well as radiation from the bladder and bowel sequestration during and for a few days post therapy. Therefore, patients are instructed to drink large amounts of fluids and use laxatives if constipated in order to avoid unnecessary radiation to the ovaries (*18*).

According to the guidelines established by the Society of Nuclear Medicine and Molecular Imaging, female patients who have the potential to be pregnant must always be tested for pregnancy using a urine or serum β-HCG test before iodine-131 treatment (*19*). Iodine-131 therapy is absolutely contraindicated in pregnant women and one attempts to avoid inadvertent exposure and this continues to be recommended in the literature. However, Hyer S, *et al*. (*20*) demonstrated that exposure to iodine-131 at this very early stage of pregnancy (pre implantation) is unlikely to result in malformations or thyroid dysfunction in surviving embryos; only exposure during thyroidogenesis (from 10 weeks gestation) and organogenesis (from 2 weeks gestation) may result in fetal thyroid ablation, birth defects and in later life, growth retardation and reduction in IQ. Generally speaking, women are advised to delay pregnancy at least 6 months after iodine-131 treatment in China, at which time there should be no risk of them suffering from miscarries or other dangers (*21*).

Another concern regarding iodine-131 treatment for childbearing-age women in China is the possible result of hypothyroidism. Nevertheless, many experts in western countries consider hypothyroidism after a single dose of iodine-131 a desired outcome of therapy because it avoids frequent office visits and laboratory testing to detect the late onset of hypothyroidism and thereby decreasing the risk of untreated, persistent, or recurrent hyperthyroidism (*19*). Once identified, use of replacement L-T4 can adjust the patients' thyroid function to the normal range diminishing possible concern regarding hypothyroid induction.

Previous studies in female patients have shown no significant effects of iodine-131 in treating thyroid cancers on fertility rate, birth weight, or congenital anomalies in offspring (*22-29*). In our study, we have the same experience in treating patients for GD. Among these 26 women patients we observed only successful pregnancy and childbirth, and no birth defects or other malformations were detected.

Of course, the present study has several limitations. The first is the retrospective nature of the study. Another limitation is the relatively small number of patients, which can lead to selection bias. Considering the non-zero frequency of mild and moderate birth disorders in untreated pregnancies, the same fraction would also be expected in the treated group. We haven't seen it yet, mainly due to the relatively small number of patients we have had so far. Our study is still in progress at present, and more patients and cases will be included in the next stage of our study. We will also concentrate on expanding the sample size, and strengthen the follow-up of treated patients by cooperation of obstetrics with endocrinology. Thus we may be able to get more powerful analysis on birth disorders, still births, normal live births and so on. We expect we can get a more authoritative data statistics in the next few years. For these reasons, we suggest further clinical trials should be undertaken, especially a prospective and multi-center study.

In conclusion, no significant harm to fetuses has been observed on child-bearing age women with GD who received iodine-131 treatment before pregnancy. No significant risk of abnormal fetal development has been observed on pregnant women with GD after a 6-month period of iodine-131 treatment. In order to more firmly establish these conclusions, it will be necessary to study larger numbers of subjects in a prospective multicenter study.

Acknowledgements

References

1. Vanderpump MP, Tunbridge WM, French JM, Appleton D, Bates D, Clark F, Grimley Evans J, Hasan DM, Rodgers H, Tunbridge F, Young ET. The incidence of thyroid disorders in the community: A twenty-year follow-up of the Whickham Survey. Clin Endocrinol (Oxf). 1995; 43:55-68.
2. Liu M, Jing D, Hu J, Yin S. Predictive factors of outcomes in personalized radioactive iodine (^{131}I) treatment for Graves' disease. Am J Med Sci. 2014; 348:288-293.

3. Solomon B, Glinoer D, Lagasse R, Wartofsky L. Current trends in the management of Graves' disease. J Clin Endocrinol Metab. 1990; 70:1518-1524.

4. Muldoon BT, Mai VQ, Burch HB. Management of Graves' disease: An overview and comparison of clinical practice guidelines with actual practice trends. Endocrinol Metab Clin North Am. 2014; 43:495-516.

5. Cruz Junior AF, Takahashi MH, Albino CC. Clinical treatment with anti-thyroid drugs or iodine-131 therapy to control the hyperthyroidism of Graves disease: A cost-effectiveness analysis. Arq Bras Endocrinol Metabol. 2006; 50:1096-1101.

6. Hyer S, Kong A, Pratt B, Harmer C. Salivary gland toxicity after radioiodine therapy for thyroid cancer. Clin Oncol (R Coll Radiol). 2007; 19:83-86.

7. Hyer SL, Newbold K, Harmer CL. Early and late toxicity of radioiodine therapy: detection and management. Endocr Pract. 2010; 16:1064-1070.

8. Sioka C, Zouboulidis A, Fotopoulos A, Dimakopoulos N. Re: risk of second primary malignancies in women with papillary thyroid cancer. Am J Epidemiol. 2007; 165:473; author reply 474.

9. Hyer S, Vini L, O'Connell M, Pratt B, Harmer C. Testicular dose and fertility in men following I(131) therapy for thyroid cancer. Clin Endocrinol (Oxf). 2002; 56:755-758.

10. Wichers M, Benz E, Palmedo H, Biersack HJ, Grunwald F, Klingmuller D. Testicular function after radioiodine therapy for thyroid carcinoma. Eur J Nucl Med. 2000; 27:503-507.

11. Ceccarelli C, Bencivelli W, Morciano D, Pinchera A, Pacini F. [131]I therapy for differentiated thyroid cancer leads to an earlier onset of menopause: Results of a retrospective study. J Clin Endocrinol Metab. 2001; 86:3512-3515.

12. Sioka C, Kouraklis G, Zafirakis A, Manetou A, Dimakopoulos N. Menstrual cycle disorders after therapy with iodine-131. Fertil Steril. 2006; 86: 625-628.

13. Franklyn JA, and Boelaert K. Thyrotoxicosis. Lancet. 2012; 379:1155-1166.

14. Georgiou HM, Di Quinzio MK, Permezel M, Brennecke SP. Predicting Preterm Labour: Current Status and Future Prospects. Dis Markers. 2015; 2015: 435014.

15. Yang M, Wang J, QIAN B, Dai J, Zhang X, Chen A, Meng Y. Monitoring and analysis of birth defects in 73498 infants. Journal of Clinical Pediatrics. 2015; 6:553-557. (in Chinese)

16. Zhang L, Liu KB, Pan Y, Zhang QL. Global progress in stillbirth study. Chinese Journal of Woman and Child Health Research. 2015; 26: 896-898. (in Chinese)

17. Dottorini ME, Lomuscio G, Mazzucchelli L, Vignati A, Colombo L. Assessment of female fertility and carcinogenesis after iodine-131 therapy for differentiated thyroid carcinoma. J Nucl Med. 1995; 36:21-27.

18. Sioka C, Fotopoulos A. Effects of I-131 therapy on gonads and pregnancy outcome in patients with thyroid cancer. Fertil Steril. 2011; 95:1552-1559.

19. Silberstein EB, Alavi A, Balon HR, Clarke SE, Divgi C, Gelfand MJ, Goldsmith SJ, Jadvar H, Marcus CS, Martin WH, Parker JA, Royal HD, Sarkar SD, Stabin M, Waxman AD. The SNMMI practice guideline for therapy of thyroid disease with [131]I 3.0. J Nucl Med. 2012; 53:1633-1651.

20. Hyer S, Pratt B, Newbold K, Hamer C. Outcome of pregnancy after exposure to radioiodine In utero. Endocr Pract. 2011; 1-10. doi: http://dx.doi.org/10.4158/EP10237.RA

21. American Thyroid Association Taskforce On Radioiodine S, Sisson JC, Freitas J, McDougall IR, Dauer LT, Hurley JR, Brierley JD, Edinboro CH, Rosenthal D, Thomas MJ, Wexler JA, Asamoah E, Avram AM, Milas M, Greenlee C. Radiation safety in the treatment of patients with thyroid diseases by radioiodine [131]I: Practice recommendations of the American Thyroid Association. Thyroid. 2011; 21:335-346.

22. Garsi JP, Schlumberger M, Rubino C, Ricard M, Labbe M, Ceccarelli C, Schvartz C, Henri-Amar M, Bardet S, de Vathaire F. Therapeutic administration of ^{131}I for differentiated thyroid cancer: Radiation dose to ovaries and outcome of pregnancies. J Nucl Med. 2008; 49:845-852.

23. do Rosário PW, Barroso AL, Rezende LL, Padrão EL, Borges MA, Purisch S. Malformations in the offspring of women with thyroid cancer treated with radioiodine for the ablation of thyroid remnants. Arq Bras Endocrinol Metabol. 2006; 50:930-933.

24. Balenovic A, Vlasic M, Sonicki Z, Bodor D, and Kusic Z. Pregnancy outcome after treatment with radioiodine for differentiated thyroid carcinoma. Coll Antropol. 2006; 30:743-748.

25. Bal C, Kumar A, Tripathi M, Chandrashekar N, Phom H, Murali NR, Chandra P, Pant GS. High-dose radioiodine treatment for differentiated thyroid carcinoma is not associated with change in female fertility or any genetic risk to the offspring. Int J Radiat Oncol Biol Phys. 2005; 63:449-455.

26. Brandao CD, Miranda AE, Correa ND, Sieiro Netto L, Corbo R, Vaisman M. Radioiodine therapy and subsequent pregnancy. Arq Bras Endocrinol Metabol. 2007; 51:534-540.

27. Fard-Esfahani A, Mirshekarpour H, Fallahi B, Eftekhari M, Saghari M, Beiki D, Ansari-Gilani K, Takavar A. The effect of high-dose radioiodine treatment on lacrimal gland function in patients with differentiated thyroid carcinoma. Clin Nucl Med. 2007; 32:696-699.

28. Vini L, Hyer S, Al-Saadi A, Pratt B, Harmer C. Prognosis for fertility and ovarian function after treatment with radioiodine for thyroid cancer. Postgrad Med J. 2002; 78:92-93.

29. Chow SM, Yau S, Lee SH, Leung WM, Law SC. Pregnancy outcome after diagnosis of differentiated thyroid carcinoma: No deleterious effect after radioactive iodine treatment. Int J Radiat Oncol Biol Phys. 2004; 59:992-1000.

Preliminary investigation of five novel long non-coding RNAs in hepatocellular carcinoma cell lines

Jufeng Xia[1], Yoshinori Inagaki[1], Tatsuo Sawakami[1], Peipei Song[2], Yulong Cai[1,3], Kiyoshi Hasegawa[1], Yoshihiro Sakamoto[1], Nobuyoshi Akimitsu[4], Wei Tang[1,*], Norihiro Kokudo[1]

[1] *Hepato-Biliary-Pancreatic Surgery Division, Department of Surgery, Graduate School of Medicine, The University of Tokyo, Tokyo, Japan;*
[2] *Graduate School of Frontier Sciences, The University of Tokyo, Kashiwa-shi, Chiba, Japan;*
[3] *Department of Bile Duct Surgery, West China Hospital, Sichuan University, Chengdu, Sichuan Province, China;*
[4] *Radioisotope Center, The University of Tokyo, Tokyo, Japan.*

Summary   **Hepatocellular carcinoma (HCC) is a highly prevalent cancer with a high mortality rate and HCC is always accompanied with a hepatitis B virus (HBV) infection, unlike many other types of cancers. Over the past few years, cancer-related long non-coding RNAs (lncRNAs) and virus-related lncRNAs have attracted the attention of many researchers, and a number of previous studies have examined the relationship between lncRNAs and various cancers and viruses. The current study used The Cancer Genome Atlas database to screen for lncRNAs up-regulated in HCC in order to identify cancer biomarkers. Results revealed five lncRNAs that were the most up-regulated. This result was then verified in 10 HCC cell lines and two normal liver cell lines. Quantitative real-time PCR revealed that the five lncRNAs were substantially up-regulated in HCC cell lines. Several of the five lncRNAs were expressed at higher levels in a few HCC cell lines that were infected with HBV or that were positive for its protein or DNA than in HCC cell lines that were not infected with HBV or that were negative for its protein or DNA. These findings suggest that the five lncRNAs might play a role in the progression of HCC and/or HBV infection, and these findings need to be studied in further detail.**

Keywords: lncRNA, hepatocellular carcinoma, cell line, hepatitis B virus

1. Introduction

The GENCODE project identified about 20,000 protein-coding genes in the human genome (*1*). The DNA in the human genome that is not genes and that does not produce proteins is referred to as "non-coding DNA" (*2*). Some parts of "non-coding DNAs" produce introns and the others are transcribed into functional non-coding RNAs (ncRNAs). NcRNAs are classified into small ncRNAs (less than 200 nts) and

long ncRNAs (lncRNAs, more than 200 nts). Small ncRNAs, and particularly microRNAs (miRNAs), are widely considered to be post-transcriptional regulators of mRNAs and their roles in cancer progression are increasingly being studied (*3,4*). A great number of lncRNAs have been identified thus far, and there is a rapidly growing number of studies of the biological functions of lncRNAs in human cancers, such as hepatocellular carcinoma (HCC), gastric cancer, prostate cancer, bladder cancer, renal cancer, colorectal carcinoma, and glioma (*5-9*). Numerous studies have suggested that lncRNAs are related to the proliferation, invasion, and metastasis of cancers as well as their poor prognosis. The relationship between lncRNAs and cancers implies that lncRNAs might serve as biomarkers and therapeutic targets. As an example, TUG1 was found to increase in different types of cancers, including B-cell malignancies, esophageal

squamous cell carcinoma, bladder cancer, HCC, and osteosarcoma (*10*). MALAT1 was identified as a prognostic marker for survival and metastasis in nonsmall cell lung cancer, cervical cancer, pancreatic cancer, and breast cancer (*11*). Another widely studied lncRNA, HOTAIR, was up-regulated and was used as an independent prognostic biomarker for breast cancer, cervical cancer, colon cancer, and gastric cancer (*12*). Unfortunately, most of the molecular mechanisms of lncRNAs have yet to be elucidated.

HCC is a type of highly malignant cancer with a poor prognosis according to many studies. Over the past few years, abnormal expression of a few lncRNAs has been found to be related to recurrence and metastasis of HCC as well as its poor prognosis (*13*). A special feature of HCC is the fact that some patients with the cancer are infected with a hepatitis virus. To the extent known, viruses play important roles in the progression of a few cancers, such as human papillomavirus in cervical cancer and the hepatitis B virus (HBV) and hepatitis C virus (HCV) in HCC (*14,15*). Numerous studies have suggested that some lncRNAs could affect virus infection and replication. For example, EGOT affects the antiviral response to HCV, lncRHOXF1 promotes replication of the Sendai virus, and NEAT1 is related to infection with the influenza virus (*16-18*). Thus, significant components of HCC treatment are steps to counter the tumor and viruses. The current study focused on five new lncRNAs from the Cancer Genome Atlas database. lncRNAs with the highest level of expression in HCC were identified and their level of expression was detected in HCC cell lines that were infected or not infected with HBV.

2. Materials and Methods

2.1. Cell lines

Ten human HCC cell lines, BEL-7402, HLF, HLE, HepG2, HepG2.2.15, Huh-1, Huh-7, PLC/PRF/5, Hep3B, and SK-Hep-1, and two normal human liver cell lines, hNHEPs and L02, were cultured in high glucose Dulbecco's Modified Eagle medium (DMEM, Gibco, USA), supplemented with 10% fetal bovine serum (FBS, Gibco, USA) in a humidified chamber at 37°C in 5% CO_2.

2.2. Identification of candidate lncRNAs from the TCGA database

The Cancer Genome Atlas (TCGA) database was searched to identify candidate lncRNAs. The TCGA online database is the result of a project, begun in 2005, to catalogue genetic mutations responsible for cancer, using genome sequencing and bioinformatics. The TCGA database contains the results of high-throughput genome analysis of about 30 sets of paracancerous

tissue and cancer tissue from patients with HCC. The current study arranged lncRNAs by level of expression from highest to lowest in order to identify lncRNAs that were up-regulated in cancer. The five lncRNAs that were up-regulated the most were selected to examine their expression in HCC.

2.3. Reverse transcription PCR

After cells were collected, total RNA was extracted from cells with the RNeasy Mini Kit (Qiagen, USA) in accordance with the manufacturer's instructions. The mRNA was then reverse-transcribed to produce cDNA using a Reverse Transcription System (Promega, Madison, USA) and random primers in accordance with the manufacturer's instructions.

2.4. Real-time PCR

cDNA was quantified using the StepOneTM Real-Time PCR System (Applied Biosystems, USA). A polymerase chain reaction (PCR) was performed using the primers (designed with Primer 3Plus online software and synthesized by Invitrogen) shown in Table 1. GAPDH served as a positive control. FastStart Universal SYBR Green Master (Rox) (Roche) was used to amplify and detect DNA during the reaction. Thermal cycling parameters for the target genes and GAPDH consisted of a hot start for 2 min at 94°C, followed by 40 cycles of 94°C for 15 s and 60°C for 30 s, and then 72°C for 30 s. The specificity of the PCR products was verified using melting curve analysis.

2.5. Statistical analysis

All experiments were performed in triplicate and the results were analyzed with one-way analysis of variance (ANOVA) in GraphPad Prism 4, followed by Student's *t* test in Microsoft Office Excel. $p < 0.05$ was considered to indicate a significant difference.

3. Results and Discussion

3.1. Identification of candidate lncRNAs from the TCGA database

The TCGA database was searched to identify candidate lncRNAs. As a result, several lncRNAs with abnormal levels of expression were identified. Five of these lncRNAs, PRC1-AS1 (Chromosome 15: 90966369-90988624), CRNDE (Chromosome 16: 54918863-54929189), RP11-334E6.12 (Chromosome 11: 119417951-119419114), LINC00665 (Chromosome 19: 36313061-36331718), and AC092171.4 (Chromosome 7: 5475804-5479811), were significantly up-regulated, so these lncRNAs were selected for further research (Figure 1).
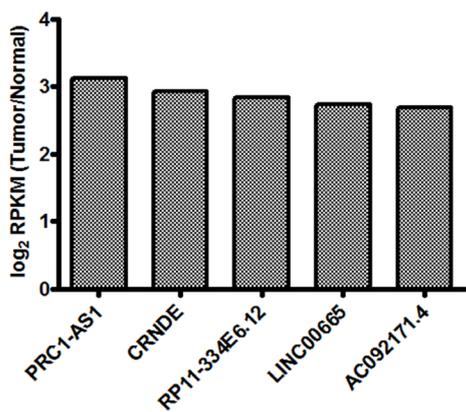
Figure 1. Five up-regulated lncRNAs identified from the TCGA database.

Table 1. Primers for quantifying lncRNAs

Primer	Sequence (5' to 3')	Product size (bp)
PRC1-AS1_F	CTCAGAGCTTTCGGTGGTTC	108 bp
PRC1-AS1_R	GGATTTCGTGGCTGGAGATA	
CRNDE_F	TGCCACTGGAAATGTTGAAA	189 bp
CRNDE_R	CTTCTGCGTGACAACTGAGG	
RP11-334E6.12_F	GACAGACCATGTCCGTGCTA	135 bp
RP11-334E6.12_R	ATGTGAGGGGTAGTGGGATG	
LINC00665_F	CCATCCACCTTTCTTGTGGT	153 bp
LINC00665_R	CAGCTGGCCTCTTTTTCACT	
AC092171.4_F	GGTTGCAGGGGACACTAAAA	160 bp
AC092171.4_R	CCTGGGTGTCCTGTTCTCAT	
GAPDH_F	AGGTGAAGGTCGGAGTCAAC	117 bp
GAPDH_R	AGTTGAGGTCAATGAAGGGG	

3.2. *Five lncRNAs were substantially up-regulated in 10 HCC cell lines*

The level of expression of the five candidate lncRNAs was measured in 10 HCC cell lines (BEL-7402, HLF, HLE, HepG2, HepG2.2.15, Huh-1, Huh-7, PLC/PRF/5, Hep3B, and SK-Hep-1) and two normal liver cell lines (hNHEPs and L02). Reverse transcription PCR and quantitative real-time PCR were used to detect the expression of these five lncRNAs in the 12 liver cell lines (Table 1). Results indicated that the five lncRNAs was significantly up-regulated in all of the 10 cancer cell lines in comparison to two normal liver cell lines (Figure 2 and Table 2).

All five lncRNAs were highly up-regulated in all of the cancer cell lines, but they tended to be expressed at a much higher level in certain cell lines. PRC1-AS1, which was the lncRNA with the highest level of expression in TCGA database, was markedly up-regulated in BEL7402, HepG2.2.15, Huh-1, and Hep3B; that level of expression was more than four-fold that in normal liver cell lines (Figure 2A). The lncRNA that was expressed at the next highest level was CRNDE, which was up-regulated in all HCC cell lines. CRNDE was expressed at higher levels in HLF, HLE,

HepG2.2.15, and Huh-1 (Figure 2B). RP11-334E6.12 was expressed at a higher level in HLF, HepG2, HepG2.2.15, and Huh-1 (Figure 2C). LINC00665 was markedly expressed in HepG2, HepG2.2.15, Huh-1, and Hep3B (Figure 2D). AC092171.4 was expressed at a higher level in HLE, HepG2, Huh-1, and Hep3B (Figure 2E). These results indicate that all five of the lncRNAs were significantly up-regulated in HCC cell lines, but each lncRNA was expressed at higher levels in certain cell lines. This finding suggests that some cell lines are a better choice for differential expression of lncRNAs.

The level of lncRNA expression in normal liver cell lines and HCC cell lines was analyzed. Figure 2F shows that all five of the lncRNAs were expressed at a significantly higher level in cancer cell lines than in normal liver cell lines. This finding coincides with the results from the TCGA database. Although each lncRNA was not expressed to the same extent as indicated in the TCGA database, the levels of expression were reasonable given the differences in clinical samples and cell lines and differences in genetic backgrounds.

3.3. *lncRNA expression was markedly up-regulated in HCC cell lines infected with HBV*

In addition to the high level of expression of the five lncRNAs in 10 HCC cell lines, results also indicated that HCC cell lines that were infected with HBV or that were positive for its protein or DNA seemed to have a higher level of expression of lncRNAs than other HCC cell lines that were negative for HBV protein or DNA (Figure 3A). In addition, the average level of expression of each lncRNA was compared in normal cell lines, HCC cell lines not infected with HBV, and HCC cell lines infected with HBV. Results revealed significant differences in expression of PRC1-AS1, LINC00665, and AC092171.4 (Figure 3B). There were no significant differences in expression of CRNDE and RP11-334E6.12 in all HCC cell lines not infected with HBV and all HCC cell lines infected with HBV. In contrast, expression of CRNDE differed significantly in HCC cell lines not infected with HBV and the PLC/PRF/5 cell line. Expression of RP11-334E6.12 differed significantly in HCC cell lines not infected with HBV and the HepG2.2.15 cell line. These results suggest that the five lncRNAs might interact with HBV or its protein or DNA. Thus, future research should involve study of the potential interaction between candidate lncRNAs and HBV.

In summary, the current study suggested that five lncRNAs were substantially up-regulated in 10 HCC cell lines in comparison to two normal liver cell lines. HCC cell lines that were infected with HBV or that were positive for its protein or DNA had a higher level of expression of lncRNAs than HCC cell lines that were not infected with HBV or that were negative for
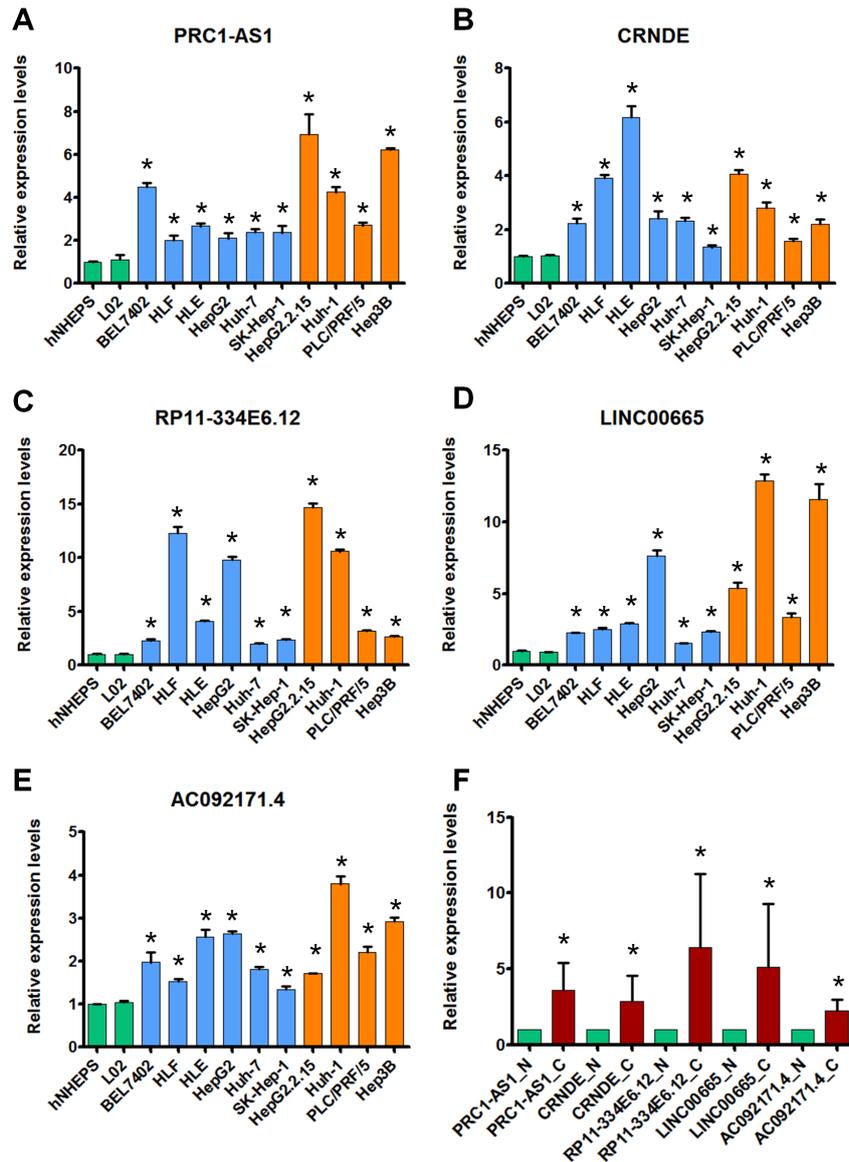
Figure 2. Relative expression of five lncRNAs in 12 cell lines. (A) The level of PRC1-AS1 expression in 12 cell lines. (B) The level of CRNDE expression in 12 cell lines. (C) The level of RP11-334E6.12 expression in 12 cell lines. (D) The level of LINC00665 expression in 12 cell lines. (E) The level of AC092171.4 expression in 12 cell lines. (F) Comparison of the expression of five lncRNAs in normal liver cell lines and HCC cell lines. N: normal liver cell lines; C: HCC cancer cell lines. Green bar: normal liver cell lines; blue bar: HCC cell lines not infected with HBV; yellow bar: HCC cell lines infected with HBV; wine red bar: HCC cell lines. Data are expressed as the mean ± S.D. ($n = 3$). *$p < 0.05$ vs. normal liver cell lines.

Table 2. Relative average level of expression of five lncRNAs in liver cell lines

Cell lines	Long non-coding RNAs				
	PRC1-AS1	CRNDE	RP11-334E6.12	LINC00665	AC092171.4
hNHEPS	1.000000	1.000000	1.000000	1.000000	1.000000
L02	1.100222	1.024768	1.03541	0.923571	1.044776
BEL7402	4.486377	2.243313	2.272536	2.257758	1.971264
HLF	2.005248	3.922631	12.25951	2.496699	1.528039
HLE	2.663165	6.190015	4.084482	2.900079	2.565964
HepG2	2.100222	2.422593	9.781447	7.655874	2.639765
Huh-7	2.389504	2.326131	1.974695	1.532592	1.809742
SK-Hep-1	2.366716	1.351478	2.367365	2.316163	1.339115
HepG2.2.15*	6.918878	4.072771	14.71719	5.375211	1.716978
Huh-1*	4.242769	2.820624	10.59926	12.87392	3.794856
PLC/PRF/5*	2.700666	1.57057	3.211381	3.346897	2.209993
Hep3B*	6.204443	2.204493	2.686601	11.57074	2.91626

*HCC cell lines that were infected with HBV or that were positive for its protein or DNA.
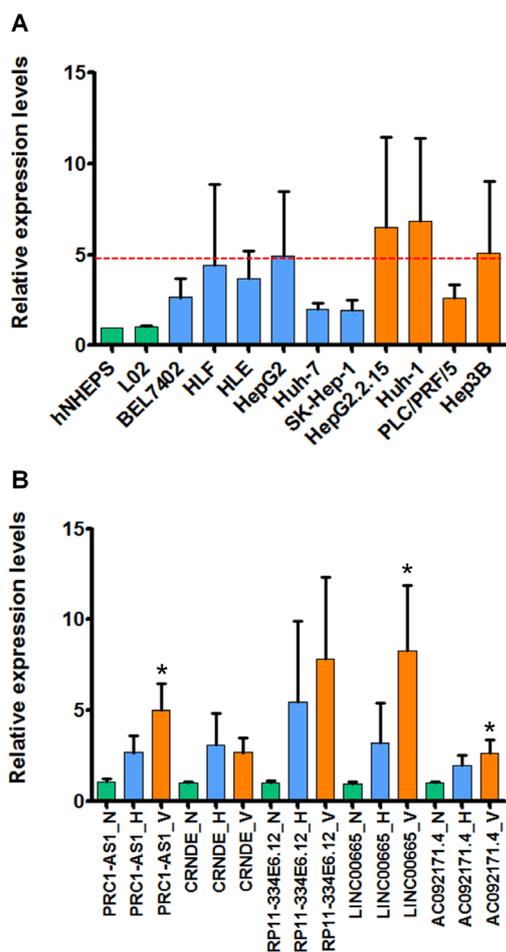
Figure 3. Comparison of HCC cell lines infected or not infected with HBV. (A) The average level of lncRNA expression in 12 cell lines. The dotted line represents the highest average level of expression in HCC cell lines not infected with HBV. **(B)** Comparison between HCC cell lines infected with HBV and HCC cell lines not infected with HBV. Cell lines expressing lncRNAs were divided into three groups: normal liver cell lines (N), HCC cell lines not infected with HBV (H), and HCC cell lines that were infected with HBV or positive for its protein or DNA (V). Green bar: normal liver cell lines; blue bar: HCC cell lines not infected with HBV; yellow bar: HCC cell lines infected with HBV. Data are expressed as the mean ± S.D. (n = 3). *p < 0.05 *vs.* HCC cell lines not infected with HBV.

its protein or DNA. These results indicate that these lncRNAs might play important roles in the progression of HCC and/or HBV infection.

Acknowledgements

References

1. The National Human Genome Research Institute (NHGRI). Statistics about the current Human GENCODE Release (version 25). *http://www.gencodegenes.org/stats/current.html* (accessed June 14, 2016).
2. Palazzo AF, Lee ES. Non-coding RNA: What is functional and what is junk? Front Genet. 2015; 6:2.
3. Clerget G, Abel Y, Rederstorff M. Small non-coding RNAs: A quick look in the rearview mirror. Methods Mol Biol. 2015; 1296:3-9.
4. Maass PG, Luft FC, Bahring S. Long non-coding RNA in health and disease. J Mol Med (Berl). 2014; 92:337-346.
5. He Y, Meng XM, Huang C, Wu BM, Zhang L, Lv XW, Li J. Long noncoding RNAs: Novel insights into hepatocelluar carcinoma. Cancer Lett. 2014; 344:20-27.
6. Fang XY, Pan HF, Leng RX, Ye DQ. Long noncoding RNAs: Novel insights into gastric cancer. Cancer Lett. 2015; 356:357-366.
7. Martens-Uzunova ES, Bottcher R, Croce CM, Jenster G, Visakorpi T, Calin GA. Long noncoding RNA in prostate, bladder, and kidney cancer. Eur Urol. 2014; 65:1140-1151.
8. Han D, Wang M, Ma N, Xu Y, Jiang Y, Gao X. Long noncoding RNAs: Novel players in colorectal cancer. Cancer Lett. 2015; 361:13-21.
9. Zhang XQ, Leung GK. Long non-coding RNAs in glioma: Functional roles and clinical perspectives. Neurochem Int. 2014; 77:78-85.
10. Li Z, Shen J, Chan MT, Wu WK. TUG1: A pivotal oncogenic long non-coding RNA of human cancers. Cell Prolif. 2016; 49:471-475.
11. Tian X, Xu G. Clinical value of lncRNA MALAT1 as a prognostic marker in human cancer: Systematic review and meta-analysis. BMJ Open. 2015; 5:e008653.
12. Bhan A, Mandal SS. LncRNA HOTAIR: A master regulator of chromatin dynamics and cancer. Biochim Biophys Acta. 2015; 1856:151-164.
13. Malek E, Jagannathan S, Driscoll JJ. Correlation of long non-coding RNA expression with metastasis, drug resistance and clinical outcome in cancer. Oncotarget. 2014; 5:8027-8038.
14. La Vecchia C, Boccia S. Oral contraceptives, human papillomavirus and cervical cancer. Eur J Cancer Prev. 2014; 23:110-112.
15. Xu C, Zhou W, Wang Y, Qiao L. Hepatitis B virus-induced hepatocellular carcinoma. Cancer Lett. 2014; 345:216-222.
16. Carnero E, Barriocanal M, Prior C, Pablo Unfried J, Segura V, Guruceaga E, Enguita M, Smerdou C, Gastaminza P, Fortes P. Long noncoding RNA EGOT negatively affects the antiviral response and favors HCV replication. EMBO Rep. 2016; 17:1013-1028.
17. Penkala I, Wang J, Syrett CM, Goetzl L, Lopez CB, Anguera MC. lncRHOXF1, a Long Noncoding RNA from the X Chromosome That Suppresses Viral Response Genes during Development of the Early Human Placenta. Mol Cell Biol. 2016; 36:1764-1775.
18. Imamura K, Imamachi N, Akizuki G, *et al*. Long noncoding RNA NEAT1-dependent SFPQ relocation from promoter region to paraspeckle mediates IL8 expression upon immune stimuli. Mol Cell. 2014; 53:393-406.

Brief Report

Cloning, purification, crystallization and X-ray crystallographic analysis of the periplasmic sensing domain of *Pseudomonas fluorescens* chemotactic transducer of amino acids type A (CtaA)

Abu Iftiaf Md Salah Ud-Din[1], Anna Roujeinikova[1,2,*]

[1] *Infection and Immunity Program, Monash Biomedicine Discovery Institute, Australia; Department of Microbiology, Monash University, Clayton, Victoria, Australia;*

[2] *Infection and Immunity Program, Monash Biomedicine Discovery Institute, Australia; Department of Biochemistry and Molecular Biology, Monash University, Clayton, Victoria, Australia.*

Summary	**Chemotaxis towards nutrients plays a crucial role in root colonization by *Pseudomonas fluorescens*. The *P. fluorescens* chemotactic transducer of amino acids type A (CtaA) mediates movement towards amino acids present in root exudates. In this study, the periplasmic sensory domain of CtaA has been crystallized by the hanging-drop vapor diffusion method using ammonium sulfate as a precipitating agent. A complete data set was collected to 1.9 Å resolution using cryocooling conditions and synchrotron radiation. The crystals belong to space group *I*222 or *I*2$_1$2$_1$2$_1$, with unit-cell parameters a = 67.2, b = 76.0, c = 113.3 Å. This is an important step towards elucidation of the structural basis of how CtaA recognizes its signal molecules and transduces the signal across the membrane.**

Keywords: Bacterial chemotaxis, chemoreceptor, sensing domain, symbiosis

1. Introduction

Pseudomonas fluorescens belongs to the plant growth promoting rhizobacteria (PGPR), the group of bacteria that provide nutrients for plant growth, induce systemic resistance against diseases, and help plants to tolerate abiotic and biotic stress (*1-3*). Some strains of *P. fluorescens* exert beneficial effects on plants by inhibiting the growth, or actions of, phytopathogenic microorganisms such as *Pythium ultimum*, *Gaeumannomyces graminis* and *Fusarium oxysporum* (*2*). They produce different types of secondary metabolites including antibiotics (mupirocin, pyrrolnitrin, pyoluteorin and 2,4-diacetylphloroglucinol), siderophores (pyocheline and pyoverdine) and hydrogen

cyanide, that prevent plant seeds and roots from fungal infection (*4-6*). Furthermore, some strains of *P. fluorescens* can degrade pollutants including styrene, trinitrotoluene and polycyclic aromatic hydrocarbons (*7-9*). In humans, *P. fluorescens* is part of the gut microflora (*10*). It can cause bacteraemia in immunocompromised patients (*11*).

Root colonization by PGPR promotes soil fertility and nutrient uptake by plants (*2*). Plant root exudates contain amino acids (*12*), organic acids (*13*) and sugars (*2*) that serve as nutrients for PGPR, and therefore are sensed by bacteria as attractants. Previous studies showed that mutation of the gene encoding the central chemotaxis regulatory protein CheA in *P. fluorescens* WCS365 resulted in less efficient colonization of tomato roots in comparison to the wild-type strain (*14*). Furthermore, a hyper-motile mutant of *P. fluorescens* F113 was shown to be a more efficient root-tip colonizer and to have a more significant effect in biological control of plant pathogenic fungi in comparison to the wild-type strain (*15*). Therefore, chemotaxis towards nutrients is thought to play a crucial role in effective root colonization by *P. fluorescens*.

Methyl-accepting chemotaxis proteins (MCPs) are membrane-embedded receptors that mediate chemotaxis

by recognizing chemical signal molecules (*16*). The binding of these molecules to the periplasmic sensing domains of MCPs initiates a chemotactic signalling cascade (*16*). The genome of *P. fluorescens* Pf0-1 encodes genes for 37 MCPs. Information on the ligands recognized by these receptors is limited. Three MCPs have been identified as chemotactic transducers of amino acids (CtaA, CtaB and CtaC) – receptors that recognize naturally-occurring amino acids (*17*). MCPs Pfl01_3768, Pfl_0728 and Pfl01_0728 were reported to recognize *L*-malate, succinate and fumarate (*18*). The metabolism of the aromatic compound 2-nitrobenzoate was shown to involve the chemoreceptor for 2-nitrobenzoate NbaY (*19*).

CtaA has a very broad ligand specificity and recognizes 16 different amino acids (*17*). The structural basis behind ligand recognition and the mechanism of signalling in response of ligand binding to CtaA remains unknown. A BLAST search against the known structures available in the Protein Data Bank (PDB) revealed that the periplasmic sensing domain of CtaA (CtaA^{peri}) has 30%, 24%, and 20% sequence identity with *V. cholerae* chemoreceptor MCP37 (PDB code 5AVE (*20*)), *Methanosarcina mazei* histidine kinase (PDB code 3li8, (*21*)) and *Campylobacter jejuni* chemoreceptor Tlp3 (PDB code 4xmr (*22*)), respectively. The periplasmic sensing domain of an amino acid chemotaxis receptor PctA from *Pseudomonas aeruginosa* that has 65% amino acid sequence identity with CtaA^{peri} (*17*) was crystallized in 2013 (*23*), but no report of the structure followed. The Pfam analysis (*24*) using the primary sequence of CtaA^{peri} revealed the presence of a Cache (*ca*lcium channels and *che*motaxis receptors) motif (residues 107-185) (*25*), which suggests that CtaA^{peri} belongs to the family of receptor proteins with two Per-Arnt-Sim (PAS) sensing domains. Recently, we have reported the crystal structure of the periplasmic sensing domain of *C. jejuni* transducer-like protein 3 (Tlp3) harboring two PAS domains. Tlp3 recognizes its ligand isoleucine directly, *via* its membrane-distal PAS domain (*22*). The structural analysis of Tlp3 and structure-guided sequence alignments revealed that receptors for amino acids, that have a tandem-PAS sensing domain that recognizes the ligand directly, contain a conserved consensus motif DXXX(R/K)CWYXXA (*22*). We note that CtaA^{peri} contains this motif and is therefore likely to bind at least some of its amino acid ligands directly. To investigate the structural basis of how CtaA recognizes its signal molecules and transduces the signal across the membrane, we have initiated structural studies on recombinant CtaA^{peri}. Here, we report its cloning, purification, co-crystallization with one of its putative ligands (serine) and initial X-ray crystallographic analysis.

2. Materials and Methods

2.1. *Gene cloning and overexpression*
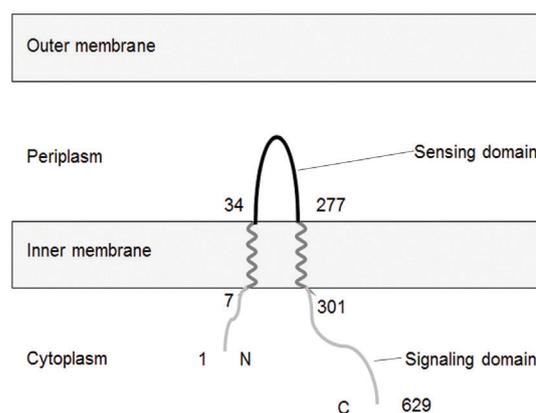
Figure 1. The predicted membrane topology of *P. fluorescens* CtaA and the boundaries (amino acid residue numbers) of the periplasmic sensory domain CtaA^{peri} characterized in this study.

The two transmembrane helices of CtaA from *P. fluorescens* Pf0-1 (GenBank: ABA76168.1) have been predicted to comprise residues 7-33 and 278-301 by the TMHMM sever v.2.0 (*http://www.cbs.dtu.dk/services/ TMHMM-2.0/*) (*26*) (Figure 1). The sequence for the periplasmic sensing domain (CtaA^{peri}, residues 34-277) was codon-optimized for expression in *Escherichia coli* and synthesized and ligated into the expression vector pET151/D-TOPO (Invitrogen) by GenScript. The protein construct had an N-terminal His$_6$-tag separated from the CtaA^{peri} coding sequence by the linker GKPIPNPLLGLDST̲ENLYFQ↓GIDPFT containing a Tobacco Etch Virus (TEV) protease cleavage site (underlined). The *E. coli* BL21 (DE3) cells (Novagen) were transformed with the expression vector, grown at 310 K in Luria Bertani broth supplemented with 50 mg/mL ampicillin to OD$_{600}$ of 0.6, and then protein expression was induced with 0.5 mM isopropyl-b-D-1-thiogalactopyranoside (Thermo Scientific) for 3.5 h at 310 K. The cells were harvested by centrifugation at 6,000 g for 15 min at 277 K.

2.2. *Purification*

The cells were resuspended in 20 mM Tris-HCl buffer pH 8.0 and 200 mM NaCl, lysed using sonication and centrifuged at 12,000 g for 30 min at 277 K. NaCl and imidazole were then added to the supernatant to final concentrations of 500 and 15 mM, respectively, and the sample was loaded onto a 5 mL HiTrap Chelating HP column (GE Healthcare) pre-washed with buffer A (20 mM Tris-HCl pH 8.0, 500 mM NaCl, 15 mM imidazole). The protein was eluted with buffer A, supplemented with 500 mM imidazole, after the column was washed with 20 column volumes of buffer A containing 20 mM imidazole. The N-terminal tag was cleaved with His$_6$-TEV protease overnight at 277 K whilst dialyzing the sample against buffer B [50 mM Tris-HCl pH 8.0, 2 mM dithiothreitol, 200 mM NaCl, 1% (*v/v*) glycerol]. NaCl
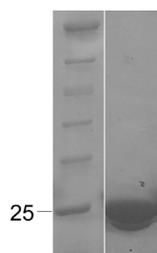
Figure 2. Coomassie Blue-stained 15% SDS-PAGE gel of recombinant CtaA^peri. The left lane contains molecular-weight marker (labelled in kDa).

and imidazole were then added to the sample to final concentrations of 500 and 15 mM, respectively, and the TEV protease and the uncleaved protein were removed on a HiTrap Chelating HP column. The flowthrough was concentrated to 2 mL in an Amicon Ultracel 10 kDa cutoff concentrator and purified further by passing through a Superdex 200 HiLoad 26/60 gel-filtration column (GE Healthcare) equilibrated with buffer C (10 mM Tris-HCl pH 8.0, 200 mM NaCl). Protein concentration was determined using the Bradford assay (*27*). The protein purity was estimated to be greater than 98% (Figure 2).

2.3. *Crystallization*

Prior to crystallization, the protein sample was concentrated to 10 mg/mL, mixed with serine solution (final concentration 2 mM), centrifuged for 20 min at 13,000 g and transferred into a clean tube. Initial crystallization screening was performed by the vapour-diffusion method in the hanging-drop format using an automated Phoenix crystallization robot (Art Robbins instruments) and Crystal Screen HT, Index Screen HT and PEG/Ion Screen HT (Hampton Research). The initial crystallization droplets comprised 100 nL protein solution mixed with 100 nL of the reservoir solution and equilibrated against 50 μL of the reservoir solution in a 96-well Art Robbins Crystalmation Intelli-Plate (Hampton Research). After one day, crystals appeared from condition No. 6 of Index Screen HT, which contained 2.0 M ammonium sulfate and 0.1 M Tris-HCl pH 8.5. This condition was further optimized to improve the crystals quality, yielding an optimal crystallization reservoir solution consisting of 2.0 M ammonium sulfate and 0.1 M Tris-HCl pH 8.0 (Figure 3).

2.4. *Data collection and processing*

Prior to data collection, crystals were transferred from the crystallization drop into a cryoprotectant solution containing 0.1 M Tris-HCl pH 8.0, 2.2 M ammonium sulfate, 2 mM serine and 30% (*v/v*) glycerol, and flash-cooled by plunging in liquid nitrogen. A complete X-ray diffraction data set was collected from a single crystal to 1.9 Å resolution using an ADSC Quantum 210r
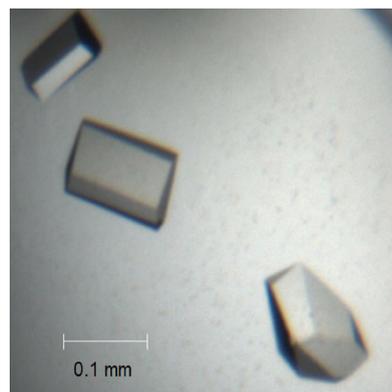
Figure 3. Crystals of a putative CtaA^peri complex with serine.
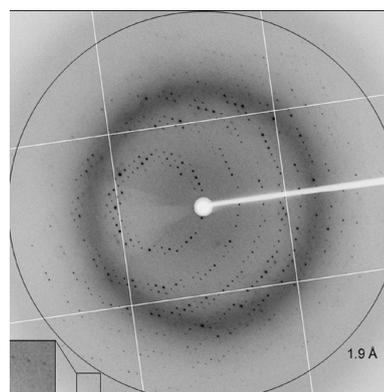
Figure 4. A representative 0.5° oscillation image of the data collected using an ADSC Quantum 210r CCD detector on the MX1 station of the Australian Synchrotron, Victoria, Australia. A magnified rectangle shows diffraction spots beyond 1.9 Å resolution.

CCD detector on the MX1 beamline of the Australian Synchrotron (AS) (Figure 4). A total of 90 images were collected using a 0.5° oscillation width. The data were processed and scaled using *iMosflm* (*28*) and *AIMLESS* (*29*) from the *CCP4* suite (*30*). The statistics of data collection and processing are summarized in Table 1.

3. Results and Discussion

Recombinant *P. fluorescens* CtaA^peri was over-expressed in *E. coli* BL21 (DE3) harboring pET151/D-TOPO plasmid upon induction of T7 polymerase. The protein was purified to >98% electrophoretic homogeneity based on Coomassie Blue staining of SDS-PAGE gels (Figure 2). It consists of amino-acid residues 34-277 of CtaA with six additional residues at the N terminus originating from the TEV cleavage site (GIDPFT). The protein migrated on SDS-PAGE with an apparent molecular weight of 25 kDa, which is in agreement with the value calculated from the amino acid sequence (27 kDa). It eluted as a single peak during size-exclusion chromatography (SEC). Estimation of its molecular weight from the mobility on the SEC column calibrated with reference to the mobility of globular proteins of

Table 1. Data collection and processing. Values for the outer shell are given in parentheses

Diffraction source	MX1 beamline, Australian Synchrotron
Wavelength (Å)	1.0
Temperature (K)	100
Detector	ADSC Quantum 210r CCD
Rotation range per image (°)	0.5
Total rotation range (°)	90
Exposure time per image (s)	1
Space group	$I222$ or $I2_12_12_1$
a, b, c (Å)	67.2, 76.0, 113.3
α, β, γ (°)	90, 90, 90
Mosaicity (°)	0.8
Resolution range (Å)	33.8-1.9
Total No. of reflections	79149 (5083)
No. of unique reflections	21256 (1353)
Completeness (%)	92.3 (94.0)
Redundancy	3.7 (3.8)
$<I/\sigma(I)>$	12.7 (2.5)
$R_{r.i.m.}$	0.029 (0.220)
Overall B factor from Wilson plot (Å2)	26.3

a known mass gave the value of approximately 23 kDa, which suggested that *P. fluorescens* CtaA^{peri} is monomeric in solution under the tested conditions.

An X-ray diffraction data set was collected for a cryo-cooled crystal of CtaA^{peri} grown in the presence of serine to 1.9 Å using the AS facility (Figure 4). Data analysis by the autoindexing routine in *iMosflm* was consistent with a body-centred orthorhombic crystal system ($I222$ or $I2_12_12_1$), with unit cell parameters a = 67.2, b = 76.0, c = 113.3 Å. The average $I/\sigma(I)$ value was 12.7 for all reflections (resolution range 33.8-1.9 Å) and 2.5 in the highest resolution shell (1.94-1.90 Å). Data processing gave an R_{merge} of 0.051 for intensities (0.346 in the resolution shell 1.94-1.90 Å) and these data were 92% complete (94% completeness in the highest resolution shell).

The calculated Matthews coefficient (*31*) for one subunit of CtaA^{peri} was 2.64 Å^3 Da^{-1}, which suggests that the asymmetric unit is highly likely to contain one protein molecule. The corresponding solvent content is approximately 53%. Molecular replacement approaches with the structures of the sensing domains of *V. cholerae* MCP37, *M. mazei* histidine kinase or *C. jejuni* Tlp3 did not yield a reliable solution. A search for heavy-atom derivatives with the aim to solve the structure using multiple isomorphous replacement and/or multi-wavelength anomalous dispersion methods is in progress. Structural analysis of the CtaA would be an important step towards our understanding of how CtaA senses its environmental signals and communicates inside the cell *via* the membrane.

Acknowledgements

References

1. Vacheron J, Desbrosses G, Bouffaud M-L, Touraine B, Prigent-Combaret C. Plant growth-promoting rhizobacteria and root system functioning. Front Plant Sci. 2013; 17:356.
2. Lugtenberg B, Kamilova F. Plant-growth-promoting rhizobacteria. Annu Rev Microbiol. 2009; 63:541-556.
3. Couillerot O, Prigent-Combaret C, Caballero-Mellado J, Moënne-Loccoz Y. *Pseudomonas fluorescens* and closely-related fluorescent pseudomonads as biocontrol agents of soil-borne phytopathogens. Lett Appl Microbiol. 2009; 48:505-512.
4. Haas D, Défago G. Biological control of soil-borne pathogens by fluorescent pseudomonads. Nat Rev Microbiol. 2005; 3:307-319.
5. O'sullivan DJ, O'Gara F. Traits of fluorescent *Pseudomonas* spp. involved in suppression of plant root pathogens. Microbiol Rev. 1992; 56:662-676.
6. Van Loon L, Bakker P, Pieterse C. Systemic resistance induced by rhizosphere bacteria. Annu Rev Phytopathol. 1998; 36:453-483.
7. Beltrametti F, Marconi AM, Bestetti G, Colombo C, Galli E, Ruzzi M, Zennaro E. Sequencing and functional analysis of styrene catabolism genes from *Pseudomonas fluorescens* ST. Appl Environ Microbiol. 1997; 63:2232-2239.
8. Pak JW, Knoke KL, Noguera DR, Fox BG, Chambliss GH. Transformation of 2, 4, 6-Trinitrotoluene by purified xenobiotic reductase B from *Pseudomonas fluorescensI*-C. Appl Environ Microbiol. 2000; 66:4742-4750.
9. Caldini G, Cenci G, Manenti R, Morozzi G. The ability of an environmental isolate of *Pseudomonas fluorescens* to utilize chrysene and other four-ring polynuclear aromatic hydrocarbons. Appl Microbiol Biotechnol. 1995; 44:225-229.
10. Wei B, Huang T, Dalwadi H, Sutton CL, Bruckner D, Braun J. *Pseudomonas fluorescens* encodes the Crohn's disease-associated I2 sequence and T-cell superantigen. Infect Immun. 2002; 70:6567-6575.
11. Scales BS, Dickson RP, LiPuma JJ, Huffnagle GB. Microbiology, genomics, and clinical significance of the *Pseudomonas fluorescens* species complex, an unappreciated colonizer of humans. Clin Microbiol Rev. 2014; 27:927-948.
12. Simons M, Permentier HP, de Weger LA, Wijffelman CA, Lugtenberg BJ. Amino acid synthesis is necessary for tomato root colonization by *Pseudomonas fluorescens* strain WCS365. Mol Plant Microbe Interact. 1997; 10:102-106.
13. Kamilova F, Kravchenko LV, Shaposhnikov AI, Azarova T, Makarova N, Lugtenberg B. Organic acids, sugars, and L-tryptophane in exudates of vegetables growing on stonewool and their effects on activities of rhizosphere bacteria. Mol Plant Microbe Interact. 2006; 19:250-256.
14. de Weert S, Vermeiren H, Mulders IH, Kuiper I, Hendrickx N, Bloemberg GV, Vanderleyden J, De Mot R, Lugtenberg BJ. Flagella-driven chemotaxis towards exudate components is an important trait for tomato root

colonization by *Pseudomonas fluorescens*. Mol Plant Microbe Interact. 2002; 15:1173-1180.

15. Barahona E, Navazo A, Martínez-Granero F, Zea-Bonilla T, Pérez-Jiménez RM, Martín M, Rivilla R. *Pseudomonas fluorescens* F113 mutant with enhanced competitive colonization ability and improved biocontrol activity against fungal root pathogens. Appl Environ Microbiol. 2011; 77:5412-5419.

16. Kato J, Kim H-E, Takiguchi N, Kuroda A, Ohtake H. *Pseudomonas aeruginosa* as a model microorganism for investigation of chemotactic behaviors in ecosystem. J Biosci Bioeng. 2008; 106:1-7.

17. Oku S, Komatsu A, Tajima T, Nakashimada Y, Kato J. Identification of chemotaxis sensory proteins for amino acids in *Pseudomonas fluorescens* Pf0-1 and their involvement in chemotaxis to tomato root exudate and root colonization. Microbes Environ. 2012; 27:462-469.

18. Oku S, Komatsu A, Nakashimada Y, Tajima T, Kato J. Identification of *Pseudomonas fluorescens* chemotaxis sensory proteins for malate, succinate, and fumarate, and their involvement in root colonization. Microbes Environ. 2014; 29:413-419.

19. Iwaki H, Muraki T, Ishihara S, Hasegawa Y, Rankin KN, Sulea T, Boyd J, Lau PC. Characterization of a pseudomonad 2-nitrobenzoate nitroreductase and its catabolic pathway-associated 2-hydroxylaminobenzoate mutase and a chemoreceptor involved in 2-nitrobenzoate chemotaxis. J Bacteriol. 2007; 189:3502-3514.

20. Nishiyama S, Takahashi Y, Yamamoto K, Suzuki D, Itoh Y, Sumita K, Uchida Y, Homma M, Imada K, Kawagishi I. Identification of a *Vibrio cholerae* chemoreceptor that senses taurine and amino acids as attractants. Sci Rep. 2016; 6:20866.

21. Zhang Z, Hendrickson WA. Structural characterization of the predominant family of histidine kinase sensor domains. J Mol Biol. 2010; 400:335-353.

22. Liu YC, Machuca MA, Beckham SA, Gunzburg MJ, Roujeinikova A. Structural basis for amino-acid recognition and transmembrane signalling by tandem Per-Arnt-Sim (tandem PAS) chemoreceptor sensory domains.

Acta Cryst D. 2015; 71:2127-2136.

23. Rico-Jiménez M, Muñoz-Martínez F, Krell T, Gavira JA, Pineda-Molina E. Purification, crystallization and preliminary crystallographic analysis of the ligand-binding regions of the PctA and PctB chemoreceptors from *Pseudomonas aeruginosa* in complex with amino acids. Acta Cryst F. 2013; 69:1431-1435.

24. Finn RD, Bateman A, Clements J, Coggill P, Eberhardt RY, Eddy SR, Heger A, Hetherington K, Holm L, Mistry J. Pfam: The protein families database. Nucleic Acids Res. 2014:gkt1223.

25. Anantharaman V, Aravind L. The CHASE domain: A predicted ligand-binding module in plant cytokinin receptors and other eukaryotic and bacterial receptors. Trends Biochem Sci. 2001; 26:579-582.

26. Krogh A, Larsson B, Von Heijne G, Sonnhammer EL. Predicting transmembrane protein topology with a hidden Markov model: Application to complete genomes. J Mol Biol. 2001; 305:567-580.

27. Bradford MM. A rapid and sensitive method for the quantitation of microgram quantities of protein utilizing the principle of protein-dye binding. Anal Biochem. 1976; 72:248-254.

28. Battye TGG, Kontogiannis L, Johnson O, Powell HR, Leslie AG. iMOSFLM: A new graphical interface for diffraction-image processing with MOSFLM. Acta Cryst D. 2011; 67:271-281.

29. Evans PR, Murshudov GN. How good are my data and what is the resolution? Acta Cryst D. 2013; 69:1204-1214.

30. Winn MD, Ballard CC, Cowtan KD, Dodson EJ, Emsley P, Evans PR, Keegan RM, Krissinel EB, Leslie AG, McCoy A. Overview of the CCP4 suite and current developments. Acta Cryst D. 2011; 67:235-242.

31. Matthews B. In: H. Neurath, Hill RL, editors. X-ray Structure of Proteins. 3. 3rd ed. Academic Press, New York, USA 1977. pp. 468-477.

Commentary

The role of family physicians contracted healthcare in China: A "Cardiotonic" or a "Band-Aid" for healthcare reform?

Qi Tang[1], Peipei Song[2],*, Lingzhong Xu[1]

[1] *School of Public Health, Shandong University, Ji'nan, Shandong, China;*
[2] *Graduate School of Frontier Sciences, The University of Tokyo, Kashiwa, Chiba, Japan.*

Summary	On June 6, 2016, as a mode expected to open a new prospect for tiered system of medical care in China, family physicians contracted healthcare was officially launched, intending to facilitate such healthcare be universal coverage by 2020.There are some doubts as to whether this goal is possible. The role of family physicians contracted healthcare in China should also be carefully identified. We hold that family physicians contracted healthcare will promote healthcare reform if it provides a "Cardiotonic" that alleviates the long-standing inequitable allocation of healthcare resources. However, this form of care faces many obstacles given the current state of medical care in China. It will just be a "Band-Aid" if the aforementioned issues of the shortage of family physicians, coordination with referring hospitals, and incomplete oversight are not resolved.

Keywords: Medical reform, family physicians, general practitioners, China

1. Introduction

Over the past five year, the Chinese Government has been exploring and establishing a tiered system of medical care tailored to China as a key step toward greater reform of the medical and healthcare system. In order to rationally allocate medical resources and promote equal access to basic medical and health care, the Chinese Government began to establish general practitioners system in 2011 (*1*).

Moreover, on June 6, 2016, family physicians contracted healthcare was officially launched as a mode expected to open a new prospect for tiered system of medical care in China, intending to facilitate such healthcare be universal coverage by 2020 (*2*). This form of care will promote healthcare reform if it provides a "Cardiotonic" that alleviates the long-standing inequitable allocation of healthcare resources. However, this form of care faces many obstacles given the current state of medical care in China. Thus, family physicians

contracted healthcare may be a "Band-Aid" that acts as a stopgap, temporarily alleviating the medical needs of the general public in China.

2. The shortage of family physicians will limit implementation

Registered general practitioners at primary care facilities are key providers of family physicians. The Chinese Government began to establish general practitioners system in 2011 (*1*). Thus far, approximately 180,000 general practitioners have been fostered, accounting for 6% of all medical practitioners. The annual growth number of general practitioners is about 30,000 from 2012 to 2014 (Figure 1). According to the data from Chinese Medical Doctor Association, if by the standard of a general practitioner serving every 2,000 residents, China needs at least 700,000 general practitioners (*3,4*). How can more than 500,000 general practitioners be rapidly fostered in just 5 years? Given the strained physician-patient relationship in China (*5-7*), how can family physicians contracted healthcare be made more attractive to primary care physicians? Can the quality of healthcare be ensured amidst unmet primary care needs? As a novel form of highly attentive medical care, how will family physicians earn the trust of patients? All of these obstacles are hampering successful implementation of contracted family physicians contracted healthcare.

*Address correspondence to:
Dr. Peipei Song, Graduate School of Frontier Sciences, The University of Tokyo, 5-1-5 Kashiwanoha, Kashiwa, Chiba 277-8563, Japan.
E-mail: ppsong-tky@umin.ac.jp
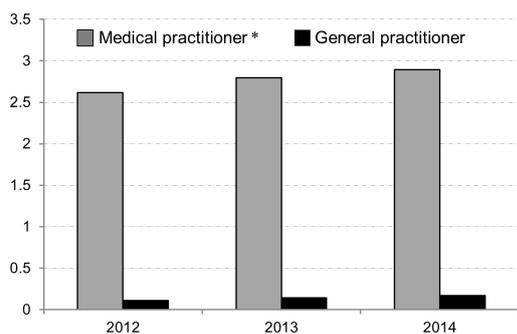
Figure 1. The number of medical practitioners and general practitioners in China from 2012-2014 based on the data from China Health Statistical Yearbook (2013-2015). *The medical practitioners include licensed medical practitioners and licensed assistant medical practitioners.

3. Giving priority to referrals will impact the "public" nature of public hospitals

Family physicians will have a certain proportion of specialists assigned, appointments will be made, and beds will be allocated, facilitating the preferential treatment and admission of contracted residents. For public hospitals, such priority will impact the "public" nature in light of many patients face difficulties in registration at large hospitals (*8*), while some patients can be provided an express route for "on-demand" healthcare. Given an imbalance in the supply of and demand for medical resources, having an initial diagnosis made by a family physician, and mutual referrals and coordination between referring hospitals and primary care facilities will also present problems. Coordinating referrals is not just the concept of a contract between family physicians, public, and referring hospitals. It is also a contract to reallocate the current medical resources.

4. Oversight to limit expenses is incomplete

Although the public is being encouraged and guided contract with nearby family physicians, the transregional contract can also be made to create an impetus for competition. In accordance with the principle of income elasticity of demand, the high income groups will pursue better medical care recruiting renowned and qualified medical personnel, which will further exacerbate the imbalance in healthcare resources. Furthermore, family physicians will provide diversified care in medication and health insurance for contracted residents. A powerful mechanism for oversight of contracted primary care is indispensable to controlling medical expenses and health insurance costs. Unfortunately, standards and measures for that oversight are lacking.

In conclusion, we sincerely hope that family physicians contracted healthcare will be a "Cardiotonic" that injects new vitality into healthcare reform in China. Nevertheless, the state of medical care in China will restrict effective implementation of this form of care. Family physicians contracted healthcare will just be a "Band-Aid" if the aforementioned issues of the shortage of family physicians, coordination with referring hospitals, and incomplete oversight are not resolved.

References

1. The State Council of China. The instructions on establishing general practitioners system. *http://www.gov.cn/zwgk/2011-07/07/content_1901099.htm* (accessed June 8, 2016; in Chinese).
2. National Health and Family Planning Commission of China. The instructions on family physicians contracted healthcare. *http://www.nhfpc.gov.cn/tigs/s3577/201606/e3e7d2670a8b4163b1fe8e409c7887af.shtml* (accessed June 7, 2016; in Chinese).
3. Chinese Medical Doctor Association. 2016 General Practitioners Training Summit: talent cultivation plan discussed by general practitioners experts. *http://www.cmda.net/gongzuodongtai/zhinengbumen/2016-04-25/15315.html* (accessed June 9, 2016; in Chinese).
4. Chinese Medical Doctor Association. Yanling Zhang: Building a primary healthcare team as pubic expect. *http://www.cmda.net/gongzuodongtai/zhinengbumen/2016-04-25/15316.html* (accessed June 9, 2016; in Chinese).
5. Zeng J, Zeng XX, Tu Q. A gloomy future for medical students in China. Lancet. 2013; 382:1878.
6. Jingang A. Which future for doctors in China? Lancet. 2013; 382:936-937.
7. Peng W, Ding G, Tang Q, Xu L. Continuing violence against medical personnel in China: A flagrant violation of Chinese law. Biosci Trends. 2016;10:240-243.
8. Yip W, Hsiao W. Harnessing the privatisation of China's fragmented health-care delivery. Lancet. 2014; 384:805-818.

BST
BioScience Trends

Guide for Authors

1. Scope of Articles

BioScience Trends is an international peer-reviewed journal. BioScience Trends devotes to publishing the latest and most exciting advances in scientific research. Articles cover fields of life science such as biochemistry, molecular biology, clinical research, public health, medical care system, and social science in order to encourage cooperation and exchange among scientists and clinical researchers.

2. Submission Types

Original Articles should be well-documented, novel, and significant to the field as a whole. An Original Article should be arranged into the following sections: Title page, Abstract, Introduction, Materials and Methods, Results, Discussion, Acknowledgments, and References. Original articles should not exceed 5,000 words in length (excluding references) and should be limited to a maximum of 50 references. Articles may contain a maximum of 10 figures and/or tables.

Brief Reports definitively documenting either experimental results or informative clinical observations will be considered for publication in this category. Brief Reports are not intended for publication of incomplete or preliminary findings. Brief Reports should not exceed 3,000 words in length (excluding references) and should be limited to a maximum of 4 figures and/or tables and 30 references. A Brief Report contains the same sections as an Original Article, but the Results and Discussion sections should be combined.

Reviews should present a full and up-to-date account of recent developments within an area of research. Normally, reviews should not exceed 8,000 words in length (excluding references) and should be limited to a maximum of 100 references. Mini reviews are also accepted.

Policy Forum articles discuss research and policy issues in areas related to life science such as public health, the medical care system, and social science and may address governmental issues at district, national, and international levels of discourse. Policy Forum articles should not exceed 2,000 words in length (excluding references).

Case Reports should be detailed reports of the symptoms, signs, diagnosis, treatment, and follow-up of an individual patient. Case reports may contain a demographic profile of the patient but usually describe an unusual or novel occurrence. Unreported or unusual side effects or adverse interactions involving medications will also be considered. Case Reports should not exceed 3,000 words in length (excluding references).

News articles should report the latest events in health sciences and medical research from around the world. News should not exceed 500 words in length.

Letters should present considered opinions in response to articles published in BioScience Trends in the last 6 months or issues of general interest. Letters should not exceed 800 words in length and may contain a maximum of 10 references.

3. Editorial Policies

Ethics: BioScience Trends requires that authors of reports of investigations in humans or animals indicate that those studies were formally approved by a relevant ethics committee or review board.

Conflict of Interest: All authors are required to disclose any actual or potential conflict of interest including financial interests or relationships with other people or organizations that might raise questions of bias in the work reported. If no conflict of interest exists for each author, please state "There is no conflict of interest to disclose".

Submission Declaration: When a manuscript is considered for submission to BioScience Trends, the authors should confirm that 1) no part of this manuscript is currently under consideration for publication elsewhere; 2) this manuscript does not contain the same information in whole or in part as manuscripts that have been published, accepted, or are under review elsewhere, except in the form of an abstract, a letter to the editor, or part of a published lecture or academic thesis; 3) authorization for publication has been obtained from the authors' employer or institution; and 4) all contributing authors have agreed to submit this manuscript.

Cover Letter: The manuscript must be accompanied by a cover letter signed by the corresponding author on behalf of all authors. The letter should indicate the basic findings of the work and their significance. The letter should also include a statement affirming that all authors concur with the submission and that the material submitted for publication has not been published previously or is not under consideration for publication elsewhere. The cover letter should be submitted in PDF format. For example of Cover Letter, please visit http://www.biosciencetrends.com/downcentre.php (Download Centre).

Copyright: A signed JOURNAL PUBLISHING AGREEMENT (JPA) form must be provided by post, fax, or as a scanned file before acceptance of the article. Only forms with a hand-written signature are accepted. This copyright will ensure the widest possible dissemination of information. A form facilitating transfer of copyright can be downloaded by clicking the appropriate link and can be returned to the e-mail address or fax number noted on the form (Please visit Download Centre). Please note that your manuscript will not proceed to the next step in publication until the JPA Form is received. In addition, if excerpts from other copyrighted works are included, the author(s) must obtain written permission from the copyright owners and credit the source(s) in the article.

Suggested Reviewers: A list of up to 3 reviewers who are qualified to assess the scientific merit of the study is welcomed. Reviewer information including names, affiliations, addresses, and e-mail should be provided at the same time the manuscript is submitted online. Please do not suggest reviewers with known conflicts of interest, including participants or anyone with a stake in the proposed research; anyone from the same institution; former students, advisors, or research collaborators (within the last three years); or close personal contacts. Please note that the Editor-in-Chief may accept one or more of the proposed reviewers or may request a review by other qualified persons.

Language Editing: Manuscripts prepared by authors whose native language is not English should have their work proofread by a native English speaker before submission. If not, this might delay the publication of your manuscript in BioScience Trends.

The Editing Support Organization can provide English proofreading, Japanese-English translation, and Chinese-English translation services to authors who want to publish in BioScience Trends and need assistance before submitting a manuscript. Authors can visit this organization directly at http://www.iacmhr.com/iac-eso/support.php?lang=en. IAC-ESO was established to facilitate manuscript preparation by researchers whose native language is not English and to help edit works intended for international academic journals.

4. Manuscript Preparation

Manuscripts should be written in clear, grammatically correct English and submitted as a Microsoft Word file in a single-column format. Manuscripts must be paginated and typed in 12-point Times New Roman font with 24-point line spacing. Please do not embed figures in the text. Abbreviations should be used as little as possible and should be explained at first mention unless the term is a well-known abbreviation (*e.g.* DNA). Single words should not be abbreviated.

Title Page: The title page must include 1) the title of the paper (Please note the title should be short, informative, and contain the major key words); 2) full name(s) and affiliation(s) of the author(s), 3) abbreviated names of the author(s), 4) full name, mailing address, telephone/fax numbers, and e-mail address of the corresponding author; and 5) conflicts of interest (if you have an actual or potential conflict of interest to disclose, it must be included as a footnote on the title page of the manuscript; if no conflict of

interest exists for each author, please state "There is no conflict of interest to disclose"). Please visit Download Centre and refer to the title page of the manuscript sample.

Abstract: The abstract should briefly state the purpose of the study, methods, main findings, and conclusions. For article types including Original Article, Brief Report, Review, Policy Forum, and Case Report, a one-paragraph abstract consisting of no more than 250 words must be included in the manuscript. For News and Letters, a brief summary of main content in 150 words or fewer should be included in the manuscript. Abbreviations must be kept to a minimum and non-standard abbreviations explained in brackets at first mention. References should be avoided in the abstract. Key words or phrases that do not occur in the title should be included in the Abstract page.

Introduction: The introduction should be a concise statement of the basis for the study and its scientific context.

Materials and Methods: The description should be brief but with sufficient detail to enable others to reproduce the experiments. Procedures that have been published previously should not be described in detail but appropriate references should simply be cited. Only new and significant modifications of previously published procedures require complete description. Names of products and manufacturers with their locations (city and state/country) should be given and sources of animals and cell lines should always be indicated. All clinical investigations must have been conducted in accordance with Declaration of Helsinki principles. All human and animal studies must have been approved by the appropriate institutional review board(s) and a specific declaration of approval must be made within this section.

Results: The description of the experimental results should be succinct but in sufficient detail to allow the experiments to be analyzed and interpreted by an independent reader. If necessary, subheadings may be used for an orderly presentation. All figures and tables must be referred to in the text.

Discussion: The data should be interpreted concisely without repeating material already presented in the Results section. Speculation is permissible, but it must be well-founded, and discussion of the wider implications of the findings is encouraged. Conclusions derived from the study should be included in this section.

Acknowledgments: All funding sources should be credited in the Acknowledgments section. In addition, people who contributed to the work but who do not meet the criteria for authors should be listed along with their contributions.

References: References should be numbered in the order in which they appear in the text. Citing of unpublished results, personal communications, conference abstracts, and theses in the reference list is not recommended but these sources may be mentioned in the text. In the reference list,

cite the names of all authors when there are fifteen or fewer authors; if there are sixteen or more authors, list the first three followed by *et al.* Names of journals should be abbreviated in the style used in PubMed. Authors are responsible for the accuracy of the references. Examples are given below:

Example 1 (Sample journal reference):
Inagaki Y, Tang W, Zhang L, Du GH, Xu WF, Kokudo N. Novel aminopeptidase N (APN/CD13) inhibitor 24F can suppress invasion of hepatocellular carcinoma cells as well as angiogenesis. Biosci Trends. 2010; 4:56-60.

Example 2 (Sample journal reference with more than 15 authors):
Darby S, Hill D, Auvinen A, *et al.* Radon in homes and risk of lung cancer: Collaborative analysis of individual data from 13 European case-control studies. BMJ. 2005; 330:223.

Example 3 (Sample book reference):
Shalev AY. Post-traumatic stress disorder: diagnosis, history and life course. In: Post-traumatic Stress Disorder, Diagnosis, Management and Treatment (Nutt DJ, Davidson JR, Zohar J, eds.). Martin Dunitz, London, UK, 2000; pp. 1-15.

Example 4 (Sample web page reference):
Ministry of Health, Labour and Welfare of Japan. Dietary reference intakes for Japanese. *http://www.mhlw.go.jp/houdou/2004/11/h1122-2a.html* (accessed June 14, 2010).

Tables: All tables should be prepared in Microsoft Word or Excel and should be arranged at the end of the manuscript after the References section. Please note that tables should not in image format. All tables should have a concise title and should be numbered consecutively with Arabic numerals. If necessary, additional information should be given below the table.

Figure Legend: The figure legend should be typed on a separate page of the main manuscript and should include a short title and explanation. The legend should be concise but comprehensive and should be understood without referring to the text. Symbols used in figures must be explained.

Figure Preparation: All figures should be clear and cited in numerical order in the text. Figures must fit a one- or two-column format on the journal page: 8.3 cm (3.3 in.) wide for a single column, 17.3 cm (6.8 in.) wide for a double column; maximum height: 24.0 cm (9.5 in.). Please make sure that the symbols and numbers appeared in the figures should be clear. Please make sure that artwork files are in an acceptable format (TIFF or JPEG) at minimum resolution (600 dpi for illustrations, graphs, and annotated artwork, and 300 dpi for micrographs and photographs). Please provide all figures as separate files. Please note that low-resolution images are one of the leading causes of article resubmission and schedule delays. All color figures will be reproduced in full color in the online edition of the journal at no cost to authors.

Units and Symbols: Units and symbols

conforming to the International System of Units (SI) should be used for physicochemical quantities. Solidus notation (*e.g.* mg/kg, mg/mL, mol/mm^2/min) should be used. Please refer to the SI Guide www.bipm.org/en/si/ for standard units.

Supplemental data: Supplemental data might be useful for supporting and enhancing your scientific research and BioScience Trends accepts the submission of these materials which will be only published online alongside the electronic version of your article. Supplemental files (figures, tables, and other text materials) should be prepared according to the above guidelines, numbered in Arabic numerals (*e.g.*, Figure S1, Figure S2, and Table S1, Table S2) and referred in the text. All figures and tables should have titles and legends. All figure legends, tables and supplemental text materials should be placed at the end of the paper. Please note all of these supplemental data should be provided at the time of initial submission and note that the editors reserve the right to limit the size and length of Supplemental Data.

5. Submission Checklist

The Submission Checklist will be useful during the final checking of a manuscript prior to sending it to BioScience Trends for review. Please visit Download Centre and download the Submission Checklist file.

6. Online Submission

Manuscripts should be submitted to BioScience Trends online at http://www.biosciencetrends.com. The manuscript file should be smaller than 5 MB in size. If for any reason you are unable to submit a file online, please contact the Editorial Office by e-mail at office@biosciencetrends.com.

7. Accepted Manuscripts

Proofs: Galley proofs in PDF format will be sent to the corresponding author via e-mail. Corrections must be returned to the editor (proof-editing@biosciencetrends.com) within 3 working days.

Offprints: Authors will be provided with electronic offprints of their article. Paper offprints can be ordered at prices quoted on the order form that accompanies the proofs.

Page Charge: Page charges will be levied on all manuscripts accepted for publication in BioScience Trends ($140 per page for black white pages; $340 per page for color pages). Under exceptional circumstances, the author(s) may apply to the editorial office for a waiver of the publication charges at the time of submission.

(*Revised February 2013*)

JOURNAL PUBLISHING AGREEMENT (JPA)

Manuscript No.:

Title:

Corresponding Author:

The International Advancement Center for Medicine & Health Research Co., Ltd. (IACMHR Co., Ltd.) is pleased to accept the above article for publication in BioScience Trends. The International Research and Cooperation Association for Bio & Socio-Sciences Advancement (IRCA-BSSA) reserves all rights to the published article. Your written acceptance of this JOURNAL PUBLISHING AGREEMENT is required before the article can be published. Please read this form carefully and sign it if you agree to its terms. The signed JOURNAL PUBLISHING AGREEMENT should be sent to the BioScience Trends office (Pearl City Koishikawa 603, 2-4-5 Kasuga, Bunkyo-ku, Tokyo 112-0003, Japan; E-mail: **office@biosciencetrends.com**; Tel: **+81-3-5840-8764**; Fax: **+81-3-5840-8765**).

1. Authorship Criteria

As the corresponding author, I certify on behalf of all of the authors that:
1) The article is an original work and does not involve fraud, fabrication, or plagiarism.
2) The article has not been published previously and is not currently under consideration for publication elsewhere. If accepted by BioScience Trends, the article will not be submitted for publication to any other journal.
3) The article contains no libelous or other unlawful statements and does not contain any materials that infringes upon individual privacy or proprietary rights or any statutory copyright.
4) I have obtained written permission from copyright owners for any excerpts from copyrighted works that are included and have credited the sources in my article.
5) All authors have made significant contributions to the study including the conception and design of this work, the analysis of the data, and the writing of the manuscript.
6) All authors have reviewed this manuscript and take responsibility for its content and approve its publication.
7) I have informed all of the authors of the terms of this publishing agreement and I am signing on their behalf as their agent.

2. Copyright Transfer Agreement

I hereby assign and transfer to IACMHR Co., Ltd. all exclusive rights of copyright ownership to the above work in the journal BioScience Trends, including but not limited to the right 1) to publish, republish, derivate, distribute, transmit, sell, and otherwise use the work and other related material worldwide, in whole or in part, in all languages, in electronic, printed, or any other forms of media now known or hereafter developed and the right 2) to authorize or license third parties to do any of the above.

I understand that these exclusive rights will become the property of IACMHR Co., Ltd., from the date the article is accepted for publication in the journal BioScience Trends. I also understand that IACMHR Co., Ltd. as a copyright owner has sole authority to license and permit reproductions of the article.

I understand that except for copyright, other proprietary rights related to the Work (*e.g.* patent or other rights to any process or procedure) shall be retained by the authors. To reproduce any text, figures, tables, or illustrations from this Work in future works of their own, the authors must obtain written permission from IACMHR Co., Ltd.; such permission cannot be unreasonably withheld by IACMHR Co., Ltd.

3. Conflict of Interest Disclosure

I confirm that all funding sources supporting the work and all institutions or people who contributed to the work but who do not meet the criteria for authors are acknowledged. I also confirm that all commercial affiliations, stock ownership, equity interests, or patent-licensing arrangements that could be considered to pose a financial conflict of interest in connection with the article have been disclosed.

Corresponding Author's Name (Signature):

Date: